ABSTRACT

POP, CRISTINA. The influence of dimer interface mutations upon the folding and activity of procaspase-3. (Under the direction of Dr. A. Clay Clark)

Procaspase-3 is the dimeric precursor of the apoptosis-executioner caspase-3 that displays little activity *in vitro*. The interface of the procaspase-3 dimer plays a critical role in zymogen maturation, although the active sites are not located at the dimer interface. We show that replacement of valine 266, the residue at the center of the procaspase-3 dimer interface, with arginine or glutamate results in an increase in enzyme activity of about 25-60-fold, representing a pseudo-activation of the procaspase. In contrast, substitution of V266 with histidine abolishes the activity of the procaspase-3 as well as that of the mature caspase. This mutant can be activated by protein exposure at pH 5, followed by dialysis at neutral pH. While the mutations do not affect the dimeric properties of the procaspase, we show that the V266E mutation may affect the formation of a loop bundle that is important for stabilizing the active sites. In contrast, the V266H mutation affects the positioning of loop L3, the loop that forms the bulk of the substrate-binding pocket. In some cases, the amino acids affected by the mutations are >20 Å from the interface. We suggest that the effects of the V266E and V266R mutations upon procaspase activity are due to the formation of buried salt bridges at the dimer interface by a mechanism similar to the activation of initiator procaspases. In addition, we suggest that inactivation of V266H is mediated by residue Y197, involved in the amino acid interaction network between the interface and catalytic loops. Equilibrium unfolding studies

show that the V266E mutant is a kinetic trap of procaspase-3, while the V266H mutant is remarkably more resistant to chemical denaturation than procaspase-3.

Overall, the results demonstrate that the integrity of the dimer interface is important for maintaining the proper active site conformation and stability of (pro)caspase-3. Procaspase-3 dimer interface mutants can be used as therapeutic tools in cancer and neurodegenerative diseases.

THE INFLUENCE OF DIMER INTERFACE MUTATIONS UPON THE FOLDING AND ACTIVITY OF PROCASPASE-3

A Dissertation

by

Cristina Pop

Submitted to the Graduate Faculty of North Carolina State University in partial fulfillment of the requirements for the Degree of Doctor of Philosophy

March 2004

Major subject: Biochemistry

APPROVED BY

_____	_____
Dr. A. Clay Clark	Dr. Carla Mattos
(CHAIR OF ADVISORY COMMITTEE)	
_____	_____
Dr. Linda Hanley-Bowdoin	Dr. Robert Kelly

DEDICATION

To my parents

BIOGRAPHY

Cristina Pop grew up in Hateg, Romania, in a small town surrounded by beautiful mountains. She attended University of Bucharest, Romania, in 1992. She graduated from Faculty of Biology in 1997 with a degree in Biochemistry. In 1998 she received a Masters of Science degree from the University of Bucharest in Molecular Biology. In 1999 she moved to Belgium, where she received training in Biochemistry at Katholieke Universiteit Leuven. In August 1999, she joined the PhD program in Molecular and Structural Biochemistry at North Carolina State University, working under Dr. A. Clay Clark's supervision. Her work was focused on the influence of the dimer interface mutations upon the folding and activity of procaspase-3. Starting June 1st 2004, she will join Dr. Guy Salvesen's laboratory at the Burhnam Institute, San Diego, CA. She is interested in pursuing a career in cancer research.

ACKNOWLEDGEMENTS

I would like to thank Dr. A. Clay Clark, my adviser, for teaching me structural biochemistry and protein folding. I appreciate his excellent guidance and supervision during my doctorate studies, as well as his generosity, kindness, friendship and understanding shown during the years.

I also thank my committee members: Dr. Linda Hanley-Bowdoin, for the flawless scientific suggestions, constructive criticism, and professional advices; Dr. Carla Mattos, for the scientific enthusiasm, friendship, passion for career advancement, and the collaboration work on caspase structure; Dr. Robert Kelly, for the promptness in suggesting ideas, and excellent teaching skills.

I owe my accomplishments in laboratory to Brett Feneey, lab manager and best friend, who carried out the molecular cloning, size exclusion chromatography, and fluorescence experiments, and helped with protein purification. I am thankful for the altruistic companionship, exceptional enthusiasm, creative ideas and persistence in completing the hardest projects shown during the year.

I thank Dr. Ashutosh Tripathy from UNC, Chapel Hill, for help with analytical centrifugation experiments, Dr. Raquel Hernandez for help with cell cultures and numerous suggestions, and Dr. Dennis T. Brown for his constant generosity.

Thanks Erin Shiver, Thora McLean and Randy Durren for the help with cloning, purification, and activity assays.

I acknowledge my friends Justin Stern, Sara Milam, Sean Casey, Vesna de Serrano, Ruby Chen, and Kakoli Bose for the good time and the interesting discussions in the lab.

I would also like to thank Ela Dragomir. She was my first Inorganic Chemistry teacher who inspired my original passion for Chemistry and heartily encouraged me ever since.

TABLE OF CONTENTS

Page

Page

Page

Page

LIST OF TABLES

Page

LIST OF FIGURES

Page

Page

Page

Page

Page

Page

Page

INTRODUCTION

Apoptotic pathways

Caspases are a family of cysteine proteases that have been identified first as key players in the cellular process termed programmed cell death or apoptosis (1). During the progression of programmed cell death, a finely organized physiological mechanism regulates the destruction and tidy disposal of unwanted cells, without participation of the inflammatory response (2). Although there are many types of cellular death, nearly all the physiological deaths in eumatozoans proceed by the process of apoptosis (3). Cell death is mandatory during the development of the multicellular organisms, participating from the tissue differentiation and harmonious shaping of the organs to the elimination of the infected cells or the suicide of cancerous cells (4).

Typical morphological changes in cells distinguish apoptosis from necrosis (4). These include chromatin condensation, DNA cleavage, cytoplasmic shrinkage, and plasma membrane blebbing that lead to the organized fragmentation of the cells into membrane-enclosed particles called ‘apoptotic bodies’ (4). Non-leakage of the intracellular content avoids the inflammation, while specific structural changes on the membrane induce the phagocytosis of the apoptotic bodies by the surrounding macrophages (4). Overall, apoptosis is differentiated from other types of death by the silent way of cellular debris removal, or “death without corpse” (2).

Abnormalities in apoptosis are the cause of many pathological situations (4). In humans, excessive cellular death is the base of neurological diseases, while insufficient apoptosis leads to autoimmune disorders or cancer (5). Due to these

reasons, the research in the pathology of cellular death received tremendous attention in the last 20 years.

Although the concept of apoptosis was introduced in 1972 (6), a clear mechanism of how apoptosis is initiated does not exist. The scientific literature shows that numerous chemicals can induce cellular death under certain conditions (4). However, in mammals, some cells die autonomously during development, meaning that the suicidal signal is intrinsically planned (4).

Two major pathways, conserved in all multicellular organisms, are generally accepted to be responsible for apoptosis initiation (7): A) Cell surface death receptor pathway; and B) Mitochondria-mediated pathway (Figure 1). Both pathways culminate with the activation of the initiator caspases, which in turn activate the executioner caspases. Minor initiation pathways include activation of the executioners by other proteases, like Granzyme B, introduced into cells by the cytotoxic lymphocytes (2).

The extracellular pathway involves ligation of the death receptors (Fas receptors or the TRAIL receptors) with their specific ligands (7) (Figure 1). The latter induce the formation of receptor micro-aggregates, followed by the recruitment of the intracellular adaptor scaffolds, and the initiator caspases. The death domain (DD) of the Fas receptor interacts with the homologous DD of the adaptor FADD (Fas associated adapter protein with a death domain). An additional domain of FADD, DED (death effector domain), interacts with the DED domain of the procaspase-8 or -10, contributing to their activation and auto-processing. The resulting caspases are released into the cytosol where they will cleave and activate the executioner

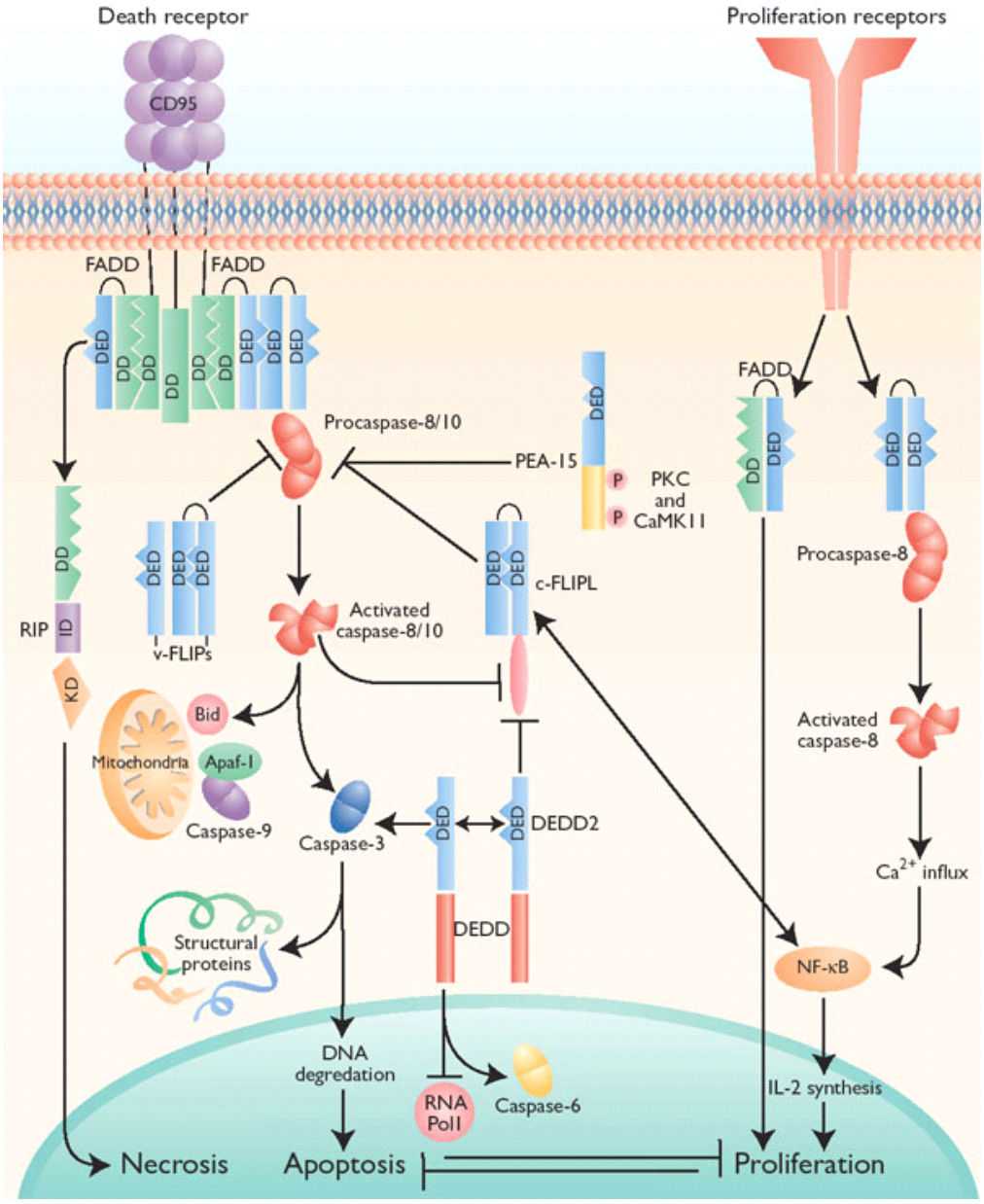

Figure 1. Apoptotic pathways. The programmed cell death is initiated via extrinsic pathway (membrane receptors) or intrinsic pathway (mitochondrial signaling) (8).

procaspases-3, -6, or -7. The executioners target the proteolysis of numerous cellular substrates (lamin, DNA repair enzymes, gelsolin, protein kinase C) (9), ultimately leading to cell dismantling (4).

On the other hand, the intracellular mediated pathway utilizes signals released by the mitochondria (7) (Figure 1). This pathway is highly ATP dependent, as the scaffold needed to activate the initiator caspase-9, called apoptosome, is formed with the participation of seven molecules of dATP per molecule of apoptosome (10). The main component of this machinery is Apaf-1, a large protein of 130 kDa, containing a caspase-recruitment domain (CARD) (at the N-terminus), a nucleotide affinity domain (in the protein core), and 12-13 WD-40 repeats (at the C-terminus) (7). In the presence of dATP and cytochrome c released by mitochondria, Apaf-1 forms a 7-unit multimeric structure (apoptosome) able to recruit and activate procaspase-9, via CARD-CARD interactions (10). Activated (pro)caspase-9 specifically targets procaspase-3 for activation (7).

The mitochondrial-signaling pathway is finely regulated by the proteins from the Bcl-2, Bcl-x, and Bax families, which control especially the release of cytochrome c from the intermembrane space (7). In addition, several endogenous inhibitors of caspases have been identified in mammalian cells, grouped into the family of IAP proteins or “inhibitors of apoptosis” (11).

Caspases in apoptosis

Caspases are cysteinyl aspartate-specific proteases that recognize a tetrapeptide motif XYZD, where the last residue is obligatorily an aspartate (12). This

high degree of specificity is found only in Granzyme B, a serine protease that also cleaves after aspartic acid and is produced by activated lymphocytes during the inflammatory response (13). There are 14 known mammalian caspases, most of them well characterized (14). Although the main cellular role of caspases is in apoptosis, some caspases are involved in other cellular processes like cytokine maturation, T-cell proliferation, cell cycle regulation, and cell differentiation (15, 16).

Several ways are used to classify caspases (14, 16) (Figure 2): a) According to their substrate preferences, caspases-1, -4, -5, and -13 belong to group I (preference for WEHD motif), caspases-2, -3, and -7 belong to group II (preference for DEXD), and caspases-6, -8, -9, and -10 belong to group III (preference for I/V/L/EXD); b) According to their cellular function, caspases are apoptotic (caspase-3, -6, -7, -8, -9), or non-apoptotic (caspase-1, 4, or 5). The latter participate in the production of the cellular cytokines, cell division and cellular attachment; c) According to the their role in apoptosis, caspases are initiators (caspase-2, -8, -9, -10) or executioners (caspase-3, -6, -7); d) According to the length of their pro-domain, caspases are long pro-domain caspases (caspase-1, -2, -4, -5, -8, -9, and -10) or short pro-domain caspases (caspase-3, -6, -7, -14).

Caspases exist in cells as dormant zymogens, which await to be activated following the apoptotic signal (17). It has been determined that the initiator procaspases are monomers, and their activation takes place only subsequent to pro-domain mediated dimerization (Figure 3). Cleavage of these procaspases is neither required nor sufficient for their activation (17). Interestingly, the mature initiator caspases have specificity for the executioners, but cannot process their own

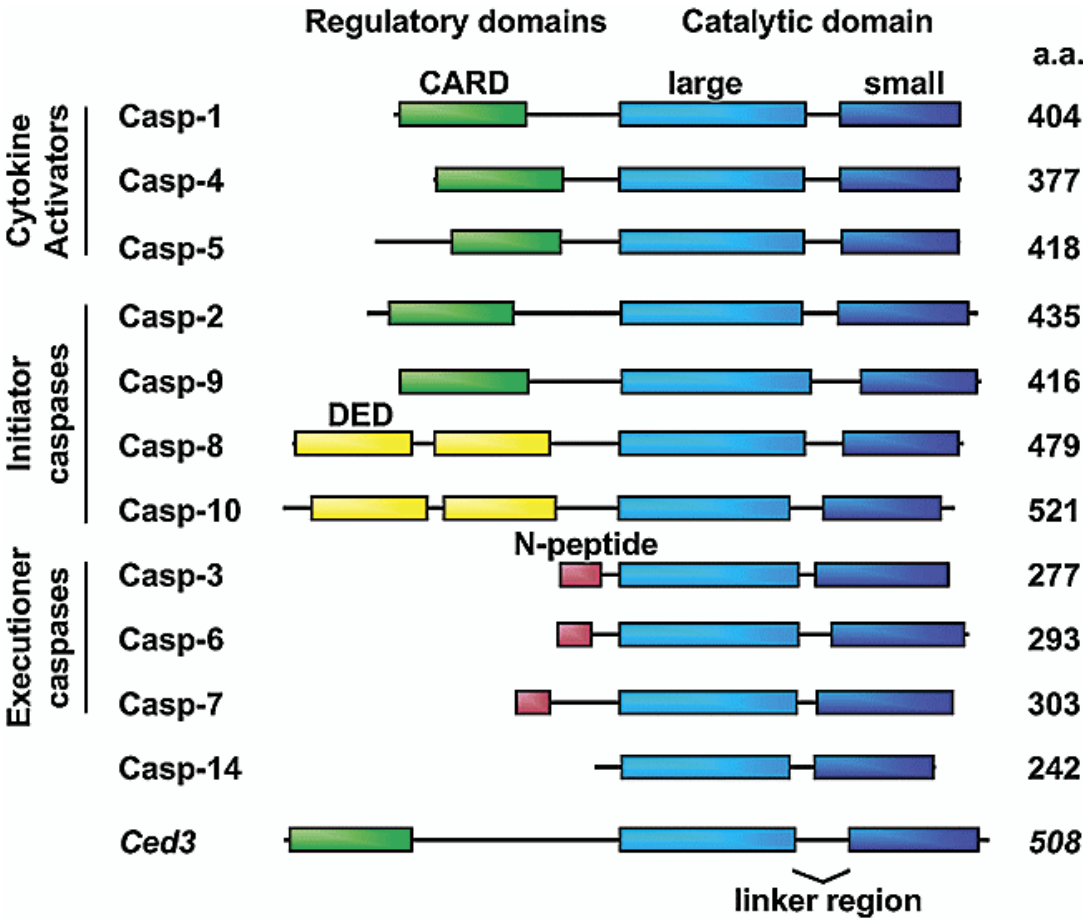

Figure 2. Caspase classification. Human caspases are classified according to their cellular function (cytokine activators, apoptosis initiators, and apoptosis executioners), and the length of the pro-domain (long pro-domain containing CARD or DED motifs, and short pro-domain). Procaspases organization includes: the pro-domain, a linker (optional), the large subunit, a linker, and the small subunit (18).

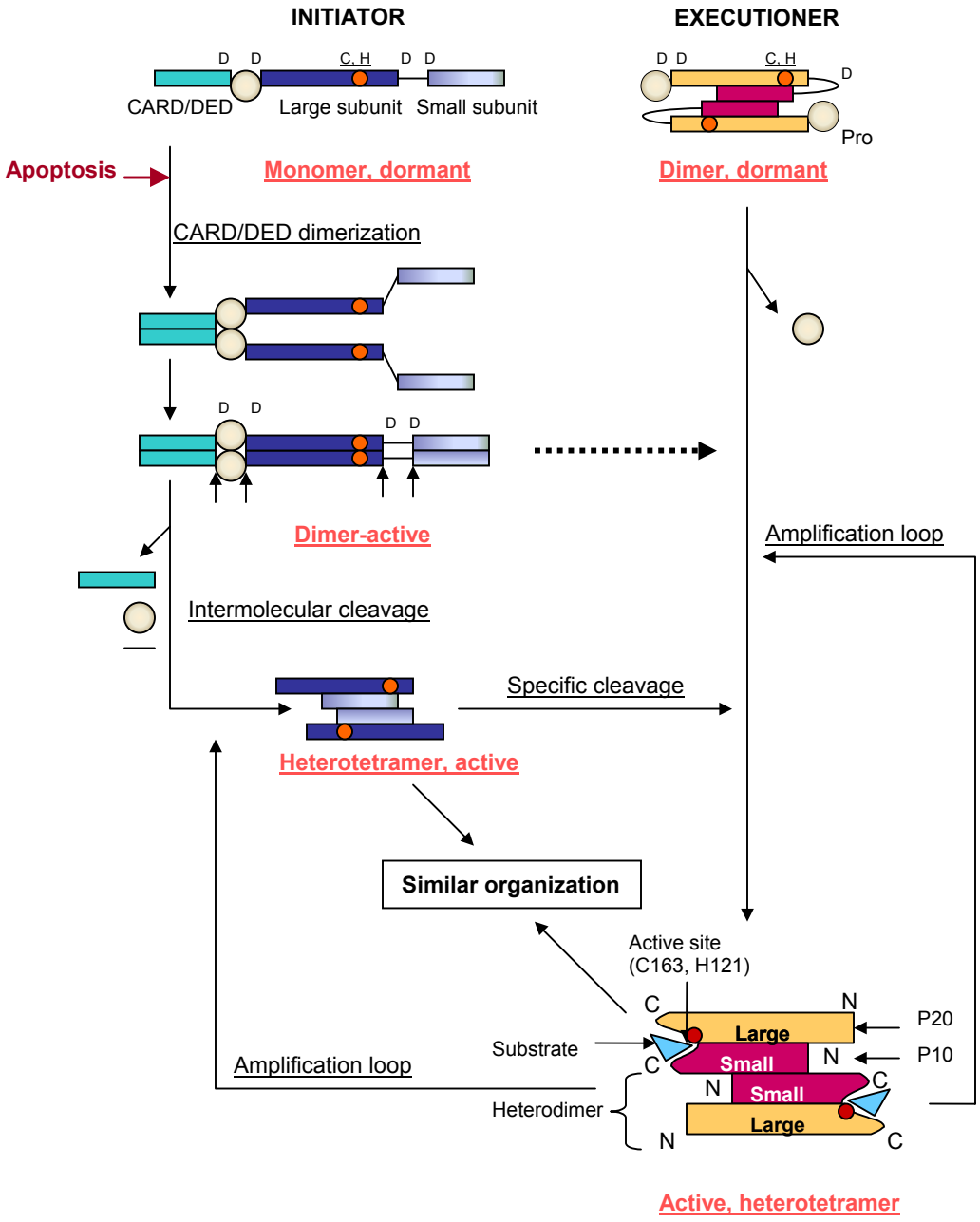
INITIATOR
EXECUTIONER
D D C, H D D
CARD/DED
Large subunit
Small subunit
D D C, H D
D
Pro
Apoptosis
Monomer, dormant
Dimer, dormant
CARD/DED dimerization
D D
D D
Dimer-active
Amplification loop
Intermolecular cleavage
Specific cleavage
Heterotetramer, active
Similar organization
Active site
(C163, H121)
C
N
Large
P20
Substrate
C
Small
N
P10
N
Small
C
Amplification loop
Heterodimer
Large
N
C
Active, heterotetramer

Figure 3. Procaspases activate via two distinct mechanisms: 1) Initiator procaspases are monomers and can be activated via CARD/DED dimerization. The resulting dimer is able to autoprocess by cleaving at the inter-subunit linker and at the CARD/DED domain (at 'D', shown by the black arrows). The resulting heterotetramer lacks the pro-domain and has full catalytic activity. 2) Executioner procaspases are dimers and can be activated via intersubunit cleavage by up-stream caspases. The resulting heterotetramer has similar organization with the initiator caspases. Executioner caspases can amplify the caspase cascade by processing other initiator or executioner procaspases. C and H are the catalytic cysteine and histidine, respectively. The red ball represents the active site.

pro-enzymes (19). By contrast, the executioner procaspases, which contain a short pro-domain, are obligatory dimers (Figure 3) (17). Their proteolysis by the up-stream caspases or other proteases is both required and sufficient for activation (20). Like the initiators, their own precursors are poor substrates (21); however, they can amplify the caspase cascade by efficiently cleaving the initiator zymogens or other effectors (18) (Figure 3). It has recently been determined that caspase-3 is active only for a short period of time during apoptosis (22). Cells are able to trigger caspase-3 degradation, a function that is dependent on the activity of caspase-3 itself. Therefore, caspases contribute to the regulation of their own turnover.

Caspase structure and organization

Caspases are organized as pro-enzymes containing a pro-domain, a linker, a large subunit, an inter-subunit linker, and a small subunit (18) (Figure 3). Cleavage of the aspartate between the small and the large subunit is responsible for mature caspase formation (18). In contrast with other protease zymogens, the dormancy of the precursors is not due to the occupancy of the catalytic site by the pro-domain (23). Upon maturation and removal of the pro-domain, caspases become organized as heterotetramers, or dimers of heterodimers of M_r~ 60 kDa (Figure 3) (18).

Crystal structures of caspase-1, -2, -3, -7, -8, and -9 have been solved and demonstrate the structural homology within the family (24-29). Caspases define a new family of proteases with respect to the global fold, topology and quaternary

structure. They are globular proteins containing six β-strands and five helices per heterodimer (Figure 4). The two heterodimers contain one large subunit (α) (~20 kDa, or p20) and one small subunit (β) (~10 kDa, or p10) and are arranged antiparallel relative to each other, in a αββα configuration (18). The β-structure forms the core of the protein, extending only one β-sheet between the large and the small subunits (Figure 4). The helices surround the β-core. The two catalytic sites, situated opposite to each other, are located between the small and large subunits and are surrounded by four catalytic loops involved in substrate binding. The catalytic residues (cysteine and histidine) belong to the large subunit, although both subunits contribute to the catalytic groove (18).

Excepting procaspase-7 (27, 30), the structure of any other procaspase has not been solved.

Caspase-3 activation

Caspase-3 (CPP32, apopain, Yama) is the main executioner of the cell death, cleaving the largest number of apoptotic substrates among all caspases (9). Procaspase-3, the precursor of caspase-3, is a protein of 277 amino acids in total with a 28 residue pro-domain. Its organization is shown in Figure 5. C163 and H121 are the catalytic residues. The motif containing the active cysteine (QACRG) is conserved in all caspases (9). Procaspase-3 crystal structure is not available.

One model for formation of active caspase assumes that procaspase dimerizes into a conformation similar to the mature enzyme prior to activation

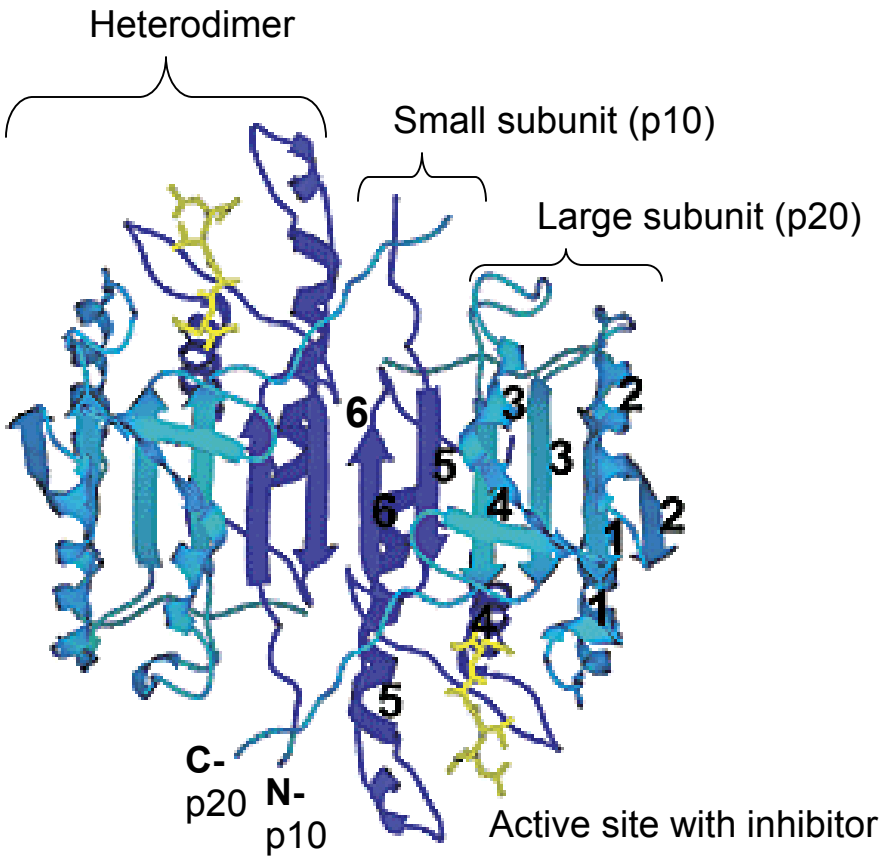

Figure 4. Caspase-3 crystal structure. A contiguous β-sheet provided by both small and large subunits forms the core of caspase-3 structure. The small subunits (p10) are colored dark blue and the large subunits (p20) are colored light blue. Helices, numbered from 1 to 5, surround the β strands, numbered from 1 to 6. In yellow it is shown the inhibitor bound to the active site (26).

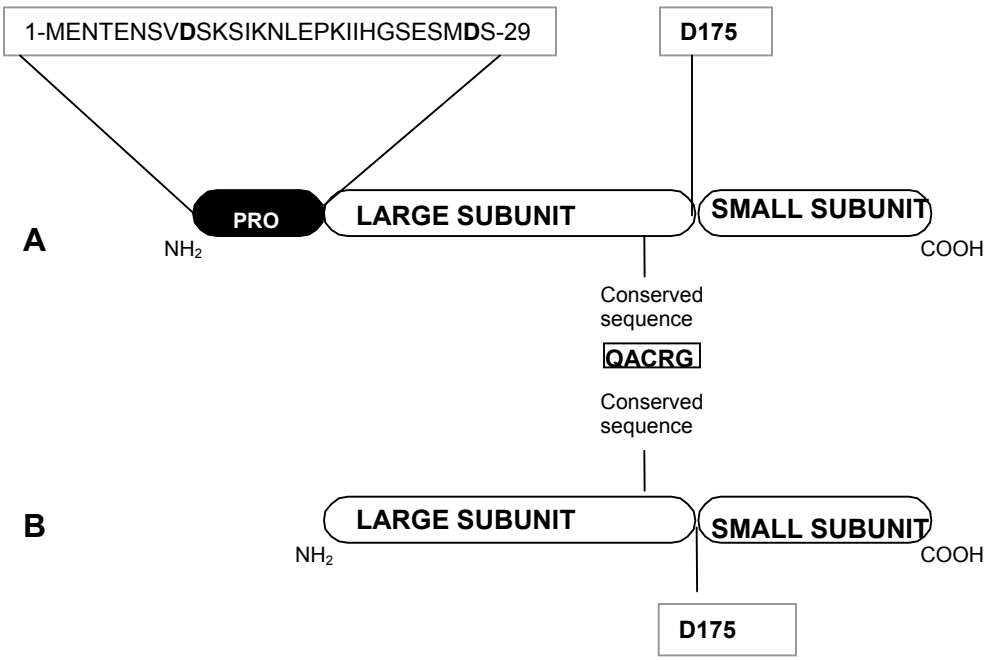

Figure 5. Procaspase-3 and pro-less variant. *Panel A*. Schematic representation of full-length procaspase-3, showing the pro-domain sequence, the conserved catalytic motif "QACRG" containing the active site C163, and the cleavage sites, D9, D28 and D175. Residues D9 and D28 from the pro-domain are shown in bold. *Panel B*. Procaspase-3 lacking the 28 amino acid pro-peptide, referred in text as 'pro-less variant.'

C

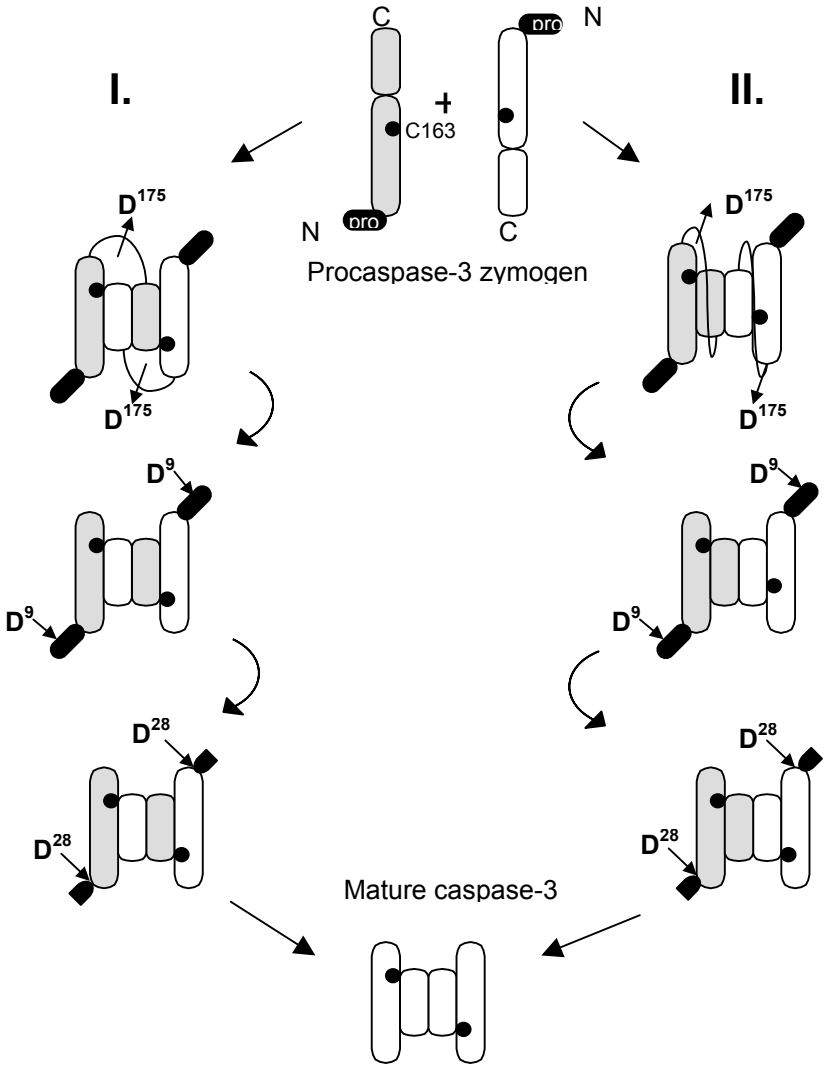

Figure 5. *Panel C*. Models for procaspase-3 assembly and maturation. Two molecules of procaspase-3 can form a dimer by interdigitation (A) or association (B), generating a structure similar to the one of caspase-3 heterotetramer. The dimeric procaspase is cleaved at D175 to form the maturation intermediate. The pro-domain is then cleaved rapidly at D9, then more slowly at D28 to give the mature heterotetramer. The catalytic site is shown as a black ball.

(Figure 5C). The dimerization can occur either by association (the heterodimer subunits come from the same precursor) or interdigitation (the subunits come from two different precursors) (24, 31). Both models have been shown to be true in the case of procaspase-1 (31). Explicitly, the large subunits of caspase-1, which were labeled with different epitope tags, could be co-immunoprecipitated when co-expressed in cultured cells (31). In addition, catalytically incompetent procaspase-1 due a mutation in p20 could be complemented by another interface mutant in the p10 subunit (31). Therefore, production of procaspase-1 dimer can occur by either model I or II of Figure 5C. Generation of mature caspase-1 is the result of procaspase-1 cleavage in the inter-subunit linker at D297 and D316, followed by pro-domain cleavage at D103 and D199 (Figure 3) (32).

In the case of procaspase-7, crystal structures (pro) caspase-7 showed that the subunits of the same heterodimer of mature enzyme originate from the same molecule of zymogen (30). Due to high similarity between procaspase-7 and procaspase-3 (9), we assume that this is also true for procaspase-3. Procaspase-3 most probably makes dimers by association, and the activation follows the model II from Figure 5C. It is assumed that the intersubunit linker of procaspase-3 connects the subunits from the same heterodimer (Figure 5C), creating the base for procaspase-3 dormancy. The resulting dimer is cleaved by the initiator caspases at D175, generating a caspase with full enzymatic activity (23). The slow cleavage of the pro-domain at D9 and D28 usually occurs auto-catalytically (33) (Figure 5C).

Mature caspase-3 subunits are 17 kDa and12 kDa, respectively. Interestingly, the C-terminus of the large subunit is in close proximity to the N-terminus of the

small subunit from the opposite heterodimer (26) (Figure 4). The two protein ends interact with each other and form the so-called “loop bundle” (further described).

The catalytic loops surrounding the active site are termed L1-L4, and are illustrated in Figure 6A. The loops include the following sequences (27): L1, residues 42-67 (large subunit), shown in yellow; L2, residues 163-175 (large subunit), shown in red; L2’, residues 176-193 (small subunit), shown in cyan; L3, residues 198-213 (small subunit), shown in blue; and L4, residues 246-263 (small subunit), shown in brown (Figure 6A).

In the case of procaspase-7, the data shows that the precursor is not enzymatically active because loop L3 is unraveled and positioned away from the active site, and the catalytic C163 is rotated away from solvent, preventing the attack of the substrate (27). Cleavage of the inter-subunit linker is critical for allowing conformational changes in other loops that must occur to remodel the active site. Removal of the covalent bond between the subunits releases the C-terminus of the large subunit, or loop L2, which flips 180° toward the N-terminus of the small subunit, or loop L2’, from the other heterodimer. The interaction between loop L2 and loop L2’ results in formation of the “loop bundle”, and allows the re-positioning of the catalytic cysteine to more hydrophobic environment. Following maturation, loop L3 moves over 10 Å toward the protein core to form the substrate-binding pocket. Loop L4 rotates in opposite direction of L3 by 60^{o} and stabilizes the other side of the catalytic groove by interacting with the loop bundle (27, 30).

A

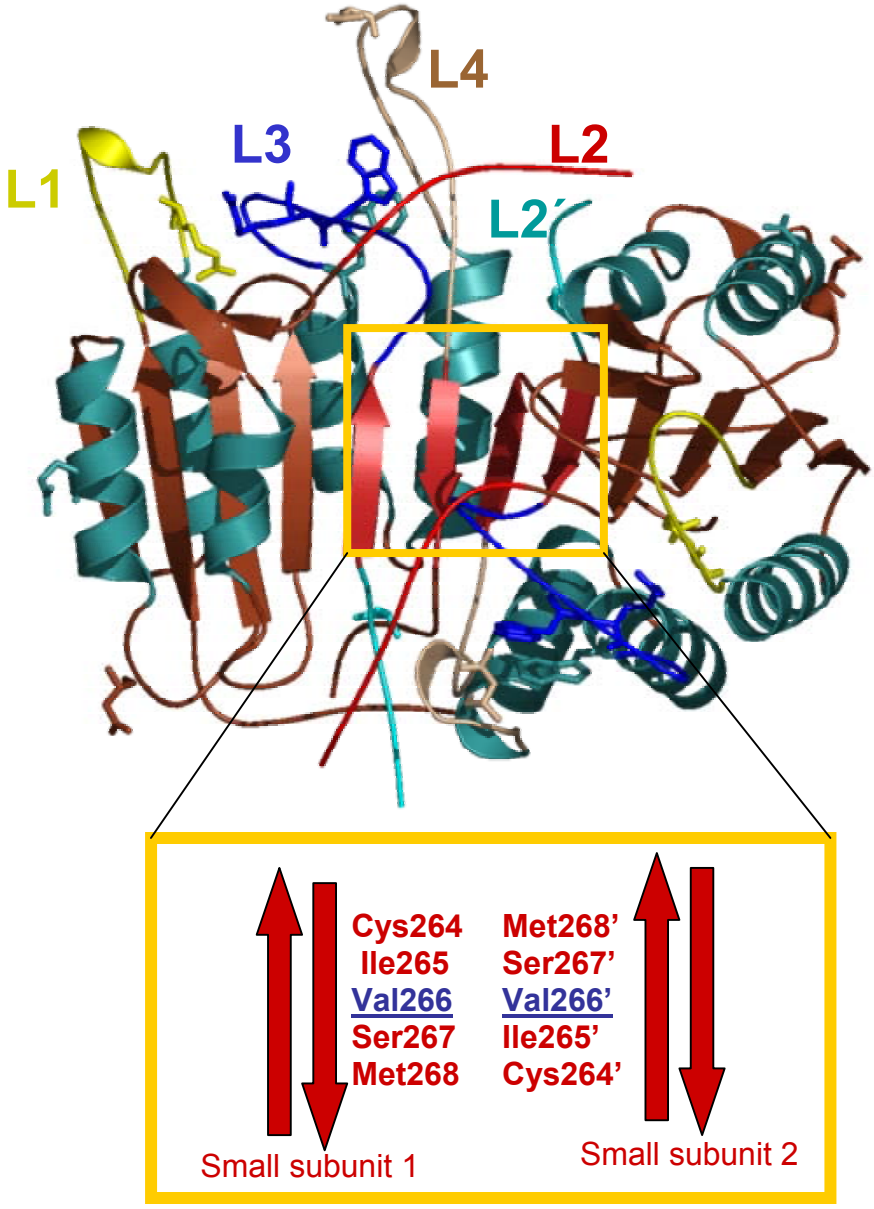

Figure 6. *Panel A*. Catalytic loops of caspase-3 (L1-L4), described in text, and the heterodimer-heterodimer interface. V266 is the symmetry axis residue, making Van der Waals contacts with the counterpart residue from the opposite heterodimer. The structure is from (26).

B

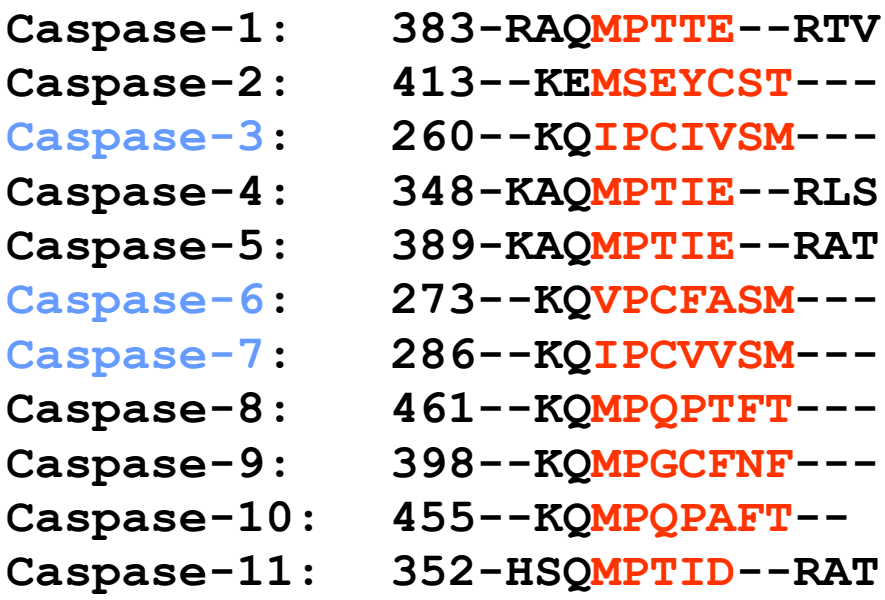

Figure 6. *Panel B*. Caspase interface alignment. Caspase-3 family is shown in blue. Residues that contribute to the formation of β-strand 6 (Figure 4) from caspase small subunit are shown in red.

Formation of the loop bundle between protein termini of two different heterodimers explains why caspases must occur as heterotetramers (Figure 6A). Stabilization of loop L2 after maturation would not be possible within the same heterodimer molecule, as the exposed residues require van der Waals contacts. Interaction of the residues from loops L2, L2' and L4 prepare the basis for caspase dimerization.

Dimeric interface of caspase-3

Caspase-3 is an obligatory heterotetramer, and its oligomeric properties are in direct link with the enzymatic activity (34). Molecular dynamics studies of the inhibitor-bound caspase-3 revealed that movements of the catalytic loops from different heterodimers are correlated, and these motions are mediated through the N-terminal region of the small subunit (35). In addition, structure-based thermodynamic analysis indicates that residues from the dimer interface of caspase-3 are critical for stabilizing the active site loops, and that a caspase-3 heterodimer could not exist thermodynamically (36).

The heterodimer-heterodimer interface of caspase-3 encloses ~2000 $Å^2$ of hydrophobic area, mainly contributed by ten residues that belong to the last two beta strands of the small subunits (26) (Figure 6). The hydrophobic contact between V266 and V266' from the opposite heterodimer is at the center of this interface. Additional interactions include H-bonding between the C-terminus of the large subunit and the N-terminus of the small subunit, and also salt bridges at the bottom of the interface involving residues E231, H234, R238, and E272 (26).

In the case of caspase-1, activity assays using the enzyme dilution method showed that caspase-1 is inactive subsequent to dissociation of the heterotetramer into heterodimers (37). In this method, the catalytic activity is measured following serial dilutions of the enzymes in assay buffer until the activity disappears. The recovery in activity is monitored by measuring the activity of the concentrated enzyme at the initial concentration values (37). In addition, initiator caspase-1, -8, and -9 can be shifted from the monomeric to the dimeric state following enzyme incubation with active site inhibitors (19, 29, 38).

The sequences of the residues residing in the dimer interface of various human caspases are shown in Figure 6B. Interestingly, the interface amino acids are not uniformly conserved in the caspase family. For example, the hydrophobic interface of caspase-3 is conserved only in caspase-6 and -7 (Figure 6B). In contrast, caspase-1 dimerization relies on electrostatic interactions between hydrophilic residues, which are preserved in caspase-4, -5, and -11. Moreover, the interfaces of caspase-2 and -9, as well as the interface of caspase-8, which is conserved in caspase -10, include both hydrophobic and hydrophilic residues (Figure 6B). In general, long pro-domain caspases contain hydrophilic residues in the dimer interface, while the short pro-domain caspases utilize hydrophobic-based interactions for oligomerization.

A distinct mechanism for the interface formation is represented by caspase-2, an initiator caspase that contains a CARD-domain and is located in the nucleus (16). In this case, a disulphide bond between C419 and C419' from the interface (Figure 6B) promotes the dimerization and stabilizes the active caspase-2 (25). Recent

studies showed that caspase-9 might also use this mechanism for activation during the oxidative stress induced apoptosis in mitochondria (39).

Protein oligomerization and caspase folding

Many cellular proteins are homo- or heterooligomers and, in some cases, their biological activity depends strictly on the quaternary structure (40). Modification of the interface of oligomeric proteins is a very specific and efficient way of drug targeting (41). More than 2000 proteins are known to occur as oligomers, and the atomic resolution structure of most of them has been elucidated (40).

Usually, in the cell, large globular proteins, rather than small proteins, associate to form soluble and functional complexes. Several evolutionary advantages can explain this feature: 1) The cooperation between subunits during the biologic activity (groEL (42) and the proteasome (43)) and during regulation (hemoglobin (44) and aspartate transcarbamylase (45)); 2) The increase in the stability due to the buried solvent-exposed surface area (46); 3) The diminution of degradation by proteases (40); 4) The facilitation of folding of large protein domains in the presence of protein assemblies (40).

In many cases, oligomerization confers unusual properties to enzymes: it may determine the direction of a reaction (lactate dehydrogenase), increase its velocity (trypthophan synthetase), modify enzyme specificity by generating new activity (lactose synthetase) or be required for substrate binding (tyrosyl tRNA synthetase) (47).

For most of the oligomeric enzymes, the catalytic activity occurs at the subunit interface. A few examples are: HIV-1 protease (48), glucose-6-phosphate isomerase (49), inosine monophosphate dehydrogenase (50), malic enzymes (51), aminoacylase (52), manganese superoxide dismutase (53). Only a few oligomeric enzymes have their active site away from the interface. However, their activity is still dependent on dimerization, like in the case of caspases (11), Rac1 GTPase (54), Cu, Zn superoxide dismutase (55), or triosophosphate isomerase (56). In this case, an interaction network between the interface and the active site residues is usually responsible for the need of association. Even fewer enzymes are active as both monomers and oligomers, as it is the case for carbamoyl-phosphate synthetase (57).

In some cases, both up-regulation and down-regulation of enzyme activity can be controlled by making use of homo- and hetero-oligomerization. An interesting example is the mechanism of caspase-8 (FLICE) activation or inhibition by means of FLIP (FLICE-like inhibitory protein) (17). FLIP is an inactive version of caspase-8 that lacks the active cysteine. Several studies indicate that FLIP expression in cultured cells can be both pro-apoptotic and anti-apoptotic (17). At low levels of expression, FLIP promotes the activation of caspase-8 by forming heterodimers with procaspase-8 at the death-inducing signaling complex (DISC) (58) (Figure 1). In contrast, at high levels of expression, FLIP competes with procaspase-8 for the same binding sites on DISC, preventing the caspase-8 activation via the induced-proximity model (59).

The number of genetic diseases generated by mutations in the dimeric interfaces of some enzymes is overwhelming. A few of these include the nonspherocytic hemolytic anemia (glucose-6-phosphate dehydrogenase) (60), hereditary sensory neuropathy type I (serine palmitoyltransferase) (61), aspartylglucosaminuria (aspartylglucosaminidase) (62), familial amyotrophic lateral sclerosis (human Cu,Zn superoxide dismutase) (62), and Parkinson's disease (human DJ-protein) (63). Most of the time, these enzyme mutations are associated with loss in catalytic activity.

Usually, the interaction between the subunits of an enzyme is tight. Thermodynamically, the association equilibrium can be shifted toward the dissociation state at low protein concentration. In practice, however, it has rarely been possible to dissociate oligomeric proteins by simple dilution. Some examples are pyruvate carboxylase, phosphofructokinase, or GroES (40). The dissociation constants for most oligomers are usually in the nanomolar range. The bulk of the conformational stability of the oligomers arises from the inter-subunit interactions (64). Due to this reason, in most of the cases, the dissociated state of a protein can only be reached by altering the environmental conditions like a change in temperature or addition of denaturants (40).

The thermodynamics of procaspase-3 unfolding at different pH values has been well characterized by our lab (65). Overall, at pH 7.2 and 25 ^{o}C, procapsase-3 unfolds via a four-state mechanism. First, the native protein, N_2, undergoes isomerization to a dimeric intermediate species, I_2. The latter dissociates to the monomeric intermediate species, I, which then unfolds to the unfolded state, U (66).

The total conformational free energy is 24 kcal/mol, suggesting that procaspase-3 is a very stable protein. The unfolding is a highly cooperative process. Dimerization of procaspase-3 occurs as a result of the association of two monomeric folding intermediates, and is considered a folding event (66). It has been predicted by theoretical thermodynamic analysis that the stability of the dimer interface of several caspases accounts for ~30-50 % of the dimer stability (36). Indeed, in our laboratory it was found that the dimerization contributes with approximately 14 kcal/mol to the conformational free energy of the protein (66). In addition, the short pro-domain of the zymogen assists in protein folding (65) as is the case for other cysteine proteases (67), but does not affect the catalytic activity (68).

Protein folding and unfolding are coupled to a range of biological phenomena, from the regulation of cellular activity to the onset of neurodegenerative diseases (69). Engineering the inter-subunit interface of oligomeric enzymes as a tool for studying protein folding and catalytic activity has been a common practice in the last twenty years.

Here we characterize in depth the correlation between hydrophobic residues in the dimer interface and the catalytic function and thermodynamics of unfolding of procaspase-3.

MATERIALS AND METHODS

Chemicals

Acrylamide, ampicillin, antifoam-C, bovine serum albumin, carbonic anhydrase, CHAPS, citric acid, cytochrome c, DEAE-sepharose, dansyl chloride, di-isopropyl fluorophosphates (DFP), DMF, DMSO, DTT, EDTA, EGTA, glycerol, IPTG, kanamycin, nickel sulfate, PIPES, PMSF, potassium iodide, monobasic and dibasic potassium phosphate, sephacryl-S15, sephacryl-S100, sodium bicarbonate, sodium citrate (dihydrate), TLCK, TPCK were from Sigma. Imidazole and urea were from ICN. Glycine, sodium chloride, Tris, tryptone, Tween-20 and yeast extract were from Fisher. His-bind resin was from Novagen. Potassium chloride and sucrose were from Mallinckrodt. HEPES was from Acros. Granzyme B was from Calbiochem. V8 protease and trypsin were from Roche Biochemicals. Ultrapure urea was purchased from Nacalai Tesque Inc (Kyoto Japan). Ac-DEVD-AFC, Ac-DEVD-CHO, Ac-DAVD-CMK and Z-VAD-FMK were purchased from Calbiochem. Polyclonal anti-caspase-3 antibody was from Cell Signaling Technology. HRP-coupled secondary antibody was from Stressgen. Non-fat dry milk was from Biorad. ECL kit was from Amersham. X-OMAT-AR film was from Kodak. Restriction enzymes were from New England Bio-labs. DMS was from Pierce.

Stock solutions

Urea stock solution (10 M) was prepared in 20 mM potassium phosphate buffer (pH 6.5-7.5), 20 mM sodium citrate buffer (pH 4.0-6.0), or 50 mM Tris HCl (pH

8.0), as previously described (70). All solutions contained 1 mM DTT and were filtered through 0.45 μm pore size filters prior to the experiment. The molarity of the urea stocks was calculated using the weight method (A) and refractive index method (B). The accepted error was ± 0.5%.

A. Calculation of molarity of urea by weight measurement

The specific gravity of a reagent solution is defined as the density relative to the density of water at the same temperature. At 25°C, the correlation between the specific gravity of a reagent solution and its weight is described by the following equation:

$$d/d_0 = 1+0.2658W + 0.0330W^2$$

where, W is the weight fraction denaturant in the solution, d is the density of the solution and d_0 is the density of water . For 10 M urea solution at 25°C, the specific gravity of the solution, d/d_0, was found to be 1.103.

Explicitly, the 10 M urea solution was prepared as follows: the desired amount of urea was weighed out in a beaker containing a stir bar. Buffer solution was then added up to a certain weight, which depended of the final volume of the solution (for example, for 40 ml of 10 M urea solution, the weight of the solution will be 40*1.103). In this calculation, the density of the buffer was approximated with the density of water as the difference is less than 0.01 g/cm^3.

B. Calculation of molarity of urea by weight measurement

The molarity of urea can be expressed in term of refractive index of urea solution by the following empirical equation:

$$M\ (urea) = 117.66(\Delta N) + 29.753(\Delta N)^2 + 185.56(\Delta N)^3$$

where, ΔN is the difference between the refractive index of the urea solution and the refractive index of the buffer. The refractive index was measured using refractometer (Fisher Scientific).

Methods

Plasmid construction

The procaspase-3 gene was amplified by PCR from pET21b-CPP32 (71), kindly provided by Dr. Emad Alnemri (Thomas Jefferson University, Philadelphia) using the primers HC3P32F (GTCGCGGATCATATGGAGAACACTG) and HC3P12R (GTGGTGGTGGTGCTCGAGGTG). This introduced an *Nde*I site at the 5' end of the gene and an *Xho*I site at the 3' end of the gene. The amplified gene product was inserted into pET21b that had been digested with *Nde*I and *Xho*I. This strategy removed fourteen amino acids at the amino terminus of procaspase-3 that arise from the vector in pET21b-CPP32. The resulting plasmid, pHC332 produces procaspase-3 with the correct amino terminus. The active site cysteine (C163) was mutated to serine using QuickChange™ site-directed mutagenesis kit (Stratagene), with the primers HCP3CS1 (5'-CATTATTCAGGCCT**C**CCGCGGTACAGAACTGGACTGTGG-3') and HCP3CS2 (5'-CAGTTCTGTACCGCGG**G**AGGCCTGAATAATGAAAAGTTTGG-3'), and plasmid pET21b-CPP32. This strategy also introduced a unique *Sac*I site (underlined) downstream of the C163S mutation (shown in bold). Plasmids were first screened by digestion with *Sac*I, and positive clones were sequenced to confirm the mutation.

The mutated gene was cloned into pET21b, as described above, to produce the plasmid pHC33201.

Plasmids pHC317 and pHC312, which harbor the genes for the caspase-3 large and small subunits, respectively, were constructed by subcloning the DNA corresponding to each subunit from pHC332, described above, into pET21b. The PCR primers for the large subunit were HC3P17F and HC3P17R (5'-CATCATCAACCTCGAGGTCTGTCTC-3'), whereas those for the small subunit were HC3P12F (5'-GCATTGAGCATATGAGTGGTGTTGATG-3') and HC3P12R. In both cases, *Nde*I and *Xho*I sites were introduced at the 5' and 3' ends, respectively. All constructs were sequenced (both strands) in order to confirm the correct sequence.

Plasmid pHC32901 was constructed by subcloning the DNA for the procaspase-3 large and small subunits from pHC33201. The primers for PCR amplification were HC3P17F (5'-GCGAATCACATATGTCTGGAATATCCC-3') and HC3P12R (5'-GTGGTGGTGGTGCTCGAGGTG-3'), generating *Nde*I and *Xho*I sites at 5' and 3' ends, respectively. The ~750 bp fragment was inserted into pET21b digested with *Nde*I and *Xho*I. The resulting proteins have carboxyl termini consisting of the sequence Leu-Glu-His_6 that arise from the vector.

The procaspase-3(D9A,D28A,D175A) mutant was made by a three-step process from plasmid pHC332, harboring the gene for wild-type human procaspase-3. First, D175 was mutated to alanine using primer 1 (5'-GTGGCATTGAGACAG**CT**AG**C**GGTGTTGATGATG-3') and primer 2 (5'-CATCATCAACACC**G**CT**AG**CTGTCTCAATGCCAC-3'). In the background of D175A, D28 was mutated to alanine using primer 3 (5'-

GGAAGCGAATCAATGG**C**C**AG**TGGAATATCCCTG-3') and primer 4 (5'-CAGGGATATTCCA**CT**G**G**CCATTGATTCGCTTCC-3'). In the background of D28A/D175A, D9 was mutated to alanine using primer 5 (5'-GAAAACTCAGTGG**CT**A**GC**AAATCCATTAAAAATTTGG-3') and primer 6 (5'-CCAAATTTTTAATGGATTT**GCT**A**G**CCACTGAGTTTTC-3'). The primers incorporated the following restriction sites for screening mutants. Primers 1 and 2: *Nhe*I; primers 3 and 4: *Bal*I (*Msc*I); primers 5 and 6: *Nhe*I. The mutations are shown in bold and the restriction sites are underlined. All plasmids were sequenced (both strands) to confirm the mutations. The resulting plasmid is called pHC33209, and we refer to this mutant as procaspase-3(D_3A). Interface mutants were created using the Quick-Change site directed mutagenesis kit (Stratagene) and the primers described below. The plasmids used as templates were pHC332, pHC33201, and pHC33209, which generated the interface mutations in wild-type caspase-3, procaspase-3(C163S), and procaspase-3(D9A,D28A,D175A), respectively. For V266H mutants, primers V266Hfwd and V266Hrev were used: V266Hfwd, 5'-CAGATTCCATGTATT**CA**TAGCATGCTCACAAAAGAACTC-3'; V266Hrev, 5'-GAGTTCTTTTGTGAGCATGCTA**TG**AATACATGGAATCTG-3'. For V266E mutants, primers V266Efwd and V266Erev were used: V266Efwd, 5'-CAGATTCCATGTATT**GAG**TCCATGCTCACAAAAGAACTC-3'; V266Erev, GAGTTCTTTTGTGAGCATGGA**CTC**AATACATGGAATCTG. Primers V266Hfwd and V266Hrev introduced a unique *Sph*1 site (underlined). The mutated bases are shown in bold. For V266R mutants, primers V266Rfwd and V266Rrev were used: V266Rfwd, 5'-CAGATTCCATGTATT**CG**T**AG**CATGCTCACAAAAGAACTC -3';

V266Rfwd, 5'-GAGTTCTTTTGTGAGCATG**CT**A**CG**AATACATGGAATCTG-3'. The introduced unique Sph1 site is underlined. For the Y197A mutants, the following primers were used: primer Y197Afwd, 5'-GGCCGACTTCTTGTATGGA**GCTAG**CA**C**AGCACCTGG-3', and Y197Arev, 5'-CCAGGTGCT**G**TG**CTAGC**TGCATACAAGAAGTCGGCC-3'. The mutations (bold) introduced the unique site NheI (underlined). For the Y197C mutants, the following primers were used: primer Y197Cfwd, 5'-GGCCGACTTCTTGTATGCAT**G**C**AGT**AC**T**GCACCTGG-3', and primer Y197Crev, 5'CCAGGTGC**A**GT**ACT**G**C**ATGCATACAAGAAGTCGGCC-3'. The mutations (bold) introduced the unique site SphI (underlined).

The plasmids were sequenced (both strands) to confirm the mutations.

Protein purification

All steps were performed at 4 ^{o}C unless otherwise noted. In separate experiments, human (pro)caspase-3 mutants were purified as C-terminal-$(His)_6$-tagged proteins from *E.coli* BL21(DE3)LysS cells harboring the described plasmids. Cells were grown in Fernbach flasks containing 1 liter of LB media with 50 μg/ml ampicillin and 0.003% antifoam-C at 37 ^{o}C. When the cultures reached an OD_{600} of ~1.2, protein expression was induced by the addition of IPTG to a final concentration of 0.5 mM and the temperature was decreased at 25 ^{o}C. The cells were harvested after ~16 hours (procaspase-3 mutants) or ~ 5 hours (caspase-3 mutants) by centrifugation at 5,000 x g for 15 minutes (GS-3 rotor). The bacterial pellets were resuspended in buffer A (Table I) (~10 ml per liter of culture) and lysed on ice using

Table I. Buffers used in the experiments

BUFFER	COMPOSITION
Buffer A	50 mM Tris-HCl, pH 7.9, 50 mM NaCl, 5 mM Imidazole, 100 μg/ml PMSF, 50 μg/ml TLCK, 100 μg/ml TPCK
Buffer B	50 mM Tris-HCl, pH 7.9, 50 mM NaCl
Buffer C	50 mM KH_2PO_4/K_2HPO_4, pH 7.2
Assay buffer	20 mM Pipes, pH 7.5, 150 mM NaCl, 1% sucrose, 0.1 % CHAPS, 10 mM DTT
Phosphate buffer	50 mM KH_2PO_4/K_2HPO_4, pH 7.5, 1mM DTT
Tris buffer	50 mM Tris-HCl, pH 7.2-9.0, 1 mM DTT
Citrate buffer	20 mM citrate pH 3.0-6.0, 1 mM DTT
Electroblotting buffer	30 mM Tris, 0.2 M glycine, pH 7.5, 20% methanol
TBS-T	20 mM Tris pH 7.6, 0.15 M NaCl, 0.1% Tween-20
Blocking buffer	TBS-T containing 5% non-fat dry milk
TEA buffer	0.2 M triethanolamine pH 8.5 1mM DTT

a French Pressure cell (16,000 psi). The supernatant was separated from cell debris by centrifugation at 28,000 x g for 30 minutes (SA-600 rotor). The pellet from this step was washed once with buffer A (Table I) (5 ml per liter of culture) and centrifuged for 30 minutes. The resulting supernatant was combined with the first. The proteins were then batch-bound for 15 minutes to His-bind resin (20 ml) equilibrated in buffer A (Table I). The resin was washed four times with four volumes of buffer A (Table I) , then four times with four volumes of buffer A (Table I) containing 80 mM imidazole. After each wash, the resin was centrifuged for two minutes at 500 g (SA-600 rotor), and the supernatant was removed. The protein was eluted with buffer A (Table I) containing 500 mM imidazole (two times of two volumes each), and the fractions were analyzed by SDS-PAGE (4-25% gradient gels). The 500 mM fractions were pooled and dialyzed overnight (2 x 80 volumes) against buffer B (Table I). The sample was applied to a DEAE-sepharose column (3 cm x 18 cm) that had been pre-equilibrated with buffer B (Table I). The proteins were eluted at a flow rate of 4 ml per minute with a linear gradient of 50-400 mM NaCl. Each fraction was tested using a mini-Bradford assay (72), and the positive fractions were analyzed by SDS-PAGE (4-25% gradient gels). The fractions (100-175 mM NaCl) containing the pure proteins were pooled, concentrated, and dialyzed overnight against buffer B (Table I). The proteins were stored at -20 ^{o}C. The protein purity was greater than 95% as assessed by SDS-PAGE.

The concentrations of procaspase-3 and caspase-3 mutants were determined using ε_{280}=26,500 $M^{-1}cm^{-1}$. The extinction coefficients were determined by the

method of Edelhoch (73) and are in good agreement with that determined previously for procaspase-3 (74). The concentrations shown here are those of the monomers.

Procaspase-3(C163S,V266E) was also purified from the insoluble fraction of *E. coli* Bl21(De3)TUNER cells. Briefly, the cells were grown at 30 ^{o}C, induced with 0.4 mM IPTG at an OD_{600} of ~1.2, and harvested after 20 h. After lysis as descried above, the inclusion bodies were washed 5 times with buffer A (Table I) and then resuspended in buffer A containing 4 M urea. The purification on His-bind resin was done as described above, except that all buffers contained additionally 4 M urea. The imidazole fractions containing the protein were concentrated, dialyzed against 50 mM Tris HCl, 50 mM NaCl, 4 M urea, 1 mM DTT, pH 7.9 and refolded in the same buffer without urea at a final concentration of 50 µg/ml, on ice. After concentration to A_{280}~0.4, the protein was stored at -20 ^{o}C.

Peptide synthesis

The wild type and mutant (D9A) pro-domains were synthesized by the Peptide Facility at the University of North Carolina at Chapel Hill. The peptides were dissolved in DMSO at a concentration of 100 mM.

Analytical ultracentrifugation

Sedimentation equilibrium experiments were performed at 25 ^{o}C in a Beckman XL-A ultracentrifuge equipped with absorbance optics and a four-hole AnTi60 rotor. The proteins were dialyzed at 4 ^{o}C into buffer C (Table I) with either 1 mM DTT (280 nm data) or 0.05 mM DTT (230 nm data). The samples were

equilibrated at three rotor speeds (14,000 rpm, 18,000 rpm, 24,000 rpm), and the absorbance was measured at 280 nm or 230 nm. For the 280 nm data, the protein concentrations were: a) procaspase-3(C163S): 3.5, 9.4, and 18.9 μM b) pro-less variant(C163S): 1.26, 4.9, and 12.9 μM; c) procaspase-3(C163S,V266E) (soluble fraction): 11.3, 18.8, and 26.4 μM; d) procaspase-3(C163S,V266H): 7.5, 18.8, and 30.1 μM; e) caspase-3(V266E): 5.6 and 15.0 μM; f) procaspase-3(C163S,V266E) (insoluble fraction): 8.4, 15.4, and 23.3 μM. For 230 nm, the protein concentrations were: a) procaspase-3(C163S): 0.45, 0.78, 1.1, 3, and 4.1 μM. b) pro-less form: 0.75, 1.25, 1.85, 2.5, and 3.7 μM. The following calculated partial specific volumes of the proteins were used: 0.713 ml/mg for procaspase-3(C163S, V266E) and procaspase-3(C163S,V266H), 0.714 ml/mg for procaspase-3(C163S) and caspase-3(V266E), and 0.715 for pro-less variant(C163S).

Size exclusion chromatography

Gel filtration experiments were done at room temperature using Sephacryl S-100 HR resin (1 cm x 30 cm) equilibrated in phosphate buffer at pH 7.2 containing 0.2 mM DTT (Table I). The proteins (13.9 μM for procasapse-3(C163S) and 14.1 μM for pro-less variant) were dialyzed in the equilibration buffer and 300 μl were applied on the column. The fractions were collected in 250 μl volume and the absorbance at 230 nm was monitored. The column was standardized using cytochrome c (~12.4 kDa), carbonic anhydrase (~29.0 kDa) and BSA (~66.0 kDa). Procaspase-3(C163S) eluted at 12.0 ml (M_r~64,773), while pro-less variant eluted at 12.25 ml (M_r~59,101).

Fluorescence and circular dichroism spectroscopy

Fluorescence emission was measured using a PTI C-61 spectrofluorometer (Photon Technologies International). Proteins (1 μM), dialyzed in buffer C (Table I) containing 1 mM DTT, were excited at either 280 nm or 295 nm, and fluorescence emission was measured from 300 to 400 nm. Circular dichroism was measured using a Jasco J600A spectropolarimeter using either a 0.1 cm (far-UV) or 1 cm (near-UV) cell. Proteins (dialyzed in buffer C containing 1 mM DTT) had concentrations between 11.3 and 20 μM. All measurements were corrected for background signal. Both instruments were equipped with thermostatted cell holders, and the temperature was held constant at 25 ^{o}C (± 0.1 ^{o}C) using a circulating water bath.

Pro-peptide labeling with dansyl chloride

Labeling of the wild-type or mutant (D9A) pro-peptide was performed as described (75), with few modifications. Briefly, wild type or mutant pro-peptide was dissolved in 0.1 M sodium bicarbonate, pH 8.6, to a final concentration of 10 mg/ml. The peptide solution was mixed while vortexing with 1/10 volumes of 10 mg/ml dansyl chloride in DMF, followed by incubation overnight at 4 °C on rotation wheel. The labeled peptide was separated from unreacted reagent using a Sephadex G-15 column (1x10 cm), equilibrated with phosphate buffer. The flow-through, containing the conjugated pro-peptide, was stored at -20 °C. The degree of labeling was determined by calculating the concentration of dansyl chloride conjugate (ε_{345}= 3400 cm^{-1} M^{-1}) and by comparison to initial concentration of pro-peptide. The degrees of

labeling of mutant pro-peptide and wild type pro-peptide were 50% and 40%, respectively.

Fluorescence anisotropy

Labeled pro-peptide (1 μM), either wild-type or D9A mutant, was incubated at 25 ^{o}C in phosphate buffer in a final volume of 2 ml. The peptide was titrated with pro-less variant between 0 μM and 10 μM, and the fluorescence anisotropy was measured as described (76). The PTI C-61 spectrofluorometer in the T-based format was used (excitation wavelength of 345 nM and emission wavelength of 450 nm).

Enzyme activity

Activity measurements were carried out as described previously using the fluorescent substrate Ac-DEVD-AFC (77). The proteins were diluted into enzyme assay buffer (Table I) and incubated at 25 °C for 15 minutes. The protein concentration was 10 times that used in the experiment. The total reaction volume was 200 μl, and the final concentration of the enzymes was 1-10 nM (caspase-3 mutants) or 10-25 nM (procaspase-3 mutants). Following the addition of the substrate, the samples were excited at 400 nm, and the fluorescence emission was monitored at 505 nm for 300 s. All fluorescence measurements were acquired using a PTI C-61 spectrofluorometer. The instrument was equipped with a thermostated cell holder, and the temperature was held constant at 25 ºC using a circulating water bath. The steady-state parameters, K_m and k_{cat}, were determined from plots of initial velocity versus substrate concentration. The dependence of the enzyme activities on

the pH was determined by measuring the initial velocity over the pH range of 5 to 10 as described (74). The assay buffer (Table I) contained: 50 mM citrate (pH 3.0 to 6.2), 20 mM Pipes (pH 6.1-7.5), 50 mM Tris HCl (pH 7.2-9.0), and 50 mM sodium bicarbonate (pH 9.2-10.6). The concentrations of CHAPS, sucrose, NaCl, and DTT were like in Table I. Final protein concentrations were 2.5-10 nM (caspase-3 mutants) or 25 nM (procaspase-3 mutants).

The enzyme activity studies in presence of the pro-domain were carried out in both assay buffer and phosphate buffer (Table I). Pro-less variant(D175A) (50 nM) was incubated with wild type pro-peptide for 1 h, at room temperature, at final pro-peptide concentrations of 0.1, 0.5, 1.0 and 2.0 μM. The fluorescent substrate was added at final concentration of 100 μM and the relative fluorescence was measured as described above.

In case of the dilution enzymatic assays, the enzyme samples were diluted in assay buffer at pH 7.5 at final concentrations shown in the figures, and incubated at 25 ^{o}C for 1 h. The substrate was added at a final concentration of 150 μM for experiments using V266E and V266H mutants, and 100 μM for experiments using V266R mutants. The initial velocity was determined as described above and plotted against the enzyme concentration.

Activation of the V266H mutant at low pH

Procaspase-3(D_3A,V266H) (25.2 μM) was dialyzed in 50 mM sodium citrate containing 1 mM DTT at pH 3.0, 4.0, 5.0, and 5.5 (1:100 volume ratio). After ~16 h of dialysis, the buffer was exchanged with buffer B (Table I) at pH 7.5 containing 1 mM

DTT, and dialyzed for additional ~19 h. In parallel, the protein was dialyzed against buffer B (pH 7.5, 1 mM DTT) for ~35 h. Fresh DTT was added in the control solution after ~16 h of dialysis. After dialysis step, the samples were centrifuged to remove the precipitate, and the concentrations were measured by reading the absorbance at 280 nm. The final concentration of the samples was: 25.2 μM (pH 7.5), 21.8 μM (pH 5.5), 12.4 μM (pH 5.0), 1.9 μM (pH 4.0) and 2.0 μM (pH 3.0). Samples dialyzed at pH 3.0 and 4.0 formed heavy precipitate after the second dialysis step. The samples were diluted to 1 μM in assay buffer and the substrate Ac-DEVD-AFC was added at final concentration of 100 μM. Initial velocity was measured as described above. The experiments were performed twice.

Granzyme B digestion

Digestion of the procaspase-3(V266H) and procaspase-3(V266H,Y197A) with granzyme B was carried out in enzyme assay buffer at 37 ^{o}C for 2 h at a final caspase: granzyme B molar ratio of 90:1. Following digestion with granzyme B, the initial velocity was measured using final enzyme concentrations of 1 nM (caspase-3) or 10 nM (caspase-3 mutants).

Limited proteolysis with trypsin

Proteins (15-20 μM) were digested with one fifteenth of their concentration (w/w) of trypsin in Tris buffer pH 7.2 or citrate buffer for pH 5.5-6.0 at 25 °C. After trypsin was added, aliquots were withdrawn at prescribed time intervals, and reactions were inhibited by TLCK (thrice the concentration of trypsin (w/w)). The

samples were frozen at -20 °C until analyzed. Samples were analyzed by SDS-PAGE using either 4-25% or 10-25% polyacrylamide gradient gels. In separate experiments, the caspase-3 inhibitor, Ac-DEVD-CHO (thrice the concentration of the protein) was included. Protein fragment identification was done by peptide sequencing.

Limited proteolysis with V8 protease

Proteins (all 15-20 μM) were digested with one fifteenth of their concentration (w/w) of V8 protease in a buffer Tris buffer (for experiments at pH 7.8 and 7.2) or a citrate buffer (for experiments at pH 6.0, 5.0 and 4.0), at 25 °C. After the addition of protease, aliquots were withdrawn at prescribed time intervals, and the reactions were inhibited with DFP (thrice the concentration of V8 (w/w)). Samples were frozen at -20 °C until analyzed. Samples were analyzed by SDS-PAGE using either 4-25% or 10-25% polyacrylamide gradient gels. In separate experiments, the caspase-3 inhibitor, Z-VAD-FMK (thrice the concentration of the protein), was included. Protein fragment identification was by peptide sequencing.

Immunobloting

All steps were done at room temperature unless otherwise noted. Proteins (5-500 ng) were resolved on 10-25% SDS-PAGE and transferred to PVDF membrane. The transfer was done in electroblotting buffer (Table I) at 30 V, overnight. The membrane was washed once for 5 min with 15 ml TBS-T solution (Table I), and then blocked with 15 ml blocking buffer (Table I) for 1 h. After washing three times with 20

ml TBS-T (5 min each), the membrane was incubated with 10 ml primary antibody (1:1000 dilution in blocking buffer) overnight at 4 ^{o}C. Following washing with TBS-T as described above, the membrane was incubated with 20 ml secondary antibody (1:3500 dilution in blocking buffer) for 1 h. The excess of secondary antibodies was removed by washing the membrane with TBS-T for 5 min, three times. The membrane was subjected to enhanced chemiluminesce as recommended by the manufacturer.

DMS cross-linking

Cross-linking with DMS was carried out as described (78). Briefly, the proteins (10-25 μM) were diluted in TEA buffer (Table I) (pH 8-8.5) or phosphate buffer (Table I) (pH 7.2), and DMS (at 10 mg/ml in the same buffer) was added at final ratio of ~1:10 (protein: DMS). The reaction mixtures were incubated for 1 h at room temperature, and the samples were analyzed by SDS-PAGE (4-25% gradient). In the case of V266R mutant, the experiemtns were also done in the presence of 1:20 molar ratio of caspase:Ac-DAVD-CMK inhibitor.

Native PAGE

Native polyacrylamide gel electrophoresis was done at pH 7.2 using the same buffers as for SDS-PAGE, lacking SDS. The molecular standards used for running included cytochrome-c (12.4 kDa), α-lactalbumin (14.2 kDa), carbonic anhydrase (29.0 kDa), chicken albumin (45.0 kDa) and BSA (66.2 kDa, 132.4 kDa).

Quenching of tryptophan fluorescence emission with acrylamide or iodide

Stock protein solutions were dialyzed against phosphate buffer, pH 7.2. Alternatively, the proteins were dialyzed against a buffer of citrate buffer, pH 6.0 to pH 3.0, or Tris buffer, pH 7.0-9.0. Stock solutions of acrylamide (5 M) or KI (2 M) (quenchers) were prepared in the same buffers. Protein solutions (1 μM) were prepared from the stocks, and the quenching agent was added to the following final concentrations: acrylamide- 0.0, 0.1, 0.15, 0.2, 0.25, 0.3, 0.4, 0.5, 0.6, 0.7, and 0.8 M; KI- 0.0, 0.01, 0.02, 0.03, 0.04, 0.05, 0.075, 0.1, 0.125, 0.15, 0.2, 0.25, 0.3 M. The samples were stirred and incubated for 1 min following each addition of quencher, and the experiments were performed at 25 °C. Samples were excited at 295 nm, and the fluorescence emission was examined from 330-350 nm. All data were corrected for background signal.

Unfolding kinetic studies

For the pH range between 6.5 and 8.0, the protein was prepared in 9.6 M urea-containing buffer at a final concentration of 4 μM in a 4 ml volume. For the pH range between 4.0 and 6.0, the final urea concentration was 5 M. The samples were vortexed and incubated at 25 °C. Fluorescence emission between 300 and 400 nm was monitored every 24 h. The average emission wavelength (<λ>) (79) was calculated for the excitation wavelengths 280 and 295 nm and plotted versus the time of unfolding. CD signal at 228 nm was monitored in parallel.

Equilibrium unfolding studies

All equilibrium unfolding experiments were performed as described previously (70, 80). Briefly, stock protein solutions were prepared in Tris buffer, pH 7.9, to be 25-100 times the final concentration used in the experiment. Phosphate buffer (20 mM) (pH 6.5-7.2), 50 mM Tris (pH 8.0) or 20 mM citrate buffers (pH 4.0-6.0), 10 M urea (stock) (pH 4.0-8.0), and stock protein solutions were mixed in microcentrifuge tubes to give final urea concentrations between 0 M and 9.6 M, and final protein concentrations of 0.5, 1.0, 2.0, 4.0 or 6.0 μM. The protein was unfolded for 24 h (pH 4.0-5.5), 48 h (pH 6.0), 72 h (pH 6.5), 144 h (pH 7.2) and 192 h (pH 8.0) at 25 °C. For refolding experiments, the protein was incubated in 8 M urea at pH 4.0-5.5 or 9.6 M urea (pH 6.0-8.0). After incubation at 25 °C as described above, the protein was rapidly diluted in buffer and urea such that the final urea and protein concentrations were as indicated in the figure legends. All samples were mixed by vortexing and were incubated in a circulating water bath at 25 °C for a minimum of 24 hours.

Fluorescence emission at each denaturant concentration was measured using a PTI C-61 spectrofluorometer. Following excitation at 280 nm or 295 nm, the fluorescence emission was monitored between 300 and 400 nm and the average emission wavelength (<λ>) was calculated. The <λ> was normalized for the native protein signal and plotted versus urea molar concentration (see data analysis).

In the case of procaspase-3(C163S,V266E) mutant, the protein (1 μM) was unfolded for ~18 h at 25 ^{o}C in 50 mM potassium phosphate, pH 7.2, 1 mM DTT containing urea at final concentrations between 0 and 8 M. The protein samples were excited at 280 and 295 nm and the fluorescence was monitored at 340 nm.

Circular dichroism signal at 228 nm was measured with a Jasco J600A spectropolarimeter using a cuvette of 1 cm path length. The data were averaged for 30 seconds. Both instruments were equipped with thermostatted cell holders, and the temperature was held constant at 25 °C using a circulating water bath.

Data analysis

Analytical ultracentrifugation

The experimental data ($\ln A_r$ versus r^2) were fit using the ORIGIN (81) version of the NONLIN algorithm (82) supplied by Beckman:

$$\ln(A_r) = \ln(A_F) + \frac{\omega^2}{2RT} M(1-\nu\rho)(r^2 - r_0^2) \qquad \text{(Eq. 1)}$$

where A_r is the solute absorbance at radius r (cm), A_F is the solute absorbance at a reference distance F, ω is the angular velocity (RPM*2π/60), R is the gas constant (R= 8.314x10^7 erg $mol^{-1}K^{-1}$), T is the temperature in Kelvin (K), M is the molecular weight (Da), ρ is the density of solution (g/ml), and ν is the partial specific volume (ml/g).

Fluorescence anisotropy

The average polarization (P) obtained for each titration was converted to anisotropy (A) using the following equation:

$$A = \frac{2P}{3-P} \qquad \text{(Eq. 2)}$$

The data were fit to a binding model that assumes a 1:1 stoichiometry as described (76) using equation 3:

$$A = A_f + \frac{[L](A_b - A_f)}{(K_d + [L])} \qquad \text{(Eq. 3)}$$

where, A is the measured anisotropy in a mixture of free and bound fluorescent molecules with the anisotropy of A_f and A_b, respectively, [L] is the concentration of the protein, and K_d is the dissociation constant.

Enzyme activity

The dependence of the experimental initial velocity on the substrate concentration was fit to the Michelis-Menten equation:

$$v_0 = \frac{k_{cat}[E][S]}{K_M + [S]} \qquad \text{(Eq. 4)}$$

where v_0 is the initial velocity (μM/s), k_{cat} is the turn-over number (s^{-1}), *[E]* is the enzyme concentration (μM), *[S]* is the substrate concentration (μM), and K_M is the Michelis-Menten constant (μM).

For the variation of the enzymatic activity with pH, the experimental initial velocity versus pH was fit to equation 5:

$$Y = C / \left(1 + \frac{[H^+]}{K_{a_1}} + \frac{K_{a_2}}{[H^+]}\right) \qquad \text{(Eq. 5)}$$

where Y is the initial velocity measured at each pH, C is the pH-independent value of Y, and K_{a1} and K_{a2} are the dissociation constants for the enzyme groups (83).

Fluorescence quenching

For acrylamide quenching, the data were fit to the Stern-Volmer equation, accounting for static and dynamic quenching (84):

$$\frac{F_0}{F} = (1 + K_{SV}[Q])e^{V[Q]} \qquad \text{(Eq. 6)}$$

where, F_0 is the fluorescence in absence of quencher, F is the fluorescence in presence of quencher, K_{SV} is the Stern-Volmer constant, *[Q]* is the quencher concentration, and V is the static quenching constant.

For quenching by iodide, the percent quenching ((F/F0)*100 was plotted versus the concentration of KI, and the data were fit to equation 7:

$$\frac{\Delta F}{F_0} \times 100 = \frac{100[Q]f_a K_{SV}}{1 + [Q]K_{SV}} \qquad \text{(Eq. 7)}$$

where (F is the change in fluorescence emission at each concentration of quencher (KI), F_0, K_{SV}, and [Q] are described in equation 5, and f_a is the fraction of the initial fluorescence emission that is accessible to the quencher.

The Stern-Volmer constants (K_{SV}), determined from the fits described by equation 7, over the pH range of 2.5 to 9, were plotted versus pH. The data were fit to equation 8:

$$\mathrm{K_{SV}} = \mathrm{A} + \Delta K_{SV_1} \frac{10^{n_1(pH - pKa_1)}}{1 + 10^{n_1(pH - pKa_1)}} + \Delta K_{SV_2} \frac{10^{n_2(pH - pKa_2)}}{1 + 10^{n_2(pH - pKa_2)}} \qquad \text{(Eq. 8)}$$

where, K_{SV} is the Stern-Volmer constant, A is the value of K_{SV} at the lowest pH, ΔK_{SV1} and ΔK_{SV2} represent the changes in the Stern-Volmer constant for each

transition, n_1 and n_2 are the number of protons titrated in each transition, and pK_{a1} and pK_{a2} are the apparent *pK*'s of the transitions.

Average emission wavelength

The average emission wavelength (<λ>) was calculated using equation (9):

$$< \lambda >= \sum_{i=1}^{N} (I_i \lambda_i) \Big/ \sum_{i=1}^{N} (I_i) \qquad \text{(Eq. 9)}$$

where <λ> is the average emission wavelength, and I_i is the fluorescence emission at wavelength λ_i.

The data versus pH were fit to equation 10,

$$< \lambda >= A + \sum_{i=1}^{3} \left[\Delta < \lambda >_i * 10^{n_i (pH - pKa_i)} / (1 + 10^{n_i (pH - pKa_i)}) \right] \qquad \text{(Eq.10)}$$

where *A* is the value of <λ> at pH >8.0, $\Delta<\lambda>_i$ is the change in average emission wavelength for the corresponding transition, n_i is the number of protons titrated in each transition, and pK_{ai} refers to the apparent p*K*'s of the transitions.

Equilibrium unfolding studies

For the fluorescence-based equilibrium studies and circular dichroism experiments, the relative signal was normalized to the value for the native protein using equation 11:

$$RS_i = \frac{S_i - S_u}{S_u - S_n} \qquad \text{(Eq. 11)}$$

where RS_i is the relative signal at urea concentration *i*, S_i is the signal of the sample *i* , S_u is the signal of the unfolded protein, S_n is the signal of the native

protein. The signal *S* is either the average emission wavelength, calculated with equation 9, in the case of the fluorescence-based experiments, either the signal in millidegrees at 228 nm in the case of the circular dichroism experiments.

For the unfolding kinetics studies, the monitored signal (*S*) versus time of unfolding (*t*) was fit to the first order kinetics equation:

$$S = S_i + \Delta S - \frac{\Delta S}{\exp\left(t \ln 2 / t_{1/2}\right)} \qquad \text{(Eq. 12)}$$

where, S_i is the initial signal, ΔS is the change in *S* with time, $t_{1/2}$ is the half time of unfolding. The signal *S* is either the <λ> at excitation 280 or 295 calculated with equation 9, either the circular dichroism signal monitored at 228 nm.

In the case of the equilibrium unfolding studies of procaspase-3(C163S,V266H) at pH 4, the fluorescence and circular dichroism data were modeled using the two state equilibrium model (85) shown in equation 13:

$$N \rightleftarrows U \qquad \text{(Eq.13)}$$

In this model, the protein is assumed to be in the monomer form (N), which unfolds to the unfolded protein (U), and *K* is the equilibrium constant for this process. The total molar concentration of the protein is $[P]_T$:

$$[P]_T = [N] + [U] \qquad \text{(Eq. 14)}$$

and the molar fraction of each species is:

$$f_N = \frac{N}{P_T} \qquad \text{(Eq.15)}$$

$$f_U = \frac{U}{P_T} \qquad \text{(Eq. 16)}$$

The sum of the two species is equal to unity, as shown by equation 17:

$$f_N + f_U = 1 \qquad \text{(Eq. 17)}$$

The equilibrium constant *K* is generated by equation 18:

$$K = \frac{f_U}{f_N} \qquad \text{(Eq. 18)}$$

From equations 17 and 18, the fraction of the unfolded species is given by equation 19:

$$f_U = \frac{K}{K+1} \qquad \text{(Eq. 19)}$$

From equations 14-19 and the relationship

$$\Delta G = -RT \ln(K_{eq}) \qquad \text{(Eq. 20)}$$

where R is the gas constant and T is the temperature in Kelvin, one may calculate the equilibrium constant and the values of ΔG at each urea concentration. We assumed the free energy change for each step in the reaction to be linearly dependent on denaturant concentration as described earlier (86) (equation 21):

$$\Delta G = \Delta G^{H_2O} - m_1 [\text{denaturant}] \qquad \text{(Eq. 21)}$$

where ΔG^{H_2O} is the free energy changes in the absence of denaturant corresponding to *K*, and m_1 is the cooperativity index associated with each step. The amplitude of the spectroscopic signal determined at each urea concentration was assumed to be a linear combination of the fractional contribution from each species (equation 22),

$$Y = Y_N f_N + Y_U f_U \qquad \text{(Eq. 22)}$$

where Y_N and Y_U are the amplitudes of the signals for the respective species. Finally, the amplitudes associated with the native and unfolded forms of the protein

were assumed to be linearly dependent on urea concentration, as shown in equations 23-24:

$$Y_N = Y_{N'} + m_2[\text{urea}] \qquad \text{(Eq. 23)}$$

$$Y_U = Y_{U'} + m_3[\text{urea}] \qquad \text{(Eq. 24)}$$

where $Y_{N'}$ and $Y_{U'}$ are the amplitudes of the signals in the absence of urea for the native and the unfolded species.

The curves were drawn in Kaleidagraph (Synergy Software, Reading, PA) and nonlinear least squares fitting of the data to these equations employed the Igor Pro software to determine the unknown parameters ΔG^{H_2O} and m_1 from each unfolding curve. Figure 7A shows the procedure file used by IgorPro to fit the two-state unfolding data.

The unfolding data at pH 4.25 to pH 5.0 were fit using a three-state model, as described by the equation 25:

$$N \rightleftarrows I \rightleftarrows U \qquad \text{(Eq. 25)}$$

This model assumes that the native species, N, is a monomer, which unfolds to an intermediate species, I, which unfolds to the unfolded state, U. The first transition is described by the equilibrium constant K_1, and the second transition is characterized by the equilibrium constant K_2. The total concentration of the protein, P_T, is a sum of all species concentration as shown in equation 26:

$$P_T = [N] + [I] + [U] \qquad \text{(Eq. 26)}$$

The molar fraction for each species is defined by the equations 27-29:

$$f_N = \frac{N}{P_T} \quad \text{(Eq.27)}$$

$$f_I = \frac{I}{P_T} \quad \text{(Eq.28)}$$

$$f_U = \frac{U}{P_T} \quad \text{(Eq. 29)}$$

The sum of all species fractions is equal to one (equation 30):

$$f_N + f_I + f_U = 1 \quad \text{(Eq. 30)}$$

The equilibrium constants are related to the mole fraction of species as shown in the equations 31-32:

$$K_1 = \frac{f_I}{f_N} \quad \text{(Eq. 31)}$$

$$K_2 = \frac{f_U}{f_I} \quad \text{(Eq. 32)}$$

From equations 27-29, 30, and 31-32 equation 33 can be generated:

$$f_U + \frac{f_U}{K_2} + \frac{f_U}{K_1 K_2} = 1 \quad \text{(Eq. 33)}$$

By solving equation 33, the fraction of each species is obtained as shown in equations 34-36:

$$f_U = \frac{K_1 K_2}{1 + K_1 + K_1 K_2} \quad \text{(Eq. 34)}$$

$$f_I = \frac{f_U}{K_2} \quad \text{(Eq. 35)}$$

$$f_N = \frac{f_U}{K_1 K_2} \quad \text{(Eq. 36)}$$

From equations 34-36 and equation 20, one may calculate the equilibrium constants and the ΔG at each urea concentration. The free energy for each transition is:

$$\Delta G_1 = \Delta G_1^{H_2O} - m_1 [\text{denaturant}] \qquad \text{(Eq. 37)}$$

$$\Delta G_2 = \Delta G_2^{H_2O} - m_2 [\text{denaturant}] \qquad \text{(Eq. 38)}$$

where $\Delta G_1^{H_2O}$ and $\Delta G_2^{H_2O}$ are the free energy changes in the absence of denaturant corresponding to K_1 and K_2, respectively, m_1 and m_2 are the cooperativity indices associated with each step. The amplitude of the spectroscopic signal determined at each urea concentration is shown by equation 39,

$$Y = Y_N f_N + Y_I f_I + Y_U f_U \qquad \text{(Eq.39)}$$

where, Y_N , Y_I, and Y_U are the amplitudes of the signals for the respective species.

Finally, the amplitudes associated with the native and unfolded forms of the protein are given by equations 21-22

$$Y_N = Y_{N'} + m_3 [\text{urea}] \qquad \text{(Eq. 40)}$$

$$Y_I = Y_{I'} + m_4 [\text{urea}] \qquad \text{(Eq. 41)}$$

$$Y_U = Y_{U'} + m_5 [\text{urea}] \qquad \text{(Eq. 42)}$$

where $Y_{N'}$, $Y_{I'}$ $Y_{U'}$ are the amplitudes of the signals in the absence of urea for the native and the unfolded species. Figure 7B shows the procedure file for the three-state equation used for data fitting by the software Igor Pro.

A.

```
Wave w

        Variable x

        Variable K=EXP(-((w[0]+w[1]*x)/(0.001987*298)))
        Variable Fu=K/(1+K)
        Variable Fn=1-Fu
        Variable Yn=w[2]+w[3]*x
        Variable Yu=w[4]+w[5]. *x
        Variable Y=Yn*Fn+Yu*Fu

        Return Y

End
```

Figure 7. *Panel A*. Procedure file for two-state monomer model of procaspase-3(C163S,V266H). w[2] is $Y_{N'}$, w[3] is m_2, w[4] is $Y_{U'}$, w[5] is m_3. The other parameters have been defined earlier.

B.

```
Wave w

        Variable x

        Variable K1=EXP(-((w[0]+w[1]*x)/(0.001987*298)))
        Variable K2=EXP(-((w[2]+w[3]*x)/(0.001987*298)))
        Variable Fn=1/(1+K1+K1*K2)
        Variable Fi= K1/(1+K1+K1*K2)
        Variable Fu= K2*K1/(1+K1+K1*K2)
        Variable Yn=w[4]+w[5]*x
        Variable Yu=w[6]+w[7]*x
        Variable Yi=w[8]+w[9]*x
        Variable Y=Yn*Fn+Yu*Fu+Yi*Fi

        Return Y

End
```

Figure 7. *Panel B*. Procedure file for three-state monomer model of procaspase-3(C163S,V266H). w[4] is $Y_{N'}$, w[5] is m_3, w[6] is $Y_{U'}$, w[7] is m_4, w[8] is $Y_{I'}$, w[9] is m_5. The other parameters have been defined earlier.

RESULTS

I. Oligomeric properties of procaspase-3 and role of the pro-domain

The oligomeric properties of the effector procaspases have not been addressed for a long period of time. Usually, the effector procaspases were drawn in the literature as monomers. The dimerization mechanism of the initiator procaspases involves protein-protein interaction mediated by the long pro-domain. However, the driving force for formation of the effector caspase heterotetramers was not known. Moreover, no role in the activation or stability of caspases could be attributed to the short pro-domain from the effector pro-caspases or to the ~30 residue linker from the initiator procaspases, following the CARD/DED domain (see Figure 2). Here, the oligomerization properties of the recombinant procaspase-3, as well as the role of the pro-domain in procapase-3 oligomerization and activity are being examined using analytical ultracentrifugation, size exclusion chromatography, cross-linking, circular dichroism, fluorescence anisotropy and activity measurements.

Recombinant procaspase-3 mutants

Procaspase-3 consists of 277 amino acids, with a M_r of 31,606. Under normal conditions in human cells the protein is not able to autoprocess; however, the recombinant full-length protein or pro-less procaspase-3 can autoprocess to caspase-3 during over-expression in bacterial cells (26, 87). In order to prevent the autocleavage of procaspase-3 during *in vitro* experiments, the active site cysteinyl residue has been mutated to serine. Mutations of C163 have been shown to

abrogate activity, but are not structurally perturbing (31, 88, 89). A histidine tag preceded by two additional residues (LEH_6) was added to the C-terminus to facilitate the purification. The recombinant histidine-tagged procaspase-3(C163S) has a M_r of 32,672 Da. In order to examine the structure of the pro-domain within procaspase, a mutant of procaspase-3(C163S) lacking the pro-peptide, called the pro-less variant, was constructed by cloning (M_r=29,658) (see Figure 5B). In this protein, the amino terminus begins with a methionine residue, which is absent from processed protease purified from cells. The amino terminus of protease purified from human cells begins with S29. Both procaspase-3(C163S) and the pro-less variant were analyzed by MALDI-TOF mass spectrometry to confirm the correct mass (data not shown).

Size exclusion chromatography

To examine the oligomeric properties of procaspase-3 and the pro-less variant, we initially examined their elution profiles by using size exclusion chromatography analysis at pH 7.2 (Figure 8). Results from these experiments showed that procaspase-3(C163S) eluted with an apparent molecular weight of 64,773 Da, approximately equal to the mass of a dimer (for the monomer, M_r=32,642). Likewise, the pro-less variant eluted with an apparent molecular weight of 59,101 Da (for the monomer, M_r=29,658). There were no additional peaks corresponding to the monomer molecular weight, suggesting that at the protein concentrations of these experiments (~15 μM) both procaspase-3(C163S) and the pro-less variant are dimers.

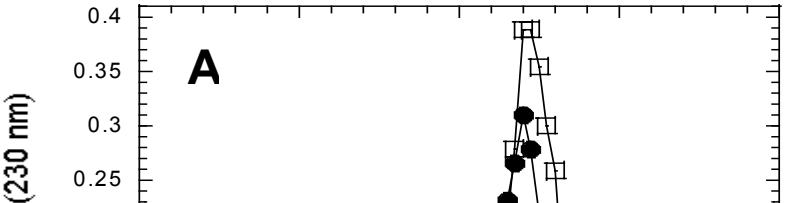

Figure 8. Gel filtration analysis. *Panel A*. Elution profiles from the sizing column of the procaspase-3(C163S) (●) and pro-less variant (□) monitored by absorbance at 230 nm. *Panel B*. Calibration curve of the sizing column (■). The arrows indicate the elution volumes of the procaspase-3(C163S) (12.0 ml) and pro-less variant (12.25 ml).

Chemical cross-linking using dimethyl suberimidate (DMS)

DMS (M_r= 273 Da) is a bi-functional chemical cross-linker that can interact slowly with the amino groups of the N-terminus or lysine residues in the range of pH 7.2-9.0 (78). Due to its short arm spacer (~11 Å), DMS can simultaneously bind two functional groups only if they are in close proximity (i.e., intramolecularly), and the proximity is maintained in time (in oligomers). DMS cannot bind two unassociated proteins, and also does not necessarily cross-link all oligomeric proteins. The absence of the cross-linked complex does not exclude the protein association (78). Procaspase-3 has numerous charged lysines on the surface, and, depending on the amount of the cross-linker that is used, a certain fraction of the protein can be shifted to a covalently bound dimer (26). Figure 9 shows that both procaspase-3(C163S) and pro-less variant are able to form cross-linked dimers in the presence of DMS at pH 7.2, indicating that chemical cross-linking is a good tool to study (pro)caspase-3 association. This assay has higher efficiency at pH 8.5 (not shown), as more lysine residues are charged at this pH. The molecular weights determined from the SDS-PAGE are ~67 kDa for the pro-less variant, and ~70 kDa for the procaspase-3(C163S), slightly higher than in the gel filtration assay. This is probably due to the DMS contribution to the M_r of the dimer.

Sedimentation equilibrium experiments

One of the most precise ways to determine the M_r of a protein is the analytical ultra-centrifugation method (82). The distance migrated by a protein in solution at

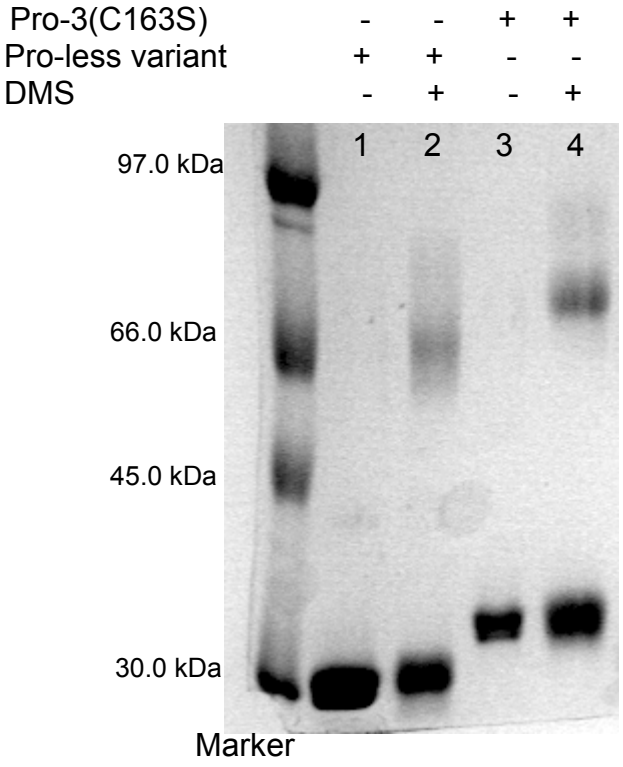

Figure 9. Cross-linking of procaspase-3(C163S) and the pro-less variant with DMS at pH 7.2. Lane 1, pro-less variant; lane 2, pro-less variant in presence of DMS, lane 3, procaspase-3(C163S), lane 4, procaspase-3(C163S) in presence of DMS.

equilibrium under the influence of low centrifugal force is directly correlated with the shape and the molecular weight of the protein, among other parameters (82).

We subjected both procaspase-3(C163S) and pro-less variant to sedimentation equilibrium studies at pH 7.2 and 25 ^{o}C. The proteins were examined over a wide range of protein concentration (0.45 μM to 20 μM) and at several rotor speeds (14,000, 18,000, and 24,000 rpm). In all experiments, the samples were allowed to equilibrate before the speed was adjusted. In addition, we monitored absorbance at 230 nm and 280 nm, as described in Methods. Representative data are shown in Figure 10.

For both proteins, the data were best fit to a single, thermodynamically ideal species that corresponds to a dimer. For procaspase-3(C163S), the average molecular weight determined from the fits of all data sets was 65,573 Da. For the pro-less variant, the average molecular weight determined from the fits of all data sets was 58,342 Da. The residuals to the fits for procaspase-3(C163S) (Figure 10, Panel A) and the pro-less variant (Figure 10, Panel C) demonstrate that the data are well fit to the model.

In Figure 10, we compare the experimental results to those expected if the proteins were a monomer or a tetramer. It is clear from this analysis that both proteins are dimers in solution, and this was true over the entire range of protein concentrations investigated. That is, there was no evidence for formation of a monomeric species, even at the lowest protein concentration (~450 nM) of the experiment. An accurate determination of the equilibrium dissociation constant is not possible under these conditions because we were unable to populate the

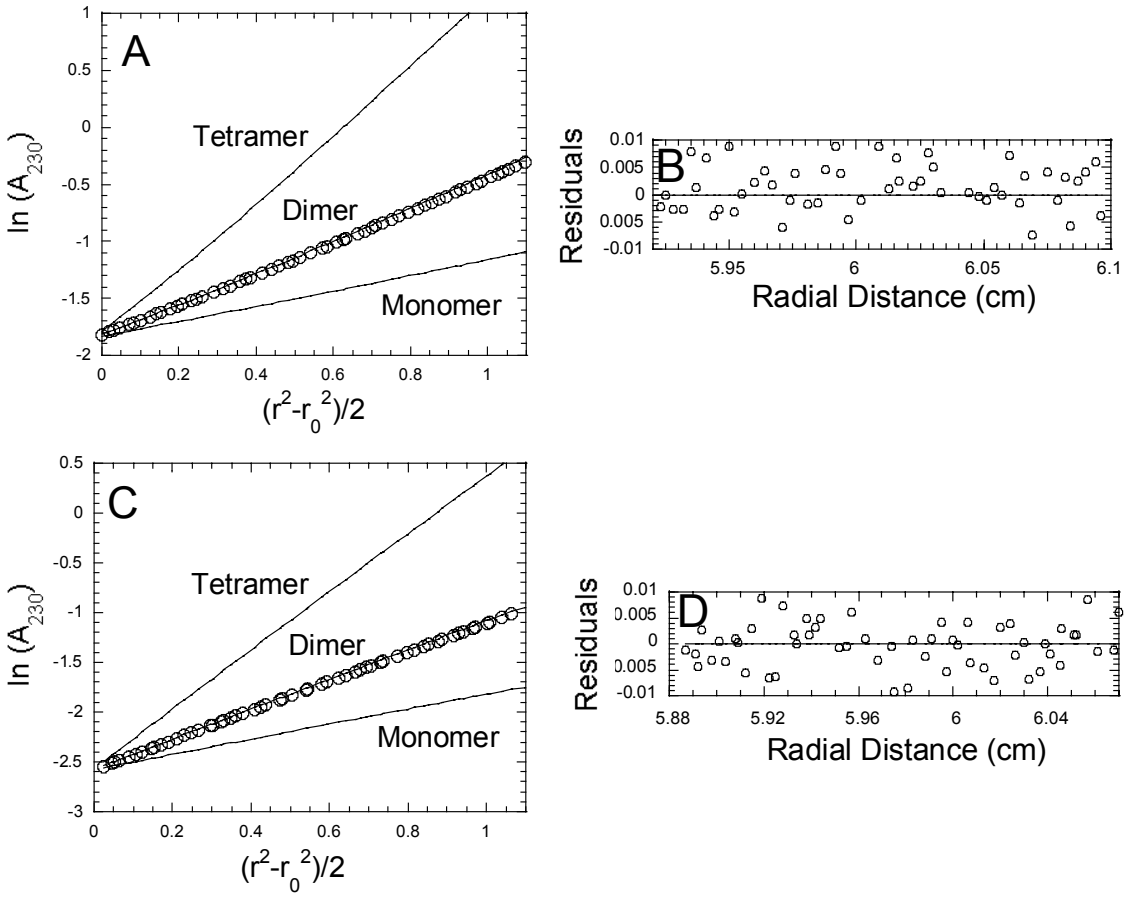

Figure 10. Analytical ultracentrifugation of procaspase-3(C163S) and pro-less variant(C163S). Proteins (0.45-19.8 μM) were dialyzed against 50 mM KH_2PO_4/K_2HPO_4, pH 7.2, containing either 1 mM or 0.05 mM DTT. The spectra were recorded at 230 nm or 280 nm at 25 ^oC, using three rotor speeds (14,000, 18,000, and 24,000 rpm). The solid lines are the theoretical plots if the proteins were monomers, dimers, or tetramers, as indicated. The circles represent the experimental data for procaspase-3(C163S) (Panel A) and pro-less variant (Panel C). Residuals to the fits are shown in Panels B and D.

monomeric species at the lowest protein concentration, which was at the detection limit of the instrument when absorbance at 230 nm was monitored.

However, if we assume a simple model for dissociation of a dimer to two monomers, and given the fact that the proteins are dimers at protein concentrations of 450 nM, we can estimate the upper limit for the equilibrium dissociation constant of the dimer to the monomer to be 50 nM, although it may be much lower.

Circular dichroism (CD) experiments

We compared the secondary and tertiary structures of procaspase-3(C163S) and the pro-less variant by monitoring near- and far-UV circular dichroism, and the data are shown in Figure 11. In the far-UV, procaspase-3(C163S) demonstrates two minima (208 nm and 215 nm) (Figure 11A, spectrum 1), although the amplitudes of the minima are very similar. While it is not possible to deconvolute these data into their component secondary structural elements due to the limitations of our instrument, the data are consistent with a protein that contains both α-helix and β-sheet elements, with the α-helical structures contributing to the minimum at 208 nm. The far-UV CD spectrum for the pro-less variant (Figure 11A, spectrum 2) is similar to that of procaspase-3 except that the minimum at 208 nm is less pronounced. In addition, there is a decrease in amplitude of approximately 10% between the pro-less variant and procaspase-3(C163S), consistent with the loss of about 10% of the total number of amino acids in the pro-less variant (28 amino acids from 285 amino acids). The spectra are superimposable when the data (spectra 1

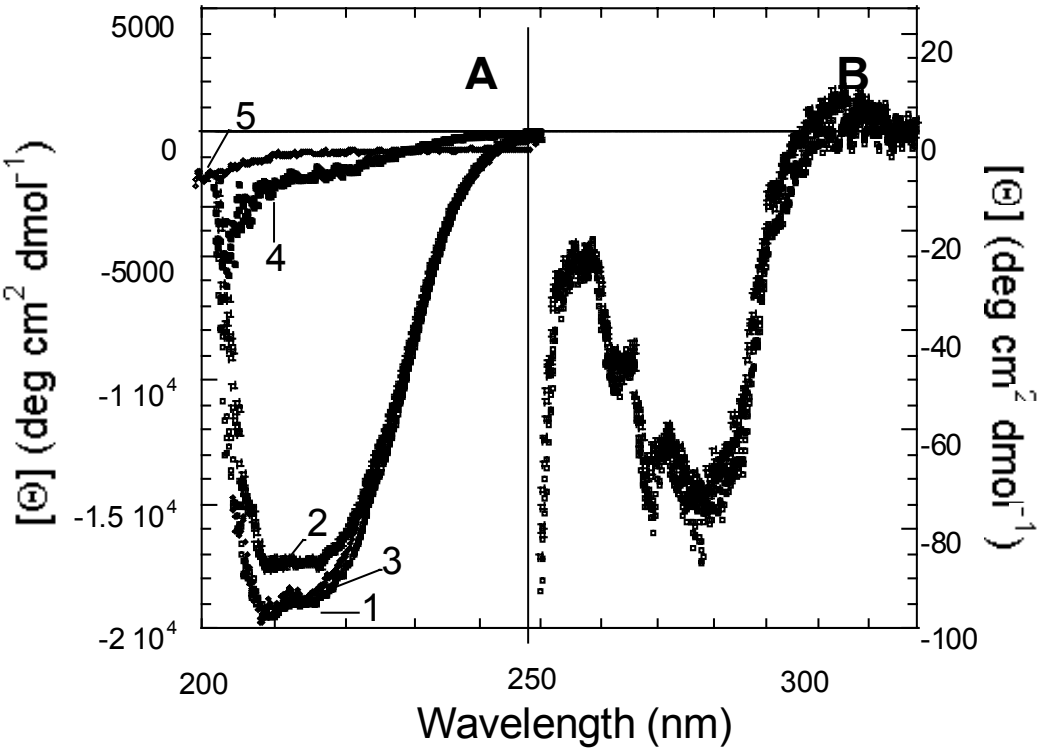

Figure 11. Circular dichroism spectra of procaspase-3(C163S), pro-less variant, and pro-peptide. *Panel A*. Far-UV circular dichroism spectra: (1) procaspase-3(C163S); (2) pro-less variant; (3) pro-less variant with pro-peptide in *trans*; (4) procaspase-3(C163S) minus pro-less variant (spectrum 1 minus spectrum 2); (5) pro-peptide, and *Panel B*. Near-UV circular dichroism spectra, (○) procaspase-3(C163S); (□) pro-less variant.

and 2 in Figure 11A) are normalized by the total number of amino acids in each protein, that is, the mean residue ellipticity (data not shown). This suggested that the secondary structure of the procaspase-3(C163S) dimer was unaffected by the loss of the pro-domain.

The near-UV CD spectra (Figure 11B) for procaspase-3 and the pro-less variant are superimposable. The data demonstrate minima at 280 nm and 270 nm as well as a maximum at 255 nm, indicative of well-packed tertiary structures. The structural changes may be localized to the environment of the two tryptophan residues in the pro-less variant.

A comparison of the far-UV CD spectra (Figure 11A) for procaspase-3(C163S) and the pro-less variant suggested that the pro-domain may contain secondary structural elements that contribute to the spectrum of the full-length protein. We have subtracted the two spectra (Figure 11A, spectra 1 and 2), and the results are shown in Figure 11A (spectrum 4). Because the mean residue ellipticity spectra are superimposable for the two proteins (data not shown), conformational changes, if any, in the protein as a result of removal of the pro-domain do not affect the far-UV spectral properties. Therefore, we suggest that spectrum 4 in Figure 11A represents the pro-domain of procaspase-3. We have examined the pro-domain (28 amino acids) under the same solution conditions as those described for procaspase-3 (Figure 11) in order to compare the far-UV CD properties of the pro-domain with those of the subtracted spectra. The far-UV CD spectrum for the pro-domain in solution is shown as spectrum 5 in Figure 11A. In the absence of the protease domain, the pro-peptide appears to contain primarily random structure. We also

examined the CD spectra at several concentrations of pro-peptide (10 μM to 100 μM) and found no change in the CD spectra with an increase in protein concentration (data not shown). These results demonstrate that the pro-domain does not self-associate under the conditions of these experiments.

Fluorescence anisotropy experiments

All the described experiments clearly indicate that the short pro-domain of procaspase-3 is not directly involved in the dimerization, as the pro-less variant can still make stable dimers. Work in our lab has shown that the secondary and tertiary structure of the procaspase-3 changes insignificantly following the pro-domain removal. This was proved by the emission fluorescence (68) and the circular dichroism spectra of the procaspase-3(C163S) and pro-less variant as shown above. However, the structure of the pro-domain in solution (random coil) becomes β-like structure when the pro-domain is bound to the procaspase-3, as shown by our lab using circular dichroism and other labs using FTIR experiments (68). In addition, the pro-domain is neither a good substrate nor a good inhibitor of caspase-3 (68).

To show that the pro-domain actually interacts with procaspase-3, we performed fluorescence anisotropy experiments. The wild-type and mutated pro-domain(D9A) was labeled with the fluorescent compound dansyl chloride, and was incubated with the pro-less variant (Figure 12). The fluorescence anisotropy was measured for different ratios of pro-peptide: procaspase-3 mixtures as shown in Figure 12. The results indicate that indeed the pro-domain can bind to the pro-less

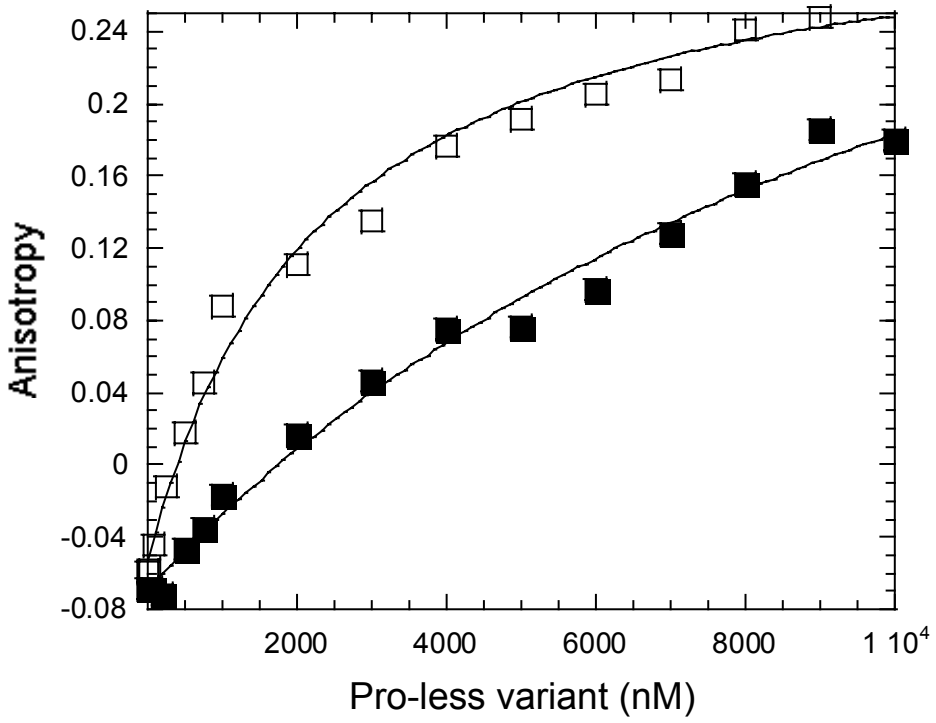

Figure 12. Fluorescence anisotropy of pro-peptide in the presence of pro-less variant. The dansyl-labeled wild-type pro-peptide (□) or the dansyl-labeled D9A mutant pro-peptide (■) (1 μM) was titrated with the pro-less variant. All assays were carried out at 25 ^{o}C in a buffer of 50 mM potassium phosphate, pH 7.5, 1 mM DTT. The solid lines represent fits of the data to a simple binding model described by equation (3), as described in *Methods*.

variant, and that the binding is more efficient with the wild-type pro-peptide than with the mutated peptide. The estimated dissociation constants for the interaction of the pro-peptide with pro-less variant are K_d~ 2.3 μM in the case of the wild-type pro-domain, and K_d~ 12 μM in the case of the mutated pro-domain.

Procaspase-3 activity in absence of the pro-domain

The best assignment for the pro-domain function is the pro-domain contribution to the folding of procaspase-3, as demonstrated by our lab (65). Although pro-less procaspase-3(C163S) is produced by *E. coli* as a dimer, the resulting protein is not able to recover the native fluorescence properties following refolding from 8 M urea. However, upon addition of the wild-type pro-domain *in trans* to the pro-less variant (two fold molar excess), the protein is able to refold correctly (65). This suggests that procaspase-3 lacking the pro-domain may be incorrectly packed during expression in bacterial cells. This change may be reflected by the enzymatic properties of the pro-less variant.

To test this hypothesis, we measured the activity of the procaspase-3 lacking the pro-domain and harboring the mutation D175A (referred to pro-less variant(D175A)). This mutant has an intact active site and cannot be cleaved by caspases due to D175A mutation. We compared the activity of the mutant with the activity of the full-length procaspase-3 mutated at all three cleavage aspartates, D9A, D28A, and D175A, in order to prevent the autoproteolysis during expression. The uncleavable procaspase-3 mutant is referred in text to procaspase-3(D_3A).

The Michelis-Menten plots showing the initial velocity versus substrate concentration for these two constructs are presented in Figure 13A. In the case of procaspase-3(D_3A) (open squares), the Michelis-Menten curve displays one step binding event for the interaction with the substrate, characteristic to the presence of two equivalent active sites in the protein (Figure 13A). The Michelis-Menten constant generated by the fit (equation 4) is K_M= 4.8±0.6 μM, and the catalytic constant is k_{cat}= 0.0021(±3.4x10^{-5})/s. In contrast with the D_3A mutant, pro-less variant(D175A) (solid squares) displays a two-step binding event for the interaction with the substrate (Figure 13A). The curve does not show saturation of the substrate binding even at concentrations > 50 μM, suggesting that the K_M is dramatically higher in this case. We suggest that the two active sites of the pro-less variant are not equivalent in the substrate binding. The estimated catalytic constant for this mutant is ~0.0018/s, close to the k_{cat} of the D_3A mutant. This implies that removal of the pro-domain from procaspase-3 structure affects mostly the enzyme affinity for the substrate, and not the catalytic turn-over.

To determine whether the presence of the pro-domain can recover the activity of the pro-less variant, we measured the initial velocity of this mutant in solutions containing the pro-peptide added *in trans* to the enzyme. The experiment was performed in assay buffer (Table I), at various concentrations of pro-peptide as shown in Figure 13B. The final concentration of the enzyme was 50 nM. As one can notice, the pro-peptide did not rescue the low activity of procaspase-3 lacking the pro-domain, even at high pro-peptide concentrations (Figure 13B). The assay buffer includes 150 mM NaCl and 0.1% CHAPS (Table I). To eliminate the

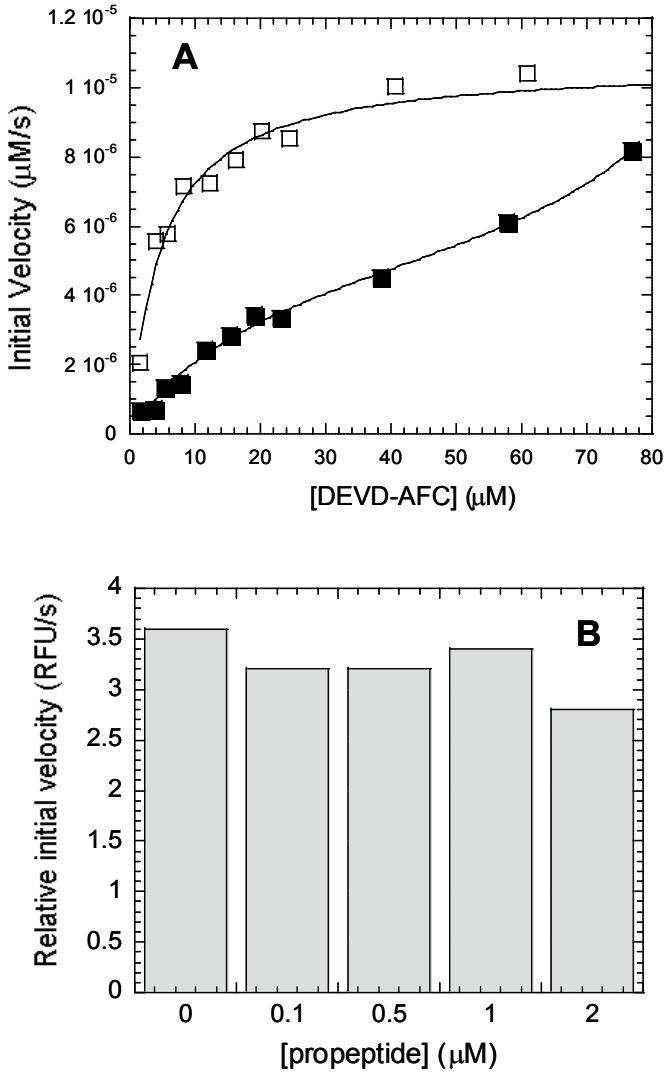

Figure 13. Pro-domain influence upon the activity of procaspase-3. *Panel A*. Michelis-Menten plots were generated for procaspase-3(D_3A) (□) and pro-less procaspase(D175A) (■) by measuring the enzyme activity in presence of various concentrations of Ac-DEVD-AFC substrate. *Panel B*. The initial velocity of pro-less procaspase(D175A) (50 nM) was measured in presence of the pro-domain added in *trans* at specified concentrations.

eventual effect NaCl and CHAPS might have upon the protein-pro-peptide interaction, the same activity assays were carried out in phosphate buffer (Table I) in the presence of 10 mM DTT. Even under these conditions, the pro-domain added *in trans* of the pro-less variant(D175A) failed to improve the enzymatic activity (data not shown).

In conclusion, although the pro-peptide of procaspase-3 is not directly involved in protein association, its presence as an intrinsic part of the protein is required to allow procaspase folding into a proper packed structure, with full catalytic activity.

II. Dimer interface substitutions in (pro)caspase-3

It has been recently shown that other effector procaspases are dimers *in vitro*, like in the case of procaspase-6 and -7 (27, 30, 90). In contrast with the initiators, the dimerization is required but not sufficient for activation of the effectors (20). The limiting factor for activation in this case is the inter-subunit cleavage.

The recent crystal structures of procaspase-7 and caspase-7 demonstrate that little differences exist in the general organization of the zymogen and the mature caspase (27, 30). The major changes concern the catalytic loops (see Figure 6A). Subsequent to maturation, the dimer interface remains unaffected. Several mutagenesis studies using initiator caspase-1, -8, and -9 have shown that some substitutions of the interface residues dramatically affect the procaspase ability to dimerize and activate (36). These experiments have not been carried out yet with the effector caspases.

Here we characterize the effect of interface V266 substitution with hydrophilic residues upon the activity and stability of (pro)caspase-3.

Designing dimer interface mutants

V266 from the dimer interface (see Figure 6A) has been substituted with two hydrophilic residues, histidine or glutamate, in the context of both caspase-3 and procaspase-3 (Figure 14). In the case of procaspase-3, two types of mutants were designed: 1) Inactive mutants that have the catalytic cysteine replaced with a serine (C163S), so that the auto-processing is prevented during expression (Figure 14A);

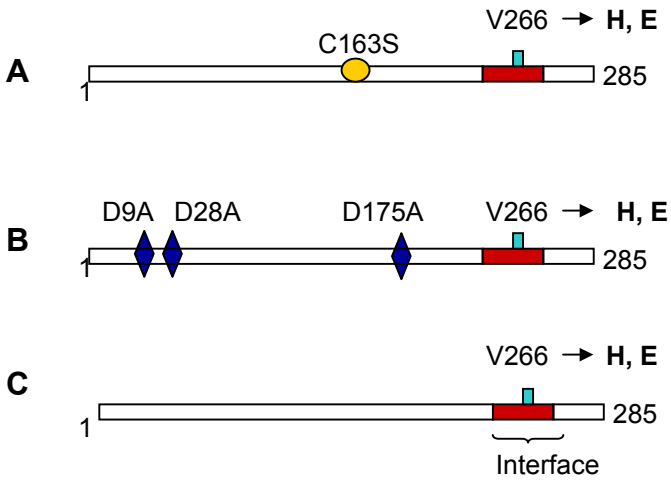

D Designed mutants:

H mutants: Pro-3(C163S,V266H), Pro-3(D_3A,V266H), Casp-3(V266H)

E mutants: Pro-3(C163S,V266E), Pro-3(D_3A,V266E), Casp-3(V266E)

Figure 14. Designing dimer interface mutants. The dimer interface mutants were designed in the context of inactive procaspase-3 (A), uncleavable procaspase-3 (B), and wild-type procaspase-3 (C). The last one generates caspase-3 by autocleavage during expression in *E. coli*. In panel D, all designed mutants are shown

2) Active mutant that have the cleavage aspartates replaced with alanine (D9A, D28A, D175A, called D_3A), so that they are unable to undergo maturation (Figure 14B). In the case of caspase-3, the interface mutants were designed in the context of wild-type procaspase, which undergoes maturation to caspase-3 during the expression in bacterial cells (Figure 14C). All mutants (Figure 14D) contain the histidine tag at the C-terminus to facilitate purification.

Oligomeric properties of the interface mutants

We have used sedimentation equilibrium studies to test whether the hydrophilic interface mutations have affected the oligomeric properties of (pro)caspase-3.

Figure 15 shows the analytical ultracentrifugation results for procaspase-3(C163S,V266E) (Panel A), caspase-3(V266E) (Panel B), and procaspase-3(C163S,V266H) (Panel C). The experimental molecular masses given by the global fit for these proteins are listed in Table II and are compared with the calculated molecular masses of the mutants. For caspase-3(V266E) the analysis has also been done in the presence of the covalently bound inhibitor, VAD-FMK. Activity measurements before and after incubation showed a complete loss of enzymatic activity, demonstrating that the inhibitor was bound (data not shown). As it can be seen in Table II, the ratio between the theoretical and experimental values is in all cases ~1/2, which shows that the proteins are stable dimers under these conditions. Even for the lowest concentrations used in the experiment (low micromolar range)

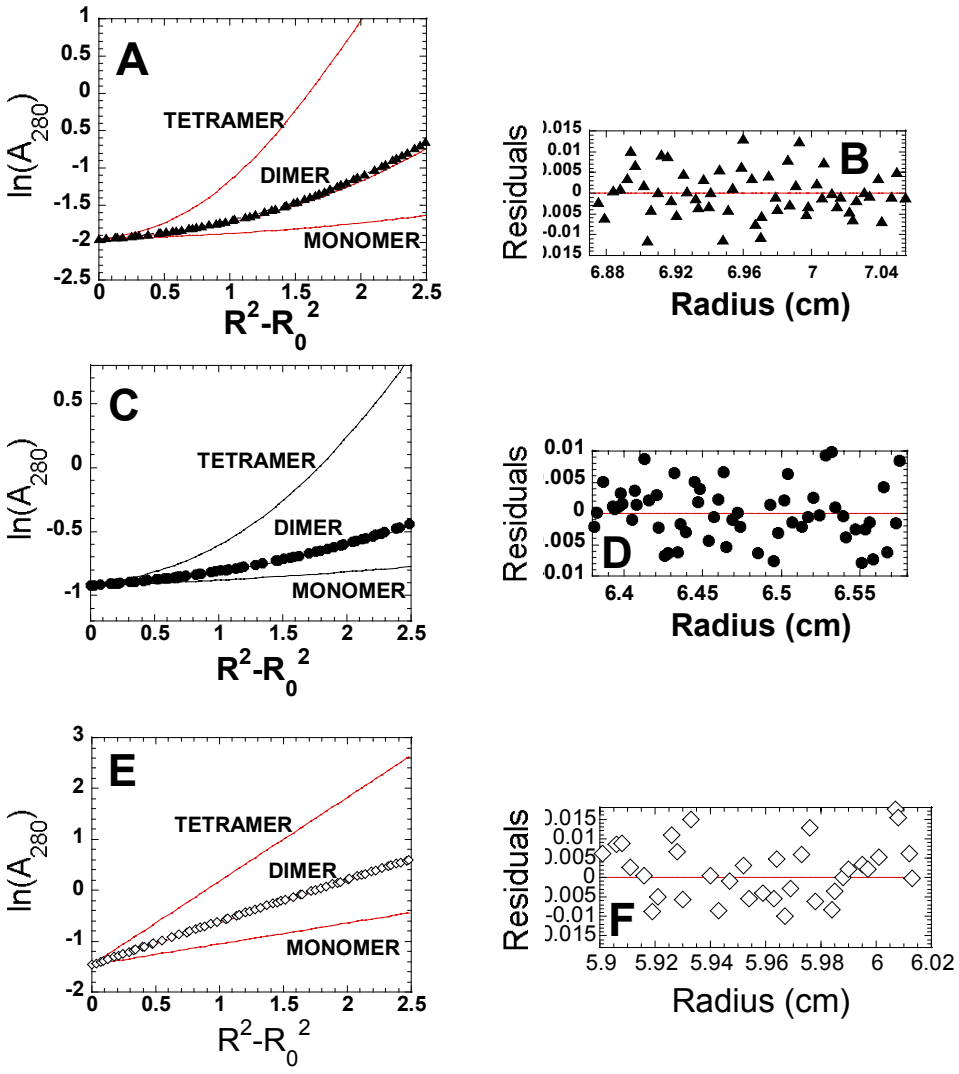

Figure 15. Sedimentation equilibrium analysis of the interface mutants: *Panel A*. Procaspase-3(C163S,V266E) (▲); *Panel B.* Residuals; *Panel* C. Caspase-3(V266E); (●); *Panel* D. Residuals; *Panel* E. Procaspase-3(C163S,V266H) (◇); *Panel F*. Residuals.

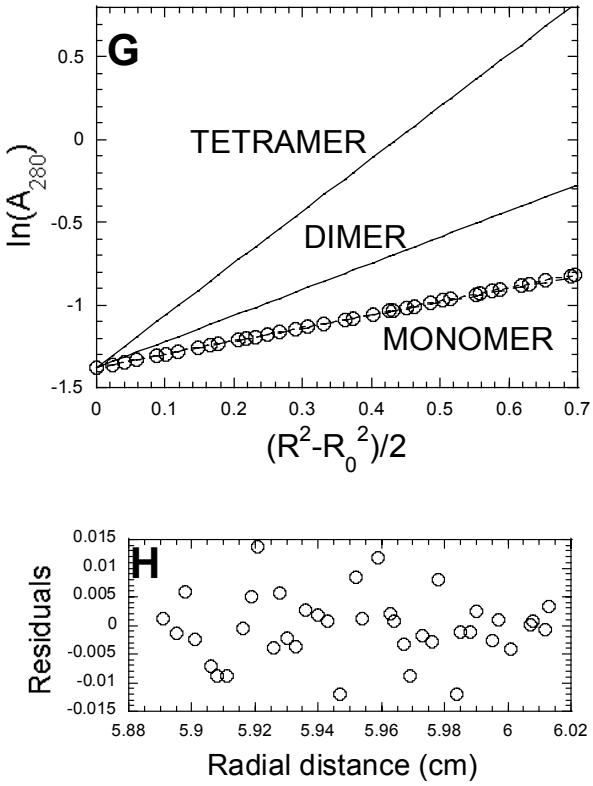

Figure 15. *Panel* G. Sedimentation equilibrium analysis of procaspase-3(C163S,V266E) purified from the insoluble fraction of *E. coli* (○); *Panel H.* Residuals.

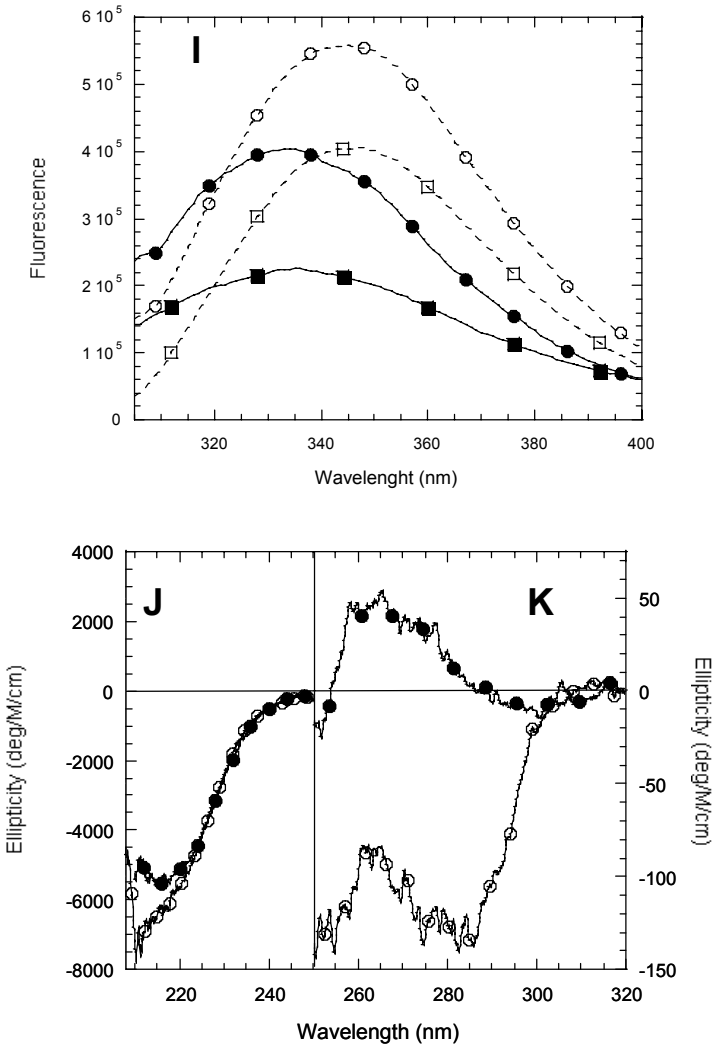

Figure 15. *Panel I*. Fluorescence emission spectra of procaspase-3(C163S,V266E) purified from soluble fraction (open symbols) and insoluble fraction (dark symbols), after excitation at 280 nm (circles) or 295 nm (squares). *Panels J and K*. Far-UV, respectively Near-UV, circular dichroism spectra for the same protein isolated from the soluble (○) or insoluble fraction (●).

Table II. Calculated and experimental molecular masses for (pro)caspase-3 interface mutants

	Calc M_r (Da)	Exp M_r (Da)
Procaspase-3(C163S,V266E) (Soluble fraction)	32,685	65, 667
Procaspase-3(C163S,V266E) (Insoluble fraction)	32,685	33,016
Procaspase-3(C163S,V266H)	32,694	67,350
Caspase-3(V266E)	29,688	63,308
Caspase-3(V266E) + Z-VAD-FMK	30,123	63,690

the fits for all proteins generated molecular masses that were twice the calculated values of the monomers (not shown).

The mutants described above have been isolated from the soluble fraction of the *E. coli* cells following induction of the protein expression (see Methods). In the case of procaspase-3(C163S,V266E), the protein was also isolated from the insoluble part of *E. coli* cells, grown at 30 ^{o}C (see Methods). The inclusion bodies were resuspended in urea and the purified protein was refolded in buffer by rapid dilution. The oligomeric properties of the mutant were investigated by analytical ultracentrifugation as described above, and the results are shown in Figure 15G. Interestingly, in contrast with the soluble procaspase-3(C163S,V266E) that is a dimer (Figure 15A), the studies show that insoluble procaspase-3(C163S,V266E) is a monomer under the same conditions (see Methods) (Figure 15G). The calculated M_r for the latter is 32,685 Da, while the global fit of the experiments gives a M_r of 33,016 Da (Table II). This result has been confirmed by gel filtration analysis done in our lab (not shown). Under the conditions used for protein expression (see Methods), about one fourth of the protein is a soluble dimer, while the rest is distributed in the inclusion bodies, as monomer, as judged from the SDS-gels (not shown). The amino acid sequencing analysis established that the N-terminus of these variants (see Figure 5) starts with the same residue sequence (“MENTE”) (data not shown), confirming that the same protein is being produced in both cases.

However, the insoluble monomer displays several features that are different from the dimer, like migration in the SDS-PAGE gels, binding the anion exchange resin, and circular dichroism and fluorescence spectra. In the case of spectral

properties, the results are shown in Figure 15, Panels I-K. The insoluble mutant presents a fluorescence emission spectrum that is remarkably more blue-shifted in comparison with the soluble mutant (Figure 15I). The emission maximum after excitation at 280 nm is 334 nm for the insoluble protein versus 344 nm for the soluble mutant. At excitation wavelength of 295 nm, the maxima are 335 nm for the monomer and 348 nm for the dimer. This suggests that the tryptophanyl residues are more solvent exposed in the soluble version of this protein and also that the we deal with proteins that have different tertiary structures.

This hypothesis was confirmed by circular dichroism (CD) studies. Far-UV CD experiments show that the secondary structure of the two V266E mutant versions is similar (Figure 15J), although the insoluble mutant displays less signal. However, the near-UV CD spectrum of the monomer is completely different than the spectrum of the soluble protein by the presence of a positive signal over the 255-285 nm range (Figure 15K). This confirms the results of the fluorescence emission studies regarding the fact that the tertiary structure is much different in the case of insoluble protein (Figure 15I).

Therefore, bacteria may have two alternatives for folding procaspase-3(C163S,V266E).

For consistency in our results, we have used in the following studies only soluble procaspase-3(C163S,V266E), considering that all the other mutants have been purified from the soluble fraction.

The oligomeric properties of the interface mutants were also studied by cross-linking experiments at pH 7.5 using either dimethyl suberimidate or

glutaraldehyde (data not shown). With no exception, the interface mutants of procaspase-3(D_3A), procaspase-3(C163S), and caspase-3 displayed gel shift bands in SDS-PAGE corresponding to the dimer form of procaspase-3.

In conclusion, introducing single hydrophilic mutations in the hydrophobic interface of (pro)caspase-3 may disrupt the oligomerization state of procaspase-3 (in the case of the insoluble V266E mutant), although a certain fraction of the produced V266E protein is able to undergo association into dimers. The histidine mutant is produced in the soluble fraction as a stable dimer. Interestingly, depending of the temperature used for expression, the V266E mutant can be synthesized either in the inclusion bodies (30-37 ^{o}C) or accumulated in the soluble fraction (18-25 ^{o}C). It remains to be investigated whether the temperature has any effect upon the folding of the glutamate mutant.

Catalytic properties of the interface mutants

We have studied the enzymatic properties of the interface mutants by monitoring the formation of the fluorogenic AFC moiety (a coumarin derivative) following the cleavage of the caspase-3 specific substrate, Ac-DEVD-AFC. For these assays we have used the uncleavable version of the procaspase mutants.

For the V266E mutant, the Michelis-Menten plots are shown in Figure 16A. The steady-state parameters, K_m (Michelis-Menten constant) and k_{cat} (turn-over number), were calculated and compared with the values for caspase-3 (wild type) and procaspase-3(D_3A) (Table III).

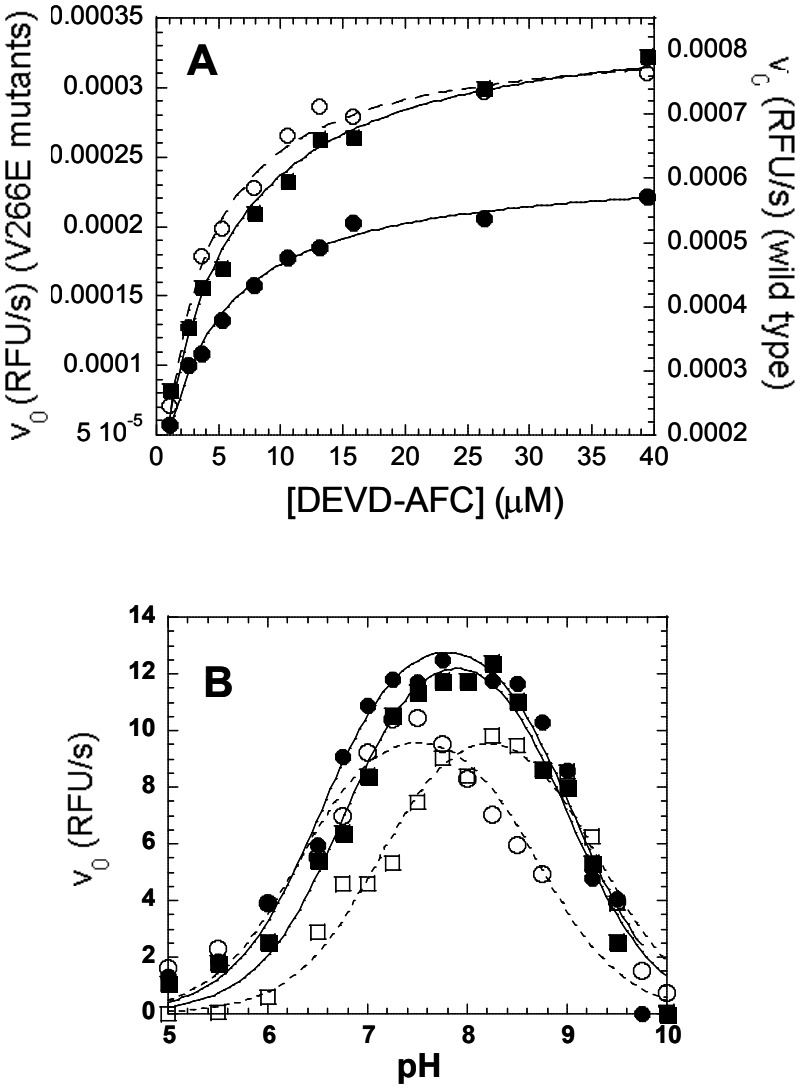

Figure 16. Catalytic parameters for the interface mutants: *Panel A*. Michelis-Menten analysis for procaspase-3(D_3A, V266E) (■) and caspase-3(V266E) (●) in comparison with the wild-type caspase-3 (○); *Panel B*. Effect of pH on the initial velocity (v_0) for procaspase-3(D_3A,V266E) (■), caspase-3(V266E) (●), procaspase-3 (□) and wild-type caspase-3 (○).

C

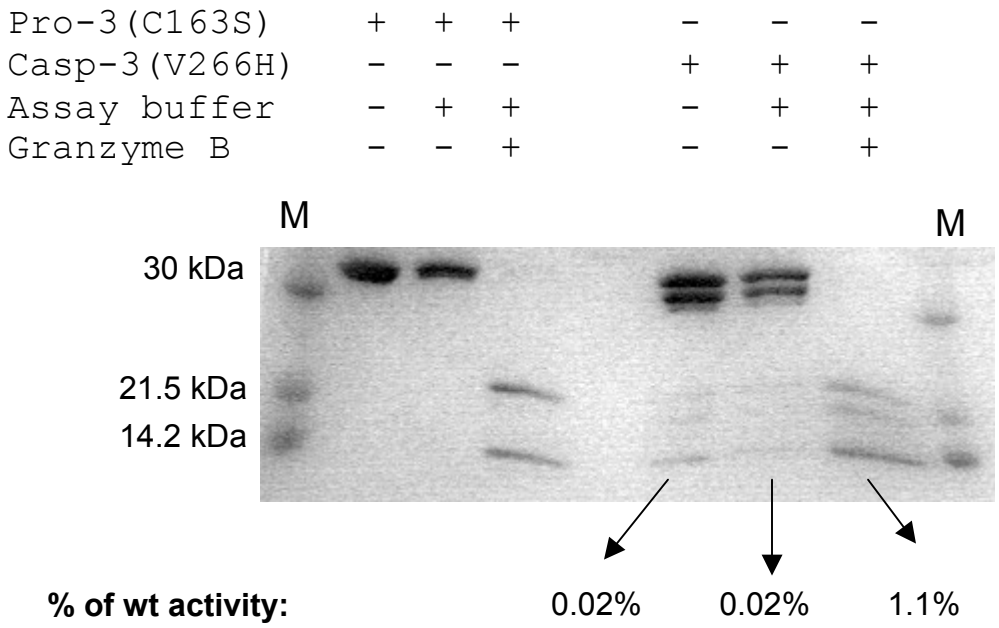

Figure 16. *Panel C.* Activation of the V266H mutant. Caspase-3(V266H) can only be activated by Granzyme B and not by autocleavage. Caspase-3(V266H) and procaspase-3(C163S) (control) were digested with Granzyme B and the activity of the resulting caspase was measured and compared with the wild-type activity.

Interestingly, while the values of K_m are similar (between ~2 and ~6 μM), the catalytic efficiency (k_{cat}) is about sixty-fold higher for procaspase-3(D_3A,V266E) compared to procaspase-3(D_3A) (Figure 16A). This results in a pseudo-activation of the procaspase because the activity is only about 2-fold lower than that of the mature caspase-3, without the corresponding cleavage of the polypeptide chain. Interestingly, there was no further increase in k_{cat} for caspase-3(V266E), following the intersubunit cleavage (Table III). Overall, the specificity constant (k_{cat}/K_M) is ~5 fold lower in V266E caspase that in the wild-type.

We have also studied the influence of pH on the initial velocity of the V266E mutants and the data were compared with caspase-3 and D_3A (Figure 16B, and Table III). Like mature caspase-3, procaspase-3(D_3A) displays a bell-shaped profile when activity is measured versus pH (74). This is consistent with the protonation and/or deprotonation of the two catalytic groups, H121 and C163, leading to one active form of the enzyme (74). For both V266E mutants, compared to procaspase-3(D_3A) (Table III), pK_{a1} decreased by at least 0.5 pH units, so that it was similar to that of the wild-type caspase-3. However, pK_{a2}, presumably the deprotonation of H121 (91) remained similar to that of the procaspase-3. These properties result in broad optimal pH ranges for both precursor and mature caspase-3(V266E) (Table III). Overall, the data suggest that the V266E mutation increases the activity of the procaspase because it affects the environment of C163. In addition, the environment of H121 is similar to that of the procaspase, even in the processed protein.

In contrast to the V266E interface mutants, both caspase-3(V266H) and

Table III. Catalytic properties of the (pro)caspase-3 interface mutants

	Caspase-3 (wt)	Caspase-3 (V266E)	Procaspase-3 (D_3A)	Procaspase-3 (D_3A,V266E)
K_M (μM)	2.2±0.5	4.7±0.3	3.5±0.8	5.6±0.4
k_{cat} (s^{-1})	0.4±0.05	0.14±0.005	(3±0.14)x10^{-3}	0.2±0.01
k_{cat}/K_M ($M^{-1}s^{-1}$)	1.8x10^5	3.0x10^4	8.6x10^2	3.7x10^4
pK_{a1}	6.3±0.14	6.4±0.08	7.3±0.10	6.7±0.09
pK_{a2}	8.5±0.14	9.0±0.07	9.1±0.11	8.9±0.08
Optimal pH	7.2-7.8	7.2-8.4	8.0-8.5	7.4-8.4

procaspase-3(D_3A,V266H) displays very little residual activity. During purification, the procaspase-3(V266H) remained mostly unprocessed; the initial velocity of this mutant is <0.1% of the initial velocity of wild-type (Figure 16C), and we attribute this residual activity to the cleaved caspase-3(V266H) formed during purification (20 kDa and 12 kDa bands). Due to this reason, the mature protein was obtained by processing with granzyme B that cleaves after D175 from the intersubunit linker. The resulting caspase displays an initial velocity of ~1% of the initial velocity of caspase-3, demonstrating that the effect was not limited to the procaspase form of the protein (Figure 14C).

Characterization of V266E and V266H interface mutants

It is possible that the activity observed for procaspase-3(D_3A,V266E) is due to contaminating mature caspase generated at alternative cleavage sites in the intersubunit linker. We show that this is unlikely by performing two control experiments.

First, we show that uncleavable procaspase-3(D_3A) does not constitute a substrate for caspase-3, while procaspase-3(C163S) can be cleaved by the caspase (Figure 17A). The two procaspases were incubated in assay buffer with caspase-3 in a molar ratio of 1:10. While procaspase-3 generated bands 1-7 corresponding to cleavage at D9, D28, D175, procaspase-3(D_3A) did not show any cleavage, even after overnight incubation. Therefore, the activity of the control procaspase does not result from an alternatively cleaved caspase-3.

A

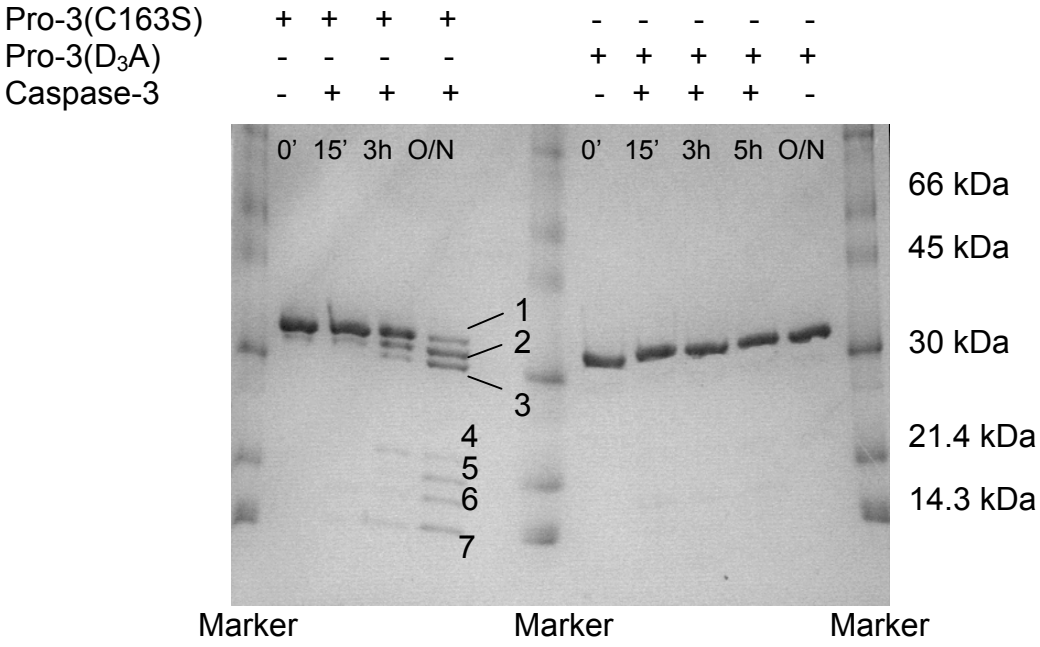

Figure 17. *Panel A*. Digestion of the procaspase-3 with caspase-3. Procaspase-3(C163S) and procaspase-3(D_3A) were digested with mature caspase-3. Bands 1-7 are: 1, full-length protein; 2, procaspase-3 cleaved at D9; 3, pro-less procaspase-3; 4, large subunit plus pro-domain; 5, large subunit plus pro-domain, cleaved at D9; 6, large subunit; 7, small subunit.

B

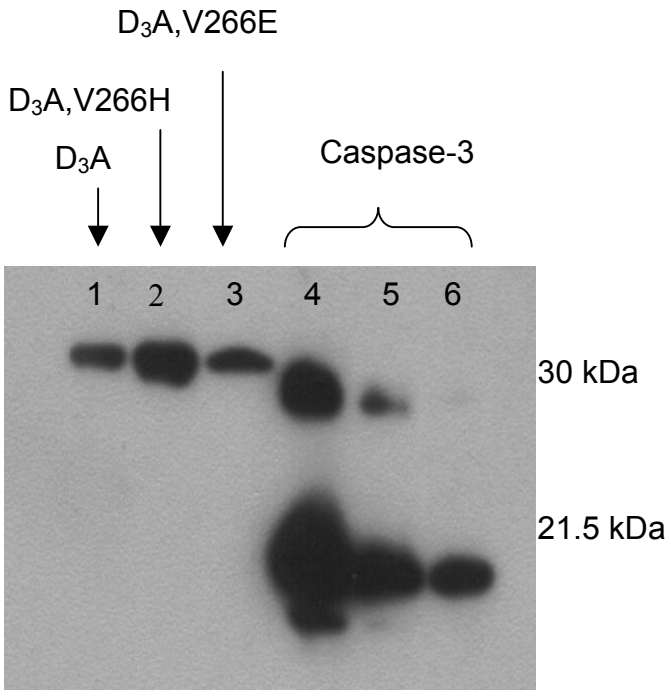

Figure 17. *Panel B.* Western blot against the large subunit of caspase-3 for procaspase-3(D_3A) (lane 1, ~500 ng), procaspase-3(D_3A,V266H) (lane 2, ~600 ng), procaspase-3(D_3A,V266E) (lane 3, ~500 ng), and caspase-3 (lanes 4-6, ~ 670, 67, and 13 ng). We explain the high intensity of caspase-3 band by the higher affinity of the antibody for caspase in comparison with the procaspase mutants.

Second, we performed Western-blotting experiments using an antibody that recognizes the large subunit of caspase-3. The results for procaspase-3(D_3A), procaspase-3(D_3A,V266E), and procaspase-3(D_3A,V266H) are shown in Figure 17B together with the wild type. Overall, the data show no evidence for a processed large subunit in this samples and further demonstrate that the activity of procaspase-3(D_3A,V266E) is not due to contaminating processed protein.

Oligomerization state of the interface mutants in nanomolar range

The experiments that tested the oligomeric state of the interface mutants used protein in the range of low micromolar concentrations (see Figure 15), while the activity assays were performed in the low nanomolar range (see Figure 16). One could argue that the inactivity of the V266H mutants and the decreased activity of the caspase-3(V266E) are the result of dimer dissociation at low concentrations. In order to examine this possibility, we have used the 'enzyme dilution assay' (37) by measuring the initial velocity of the interface mutants over 800-1000 fold difference in the concentration of enzyme. The results are presented in Figure 18A. Due to low residual activity of the V266H mutant, the lowest concentration tested was 50 nM, while for the V266E mutants the lowest concentration was 1 nM. We represented the logarithm of initial velocity versus the logarithm of the protein concentration. As it can be seen, the initial velocity is a linear function of the enzyme concentration for all the tested mutants (Figure 18A). In case of loss in activity due to dimer dissociation, the initial velocity would decrease nonlinearly with concentration of the protein, so that the plot of log(initial velocity) versus log(enzyme concentration) would show

A

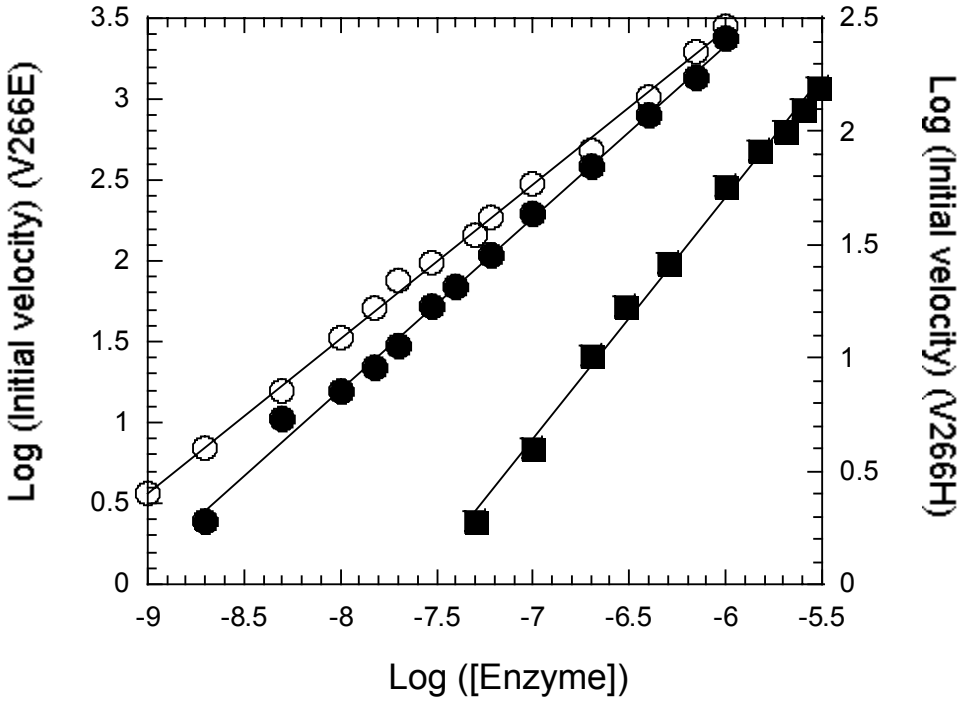

Figure 18. *Panel A.* Initial velocity dependence on the enzyme concentration for Procaspase-3(D_3A,V266E) (●), caspase-3(V266E) (○), procaspase-3(D_3A,V266H) (■). The logarithm of initial velocity plotted against the logarithm of enzyme concentration (in molar) shows a linear dependence in the case of all mutants.

B

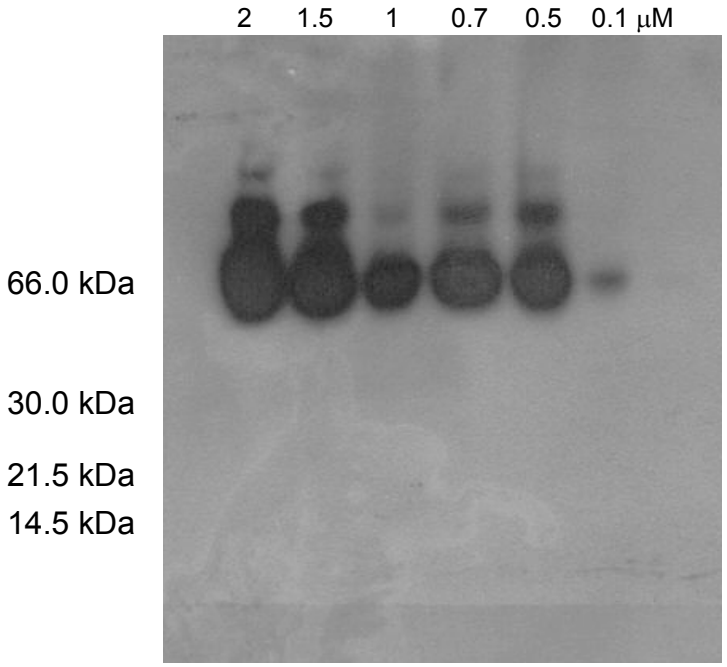

Figure 18. *Panel B.* Native gel Western-blotting of procaspase-3(C163S,V266H) .

The used antibodies were developed against the large subunit of caspase-3

two slopes. This proves that all the interface mutants described here remain dimers even at low nanomolar concentrations. Therefore, the low activity of the V266H mutants is not due to dimer dissociation.

In addition, procaspase-3(C163S,V266H) was subjected to native gel electrophoresis coupled to Western blotting against the large subunit of caspase-3 (Figure 18B). The investigated range was 0.1 μM- 2 μM. The protein migrated only as a dimer, and the presence of monomer protein could not be detected.

Limited trypsin proteolysis

We examined the positioning of the active site loops using limited proteolysis with trypsin and V8 proteases. In these studies, we used the enzymatically inactive forms of the procaspases, C163S, although the results were the same for the interface mutants in the context of C163S or D_3A. In all assays, the molar ratios of protein to trypsin, as well as the temperature were constant.

Both procaspase-3(C163S) and mature caspase-3 are cleaved by trypsin in two of the active site loops (92). Discrete cleavages occur at K57 and R64, in loop L1, and R207, in loop L3. The fragments generated by trypsin digestion of the interface mutants, procaspase-3(C163S,V266H) and procaspase-3(C163S,V266E), are shown in Figure 19. For the V266H mutant (Figure 19A), trypsin cleaved first at R207, producing two fragments of ~23 and ~9 kDa. In a somewhat slower reaction, the protein was cleaved at K57/R64, generating a fragment of ~16 kDa. The pro-domain was also cleaved at K19. These results are in contrast to those of procaspase-3 (92), where cleavage at K57/R64 occurred first, generating a fragment

A

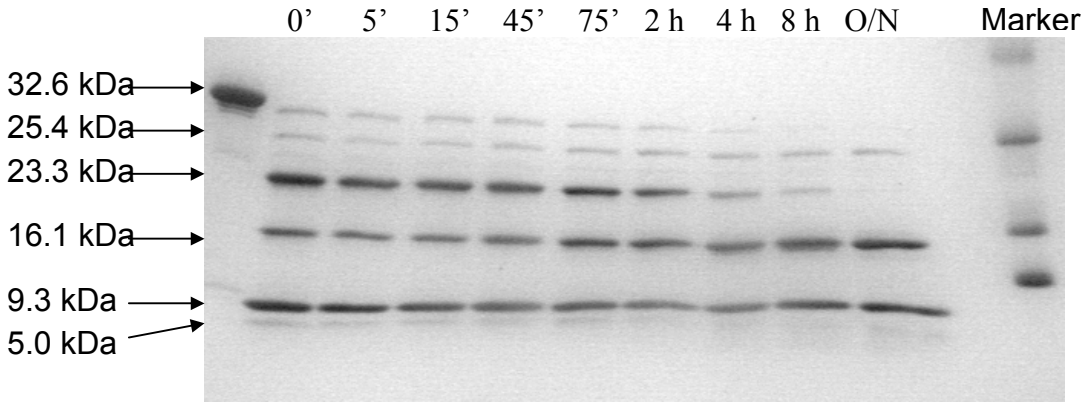

Figure 19. *Panel A.* Trypsin digestion of procaspase-3(C163S,V266H) at pH 7.2. The 32.6 kDa band represents the full-length protein, whereas the 25.4, 23.3, 16.1, 9.3, and 5.0 kDa bands are the cleavage products. Cleavage of the full-length protein at R207 generates the 23.3 and 9.3 kDa bands.

B

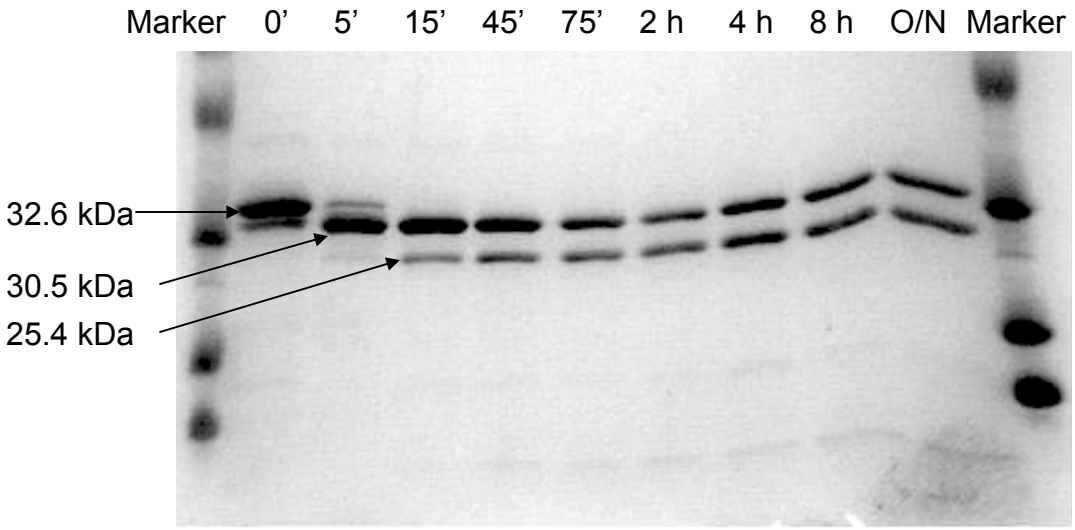

Figure 19. *Panel B*. Trypsin digestion of procaspase-3(C163S,V266E) at pH 7.2. The full-length protein (32.6 kDa) is cleaved at K19 generating the 30.5 kDa band and at R64, generating the 25.4 kDa band.

C

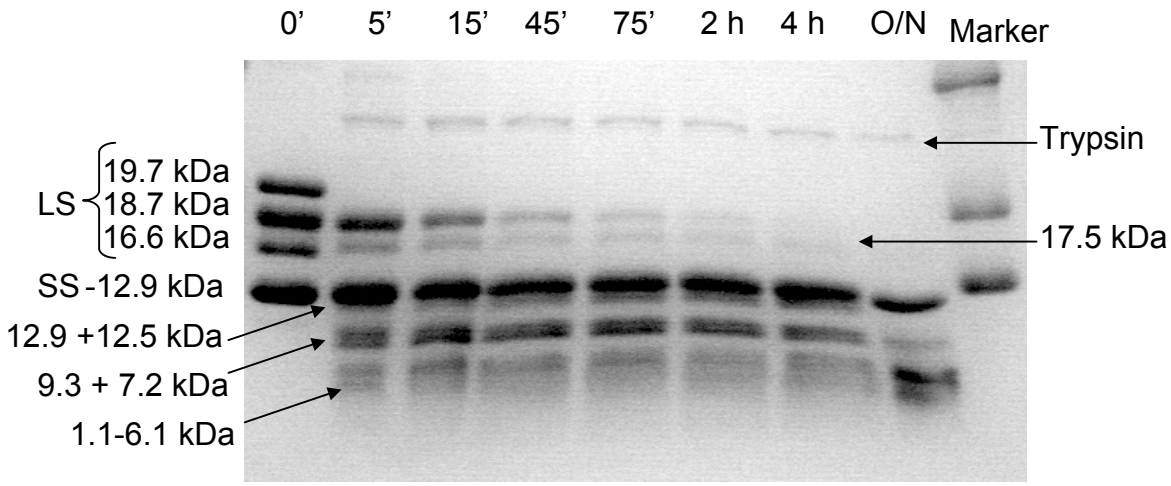

Figure 19. *Panel C*. Trypsin digestion of caspase-3(V266H) at pH 7.2. Caspase-3(V266H) was completely pre-cleaved with Granzyme B into large (LS) and small (SS) subunits (see Figure 16C). LS underwent auto-digestion at D9 and D28 during expression in *E. coli*, generating the fragments of 18.7 and 16.6 kDa (time 0'). Trypsin digestion cleaves as follows: LS (at R64, K19)- 17.5, 12.5, 7.2, 5.0 and 2.1 kDa; LS lacking 1-9 residues (at R64, K19)- 17.5, 12.5, 6.1, 5.0, 1.1 kDa; LS (at R64)- 12.5 and 5.3 kDa; SS (at R207)- 9.3 and 3.6 kDa.

D

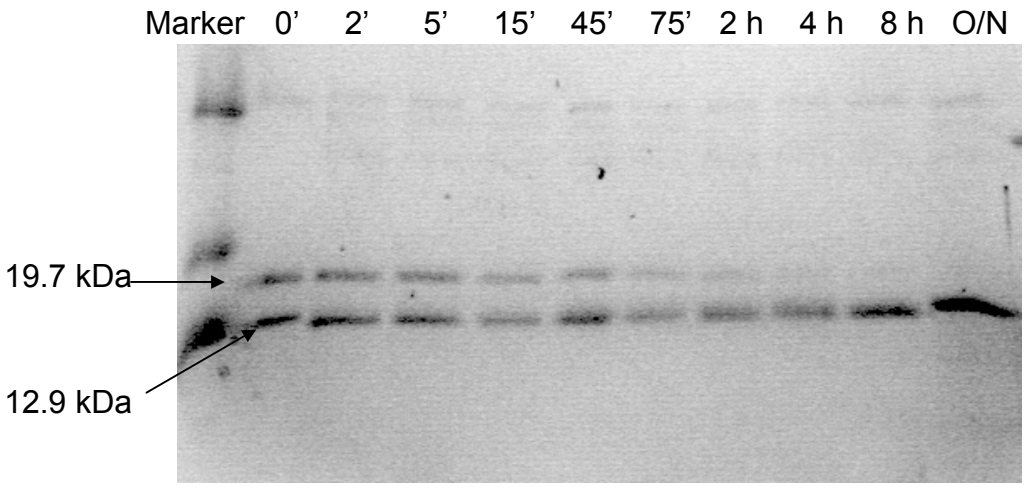

Figure 19. *Panel D*. Trypsin digestion of caspase-3(V266E) at pH 7.2. The large subunit (19.7 kDa) is slowly cleaved at R64, generating the 12.5 kDa band, which makes a doublet with the small subunit (12.9 kDa). The small subunit does not undergo cleavage at R207 as shown by the absence of the 9.3 kDa band.

E

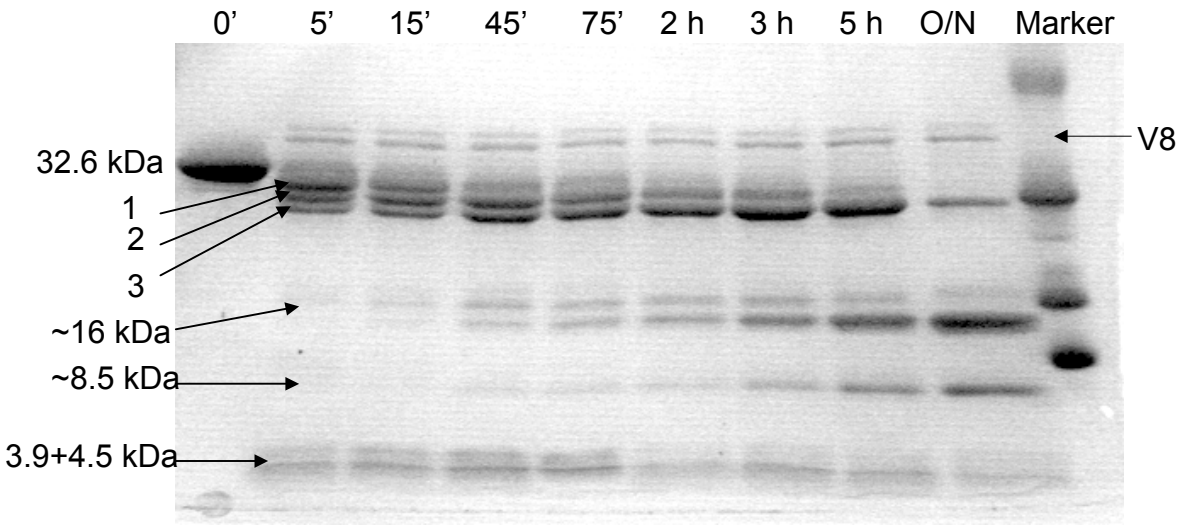

Figure 19. *Panel E.* V8 protease digestion of the procaspase-3(C163S,V266H) at pH 7.2. The full-length protein (32.6 kDa) is cleaved first at E248/D253 generating band 1 (mixture of 28.1 and 28.7 kDa fragments) and the ~4 kDa bands. Next cleavage occurs at D9, raising band 2 (27.1 and 27.7 kDa fragments), and then at E25, producing band 3 (25.3 and 25.9 kDa products). Simultaneous cleavage at E98/ E106 and E173/ D190 produces the mixture of bands at 16 kDa and 8.5 kDa.

F

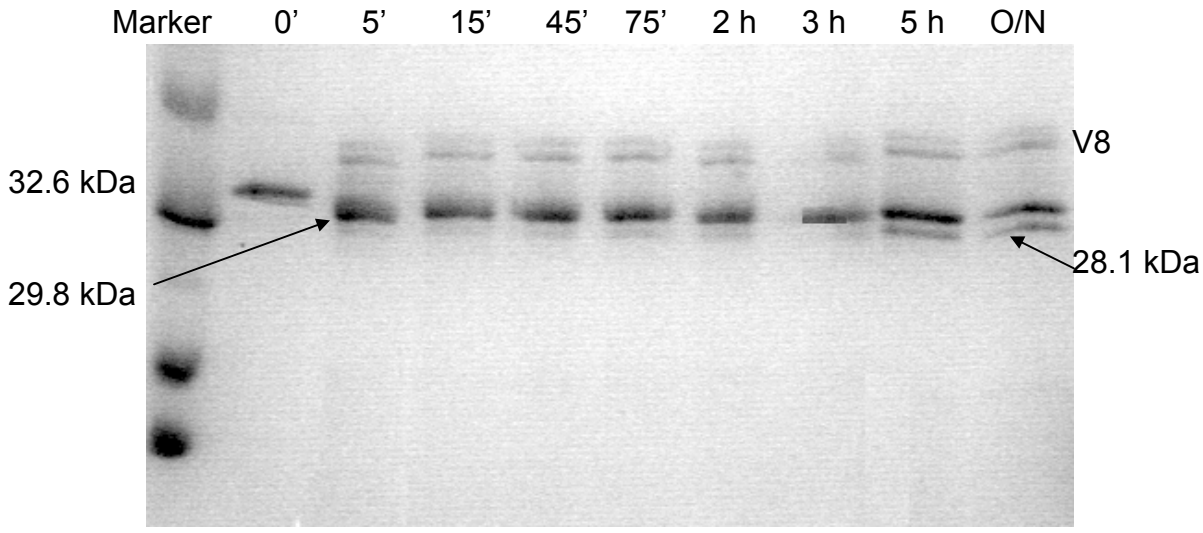

Figure 19. *Panel F.* V8 protease digestion of the procaspase-3(C163S,V266E) at pH 7.2. The full-length protein (32.6 kDa) is cleaved first at E25 generating the 29.8 kDa fragment. The second cleavage occurs at E272, producing the 28.1 kDa band. No cleavage occurs at E98/ E106, E173/ D190, or E248/D253.

G

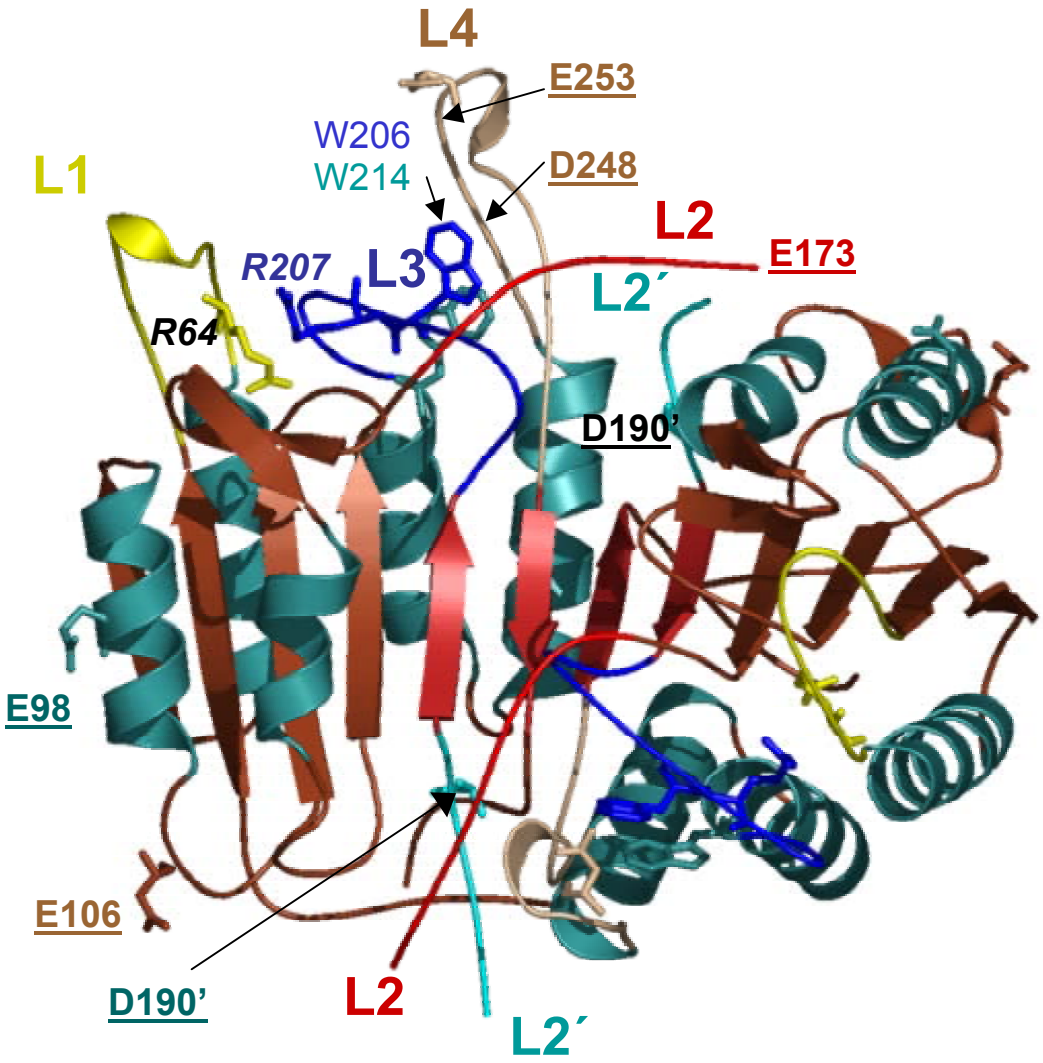

Figure 19. *Panel G*. Mapping the trypsin and the V8 protease cleavage of the interface mutants on the caspase-3 structure. Residues accessible to trypsin are shown in italic. Residues accessible to V8 protease are underlined. Catalytic loops are abbreviated as L1 (loop 1, in yellow), L2 (loop 2, in red), L2' (intersubunit linker, in cyan), L3 (loop 3, in blue), and L4 (loop 4, in gold).

H

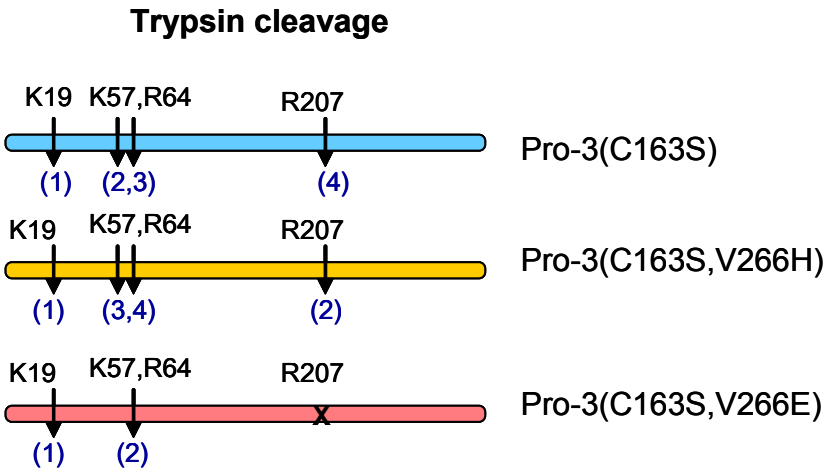

I

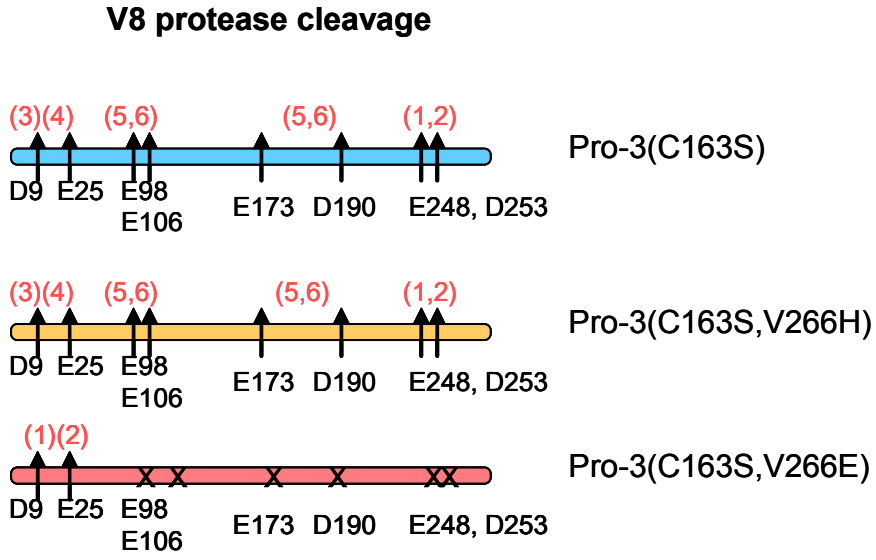

Figure 19. Summary for the kinetics of cleavage of the interface procaspase mutants in the case of trypsin proteolysis (*Panel H*) and in the case of V8 protease proteolysis (*Panel I*).

of 25 kDa, followed by cleavage at R207. In the V266H mutant, the ~25 kDa fragment is observed to be a minor component (Figure 19A). In contrast to procaspase-3, there was no protection of R207 in the presence of caspase-3 inhibitor (not shown), but based on the activity studies it is likely that the mutant does not bind the inhibitor. Overall, the results suggest that R207 in loop L3 is hyper-exposed in procaspase-3(V266H) relative to the position in procaspase-3.

In the V266E mutant (Figure 19B), trypsin cleaved first at K19 in the pro-domain, generating a fragment of 30.5 kDa, then a second cleavage occurred at R64 (loop L1), which generated a fragment of 25.4 kDa. There was no evidence for cleavage at K57 in loop L1. The kinetics of cleavage at R64 was slower than observed for procaspase-3(C163S) (92), suggesting that R64 is somewhat less accessible to the protease. There was no cleavage at R207, suggesting that this residue is inaccessible to the trypsin (Figures 19B, 19H). In the presence of caspase-3 inhibitor, DEVD-CHO, R64 was protected (not shown). Overall, the data suggest that the V266E mutation affects the positions of active site loops L1 and L3 in the procaspase.

Caspase versions of the interface mutants were also analyzed by trypsin proteolysis. The results are shown in Figures 19C and 19D. In case of the caspase-3(V266H), the protein was initially digested with granzyme B to completely convert the full-length protein to mature subunits (see Figure 16C). Due to residual activity of this mutant, auto-cleavages in the pro-domain at D9 and D28 also occurred so that the protein shows four bands in the gel (Figure 19C, time 0'): 19.7 kDa band represents the large subunit containing the pro-domain, 18.7 kDa band is the large

subunit plus residues 9-28, 16.6 kDa band is the large subunit, while the 12.9 kDa band represents the small subunit. Trypsin cleaves at the same sites as in the procaspase-3(C163S,V266H) (Figure 19A) and caspase-3 (92) at K19, R64, and R207, and the generated bands are shown in Figure 19C. It is not possible to determine whether R207 cleavage in caspase(V266H) is faster than in caspase-3 (in other words, if loop L3 is over-exposed in the interface mutant), as R207 digestion seems to occur with fast kinetics in both proteins ($t_{1/2}$< 2 min).

In the case of caspase-3(V266E) (Figure 19D), the large subunit is cleaved by trypsin at R64 generating a band of 12.5 kDa that overlaps with the band produced by the small subunit. The kinetics of R64 cleavage is much slower ($t_{1/2}$ ~ 30 min) than in caspase-3 ($t_{1/2}$ < 2 min) (92), which demonstrates that, like in procaspase-3(C163S,V266E), loop L1 is also less exposed in the caspase form of this mutant than in caspase-3. Caspase-3 inhibitor DEVD-CHO prevented the cleavage at R64 (data not shown). Interestingly, the small subunit is not cleaved at R207, as judged by the lack of the 9.3 kDa band (Figure 19D). This suggests that the conformation of loop L3 from procaspase-3(C163S,V266E), probably buried, is maintained following the cleavage of the intersubunit linker.

Limited V8 proteolysis

Our lab has shown that V8 protease cleaves procaspase-3(C163S) at residues D9, E25, E98, E106, E173, D190, E248 and D253 (92).

The same cleavage pattern and kinetics of cleavage is displayed by the procaspase-3(C163S,V266H) mutant (Figures 19E, 19I). At times of cleavage from 5

to 15 minutes, the data demonstrate three closely spaced bands between 32 and ~27 kDa, referred to as bands 1-3. Cleavages at E248 and D253, in loop L4, generate two fragments of ~29 kDa (band 1) and ~4 kDa. Band 1 is cleaved further at D9, to give band 2, and at E25, to give band 3. Band 3 is then cleaved simultaneously at positions E98/D106 and E173/D190, giving rise to a mixture of ~16 kDa and ~8.5 kDa bands. The data shown here suggest that there is no difference in the accessibility of loop L4 (E248/D253) or the intersubunit linker for procaspase-3(C163S,V266H) in comparison with procaspase-3(C163S) (92).

We also characterized the limited proteolysis of procaspase-3(C163S,V266E) with V8 protease and the results are shown in Figure 19F. Significantly fewer cleavages occurred in this mutant in comparison with the other proteins. V8 protease cleaved the N-terminus (E25) and then the C-terminus (E272), to generate two fragments of ~30 and ~28 kDa (Figures 19F, 19I). Importantly, there are no cleavages observed for the E98/E106, E173/E190, or the E248/D253 sites. This suggests a conformational change that affects loop L4 (E248/D253), the intersubunit linker (E173/E190) and the region containing the residues E98 and E106.

In addition, caspase-3(V266E) digestion with V8 protease generated only one cleavage in the small subunit (data not shown). Based on the molecular weight estimated from the SDS-gel, the data suggests that this cleavage occurred at E248/D253 in loop L4.

We have mapped the cleavage sites for trypsin and V8 proteolysis on the structure of caspase-3, and the results are shown in Figure 19G. In case of trypsin digestion, K57 and R64 reside in the catalytic loop L1, which interact with the

substrate via R64. R207 resides in the catalytic loop L3, and it also interacts with the substrate. Interestingly, although there are many positively charged residues on the surface of (pro)caspase-3 (26), trypsin cleaves only in the active site. Cleavage patterns of interface mutants suggests that loop L3 is inaccessible for proteolysis in V266E mutants, or it is overexposed in the V266H mutants, and also that loop L1 is less accessible in the V266E mutants.

V266E mutants have features of both the procaspase and of the mature caspase. For example, limited proteolysis by V8 protease suggests a conformational change that affects loop L4 (E248/D253), the intersubunit linker (E173/E190) and the region of E98/E106 (Figure 19F, 19H). In the mature caspase-3, residue E106 interacts with R86 to form a salt-bridge. These contacts do not occur in procaspase-3, and consequently, the procaspase is cleaved by V8 protease at E106 (92). Overall, the data for procaspase-3(C163S,V266E) show that loop L4 is protected from cleavage by V8 protease, that the contacts between E106 and R86 may have formed in the procaspase, and that loop L2' (E173/D190) is less accessible for cleavage by V8 protease. The latter two points are observed in mature caspase-3. The lack of cleavage at D190 is interesting because the exposed loop L2' (intersubunit linker) in procaspase-3 becomes less accessible to V8 protease after zymogen processing (Figure 19G). In this case, the loop flips 180° so that it makes new contacts with loops L2 and L4 of the second monomer. Because loop L2' is covalently connected to loop L2 in the procaspase, preventing its flipping, it is not clear why E173/D190 would be protected in V266E mutants. On the other hand,

cleavage of the intersubunit linker in procaspase-3(C163S,V266E) allows loop L4 proteolysis by the V8 protease, like in the case of caspase-3.

Remarkably, based on these studies, all loops in the procaspase-3(C163S,V266E) seem to be affected by the interface V266E substitution.

Fluorescence quenching and average emission wavelength versus pH

Each monomer of caspase-3 contains two tryptophan residues, W206 and W214, and both reside in the active site (see Figure 19G). To further examine loop L3, which contains W206, in the interface mutants, we measured quenching of fluorescence emission upon the addition of potassium iodide and acrylamide. Quenching by potassium iodide depends on the accessibility of the tryptophans in protein structure as well as on the charge of the residues occurring around the tryptophans. Acrylamide quenching is only dependent on the aromatic residue relative exposure.

Figures 20A and 20B present the KI quenching of the interface mutants fluorescence. In these experiments, the percent quenching was plotted versus the concentration of quencher, and the data were fit to a modified form of the Stern-Volmer equation to obtain the quenching constant, K_{SV} (equation 8). The values of K_{SV} were determined from pH 3 to 9.5.

Figure 20A shows the potassium iodide quenching for the caspase-3 mutants in comparison with caspase-3. For caspase-3 and caspase-3(V266H) the data are described by two transitions, while caspase-3(V266E) data show three transitions (Figure 20A). The first transition results in consistent decrease of the

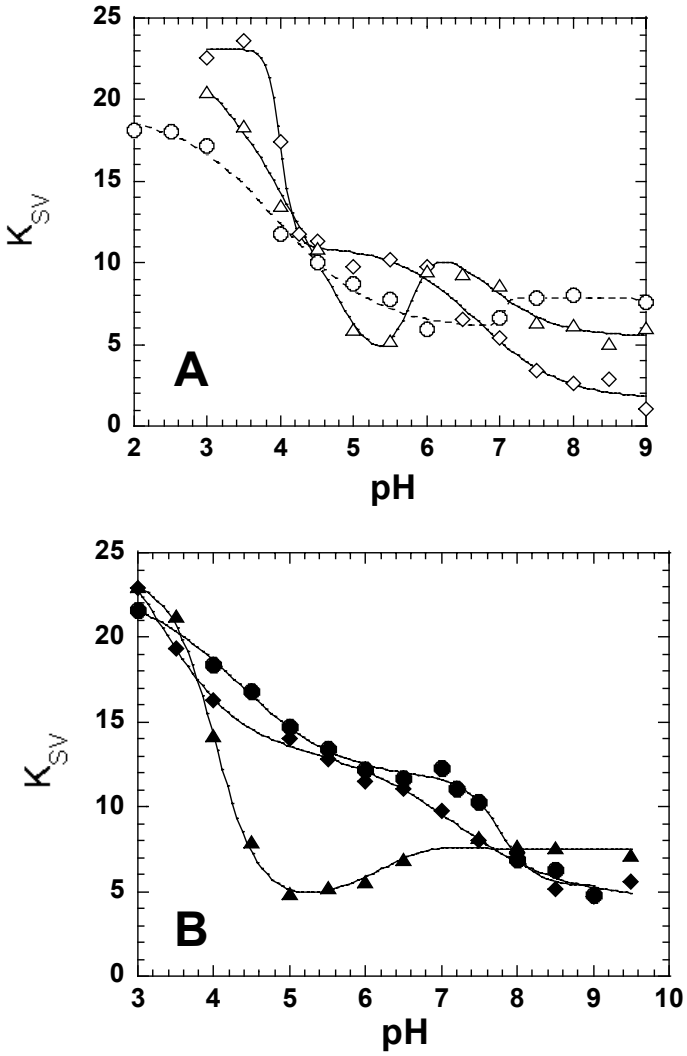

Figure 20. Fluorescence quenching studies for the interface mutants versus pH. *Panel A*. Fluorescence quenching by iodide for caspase-3 (○), caspase-3(V266E) (△), caspase-3(V266H) (◇). *Panel B*. Fluorescence quenching by iodide for 3(C163S) (●), procaspase-3(C163S,V266E) (▲), and procaspase-3(C163S,V266H) (◆). The curves represent fits to equation 8. In the case of caspase-3(V266E), equation 8 has been modified to the three state transition model, by adding another term to the equation.

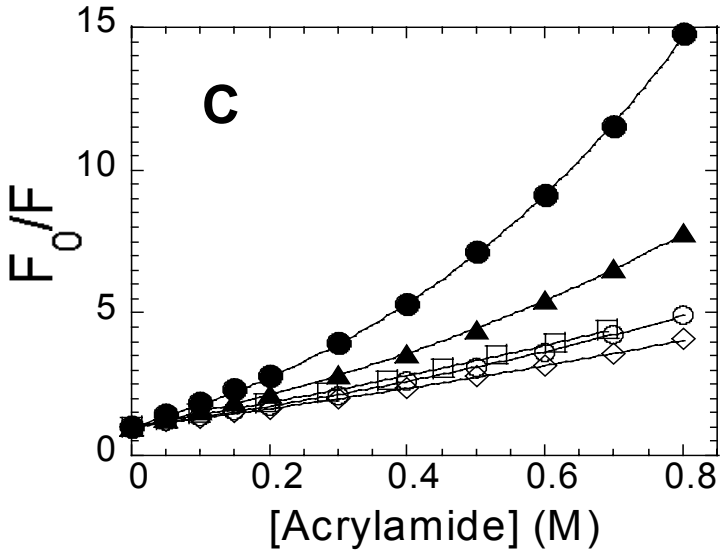

Figure 20. *Panel C*. Fluorescence quenching by acrylamide at pH 7.2. The curves represent fits to the Stern-Volmer equation for: caspase-3 (○), caspase-3 in 8 M urea (●), procaspase-3(C163S) (□), procaspase-3(C163S, V266H) (◇), and procaspase-3(C163S,V266E) (▲). The curves represent fits to equation 6.

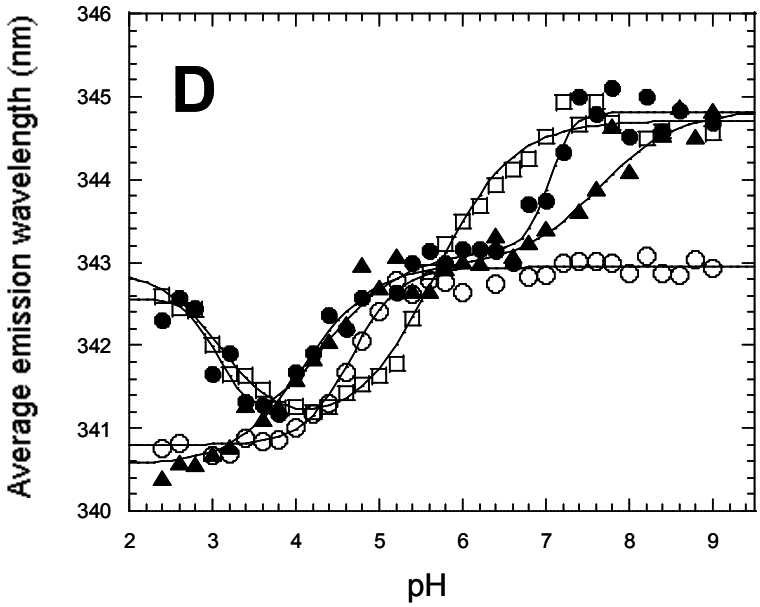

Figure 20. Panel D. Average emission wavelength (<λ>) versus pH for caspase-3 (□), procaspase-3(C163S) (○), procaspase-3(C163S,V266H) (◇), procaspase-3(C163S,V266E) (▲), and caspase-3(V266E) (●). Solid lines represent fits of the data to equation 10 as described in Methods.

K_{SV} value, having a pK_a value of ~4 for all mutants: caspase-3 (pH 2-6), pK_{a1}= 4.0±0.2; caspase-3(V266H) (pH 3-4.5), pK_{a1}= 4.0±0.02; caspase-3(V266E) (pH 3-5.5), pK_{a1}= 4.2±0.5. This transition corresponds to high accessibility of tryptophan residues at low pH. For the second transition, the K_{SV} decreases for the wt and V266H mutant, and increases for the V266E mutant. The pK_a values are: pK_{a2}= 7.2±0.4 for caspase-3 (pH 6-9); pK_{a2}= 6.5±0.2 for caspase-3(V266H)) (pH 6-9); and pK_{a2}= 5.5±0.5 for caspase-3(V266E) (pH 5-6). The third transition of the caspase-3(V266E) mutant occurs between pH 6.5-9 and has a pK_{a3} of 7.3±0.6. Overall, V266E mutant and caspase-3 display a similar pattern of iodide quenching at pH< 4.5 and pH>7, while quenching of V266H mutant and caspase-3 is alike over pH range from 4.5 to 6.5.

For the procaspase-3 interface mutants the results are shown in Figure 20B. The data for procaspase-3(C163S) are shown here for comparison. For all proteins at pH>8, values of K_{SV} are ~5-8. Between pH 9.5 and 5.5, K_{SV} increased to ~13 for procaspase-3(C163S) and procaspase-3(C163S,V266H), whereas it decreased from ~8 to ~5 for procaspase-3(C163S,V266E). For procaspase-3(C163S,V266H) the data are similar to those of procaspase-3(C163S) and are described by two transitions. Between pH 3 and 5, the first transition has pK_{a1} = 3.7±0.3. The second transition occurs at pH>6.5, where pK_{a2} = 7.2±0.3 and results in a decreased in the K_{SV}. In case of procaspase-3(C163S,V266E), the data are also described by two transitions (Figure 20B) The first transition (pH 3 to pH 5) has pK_{a1} = 4.0±0.4, while the second transition (pH 6 to pH 9) has pK_{a2} = 6.2±0.2. The transition results in a decrease in iodide accessibility for procaspase-3(C163S,V266E) and an increase in

accessibility for procaspase-3(C163S) and procaspase-3(C163S,V266H). Therefore, according to these data, it seems that only procaspase-3(C163S,V266H) preserved the electrostatic environment around the tryptophan residues. The results of iodide quenching can be interpreted as the unraveling at lower pH and solvent exposure of loop L3, containing the W206, which would be consistent with the positioning of this loop in procaspase-7 (27, 30).

In order to test this hypothesis, we have examined the quenching of the tryptophan fluorescence using acrylamide. The plots of F_0/F versus acrylamide concentration are displayed in Figure 20C. The results show that there was no difference between procaspase-3(C163S), procaspase-3(C163S,V266H) and caspase-3, where values of K_{SV} were ~2.7-3.7. Acrylamide was slightly more effective for quenching of procaspase-3(C163S,V266E), where K_{SV} was ~4.7. The data are compared to caspase-3 unfolded in 8 M urea-containing buffer. Under these conditions the protein is unfolded, and the tryptophanyl residues are exposed to solvent (K_{SV}~ 5.7). Importantly, the values of K_{SV} did not change from pH 7 to 3 for procaspase-3(C163S) (92) and for the mutants (data not shown), demonstrating that loop L3 is not unraveled at the lower pH. Although the precise groups are not yet known, the results for all proteins suggest that the titration at lower pH affects the electrostatic environment of the tryptophanyl residues rather than unraveling loop L3.

Overall, the data suggest that the V266H mutation has minimal effects on the electrostatic environment of the tryptophans in the procaspase but affects the caspase structure. This is shown by the experiments using limited proteolysis with

trypsin (Figure 19A). Moreover, the V266E mutation affects caspase and procaspase in a different manner, which suggests that the zymogen undergoes a conformational change upon maturation.

Fluorescence emission scans of the V266E and V266H interface mutants were examined over the pH range of 2.5 to 9, and the average emission wavelength (79), $\langle\lambda\rangle$, was calculated at each pH using equation 9 (Figure 20D). The data for caspase-3 have been described (92) and are shown here for comparison. For procaspase-3(C163S,V266H), $\langle\lambda\rangle$ is constant at 343 nm between pH 5.5 and 9. Below pH 5.5, there is a cooperative decrease in $\langle\lambda\rangle$ such that at pH<4, $\langle\lambda\rangle$ is 340.8 nm. This represents a blue-shift in the fluorescence emission and bringing evidence that loop L3, containing W206, is not unraveled and solvent exposed at low pH. The results for this protein are nearly identical with those of procaspase-3(C163S), described previously (92), except that a small inflection at pH 4 ($\langle\lambda\rangle$=341.4 nm) is missing in the interface mutant. The pK_a that describes the single transition was 4.7±0.04. In contrast, the results for the mature caspase-3 are described by two transitions. Between pH 7 and 9, $\langle\lambda\rangle$ reached a maximum of 344.6 nm. Below pH 7, there was a cooperative decrease in $\langle\lambda\rangle$ to 341.2 nm at pH 4. A second cooperative transition occurred below pH 4 that resulted in an increase in $\langle\lambda\rangle$, representing a red-shift in the fluorescence emission so that $\langle\lambda\rangle$=342.5 nm. The data were fit to equation 10, and the following pK_a's were determined for the two transitions*:* pK_{a1}=3.0±0.2, pK_{a2}=5.7±0.1. The results for the V266E interface mutants in this assay were surprising. At pH>8, both mutants reached a maximum in $\langle\lambda\rangle$ of 344.6 nm, the same as for the mature caspase-3. Between pH 8 and 5, there was a

cooperative decrease in <λ> to 343 nm, which was the same <λ> as that of procaspase-3(C163S) or procaspase-3(C163S,V266H). The pK_a's for the transition were 7.6±0.2 (procaspase-3(C163S,V266E)) and 7.0±0.2 (caspase-3(V266E)). Between pH 5 and ~4, there was a cooperative decrease in <λ> to 341.2 nm. The pK_a's for the second transition were 4.1±0.1 (procaspase-3(C163S,V266E)) and 4.3±0.4 (caspase-3(V266E)). This represents a small decrease in pK_a for the procaspase (4.7 versus 4.1) but a large decrease in pK_a for the mature caspase (5.7 versus 4.3). In caspase-3(V266E), a third transition occurred below pH 4 that resulted in an increase in <λ> to 343 nm, similar to that observed for the mature caspase-3. The pK_a for this transition was 3.0±0.2.

In summary, the V266E mutants display <λ> values intermediate to the values of mature caspase-3 and zymogen, while procaspase-3(C163S,V266H) resembles only procaspase-3 from this point of view.

Circular dichroism studies

Several assays using circular discroism (CD) are helpful to characterize better the global conformational changes that occur in the (pro)caspase-3 interface mutants versus the wild type proteins.

Figures 21A and 21B show the CD spectra in far-UV and near-UV for the procaspase-3 mutants at pH 7.5. In the V266H mutant, the magnitude of the far-UV CD signal is unaltered, but decreases ~30% in the case of procaspase-3(C163S,V266E) (Figure 21A). This decrease may be associated with a loss in the secondary structure. In the case of the near-UV CD data, there is an increase in the

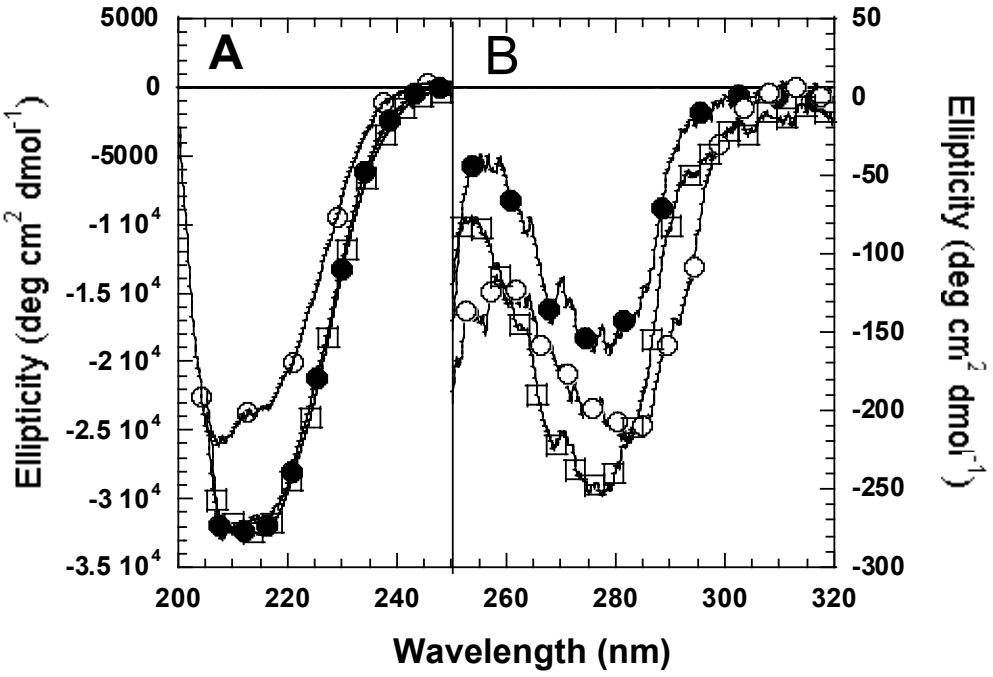

Figure 21. Far-UV circular dichroism (FUV-CD) (*Panel A*), and Near-UV circular dichroism (NUV-CD) (*Panel B*) for procaspase-3(C163S) (●), procaspase-3(C163S,V266E) (○), and procaspase-3(C163S,V266H) (□).

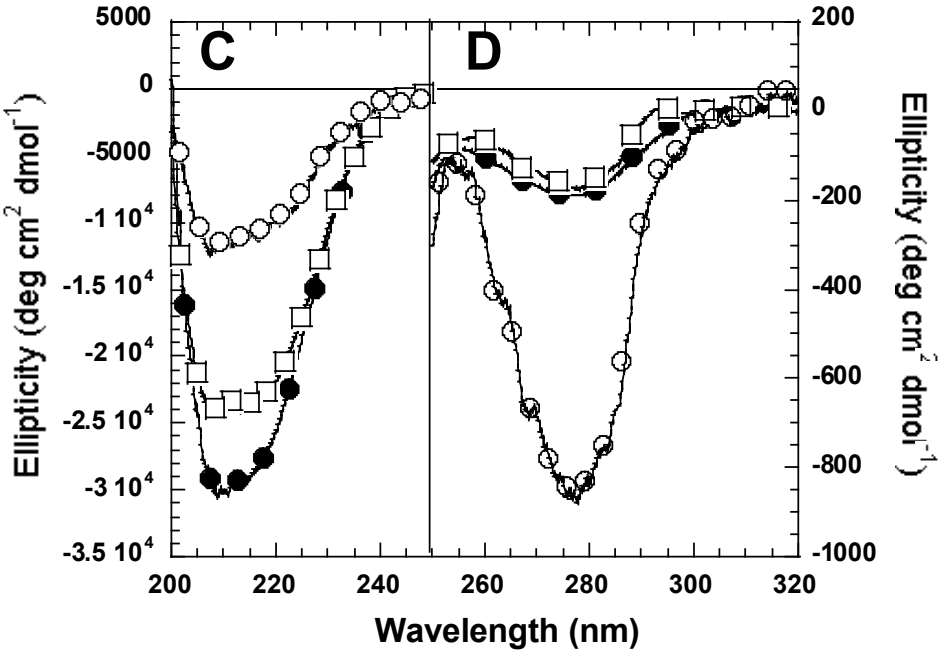

Figure 21. Far-UV circular dichroism (*Panel A*), and Near-UV circular dichroism (*Panel B*) for caspase-3 (●), caspase-3(V266E) (○), and caspase-3(V266H) (□).

magnitude of the signal versus the procaspase-3(C163S) for both mutants; in addition, procaspase-3(C163S,V266E) displays a red-shift of ~6 nm of the signal minimum (Figure 21B). This result may be due a higher exposure of the aromatic residues in V266E mutant, in agreement with the acrylamide quenching and the fluorescence emission assays. The acrylamide assay suggests that the tryptophan residues are more accessible for quenching in V266E mutant than in procaspase-3 at pH 7.2 (Figure 20C). In addition, the average emission wavelength for V266E mutant is red-shifted between pH 6.8 and 9.0 versus procaspase-3 (Figure 20D).

Figures 21C and 21D show the far-UV or near-UV CD spectra, respectively, for caspase-3 mutants. In comparison with caspase-3, the far-UV CD spectra show an increase in the ellipticity for caspase-3(V266H) of ~35% and a decrease in the signal for caspase-3(V266E) of ~47% (Figure 21C). The signal in the near-UV CD does not change for caspase-3(V266H), but it is much more pronounced for the caspase-3(V266E) (Figure 21D).

The data also show that while the magnitude of the far-UV CD signal decreases upon maturation, the magnitude of the near-UV CD signal increases, consistent with conformational changes upon maturation. Overall, the results suggest that the interface mutants are folded with well-packed tertiary structures. While it should be noted that the mutations might affect other regions of the proteins, the changes in the near-UV CD spectra are consistent with the changes in the active site loops described above.

Models for the structural changes in the interface mutations

We have shown that several important changes of (pro)caspase-3 conformation and function occur after replacing Val266 in the dimer interface with glutamate. First, the activity of the procaspase increases by 60-fold (Table III). This pseudo-activation is likely the result of stabilizing contacts in the loop bundle, including loop L4, which are mediated by movements in the intersubunit linker (Figure 19G). Secondly, the mutation reduces the exposure of all catalytic loops, L1-L4 (Figures 19B and 19F), and increases the tryptophan fluorescence (Figure 20D). Although further cleavage of the inter-subunit linker does not increase the catalytic activity (Table III), the resulting caspase is accessible for cleavage in loop L4 (Figure 19D) and displays a different electrostatic environment around the tryptophans (Figure 20A).

Based on the described studies, the V266E mutants have intermediate properties of the procaspase and of the mature caspase. For example, V8 protease cleaves procaspase-3 at E98/E106, but not caspase-3 or the V266E mutants (92) (Figure 19F). The reason for this is that E106 forms a salt bridge with R86. The interaction appears to be lacking in procaspase-3 (92). In addition, V8 cleavage at E173/D190 (L2) does not occur in caspase-3 or the V266E mutants but occurs in procaspase-3 (92). Since subsequent to the inter-subunit cleavage loop L2 interacts with L2' and L4' from the second monomer to stabilize the 'loop bundle' structure, it is assumed that L2 from the V266E zymogen re-locates to a position similar to that in caspase-3, such that it improves the activity and in addition hampers the access to loop L4. This is supported by the red shift in the fluorescence emission that

probably results from movements of loop L2 and/or L4 away from the active site and formation of the loop bundle (Figure 20D). The weaker contacts in the loop bundle may also explain the lower activity of caspase-3(V266E) compared to the wild-type caspase-3 (Table III).

While the mechanism of the loop movements is not clear, we suggest that the effects of V266E are mediated through contacts with R164 on loop L2. Figure 22A shows the positioning of the catalytic loops, active cysteine (C163) and R164 versus the dimer interface in the caspase-3 structure. During maturation of the caspase, R164 rotates away from the active site and points toward the dimer interface (Figure 22A). Loop L3 inserts next to the dimer interface with the “elbow loop” containing the proline 201. The side-chain of R164 intercalates between Y197 and P201, on the “elbow loop,” and these contacts appear to stabilize loop L3. The positive charge of R164 is neutralized by E124, which resides on a loop above the interface. This loop is important because it contains H121 and G122, which forms part of the oxyanion hole (26). Schematically, the same interactions are shown more clearly in Figure 22B, which has been constructed to explain the activation model of V266E mutants and inactivation model of V266H mutants.

We suggest that the V266E mutation positions the E266 side-chain so that it interacts with the guanidinium group of R164 (Figure 22C). Indeed, these contacts are observed in caspase-1, where E390, the comparable position in the interface, is within 2.5 Å of the arginine side-chain (93) (Figure 6B). In this case, the buried salt bridge formed at the interface of procaspase-1 does not interfere with dimerization (31). For the V266E mutants, correct positioning of R164 facilitates insertion of the

A

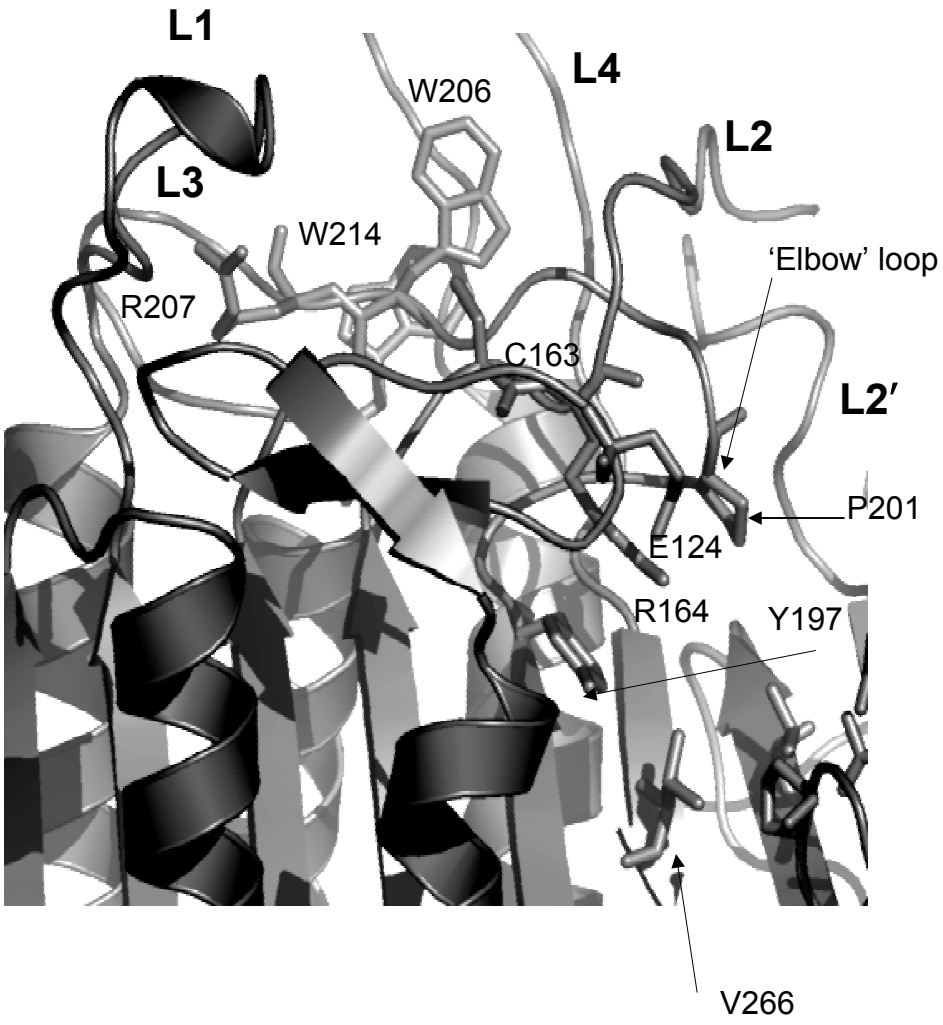

Figure 22. *Panel A.* Caspase-3 showing the amino acid network lying between the heterodimer-heterodimer interface and the catalytic loops. R164 from loop L2 is stabilized between the Y197 (core) and E124. Structure was generated by *PyMol.*

B

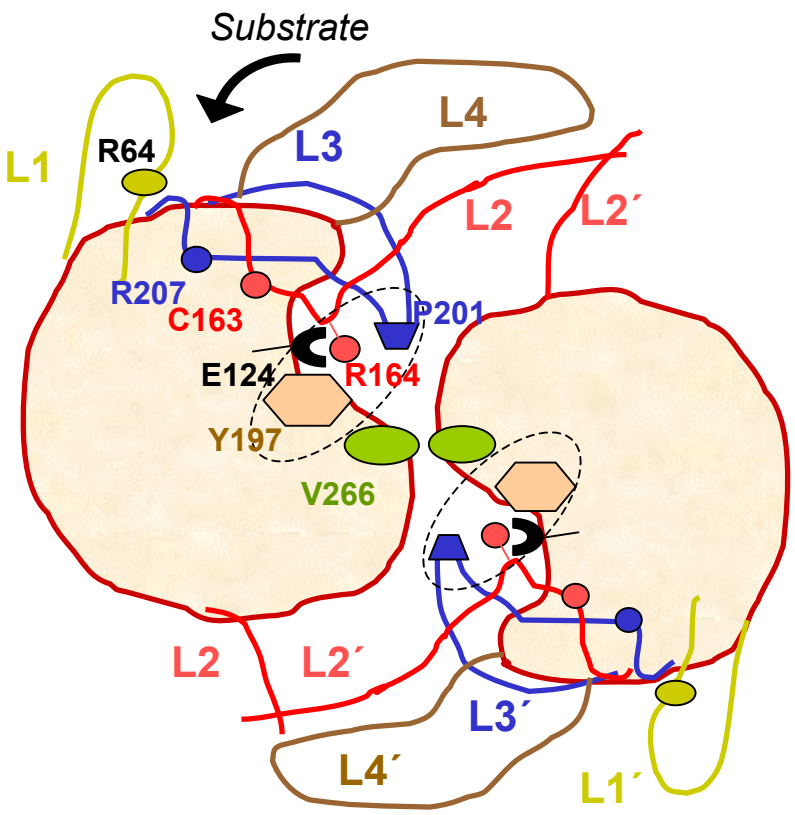

Figure 22. *Panel B.* Schematic representation of caspase-3 dimer showing the positioning of the Y197 versus the interface residue V266. Y197 and P201, from the elbow loop (blue), stabilize the interaction between R164 from loop L2 (red) and E124 (shown as a dotted circle). Insertion of R164 and elbow loop close to the dimer interface allows the correct positioning of C163 for the catalytic attack and of R207 for the substrate binding.

C

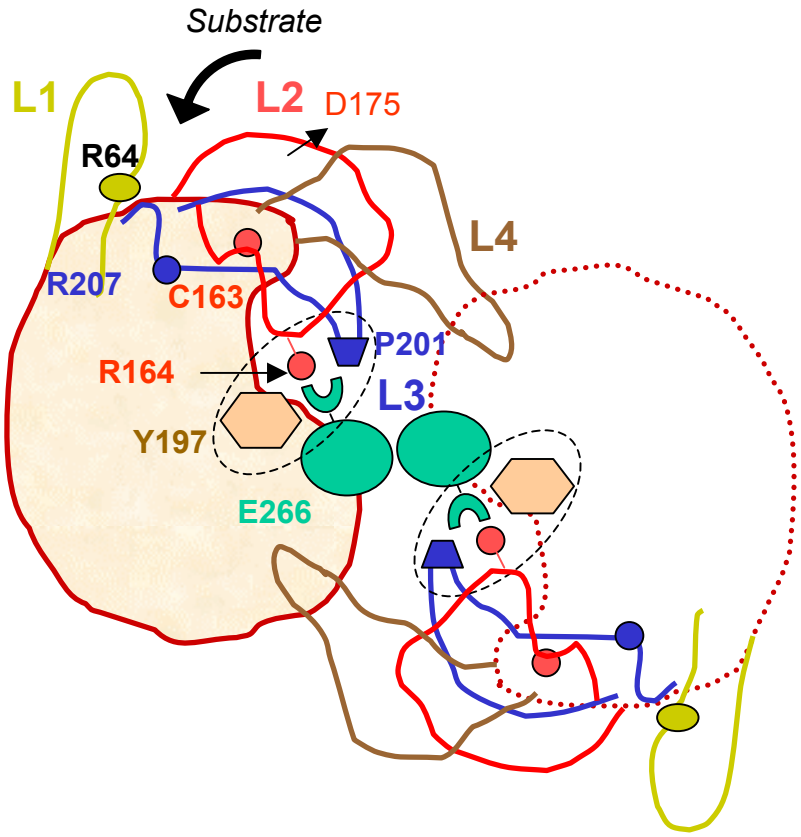

Figure 22. *Panel C.* Model for procaspase-3(V266E) pseudo-activation. The schematic representation shows the buried salt bridge between E266 and R164, which allows loop L2 (red) to insert properly. This permits the elbow loop to descend next to R164, making room for the substrate in the catalytic site. Full activation of caspase-3(V266E) after cleavage of the inter-subunit linker may not be possible due to alterations in loop L4.

D

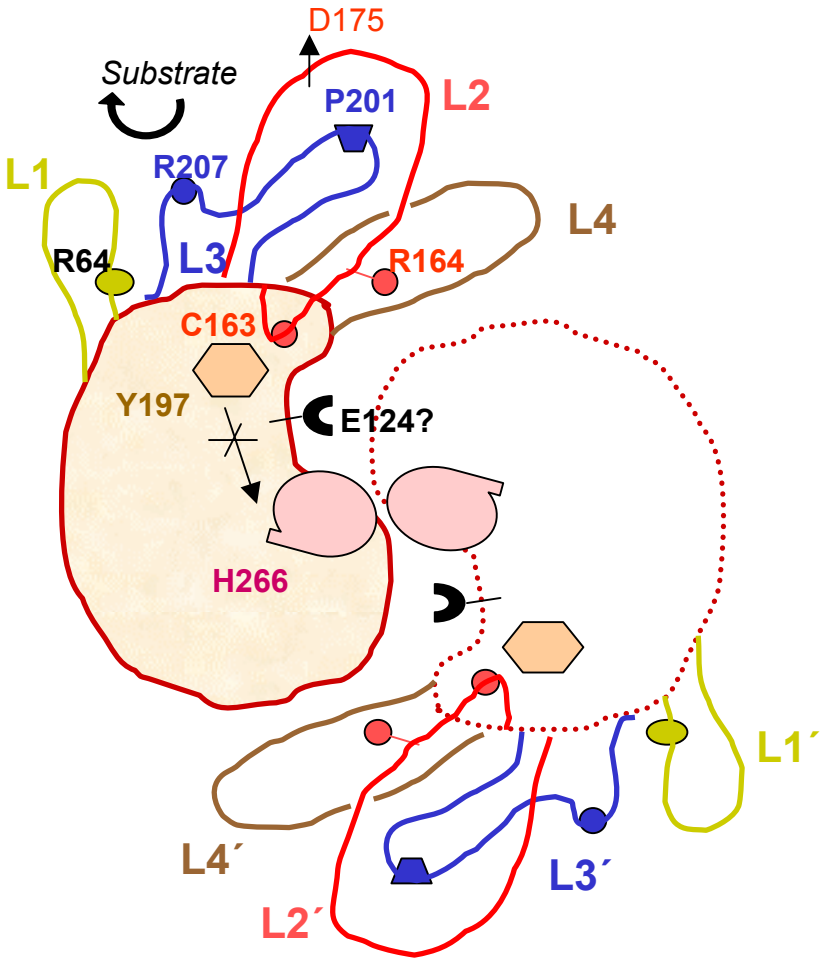

Figure 22. *Panel D.* Model for procaspase-3(V266H) inactivation. Schematic representation showing the steric hindrance generated by H266 following the V266H mutation. Y197 is misplaced and cannot stabilize R164. Consequently, the elbow loop of loop L3 (blue) is not properly inserted, resulting in substrate inaccessibility to the catalytic groove.

elbow loop, and flattens the active site, which binds the substrate (Figure 22C). In addition, we believe that active C163 reaches the location occurring in the wild-type caspase-3 and that the active site opening exposes more the tryptophans within loop L3 (Figure 22B). This mechanism explains the pseudo-activation, L3 and L2 inaccessibility by proteolysis and the increase in the fluorescence in V266E mutants. Nonetheless, it is not clear how interactions between R164 and E266 affect movements in the intersubunit linker and loop L4. In addition, the model does not explain why the activity does not increase after the cleavage of the intersubunit liker (Table III). However, it is remarkable to acknowledge that a point mutation in the dimer interface of procaspase-3 affects the conformations of three of the five active site loops and results in a significant increase in the enzyme activity, dispensing the need of cleavage.

In contrast to V266E, replacing V266 with histidine abolishes activity in the procaspase and in the mature caspase (Table III). As shown in Figure 19A, the V266H mutation results in a hyper-exposed R207, which is cleaved rapidly by trypsin. Based on the proteolysis and fluorescence emission studies (Figures 19E and 20D), the V266H mutation does not appear to affect loops L1, L4, or the intersubunit linker. Loop L3 forms the bulk of the substrate-binding pocket, thus the hyper-exposed R207, on loop L3, is consistent with the lack of enzyme activity. While the mechanism remains unknown, the effect of V266H occurs over long distances (~20 Å between V266 and R207). We suggest that the effects of H266 may be mediated through Y197 (Figure 22A). Upon maturation, the side chain of Y197 rotates away from the active site and toward the dimer interface (Figure 22B).

Modeling studies with H266 in the interface suggest that steric clashes exist between the side-chains of H266 and Y197, which may prevent the proper rotation of Y197. This model is depicted in Figure 22D, which represents H266 as a bulky residue limiting Y197 flexibility. Subsequently, the interaction between R164 and E124 shown in Figure 22B may not take place in the proper way, which can have dramatic consequences on the activity. This mechanism is observed in caspase-9, which contains a phenylalanine at position 404 (comparable to 266 in caspase-3) (see Figure 6B). In that case, the presence of two phenylalanyl side-chains in the interface prevents proper positioning of Y197, and this results in only one intact active site rather than two (29). Aside from an increase in side-chain volume between valine and histidine, the effect of a positive charge on H266 cannot be ruled out at this point.

III. Testing the models proposed for the interface mutants

A. Tyr197 designed mutants

We suggest that the bulky histidine in the interface of (pro)caspase-3 prevents the correct insertion of Y197 and subsequent location of the catalytic loops, especially L3. If this is the case, then substitution of the Y197 with a smaller amino acid (i.e., alanine or cysteine) might allow recovery of the enzymatic activity of the V266H mutants. It is worth noting that caspases-1, -4, -5, and -13 contain a cysteine at position 197, while Y197 is conserved in all effector caspases (caspase-3, 6, and 7) and in caspase-9.

To test this model, we have mutated Y197 to either cysteine or alanine in the context of caspase-3(V266H) and procaspase-3(D_3A,V266H). We have also designed mutants that contained single mutations Y197A or Y197C to assess the influence of these substitutions on the activity of (pro)caspase-3. All mutants contained the C-terminal His-tag and were purified like the other mutant proteins.

Catalytic parameters of the (V266H,Y197A/C) caspase mutants

We have determined the catalytic parameters of the caspase mutants containing V266H/Y197A and V266H/Y197C mutations and we compared the obtained values with the values for the wild type and the control mutants. Except for caspase-3(V266H,Y197A), which was partially processed after purification, all other caspase mutants displayed two bands in the denaturating gel, equivalent to the small (~12.9 kDa) and the large subunit (~17.1 kDa) (Figure 23). For full processing, caspase-3(V266H,Y197A) required the digestion with Granzyme B (Figure 23A).

Figures 24A and 24B show the Michelis-Menten plots for Y197A and Y197C caspase mutants. The catalytic parameters for these mutants, K_m, k_{cat}, and k_{cat}/K_m, are listed in Table IV.

First, caspase-3(V266H,Y197A) displayed 0.1% of the wild-type activity before digestion with Granzyme B (data not shown). Following digestion with Granzyme B the enzyme recovered only ~1% of the activity (Table IV, Figure 24A), similar to that of caspase-3(V266H) (see Figure 16 C). This mutant underwent very little auto-processing at the high protein concentrations used during purification (~20 μM), and it could be considered practically inactive (Figure 23A). By

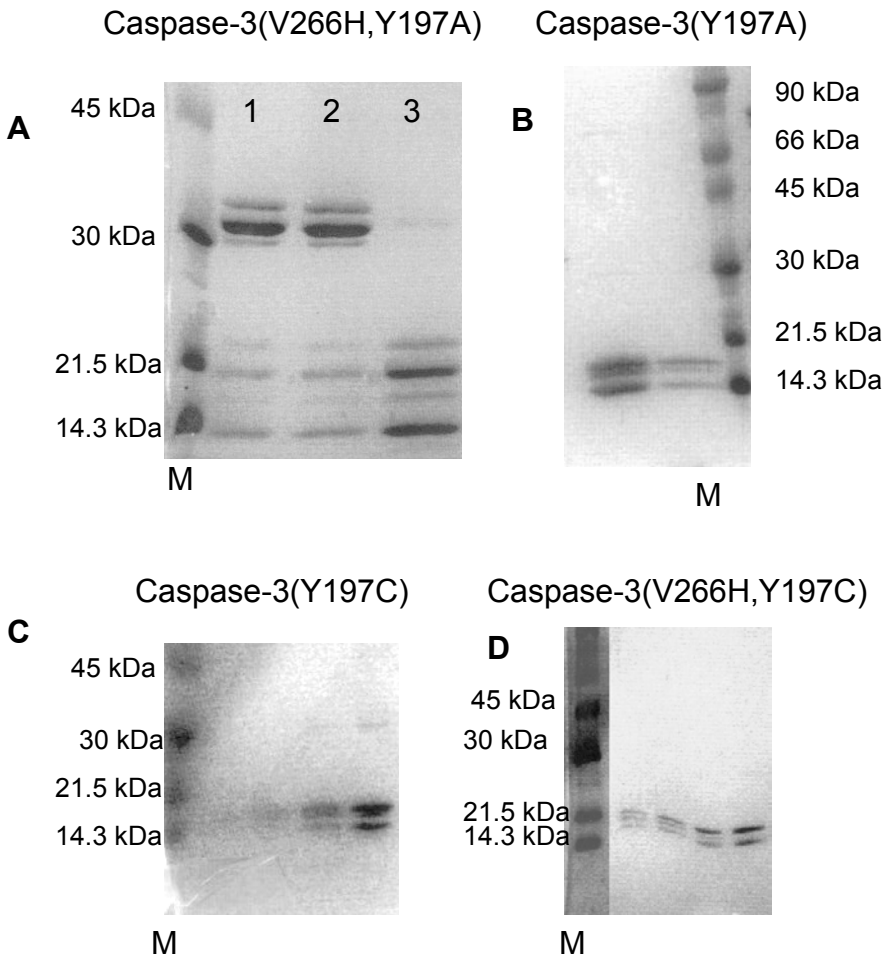

Figure 23. SDS-PAGE gels for Y197A and Y197C mutants. *Panel A*. Caspase-3(V266H,Y197A): lane 1, protein in Tris buffer following purification on anion exchange resin; lane 2, protein incubated in assay buffer; lane 3, protein digested with Granzyme B. *Panel B.* Caspase-3(Y197A) following purification on His-bind resin. *Panel C.* Caspase-3(Y197C) after purification on DEAE anion exchange. *Panel D*. Caspase-3(V266H,Y197C) after purification on DEAE anion exchange. "M" refers to molecular weight marker.

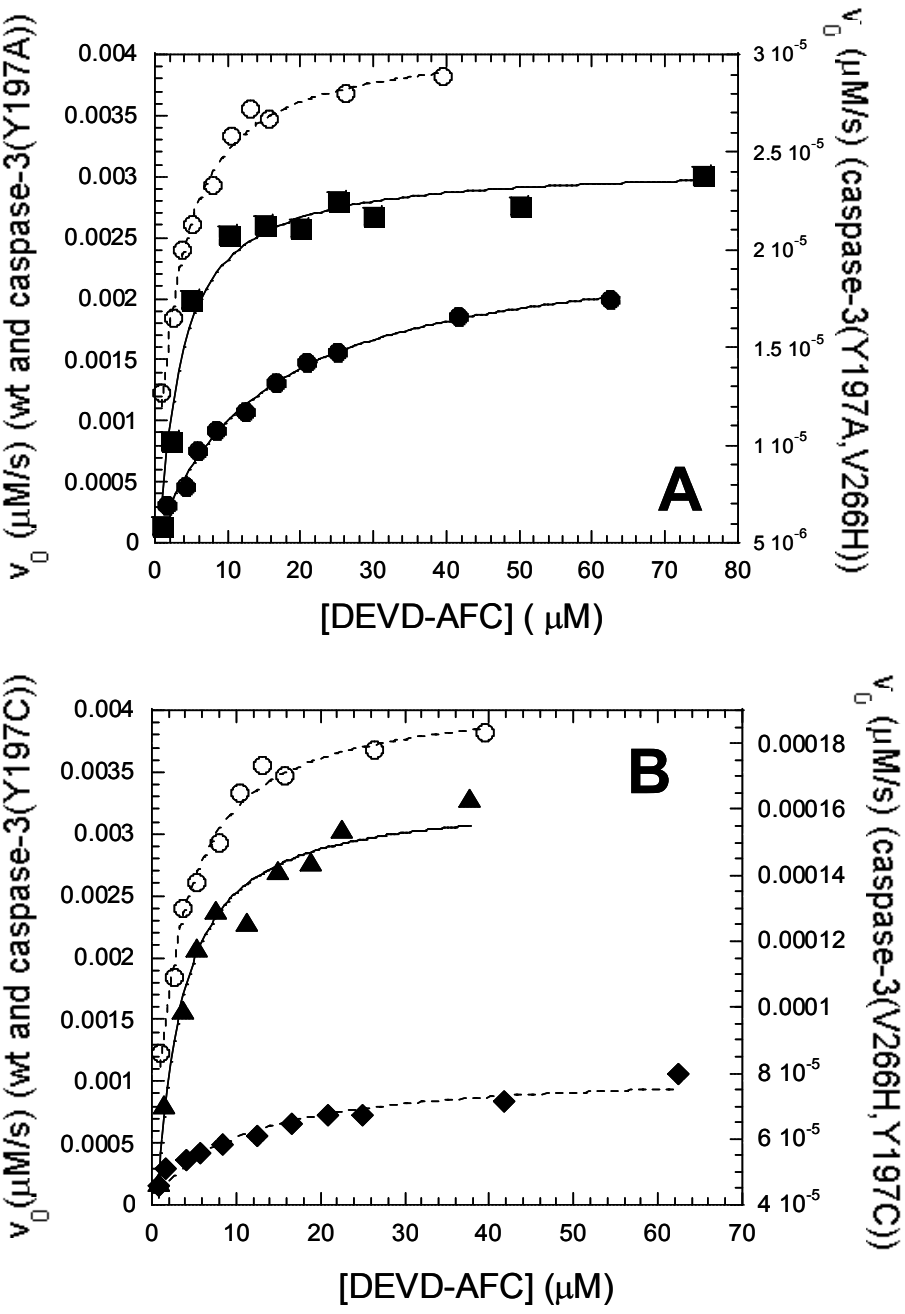

Figure 24. Michelis-Menten analysis for the Y197 caspase-3 mutants. *Panel A*. Caspase-3 (○), caspase-3(Y197A) (●), and caspase-3(Y197A,V266H) (■). *Panel B*. Caspase-3 (○), caspase-3(Y197C) (◆), and caspase-3(Y197C,V266H) (▲).

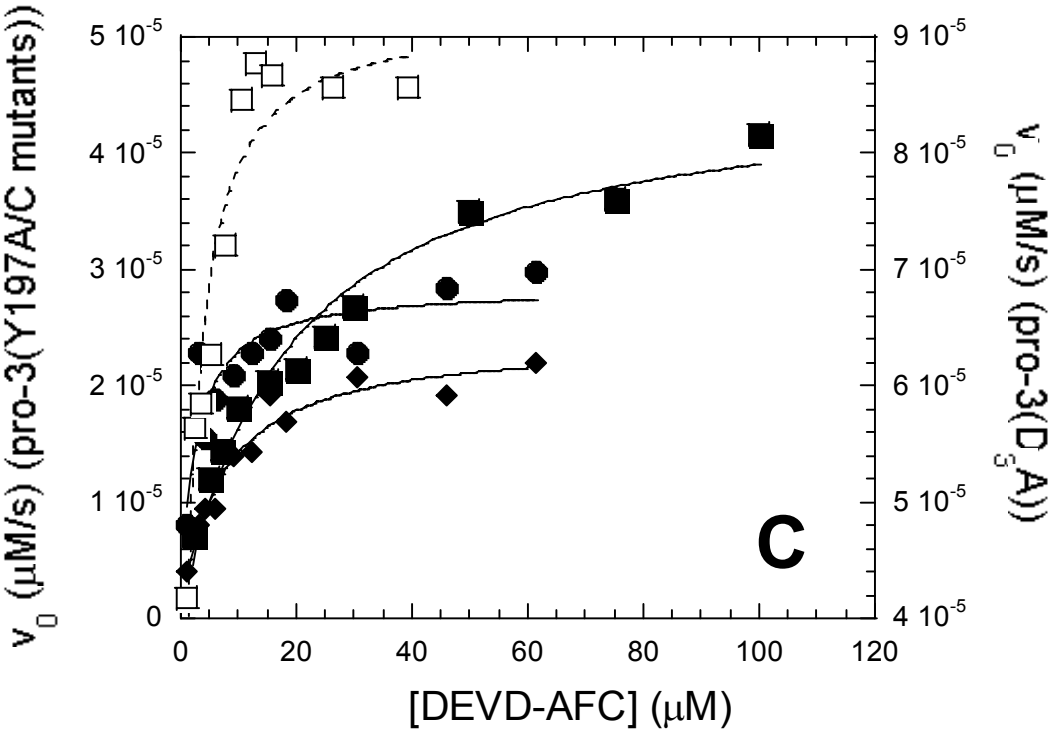

Figure 24. *Panel C*. Michelis-Menten analysis for the Y197 procaspase-3 mutants: procaspase-3(D_3A) (□), procaspase-3(D_3A,Y197A) (●), procaspase-3(D_3A,Y197C) (◆), and procaspase-3(D_3A,Y197A,V266H) (■). For the mutant procaspase-3(D_3A,Y197C,V266H), the catalytic properties could not be measured due to very low residual activity.

Table IV. Catalytic parameters for the caspases harboring V266H and/or Y197A/C mutations

	K_M (μM)	k_{cat} (s^{-1})	k_{cat}/K_M (M^{-1} s^{-1})
Caspase-3	2.2±0.5	0.4±0.05	1.8×10^{5}
Caspase-3(V266H,Y197C)	2.2±0.2	$(1.6\pm0.04)\times10^{-2}$	7.2×10^{3}
Caspase-3(V266H,Y197A)* (+ Granzyme B)	2.1±0.4	$(2.3\pm0.07)\times10^{-3}$	1.0×10^{3}
Caspase-3(Y197C)	9.8±2.2	$0.1\pm(8.3\times10^{-3})$	1.0×10^{4}
Caspase-3(Y197A)	14.9±1.0	$0.3\pm(7.2\times10^{-3})$	1.9×10^{4}

* This mutant is inactive prior to Granzyme B digestion.

contrast, caspase-3(V266H,Y197C) could cleave itself (Figure 23D) and displayed ~4% of the activity of mature caspase-3 (Table IV, Figure 24B). The inability of this mutant to recover full catalytic activity could be due to Y197C mutation. Table IV shows that both control caspases harboring Y197A and Y197C mutations have K_m values ~4-6 fold higher that the K_m values for wild-type, and k_{cat} values ~1-4 fold lower than caspase-3 values. Overall, single caspase-3 mutants, Y197 and Y197C, retain only 6-10% of caspase activity. Interestingly, the K_m values were not affected in the double mutants containing the V266H and Y197A/C substitutions (Table V).

By subtracting the Y197A and Y197C contributions to the decrease in the catalytic activity, the V266H mutant containing these mutations is able to recover ~52-72 % of the caspase-3 activity.

Catalytic parameters of the (V266H,Y197A/C) procaspase mutants

For the procaspase-3(D_3A,V266H) mutants, Y197 replacing with either alanine or cysteine has a different effect on the enzymatic activity in comparison with the caspase-3 mutants (Table V and Figure 24C). In this case, V266H/Y197C mutation did not seem to be successful in recovering the catalytic activity. The initial velocity of this mutant was extremely low, so that the catalytic parameters could not be determined. In contrast, the V266H/Y197A mutation could re-generate ~60% of the k_{cat} value of procaspase-3, although the substrate affinity was only partially recovered (Table V, Figure 24C). The K_m value for this mutant is ~5 fold higher, so that the overall catalytic efficiency of the procaspase-3(D_3A,V266H,Y197A) accounts

Table V. Catalytic parameters for the procaspases harboring V266H and/or Y197A mutations

	K_M (μM)	k_{cat} (s^{-1})	k_{cat}/K_M(M^{-1} s^{-1})
Pro-3(D_3A)	3.5±0.8	(3±0.14)x10^{-3}	8.6x10^2
Pro-3(D_3A,V266H,Y197C)	Inactive	Inactive	Inactive
Pro-3(D_3A,V266H,Y197A)	18.2±2.8	(1.8±0.42)×10^{-3}	1.0×10^2
Pro-3(D_3A,Y197C)	6.8±1.1	(9.6±0.5)×10^{-4}	1.4×10^2
Pro-3(D_3A,Y197A)	2.4±0.8	(1.14±0.08)×10^{-5}	4.2×10^2

for only ~12 % of the procaspase-3(D_3A) value (Table V). As far as it concerns the control enzymes, the procaspase activity is affected by the Y197C and Y197A single mutations (Table V). The overall catalytic efficiency decreases ~2 fold for the Y197A mutant, and ~7 fold for the Y197C mutation.

Overall, we can state that Y197A but not Y197C substitution is able to rescue partially the activity of procaspase-3(D_3A,V266H).

It is interesting comparing the substrate affinities of (pro)caspase containing different combinations of V266H, Y197A, and Y197C mutations (Tables IV and V). In the context of caspase single mutants, Y197C and Y197A mutations increase the K_m by ~4-7 fold. This does not occur in the context of procaspase single mutants or caspase double mutants. However, procaspase-3(D_3A,V266H,Y197A) has the highest K_m (~18 μM) of the mutants, and it is not clear why this combination of mutations generates low substrate affinity. One explanation is that in procaspase(D_3A,V266H) the K_m is very elevated (> 50 μM), which explains its inactivity. The introduced mutation Y197A but not Y197C could decrease this value to a range where the activity becomes measurable.

Taking all the results in account, Y197C mutation seems to be helpful for recovering the activity of caspase-3(V266H), while Y197A mutation seems more beneficial to the activity of procaspase-3(D_3A,V266H) than of caspase-3(V266H).

Limited proteolysis with trypsin

In order to test how the catalytic loops were affected by the tyrosine mutations, we subjected procaspase-3(D_3A,V266H,Y197A) and procaspase-3

A

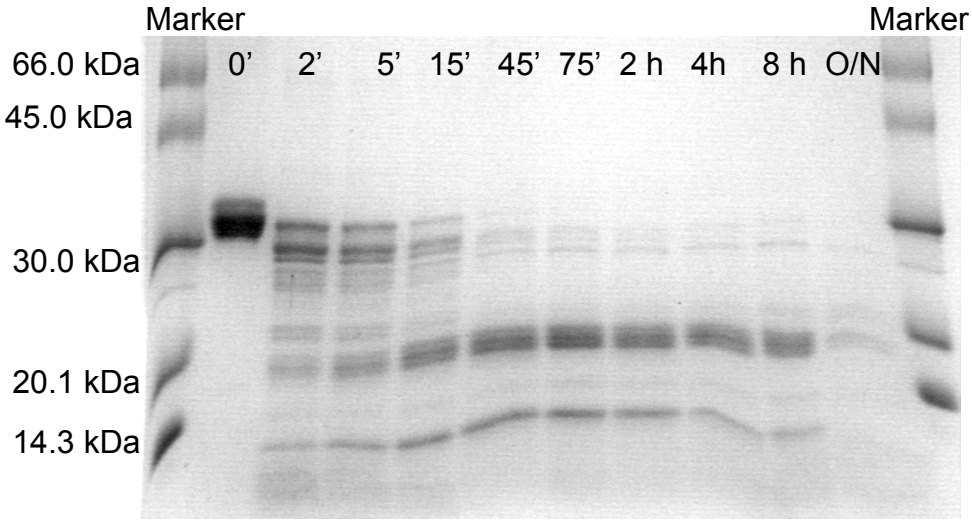

B.

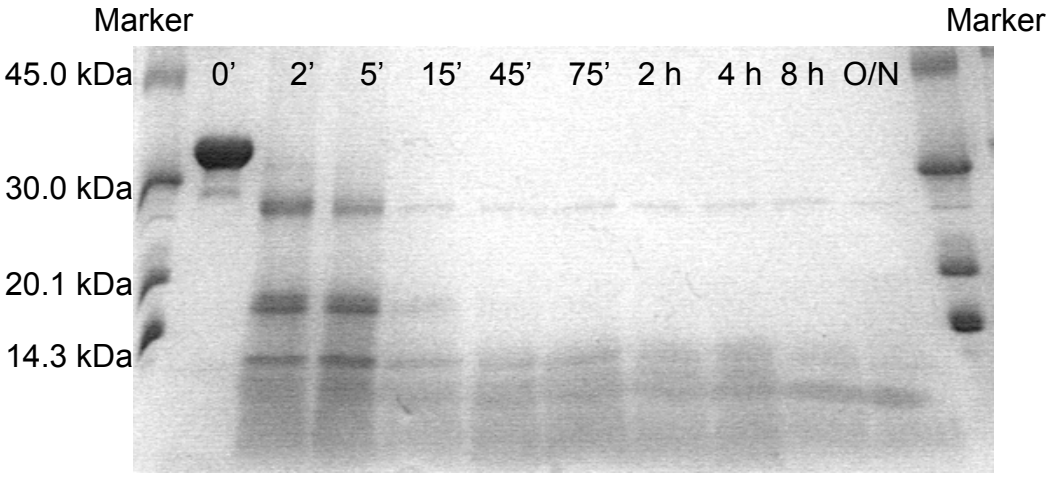

Figure 25. *Panel A.* Trypsin digestion of procaspase-3(D_3A,V266H,Y197A). *Panel B.* Trypsin digestion of procaspase-3(D_3A,V266H,Y197C). The full-length protein (32.6 kDa) does not show major cleavage at R207 as judged by the lack of the 23.3 kDa band (see Figure 19A). The mutation at Y197 recovers the overexposure of loop L3 due to the V266H mutation in the context of procaspase-3.

C.

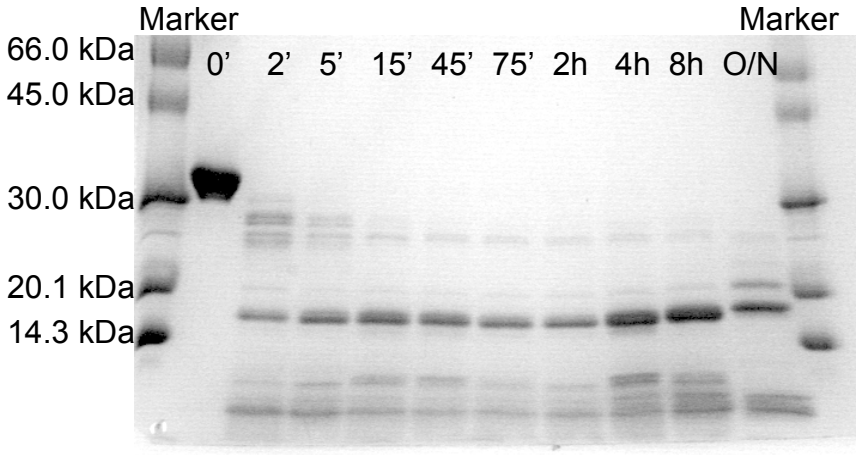

D.

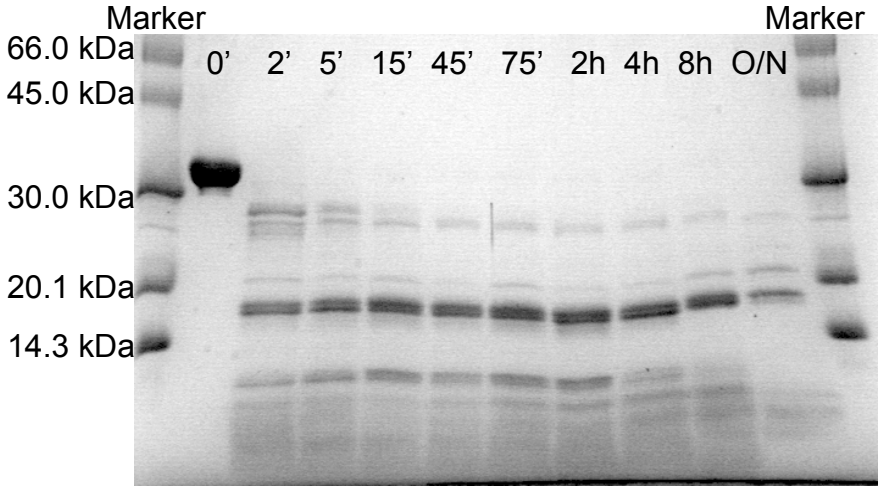

Figure 25. *Panel C.* Trypsin digestion of procaspase-3(D_3A,Y197C). *Panel D.* Trypsin digestion of procaspase-3(D_3A,Y197A). In the context of the procaspase-3(D_3A), the mutations at Y197 do not affect the cleavage at the loops L3 and L1.

E

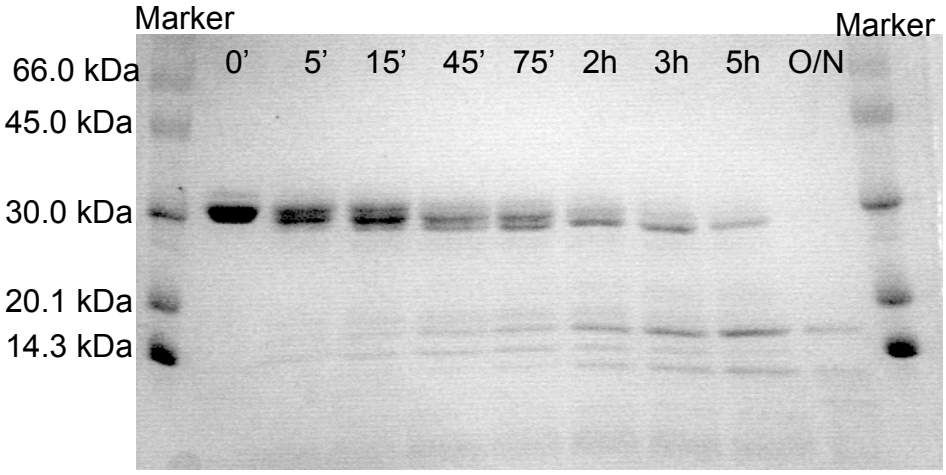

Figure 25. *Panel E.* V8 protease digestion of the procaspase-3(D_3A,V266H,Y197A). The absence of ~4 kDa bands indicates that the cleavage at D248/E253 residues within loop L4 does not occur in this mutant (see Figure 19E).

F

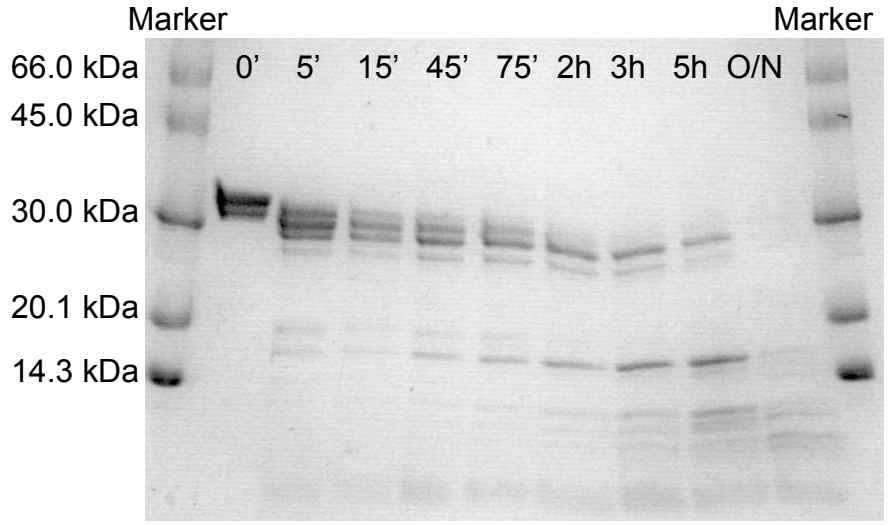

G.

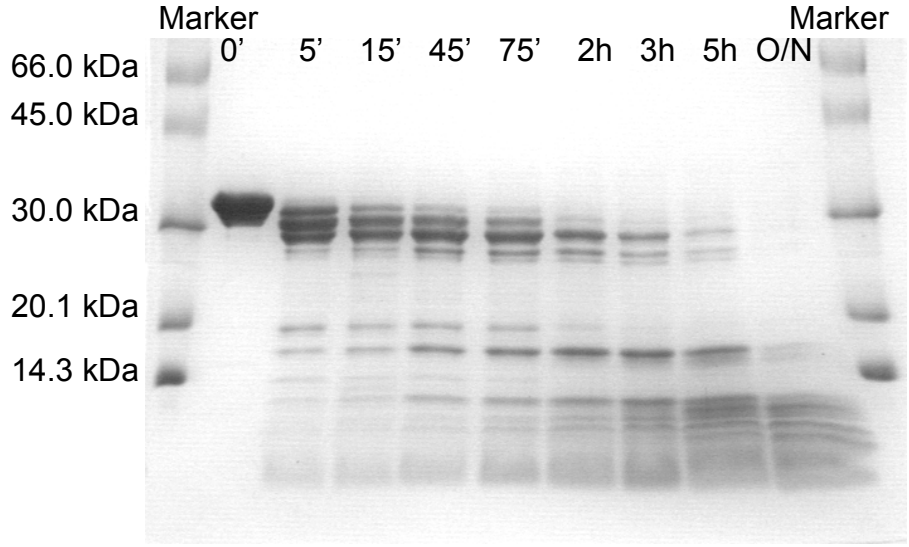

Figure 25. *Panel F.* V8 protease digestion of procaspase-3(D_3A,Y197C). *Panel G.* V8 protease digestion of procaspase-3(D_3A,Y197A). In the context of the procaspase-3(D_3A), the mutations at Y197 do not affect the cleavage at the loops L2, L4, and E98/E106.

(D_3A,V266H,Y197C) to trypsin proteolysis. This assay is important to show whether loop L3 is re-located at the position found in the wild-type procaspase-3 due to the Y197 substitution. We expect to see this the case of Y197A mutant, which is active. The results are shown in Figure 25A and 25B and are compared with the published data for procaspase-3 (92), and with the procaspase-3(C163S,V266H) limited proteolysis (Figure 19A). As shown, for both tested mutants the cleavage pattern is similar, although with a faster kinetics for the Y197C mutant. More importantly, in neither case a band corresponding to the 23 kDa fragment is observed in gel (Figures 25A and 25B). This demonstrates that the kinetics of R207 cleavage is slower than the kinetics of R64 cleavage, as it is the case for procaspase-3 (92). Therefore, loop L3 is no longer over-exposed when procaspase-3(D_3A,V266H) additionally acquires one of Y197A or Y197C mutation. However, it is not clear why procaspase-3(D_3A,V266H,Y197C) remains inactive. It is possible that loop L3 overexposure may not the cause for the inactivation of V266H mutants. Y197C mutation may only be beneficial to the structure and not to the catalysis.

Controls for the trypsin proteolysis assay are procaspase-3(D_3A,Y197C) and procaspase-3(D_3A,Y197A), shown in Figures 25C and 25D. As expected, the pattern and the kinetics of digestion are identical with the those of procaspase-3 (92). Hence, Y197A/C mutations do not affect the protease accessibility to the loops L1 and L3 from procaspase.

Trypsin digestion assays were also performed with the caspase form of the described mutants (data not shown). Except for caspase-3(V266H,Y197C), which showed a slightly reduced kinetics of cleavage at R64, the digestion pattern and the

kinetics for the other mutants, caspase-3(V266H,Y197A), caspase-3(Y197A), and caspase-3(Y197C)) (data not shown), were identical with the caspase-3 cleavage pattern and kinetics (92).

Limited proteolysis with V8 protease

V8 proteolysis was performed with the procaspase versions of the Y197 mutants (Figure 25E-G). In comparison with procaspase-3 (92), procaspase-3(D_3A,V266H,Y197A) displayed a faster cleavage of the pro-domain region (E25), a slower cleavage kinetics at the residues E98/E106 and E173/D190, and no cleavage at E248/D253 (Figure 25E). This means that loop L4, the inter-subunit linker, as well as the helix containing E98/E106 have been affected. The single mutations Y197A and Y197C in the context of the procaspase-3(D_3A) did not influence the cleavage at these residues as shown by Figure 25F and 25G.

Although these experiments do not give clear indication of what happens with the (pro)caspase-3 structure, we believe that the Y197 substitution recovers only partially the activity of the V266H mutants. Y197 is conserved in many caspases (35). The hydroxyl group of Y197 is probably involved in hydrogen bonds in caspase but not procaspase, and this explains the need of cysteine instead of alanine for auto-activation of caspase-3(V266H,Y197C). One possible partner for this interaction is the carbonyl group of F158, conserved in all caspases except caspases-1, -4, -5, and -13, where this residue is an isoleucine (9). F158 is positioned on the β-strand 5 from the small subunit (see Figure 4). Indeed, in procaspase-7, the equivalent residue of Y197 is rotated 90^o relative to the position in

the caspase, and the hydrogen bonding with F158 cannot occur (27, 30). In caspase-1, Y197 is replaced by a cysteine (C331), which is at large distance of I280, the equivalent residue of F158 in caspase-3 (93). The sulphydryl group of C331 is within hydrogen bond distance of the carbonyl group of T388, located in the dimer interface (93) (see Figure 6B). It is possible that in the case of caspase-1, formation of the hydrogen bond between C331 and interface T338 occurs both in the zymogen and the mature form.

B. V266R designed mutants

In order to test the proposed model for the pseudo-activation of procaspase-3(D_3A,V266E), we have designed mutants that replace the valine 266 from the interface with arginine. In this case, the new introduced R266 should prevent proper rotation/insertion of R164 due to electrostatic repulsion (see Figures 22A and 22B). This may result in improper insertion of loops L3 or L2. We expect to observe lack of activity of the resulting mutants and possibly dissociation to monomers.

The V266R mutation has been introduced in the context of caspase-3, procaspase-3(C163S), and procaspase-3(D_3A), as C-terminal histidine-tagged proteins (see Figure 14). Caspase-3(V266R) expression in the soluble fraction was very poor, and the amount of the purified protein was insufficient for fluorescence, proteolysis and circular dichroism studies. For this mutant, only the activity studies could be carried out.

Catalytic parameters for V266R interface mutants

First, we have remarked that during purification of caspase-3(V266R) the protein underwent complete auto-maturation to the small and large subunits, like V266E mutant (data not shown). This is indicative of sufficient intrinsic enzymatic activity that allows the cleavage, in contrast with the inactive V266H mutant. Secondly, we noticed that caspase-3(V266R) was highly unstable at freeze-thaw cycles and also lost some enzymatic activity by storage at -20 ^{o}C.

For determining the catalytic parameters, we have used freshly purified caspase-3(V266R) and procaspase-3(D_3A,V266R) that were not subjected to freezing temperature. The results are displayed in Figure 26A and Table VI.

As shown, the V266R mutation does not eliminate the catalytic activity of caspase or of procaspase-3 (Figure 25A and Table VI). The k_{cat} value for caspase-3(V266R) is only ~4.5 fold less than k_{cat} for the wild-type. Totally unexpected is the ~26-fold increase in the k_{cat} value of procaspase-3(D_3A,V266R) in comparison with the value for procaspase-3(D_3A) (Figure 25A and Table VI). This feature also characterizes procaspase-3(D_3A,V266E) (Table III). In addition, the k_{cat} values of the V266R mutants are similar, and they are comparable with the values for the V266E mutants (Tables III and IV). Distinctly different, the K_m constants for V266R mutants exceed the values acquired for caspase-3 and V266E mutants by ~5-7 fold. This indicates that the effect of V266R interface substitution is translated to the catalytic loops and affects both catalysis and binding of the substrate.

We have also determined the effect of pH upon the initial velocity of the V266R mutants. The curves are shown in Figure 26B, along with the data for the

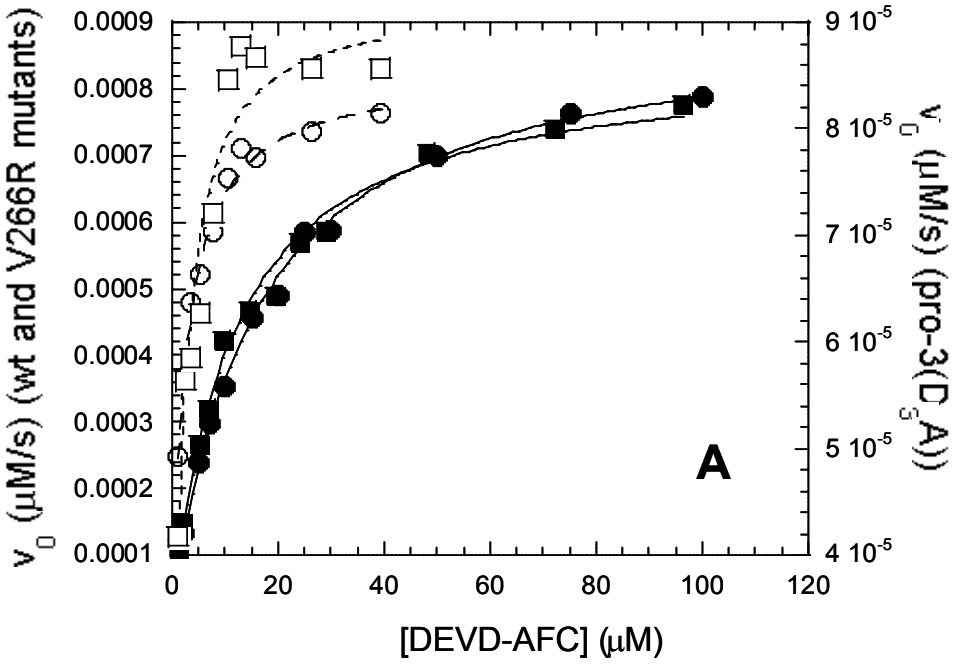

Figure 26. *Panel A.* Michelis-Menten analysis of the V266R mutants: caspase-3 (○) (1 nM), caspase-3(V266R) (●) (10 nM), procaspase-3(D_3A) (□) (10 nM), procaspase-3(D_3A,V266R) (■) (10 nM).

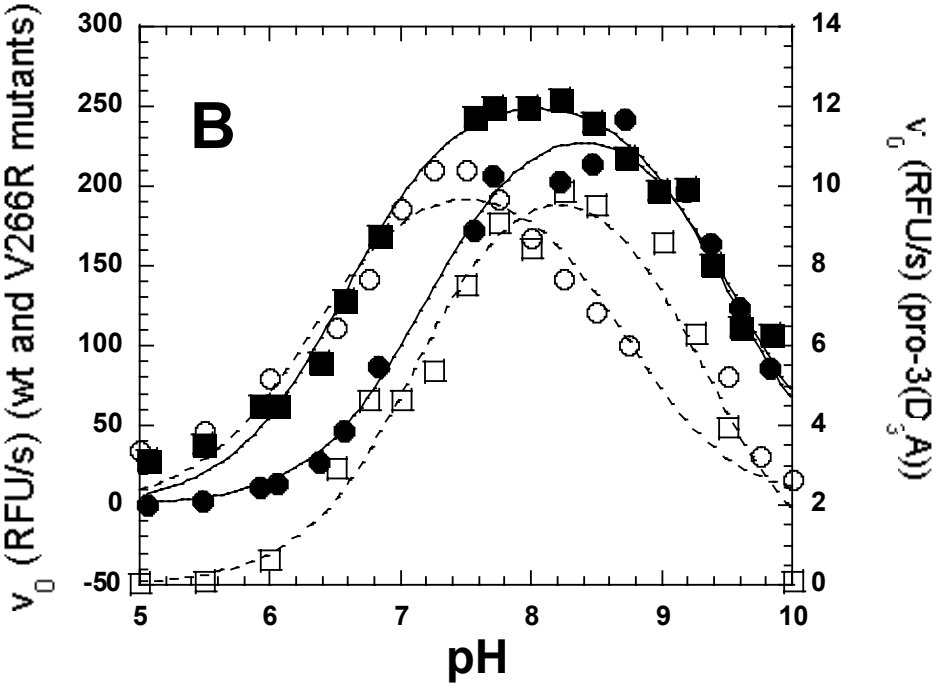

Figure 26. *Panel B*. Initial velocity dependence versus pH: caspase-3 (○) (1 nM), caspase-3(V266R) (●) (25 nM), procaspase-3(D_3A) (□) (10 nM), procaspase-3(D_3A, V266R) (■) (25 nM). The plot scaling does not reflect the working protein concentrations.

Table VI. Catalytic properties of the V266R mutants

	Caspase-3 (wt)	Caspase-3 (V266R)	Procaspase-3 (D_3A)	Procaspase-3 (D_3A, V266R)
K_M (μM)	2.2±0.5	14.8±0.8	3.5±0.8	10.9±1.0
k_{cat} (s^{-1})	0.4±0.05	(9.0±0.2)x10^{-2}	(3±0.14)x10^{-3}	(8.0±0.2)x10^{-2}
k_{cat}/K_M ($M^{-1}s^{-1}$)	1.8x10^5	6.0x10^3	8.6x10^2	7.3x10^3
pK_{a1}	6.3±0.14	7.1±0.06	7.3±0.10	6.5±0.04
pK_{a2}	8.5±0.14	9.5±0.05	9.1±0.11	9.5±0.04
Optimal pH	7.2-7.8	7.6-9.3	8.0-8.5	7.3-8.7

wild-type proteins. The optimal pH for caspase-3(V266R) is very broad (pH 7.6-9.3), and is different than the optimal pH for procaspase-3(D_3A,V266R) (pH 7.3-8.7) (Table VI). Regarding the pK_{a1} value of the first transition, V266R procaspase mutant is comparable with caspase-3 (6.5 versus 6.3), while V266R caspase is comparable with the procaspase(D_3A) (7.1 versus 7.3). The pK_{a2} values for the second transition are ~9.5 for both V266R mutants, slightly higher that of the zymogen (~9.1).

The difference in the bell-shapes profiles of the V266R mutants and wild-type proteins indicates that there is an important structural change in the environment of both C163 and H121 from the active site, as both pK_{a1} and pK_{a2} are affected. Moreover, following the inter-subunit cleavage, the environment around the C163 changes and becomes similar to the environment within procaspase-3 (Figure 26B).

Oligomeric properties at high concentration

We then examined the oligomeric properties of the V266R mutants by using cross-linking experiments with DMS and the results are shown in Figure 27A and 27B. Figures 27A (lanes 5-6) and 27B (lanes 2-3) show that, in the presence of DMS, procaspase-3(C163S,V266R) is able to form cross-linked dimers. The protein concentration used in the assay was ~10 μM. However, in comparison with procaspase-3(C163S) (Figure 27A, lanes 2-3, and Figure 27B, lane 5), the efficiency of the cross-linking reaction is lower. The intensity of the bands corresponding to the dimer is ~3-4 times less in case of the mutant. This suggests that procaspase-3(C163S,V266R) may be a mixture of monomer and dimer at pH 7.5. We have done

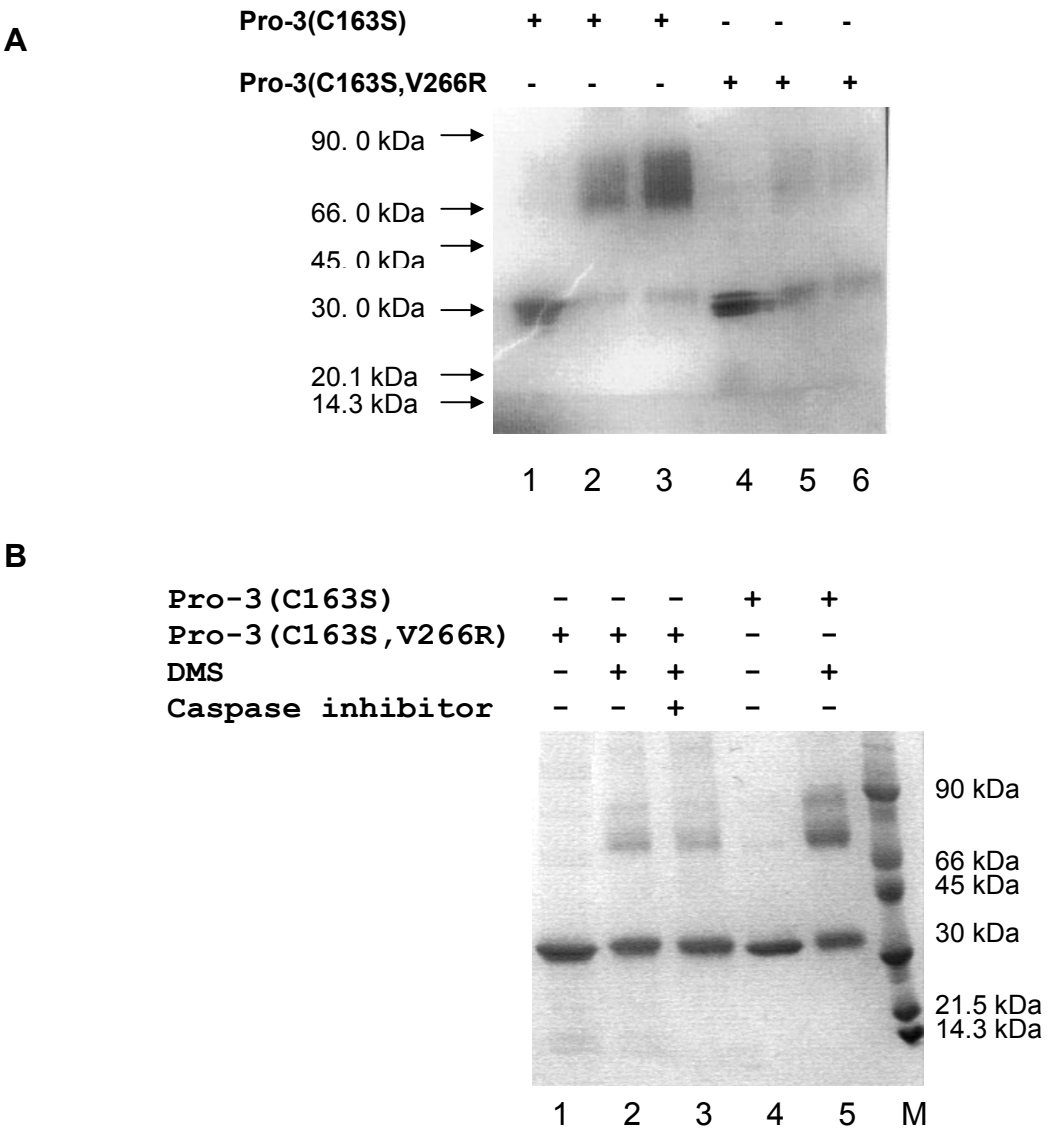

Figure 27. Cross-linking experiments with DMS. *Panel A*. Procaspase-3(C163S) (32.6 kDa) (lanes 1-3) and procaspase-3(C163S,V266R) (32.7 kDa) (lanes 4-6) were cross-linked with DMS and the reaction products were analyzed by 4-25% SDS-PAGE. The DMS:protein ratios are 10:1 (+) and 20:1 (++). *Panel B.* Same experiments were performed in presence of caspase-3 inhibitor, Ac-DAVD-FMK (lane 3). "M" refers to molecular weight marker.

C

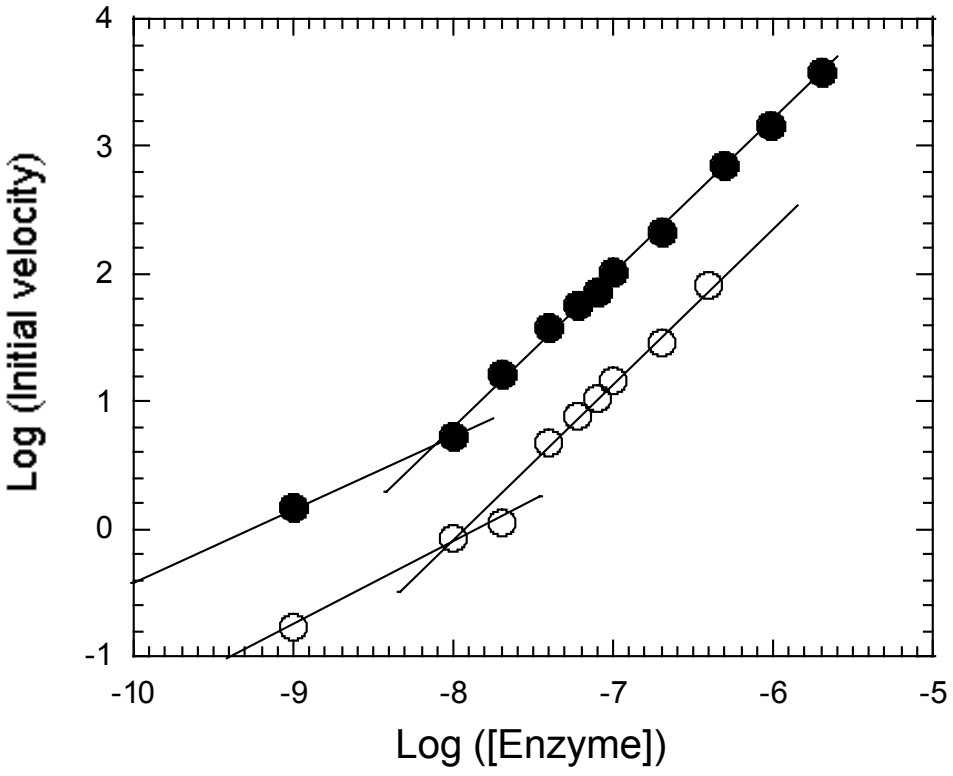

Figure 27. *Panel C.* Initial velocity dependence on the enzyme concentration for procaspase-3(D_3A,V266R) (●) and caspase-3(V266R) (○). The enzyme concentration is in molar. For each mutant, the graph can be fit to two different linear equations with different slopes. The final concentration of substrate used in this assay is ~100 μM.

the same experiment in the presence of caspase-3 inhibitor, Ac-DAVD-CMK (Figure 27B, lane 3), to see whether the inhibitor shifts the monomer to the dimeric state. The reaction did not occur with a better efficiency (Figure 27B, lanes 2 and 3). In the case of monomer caspase-9, addition of the substrate or inhibitor facilitates formation of the dimer, which represents the active form of caspase-9 (29). We cannot rule out the possibility that DMS does not bind efficiently the V266R mutant due to changes on the surface of the protein.

Work in our lab has analyzed procaspase-3(C163S,V266R) by size exclusion chromatography at ~14 μM final protein concentration at pH 6 and pH 7.8 (data not shown). At both pH values, the protein eluted from the sizing column in a single peak fraction corresponding to a molecular weight value between the dimer and monomer procaspase. This feature is characteristic for the proteins occurring at the monomer-dimer equilibrium. More work is necessary to establish the K_d of dimer dissociation for the V266R mutants.

At least in the micromolar range of protein concentration, procaspase-3(C163S,V266R) forms dimers.

Oligomeric properties at low concentrations

We have performed enzymatic dilution assays by measuring the initial velocity at different protein concentrations of caspase-3(V266R) or procaspase-3(D_3A,V266R). The same experiments showed that the activity of V266E mutants decreased linearly with the protein concentration (Figure 18A), likely suggesting that the proteins are dimers over the investigated range (low nanomolar to low

micromolar). The enzymatic assays of V266R mutants versus protein concentration are shown in Figure 27C. The experiments shown in this section used enzyme that was subjected to freeze-thaw cycles.

For both V266R mutants, the plot of the log(initial velocity) versus log(protein concentration) no longer can be fit with one linear equation (Figure 27C). At higher enzyme concentrations (>200 nM), the activity increases non-proportionally. Assuming that monomeric mutants lack enzymatic activity, we suggest that this feature is the result of populating the dimeric state of V266R as the concentration increases. Therefore, it is possible that V266R mutation destabilizes the monomer association at low protein concentrations. We base this statement on two observations: 1) First, Table VI shows that the activities of the V266R mutants are comparable, while in this assay caspase-3(V266R) displays ~7.5 fold less activity than the (D_3A,V266R) mutant (Figure 27C). This is due to the fact that the activity of the caspase-3(V266R) decreases in time much faster that the activity of the D_3A mutant, i.e. due to dimer dissociation. 2) Secondly, it is possible that during protein expression only the dimer form of this protein remains in the soluble fraction, while the monomer accumulates in high amounts into the inclusion bodies. This is the case for procaspase-3(C163S,V266E), which is a monomer when it is separated from the insoluble fraction, as shown by analytical ultra-centrifugation (Figure 15G).

The catalytic parameters determined in Table VI were calculated at the final enzyme concentration of 10 nM. This concentration is probably much below the K_d of dimer dissociation, if the plot from Figure 27C is indeed related to dimer dissociation. The real catalytic parameters of the V266R mutants may be much

higher, comparable with caspase-3. At the working concentration of 10 nM only a small fraction of the active dimer may be populated. However, it is also possible that the presence of the substrate induces dimerization of the V266R mutants, like in the case of caspase-9 (29). As the initial velocity is measured in the first 100-300 s following the substrate addition, the time the enzymes spends in the presence of substrate may not be sufficient for complete protein dimerization. Future studies using the irreversible inhibitor Ac-DAVD-CMK bound on the procaspase-3(D_3A,V266R) and assays like native gel Western Blotting and sizing column chromatography will confirm whether the inhibitor induces the dimerization.

A less likely possibility is that the monomer of caspase-3(V266R) is also active, although with lower activity. Further work is required to demonstrate this hypothesis. Monomeric caspases displaying catalytic activity have never been reported in the literature.

Limited proteolysis with trypsin and V8 protease

The technique of limited proteolysis with trypsin and V8 protease was used yet again to check the eventual modifications on the surface of procaspase-3(C163S,V266R).

In the case of trypsin digestion studies, the proteolysis pattern is shown in Figure 28A. The results are compared with the cleavage of procaspase-3(C163S) (92). Trypsin cleaves this mutant at the same sites and in the same order as in procaspase-3(C163S): K19, R64, and R207, except that the kinetics of cleavage at R207 is slower ($t_{1/2}$ ~7 min versus $t_{1/2}$ < 1 min). The result may explain the increase

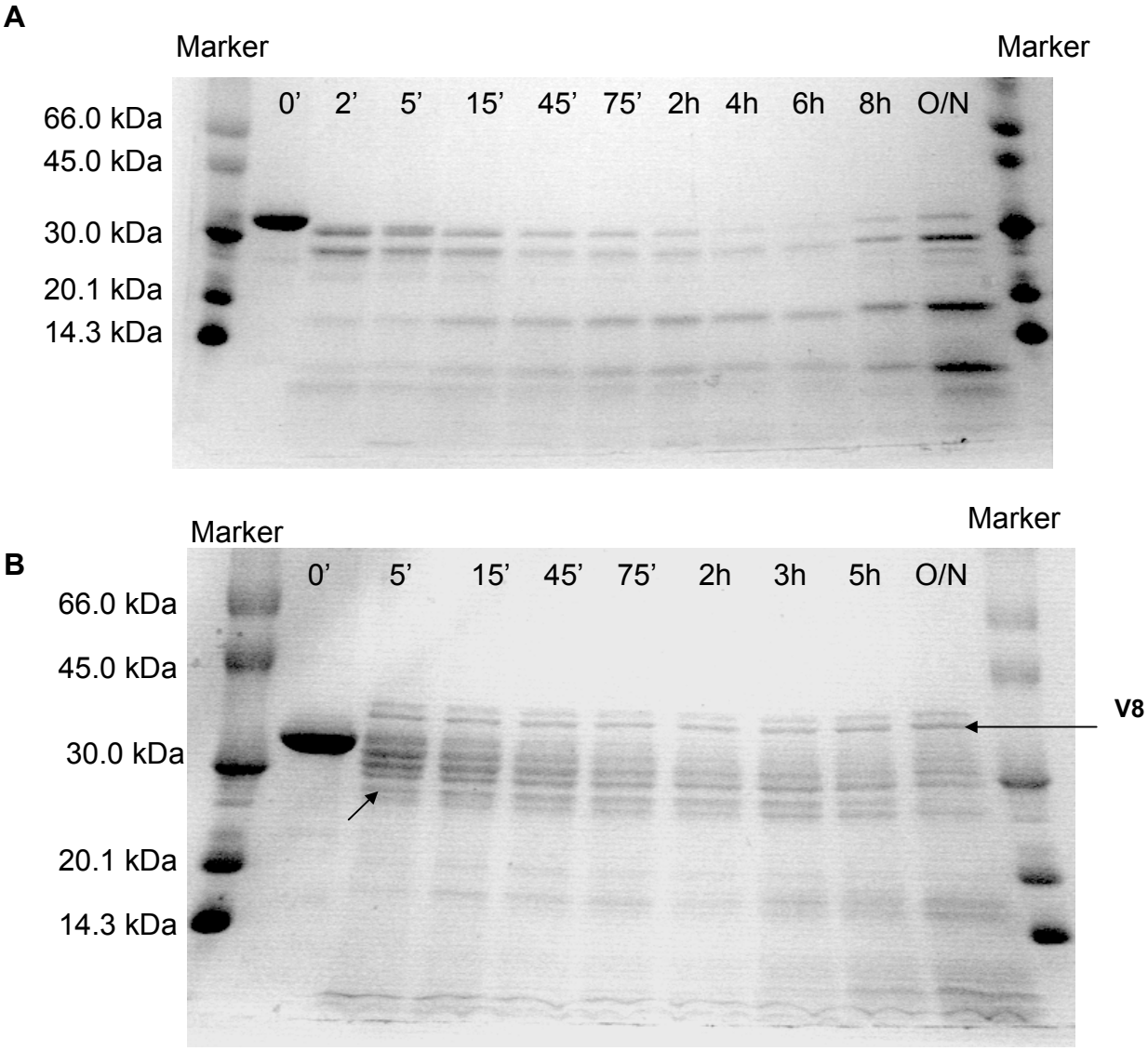

Figure 28. *Panel A*. Trypsin digestion of procaspase-3(C163S,V266R). *Panel B*. V8 protease digestion of procaspase-3(C163S,V266R). Procaspase-3(C163S,V266R) presents the same cleavage pattern as procaspase-3(C163S) (92), except for two additional cleavages by V8 protease pointed by the black arrow (~23kDa).

in the K_m from the activity studies (Table VI), as a misaligned R207 could affect the binding of the substrate.

In the case of V8 protease digestion, the results are shown in Figure 28B. In comparison with procaspase-3(C163S) (92) the cleavage pattern is the same, except for two additional cleavages that generate ~23-26 kDa bands (marked with an arrow on Figure 28B). These sites are not yet characterized. Judging from the size of the bands and considering the other cleavages, the only possibilities are the N-terminus proteolysis at D40 or E43, and the C-terminus proteolysis at D228. All of these residues are exposed in the structure of caspase-3 (not shown). Fragment D40/E43-D248 has a molecular weight of ~23.5 kDa, and fragment E25-D228 has a molecular weight of ~22.9 kDa. Spatially, all these residues come close to each other in a region opposite from the active site (26). In case that procaspase(C163S,V266R) is partially monomeric, the cleavage at D228 is favored due to exposure of the dimer interface to the solvent.

Overall, it seems that the V266R mutation slightly relaxes the structure of procaspase-3 at the C- or N-terminus and changes the exposure of loop L3.

Circular dichroism and quenching studies

The influence of the V266R mutation on the general folding of procaspase-3 has been investigated by using circular dichroism (CD). Figure 29A displays the far-UV CD spectrum, and Figure 29B shows the near-UV CD spectrum. The secondary structure content monitored by far-UV CD does not seem to be much affected by the V266R mutation (Figure 29A). The spectrum overlaps well with the control spectrum

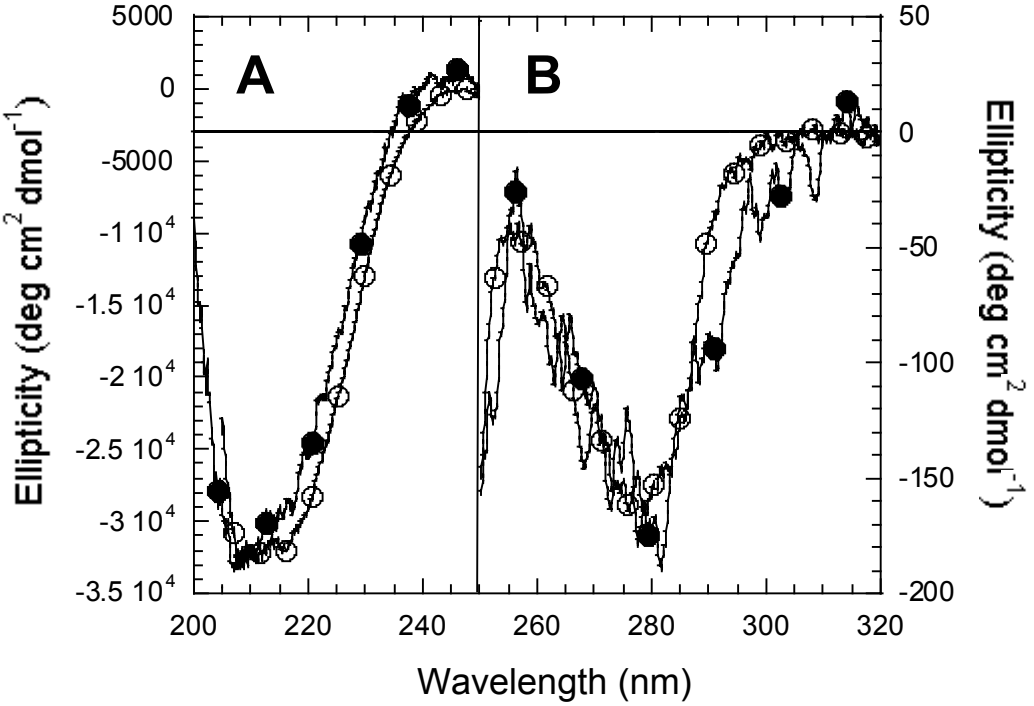

Figure 29. Far-UV circular dichroism (FUV-CD) (*Panel A*), and Near-UV circular dichroism (NUV-CD) (*Panel B*) for procaspase-3(C163S) (○) and procaspase-3(C163S,V266R) (●).

C

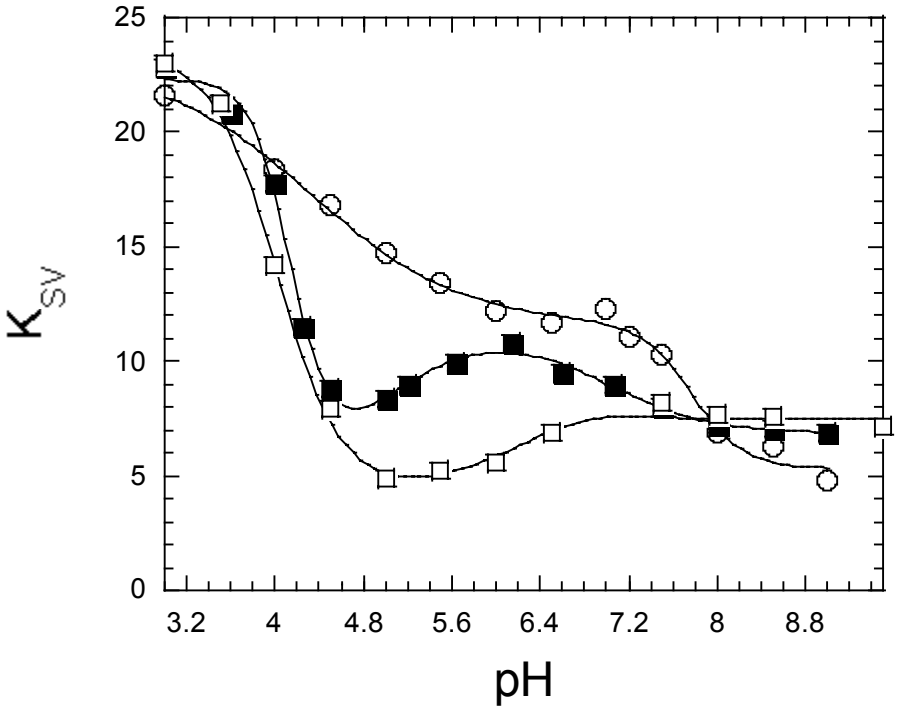

Figure 29. *Panel C*. Potassium Iodide quenching versus pH for procaspase-3(C163S) (○), procaspase-3(C163S,V266E) (□), and procaspase-3(C163S,V266R) (■).

(procaspase-3(C163S)), except for a somewhat lower signal minimum around 218 nm. This can be interpreted as loss in helical structure in the favor of beta structure or random coil formation. In case of the tertiary structure, procaspase-3(C163S,V266R) display a red shift in the signal minimum from 278 nm to 282 nm, similar with the red shift observed for procaspase-3(C163S,V266E) (Figure 21B). Again, this may be due to overexposure of the aromatic residues around the catalytic site.

In order to test the accessibility of the aromatic residues in the V266R mutant, we have carried out iodide quenching of the fluorescence emission. Potassium iodide quenching tests the electrostatic environment around the tryptophanyl residues. As it can be observed in Figure 29C, the effect of KI quenching on the fluorescence of procaspase-3(C163S,V266R) is opposite to the effect on the procaspase-3(C163S,V266E) over the pH range of 4.6-5.5 and is similar over pH 3.0-4.6. Three transitions describe the plot of K_{SV} versus pH for the V266R mutant. First transition shows a steep decrease in the quenching constants over pH 3.0 to 4.6 (from K_{SV} ~23 to ~8), and has a pK_a of ~4.1±0.08. The second transition, between pH 4.8-6.5, slightly increases the K_{SV}, and has a pK_a of ~5.0±1.2. Between pH 6.5-9.0, the third transition (pK_a of ~7.2) brings the K_{SV} value down to ~7, a usual value for procaspase-3 mutants.

Overall, the secondary and tertiary structure of the procaspase-3(C163S,V266R) is not significantly affected by the interface mutation, and resembles more the structure of procaspase-3(C163S,V266E) than of the procaspase-3(C163S). However, the electrostatic environment and the positioning of

the tryptophans in the V266R mutant are different than in the V266E mutant. It is possible that this difference comes from the re-location of the R207 resdiue.

Once again, it is remarkable to acknowledge that V266R substitution in the dimer interface preserves so many features of the wild type (pro)caspase, including the catalytic activity and the oligomeric properties. A model that could explain both characteristics is based on the stabilization of the interface R266 by one of the nearby negatively charged residues. A good candidate is E124, which is positioned close to the interface (Figures 22B and 22C). The local rearrangements of the loops due to the R164 lacking the E124 natural partner may result into the pseudo-activation of the procaspase-3 containing V266R mutation. More research is required to prove this mechanism of activation.

In conclusion, the V266R mutation in the dimer interface did not confirm the proposed model for the activation of procaspase-3 containing V266E mutation.

IV. Folding and stability of procaspase-3(C163S,V266H)

We showed that the V266H interface mutation affects the enzymatic activity of the (pro)caspase-3 without affecting the oligomeric properties of the protein. At least at neutral pH, the dimer stability seems to be the unaffected by the V266H mutation. Size exclusion chromatography studies suggest that at lower pH (pH<5.5), procaspase-3 dimer harboring theV266H mutation is more susceptible to dissociation than the wild-type dimer (data not shown). This may be due to the protonation of the interface H266 that increases the chances for dimer dissociation, thereby decreasing the procaspase dimer stability.

Our lab has characterized well the folding and assembly of procaspase-3(C163S) over the pH range of 4.0 to 9.0 (65). The dimer dissociation is a folding event, and the stability of the dimer contributes with ~75% of the conformational free energy of the protein (18 kcal/mol of 24 kcal/mol) (66).

Here we investigate the effect of the interface substitution V266H upon the thermodynamic parameters for unfolding, ΔG and m values, of the procaspase-3(C163S) over the pH range from 4.0 to 8.0.

Kinetics of unfolding of procaspase-3(C163S,V266H) in urea

First, we have determined the time required for procaspase-3(C163S,V266H) to unfold in urea at different pH values. As determined previously in our lab, the half-time for unfolding ($t_{1/2}$) of procaspase-3 in 8 M urea at pH 7.2 and 25 ^{o}C is ~8.5 h (not published).

The unfolding $t_{1/2}$ of procaspase-3(C163S,V266H) at different pHs was determined by monitoring the fluorescence emission and the circular dichroism signal versus the unfolding time of the denatured samples. The protein was unfolded in 9.6 M urea (pH 6.5 to 8.0), and respectively in 5 M urea (pH 4.0-6.0) and the spectral signals were monitored in time. For the low pH range, 5 M urea is the denaturant concentration that characterizes the middle of the unfolding transition.

The results for the kinetics of unfolding are shown in Figure 30, and the unfolding $t_{1/2}$ values are presented in Table VII. In the case of unfolding at pH 8.0 (Figure 30A), 7.2 (Figure 30B), and 6.5 (Figure 30C), it is obvious that the protein requires several days to unfold and equilibrate in 9.6 M urea solution. The $t_{1/2}$ values for these pH-s are ~24 h (pH 8.0), ~13 h (pH 7.2), and ~7 h (pH 6.5) (Table VII). Especially for the unfolding at pH 8 and 7.2, these $t_{1/2}$ values are very high, unusual for most proteins, and characteristic for fibrous proteins. (94). The chosen incubation times for the unfolding equilibrium studies were 4 days for pH 6.5, 6 days for pH 7.2 and 7 days for pH 8.0. For denaturation at pH<6.5, the half-time of unfolding decreases considerably to ~4-6 h (see Table VII and Figure 30 D-I). Although at low pH the unfolding $t_{1/2}$ may have not been accurately determined due to insufficient measurements during the first 24 h, we considered that an incubation time ~24 h is adequate for the unfolding equilibrium studies under these conditions.

Therefore, procaspase-3(C163S,V266H) necessitates much longer time and higher denaturant concentration for complete unfolding in urea in comparison with procaspase-3(C163S). It seems that the V266H mutation significantly stabilizes procaspase-3 versus chemical denaturation. Performing denaturation equilibrium

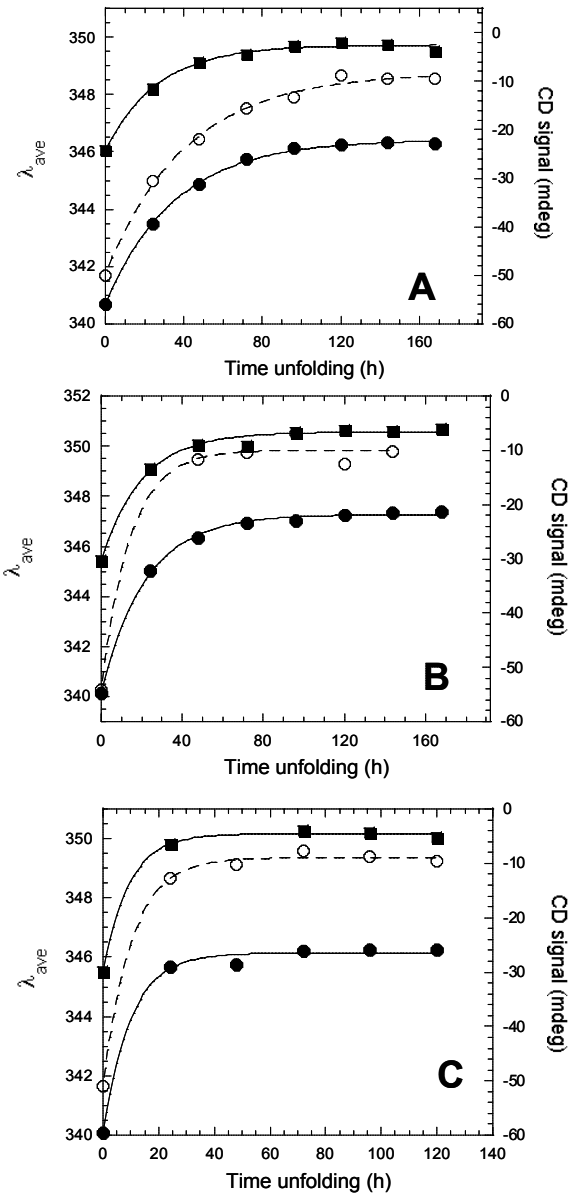

Figure 30. Kinetics of unfolding of procaspase-3(C163S,V266H) at pH 8.0 (*Panel A*), pH 7.2 (*Panel B*), and pH 6.5 (*Panel C*). Protein was unfolded in 9.6 M urea. The average emission wavelength after excitation at 280 nm (●) or 295 nm (■) and the CD signal at 228 nm (○) were monitored in solutions.

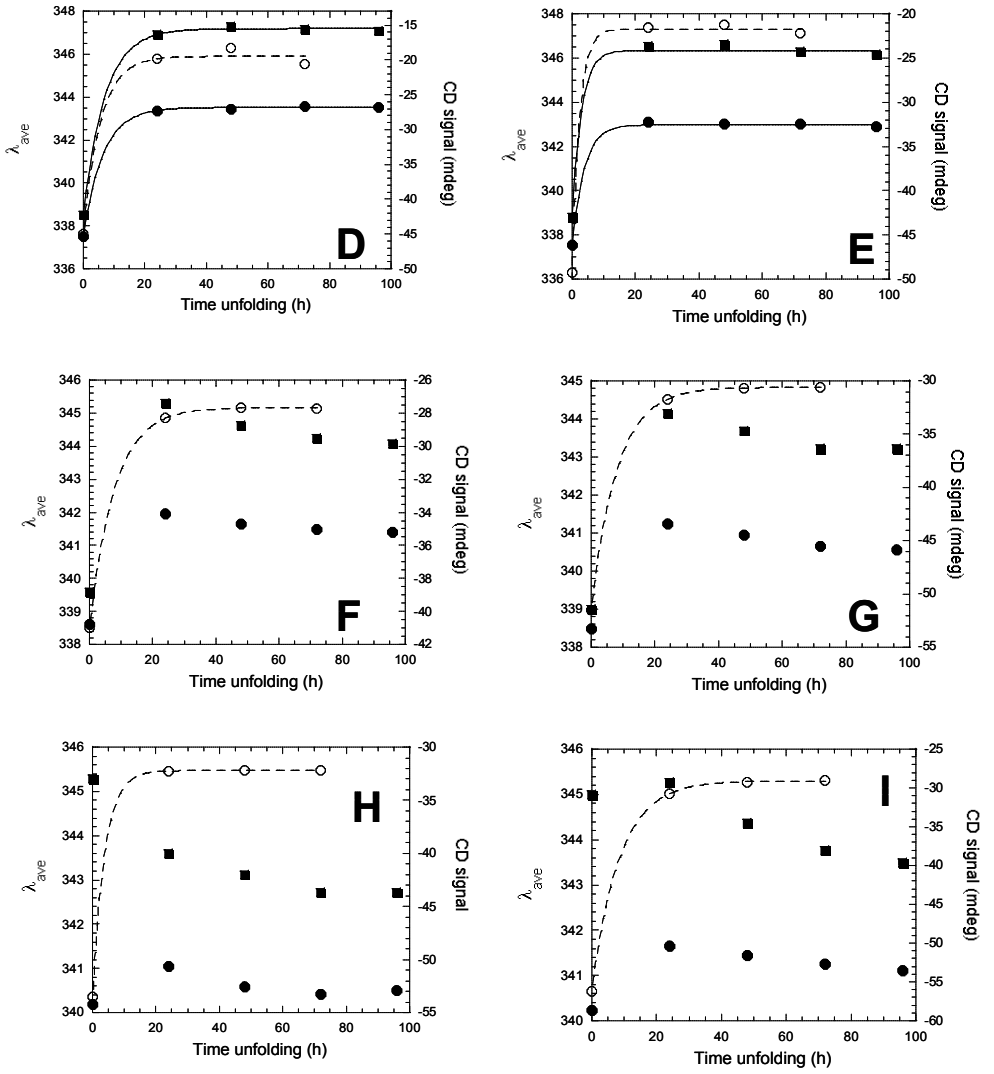

Figure 30. Kinetics of unfolding of procaspase-3(C163S,V266H) at pH 4.0 (*Panel D*), pH 4.25 (*Panel E*), pH 4.75 (*Panel F*), pH 5.0 (*Panel G*), pH 5.5 (*Panel H*), and pH 6.0 (*Panel I*). Protein was unfolded in 5.0 M urea and the emission fluorescence after excitation at 280 nm (●) or 295 nm (■) and the CD signal at 228 nm (○) were monitored in solutions.

Table VII. Half time of unfolding for procaspase-3(C163S,V266H) in 9.6 M urea (pH 6.5-8.0) or 5.0 M urea (pH 4.0-6.0).

pH	$t_{1/2}$ (hours)
pH 8	23.8±1.6
pH 7.2	13.05±2.5
pH 6.5	6.76±1.01
pH 6.0	5.9±0.23
pH 5.5	2.65±0.18
pH 5.0	5.6±0.07
pH 4.75	5.49±0.2
pH 4.25	<4
pH 4.0	4.3±2.0

studies at different pH values will answer which of the unfolding species, the dimeric form or the monomeric form, is more resistant to unfolding.

Kinetics of refolding of procaspase-3(C163S,V266H) in urea

We also analyzed the kinetics of refolding of procaspase-3(C163S,V266H) at pH 4.0-8.0. In the case of pH 4.0 to pH 6.0, we have noticed that refolding of the protein from 8 M to 0.9 M urea is reversible and requires less than 16 h for reaching the native state (data not shown). We are going to present here only the kinetics of refolding at pH 6.5-8.0.

The protein was first unfolded in 9.4 M urea for the time necessary for complete denaturation (see Table VII). As a control, procaspase-3(C163S,V266H) was also incubated in 2 M urea for the same amount of time. The denatured protein was then refolded in a buffer at final urea concentration of 2 M. We have chosen final urea concentration of refolding of 2 M due to the low stability of the refolded protein in 0.9 M urea at pH>6.5 (data not shown). The average emission wavelength after excitation at 280 nm and 295 nm was measured versus time of refolding, and the results are shown in Figure 31.

For all pH range studied the results for the refolding kinetics seemed noisy and hard to interpret (Figure 31). In all panels, the signal of the protein in 2 M urea ("native" signal) is represented by a constant dotted line. For all pH's, pH 6.5 (Figures 31A and 31B), pH 7.2 (Figures 31C and 31D), and pH 8.0 (Figures 31E and 31F), the proteins seems to require more than 48 h of refolding. Refolding data using protein refolded more than 4 days presented much noise. We have chosen 72 h of

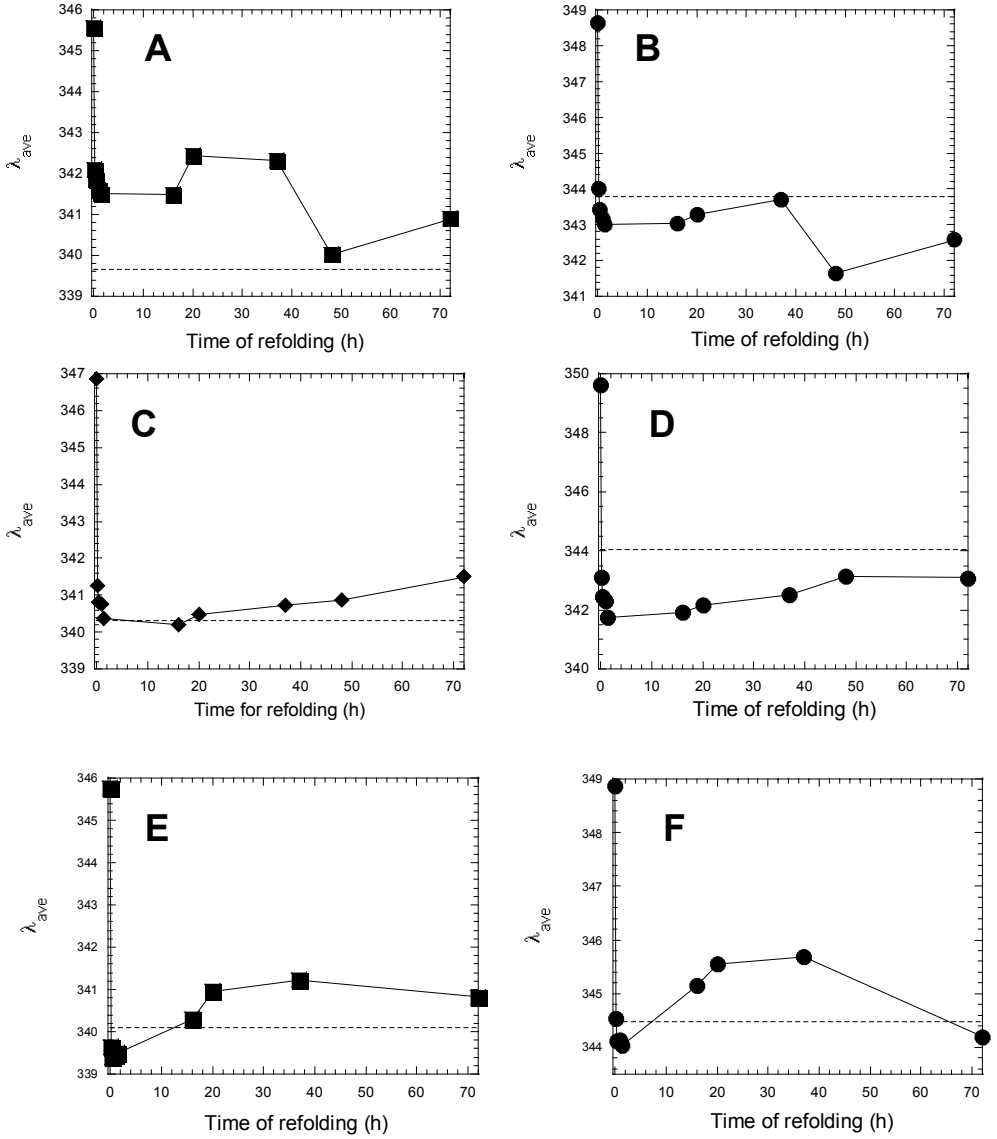

Figure 31. Kinetics of refolding of procaspase-3(C163S,V266H) at different pH values. The protein was refolded from 9.4 M urea to 2 M urea at pH 6.5 (*Panels A* and *B*), 7.2 (*Panels C* and *D*), and 8.0 (*Panels E* and *F*). The average emission wavelength (λ_{ave}) was measured after excitation at 280 nm (■) and 295 nm (●), and compared with the λ_{ave} for the protein in 2 M urea (dotted line). The points were connected with a solid line.

refolding for our refolding experiments at pH>6.5. To determine a more accurate refolding time for procaspase-3(C163S,V266H), the refolding kinetics should also be monitored by circular dichroism.

Equilibrium unfolding studies of procaspase-3(C163S,V266H)

We examined the equilibrium unfolding of procaspase-3(C163S,V266H) over the pH range of 4.0 to 8.0 by unfolding the protein in urea solutions of different concentrations (0 to 9.6 M). During the unfolding experiments, we monitored changes in tertiary structure of the protein by fluorescence, following excitation at 280 and 295 nm, and changes in secondary structure of the protein by monitoring the circular dichroism signal at 228 nm. In addition, we examined the effect of protein concentration on the equilibrium unfolding in order to characterize the thermodynamics of the dimer dissociation. We compared the results with the results produced for procaspase-3(C163S) (65). The fitting of the data was only possible in the case of unfolding at pH 4.0, 4.25, 4.75 and 5.0, and the thermodynamic parameters, ΔG and *m* values, were only calculated in these cases. As the mechanism of unfolding was more complicated at higher pH values (pH 5.5 to 8.0), we could not generate yet models that acceptably approximated our unfolding results.

Figure 32 shows the equilibrium unfolding of procaspase-3(C163S,V266H) at pH 8.0. For the fluorescence experiments, the data display little change in the signal between 0 and 6 M urea (Figure 32A and 32B). The transition of unfolding

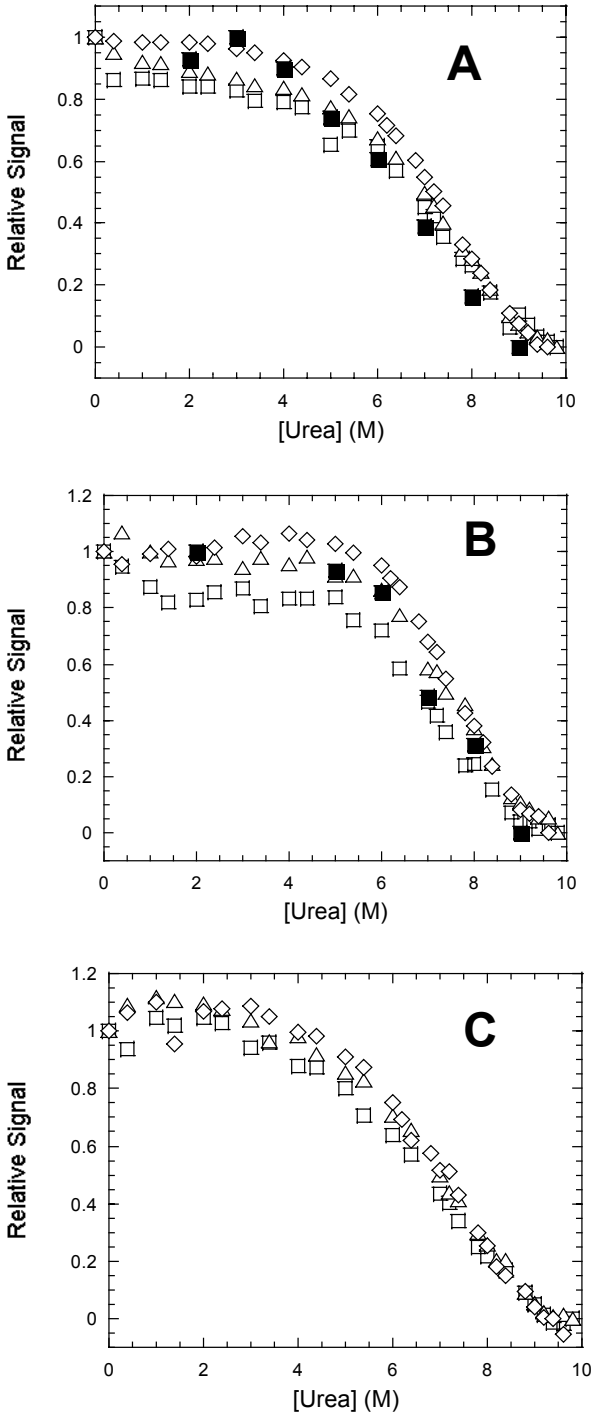

Figure 32. Equilibrium unfolding of procaspase-3(C163S,V266H) at pH 8.0. *Panel A*. Relative fluorescence signal with excitation at 280 nm. *Panel B*. Relative fluorescence signal with excitation at 295 nm. *Panel C*. Circular dichroism signal monitored at 228 nm. The protein concentrations are as follows: 1.0 μM (□), 2.0 μM (△), and 4.0 μM (◇). Closed symbol (■) represents refolding data at 1.0 μM concentration.

curve starts at ~6 M urea and has $[urea]_{1/2}$ for unfolding of ~7.2-7.5 M. In the case of the circular dichroism measurements, the signal does not change significantly between 0 and 3.5 M urea, and the transition of unfolding ranges between 4 and 9 M urea.

As judged from the experiments using fluorescence emission at 295 nm excitation (Figure 32B), the unfolding pattern of procaspase-3(C163S,V266H) follows at least four stages. The first transition occurs between 0 and 2 M urea as a slight decrease in the relative signal, indicating loss of the tertiary structure of the native protein (N) and formation of an intermediate of unfolding (I_A). In the second transition (2-3.5 M urea), the fluorescence comes back to the native signal (blue shift of the fluorescence) and remains constant between 3.5 and 4.5 M urea, indicating the presence of a second intermediate of unfolding (I_B). The latter undergoes complete unfolding between 5 and 9.2 M urea to the final unfolded state, U. In the case of fluorescence experiments collected at 280 nm (Figure 32A) and circular dichroism studies (Figure 32C), the presence of the I_A and I_B species is not evident.

The unfolding of procaspase-3(C163S,V266H) is dependent on the protein concentration on the range from 0 to 6 M urea (Figure 32A, B, and C), which suggests that dimer dissociation occurs in this range of urea concentration or I_B species is monomeric. The protein concentrations used in the experiments were 1, 2, and 4 μM (Figure 32). The unfolding is reversible, shown in the figure by the solid symbols.

The dependence on the protein concentration is less visible in the case of circular dichroism studies (Figure 32C), indicating that there is little difference in the

secondary structure between the dimeric state and the monomeric state of the protein. From these experiments, it is not clear whether species I_A is a dimer, a monomer, or a mixture of two different species, dimer I_A' and monomer I_A''.

In comparison with the unfolding of procaspase-3(C163S) at pH 8.0, also described by a 4-state model (65), several significant changes characterize the unfolding of V266H mutant. First, the third unfolding transition of V266H mutant has a midpoint of 7.2 M urea versus 5.5 M in wild-type procaspase. This suggests that one of the intermediate species of procaspase-3(C163S,V266H) is remarkably more stable than the monomeric intermediate of the procaspase-3(C163S). Second, the dependence on the protein concentration during unfolding of procaspase-3(C163S) is clear in the case of all three spectroscopic assays, indicating that the intermediates of unfolding undergo large changes in the secondary and tertiary structure in comparison with the native protein (65). This is not the case for procaspase-3(C163S,V266H) where the concentration dependence is poor (Figures 32A and 32C). Third, the refolding of procaspase-3(C163S,V266H) at pH 8.0 is much slower than procaspase-3(C163S), requiring ~72 h for reaching the equilibrium.

The unfolding experiments of procaspase-3(C163S,V266H) in urea at pH 7.2 are shown in Figure 33. Like in the case of unfolding at pH 8.0, the denaturation curves at pH 7.2 show little change in the monitored signals between 0 and 5.5 M urea. The unfolding transition ranges between 5.5 and 9.6 M urea and has the midpoint at ~ 7.0 M urea (Figure 33). Data using circular dichroism and fluorescence

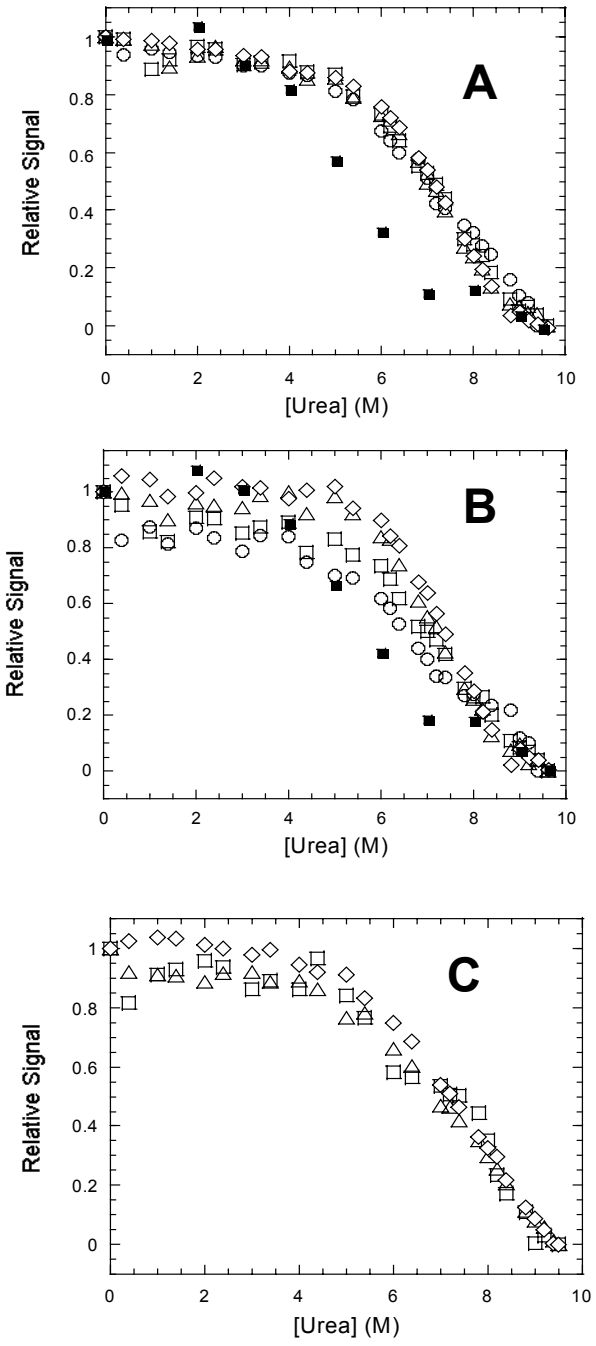

Figure 33. Equilibrium unfolding of procaspase-3(C163S,V266H) at pH 7.2. *Panel A*. Relative fluorescence signal with excitation at 280 nm. *Panel B*. Relative fluorescence signal with excitation at 295 nm. *Panel C*. Circular dichroism signal monitored at 228 nm. The protein concentrations are as follows: 0.5 μM (○), 1.0 μM (□), 2.0 μM (△), and 4.0 μM (◇). Closed symbol (■) represents refolding data at 1.0 μM concentration.

at 280 nm shows very little or no unfolding dependence on the protein concentration (Figure 33A and 33C). The protein concentration in these experiments was 0.5, 1, 2, and 4 μM. Data using fluorescence signal at 295 nm displays protein concentration dependence between 0 and 7 M urea, and manifests about four states in the equilibrium unfolding process. However, there is too much scatter in the data and the four states are not obvious. Most probably the native state, N, first isomerizes to an intermediate I_A, (dimer) shown as a slight inflexion in the curve at ~1.5 M urea (Figure 33B). The second intermediate, I_B, shown as shoulder at ~4-5 M urea, is the monomeric species that completely unfolds to the unfolded state, U, as judged from the low protein concentration dependence of the last transition (Figure 33B). This mechanism is hard to confirm, especially because the data using fluorescence at 280 nm and circular dichroism show at most three states of unfolding and are not dependent on the protein concentration (Figure 33A and 33C).

Overall, unfolding of procaspase-3(C163S,V266H) in urea at pH 7.2 differentiate of procaspase-3(C163S) unfolding by the following aspects: 1) Procaspase-3(C163S) shows four distinct stages of unfolding process (N_2, I_2, I, U) (66), while this mechanism is not evident for procaspase-3(C163S,V266H) (Figure 33A-C); 2) The midpoint of the transition that describes the unfolding of the monomeric intermediate is 5.6 M for procaspase-3(C163S) (66) and, respectively, 7.2 M for procaspase-3(C163S,V266H) (Figure 33); 3) The dissociation of the dimer procaspase starts at ~1.5-2 M urea in the case of procaspase-3(C163S) (66), whereas in the case of procaspase-3(C163S,V266H) the dissociation begins at much lower urea concentrations (~0.4 M); 4) The signal for unfolding of procaspase-

3(C163S,V266H) does not show dependence on the protein concentration in the fluorescence assay at 280 nm and the circular dischroim assay (Figure 33A and 33C). The refolding curve does not follow accurately the unfolding curve, although the fluorescence signal comes back to the native signal after refolding (Figures 33A and 33B). This phenomenon is known as hysteresis of refolding and it is probably due to the insufficient amount of time used for refolding.

Unfolding of the procaspase-3(C163S,V266H) in urea at pH 6.5 is shown in Figure 34. Excepting the assay using the fluorescence at 295 nm excitation (Figure 34B), the data using fluorescence at 280 nm and circular dichroism (Figures 34A and 34C) are similar with the data at pH 7.2 (Figures 33A and 33C). The midpoint of the main transition is ~6.5 M urea (Figure 34) versus 5 M in the case of procaspase-3(C163S) at this pH (65). In the case of the data monitored by fluorescence at 295 nm, the unfolding can be described by three states (Figure 34B). The native dimer protein, N, dissociates to an intermediate monomer, I, between 2 and 4 M urea. The intermediate, I, unfolds completely to unfolded state, U, between 5.5 and 9.2 M urea. The presence of another intermediate at ~2 M urea (dimeric species) is also possible (Figure 34B). It is interesting noting that, between 0 and 2 M urea, the unfolding curve is independent of protein concentration in contrast with the data collected at pH 7.2 and pH 8.0 (Figures 32B and 33B).

The refolding curve of the protein at pH 6.5 shows little hysteresis, similar to the data at pH 7.2 (Figure 33). Most of the native fluorescence signal is recovered in the refolding curve (Figures 34A and 34B).

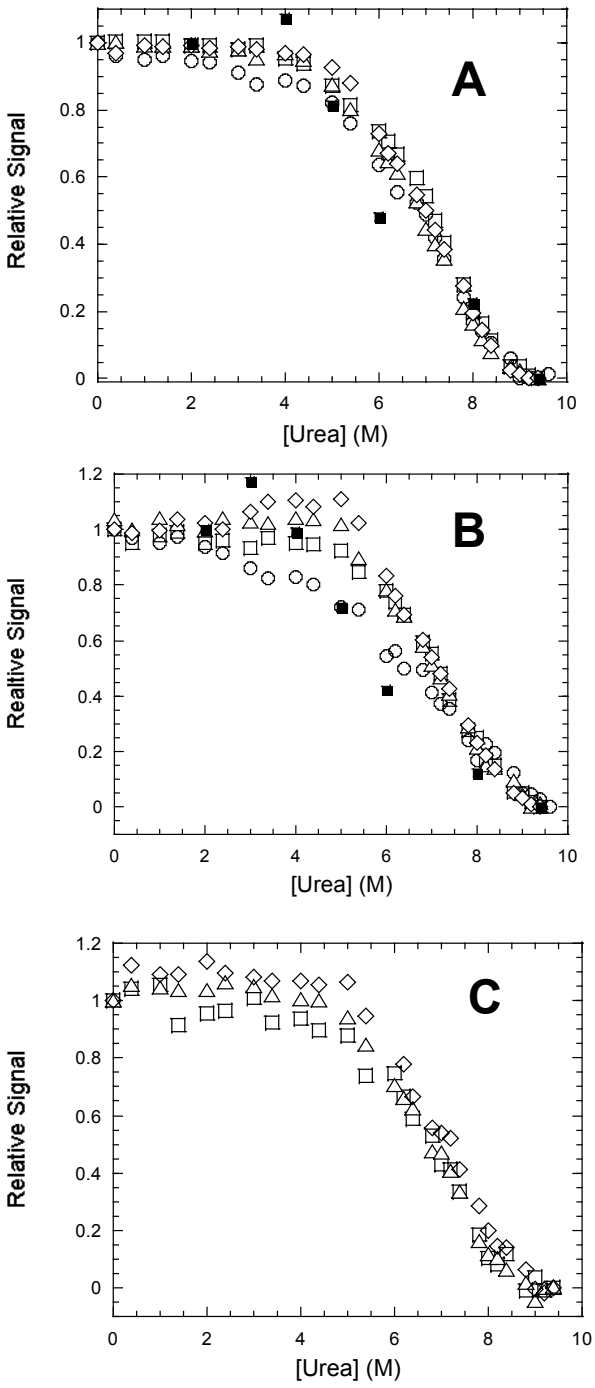

Figure 34. Equilibrium unfolding of procaspase-3(C163S,V266H) at pH 6.5. *Panel A*. Relative fluorescence signal with excitation at 280 nm. *Panel B*. Relative fluorescence signal with excitation at 295 nm. *Panel C*. Circular dichroism signal monitored at 228 nm. The protein concentrations are as follows: 0.5 μM (○), 1.0 μM (□), 2.0 μM (△), and 4.0 μM (◇). Closed symbol (■) represents refolding data at 1.0 μM concentration.

Unfolding data of procaspase-3(C163S,V266H) in urea at pH 6.0 are shown in Figure 35. At this pH, all three spectroscopic probes show similar unfolding pattern for this mutant. Between 0 and ~2.4 M urea the native signal does not show significant change, followed by a cooperative decrease between 2.4 and 4.4 M urea (Figure 35A and 35C) or increase in the case of 295 nm fluorescence data (shoulder region) (Figure 35B). This transition is dependent on the protein concentration in all three assays. The protein concentrations used in the experiment were 1, 2, and 4 μM. The final transition occurs between 4.4 M and 7 M urea and has a midpoint at ~5 M urea. The refolding is reversible as shown by the closed symbols in Figure 35A and 35B.

The unfolding process at pH 6 could be characterized by a three state model, with the native dimer state (N_2) forming an intermediate monomer (I) at ~4 M urea, which then unfolds to the completely denaturated state, U. This model is identical to the model proposed for pH 6.5 (Figure 34), except that in this case all three spectroscopic probes support the mechanism (Figure 35A-C). At pH 6, procaspase-3(C163S) unfolds via a four-state model similar to the models proposed for pH>6 (65). The midpoint for the last transition described by the unfolding of the monomeric species is ~4.8 M urea, close to ~5.0 M obtained for the V266H mutant. It is remarkable to notice that between pH 6.5 and pH 6.0 the midpoint of the unfolding transition decreases with ~1.5 molar units (Figures 34 and 35).

Unfolding data of procaspase-3(C163S,V266H) at pH 5.5 are shown in Figure 36. Protein concentrations used in these assays were 0.5, 1, 2, 4, and 6 μM. A four-state model can describe the unfolding process. The fluorescence data at 280

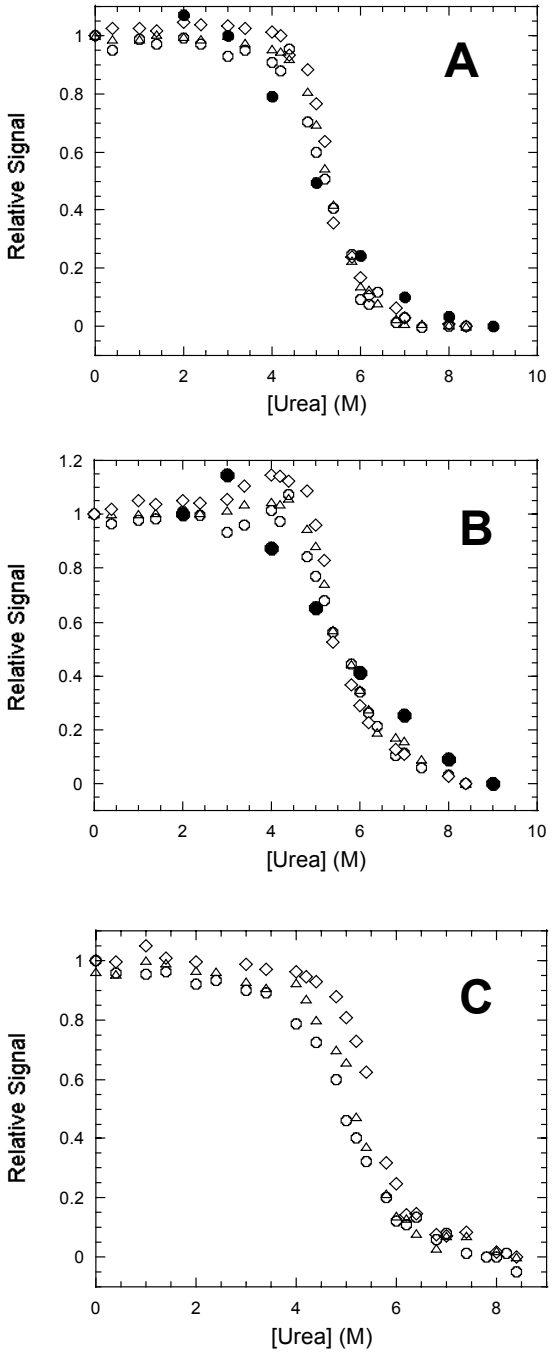

Figure 35. Equilibrium unfolding of procaspase-3(C163S,V266H) at pH 6.0. *Panel A*. Relative fluorescence signal with excitation at 280 nm. *Panel B*. Relative fluorescence signal with excitation at 295 nm. *Panel C*. Circular dichroism signal monitored at 228 nm. The protein concentrations are as follows: 1.0 μM (○), 2.0 μM (△), and 4.0 μM (◇). Closed symbol (●) represents refolding data at 1.0 μM concentration.

nm show little change in the signal between 0 M urea (native state, N) and 2 M urea, except for the data using 6 μM protein, which displays an increase in the relative signal (small shoulder) (Figure 36A). This is indicative of an intermediate species presence, I_A. For the same urea range, the circular dichroism data show a cooperative decrease of the signal, associated with loss in secondary structure (Figure 36C), while the fluorescence data at 295 nm display a consistent increase of the signal (blue shift of the fluorescence), shown as a pronounced shoulder, confirming the presence of I_A (Figure 36B). Between 2 and 4 M urea, all three probes show a cooperative decrease in the relative signal, describing a transition with the midpoint at ~3 M urea. A second signal shoulder between 4 and 5 M urea suggests the presence of a second intermediate, I_B, in all three probes that were used (Figure 36A-C). The last transition describes the unfolding of the I_B to the unfolded state, U, and has a midpoint of ~5.5 M urea. If the first and the second transitions are concentration dependent, the last one is independent of the protein concentration. Due to this fact, we propose the following model for unfolding: N (dimer) isomerizes to I_A (dimer), which forms I_B (monomer), and then unfolds to U (monomer). The unfolding process is reversible, as shown by the close symbols in Figure 36A and 36B, describing refolding at 1 μM.

The data described for procaspase-3(C163S,V266H) are very similar with the data for procaspase-3(C163S) unfolding at pH 5.5 (65). In this case, the protein unfolding also follows a four-state equilibrium model (N_2 to I_2 to I to U). The midpoint of the last transition is ~5.3, close to 5.5 observed for the V266H mutant. Data for the fluorescence signal at 280 and 295 nm look similar in the case of the two

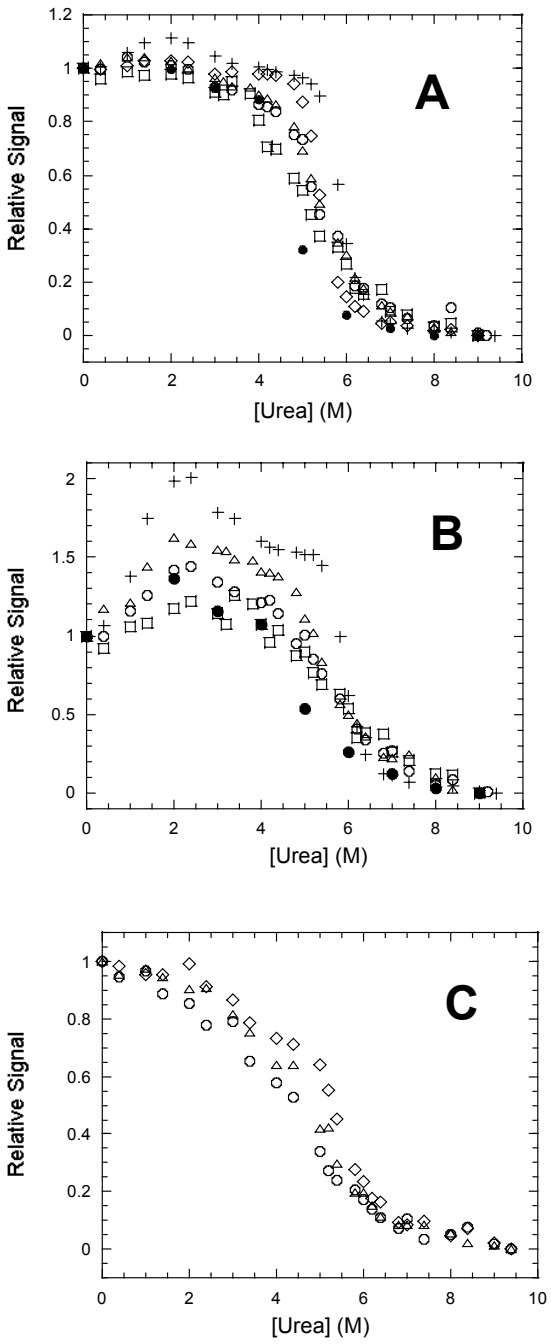

Figure 36. Equilibrium unfolding of procaspase-3(C163S,V266H) at pH 5.5. *Panel A*. Relative fluorescence signal with excitation at 280 nm. *Panel B*. Relative fluorescence signal with excitation at 295 nm. *Panel C*. Circular dichroism signal monitored at 228 nm. The protein concentrations are as follows: 0.5 μM (□), 1.0 μM (○), 2.0 μM (△), 4.0 μM (◇), and 6.0 μM (+) μM Closed symbol (●) represents refolding data at 1.0 μM concentration.

proteins, while circular dichroism data show a more clear plateau corresponding to the second intermediate in the case of procaspase-3(C163S) (65). In conclusion, it is possible that at pH 5.5 procaspase-3(C163S) and procaspase-3(C163S,V266H) have a comparable fold. However, we predict that the V266H dimer is less stable and dissociates at lower concentrations of urea than the procaspase-3 dimer.

For pH's 4.0, 4.25, 4.75 and 5.0, the data did not show any concentration dependence for all three probes that were used. The protein concentrations were 0.5, 1, 2, and 4 μM. Due to this reason, the data were averaged and were globally fit to a two state equation (pH 4.0) or three state equation (pH 4.25-5.0) as described in Methods.

Unfolding data of procaspase-3(C163S,V266H) at pH 5.0 are shown in Figure 37. Between 0 and 4 M urea, all three spectroscopic probes show a cooperative decrease in the relative signal, followed by a small shoulder at 4-4.2 M urea. A second cooperative decrease ranges between 4.2 and 8 M. Three states may characterize the unfolding at pH 5.0: the native protein, N, unfolds to an intermediate, I (midpoint of the first transition is ~2.4 M urea), which unfolds to the unfolded state, U (midpoint of the second transition is ~5.4 M urea). The unfolding is reversible, as shown by the solid symbols in Figures 37A and 37C. It is unclear whether the native protein is dimer or monomer. Size exclusion chromatography experiments done in our laboratory showed that procaspase-3(C163S,V266H) is a dimer at pH 5.0, at ~10 μM concentration (data not shown). It is possible that at the 1-4 μM protein concentration used in the unfolding experiments, the protein is a mixture of monomer and dimer. Alternatively, the native protein is a dimer at 4 μM

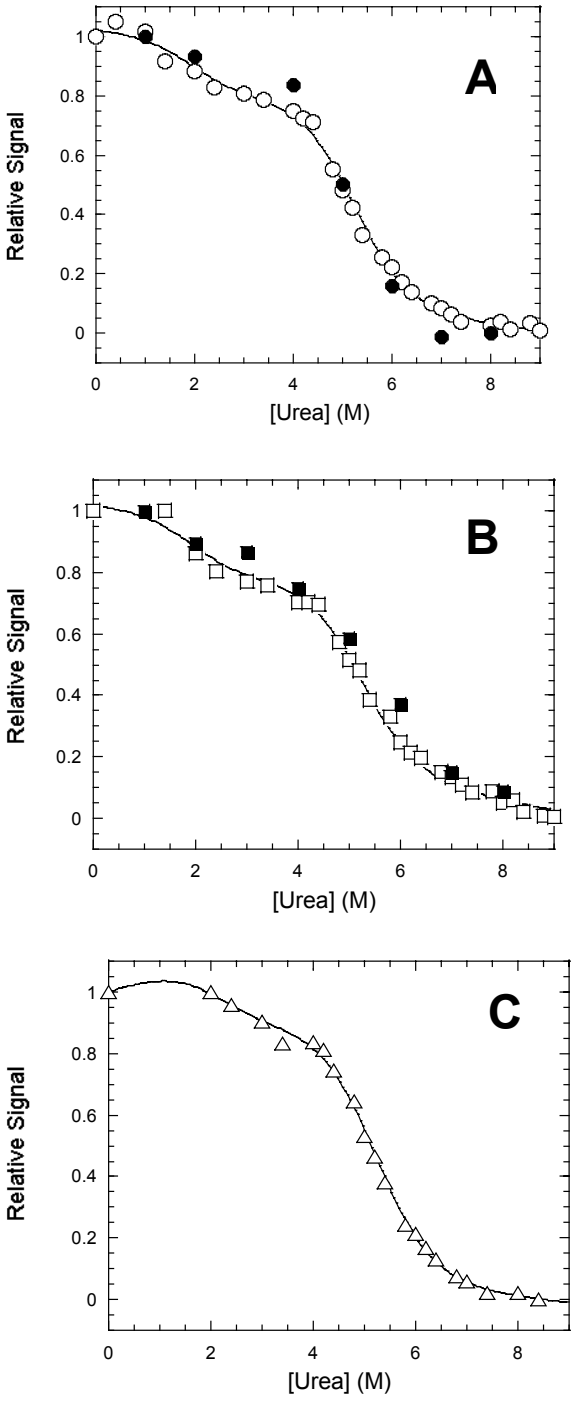

Figure 37. Equilibrium unfolding of procaspase-3(C163S,V266H) at pH 5.0. *Panel A*. Relative fluorescence signal with excitation at 280 nm (○). *Panel B*. Relative fluorescence signal with excitation at 295 nm (□). *Panel C*. Circular dichroism signal monitored at 228 nm (△). Closed symbols (●,■) represent refolding data at 1 μM concentration. For all panels, the data represents average of three data sets collected at protein concentrations of 1.0, 2.0, and 4.0 μM. The solid lines represent fits to the data described under Materials and Methods.

that dissociate at very low concentrations of urea. The thermodynamic parameters generated by the global fits are: ΔG_1=2.2 kcal/mol and m_1=-1.1kcal/mol/M, for the first transition, respectively, ΔG_2=5.6±0.3 kcal/mol and m_2=-1.09±0.05 kcal/mol/M, for the second transition. The last two values are close to the values obtained for the last transition of procaspase-3(C163S) unfolding at pH 5.0, respectively ΔG=5.3±0.5 kcal/mol and m=-1.24±0.05 kcal/mol/M (65).

The unfolding of procaspase-3(C163S,V266H) at pH 5.0 differs from the unfolding of procaspase-3(C163S) by the following aspects: 1) Procaspase-3(C163S) unfolds via a four-state model, displaying concentration dependence between 1 and 6 M urea, similar to the process at pH 5.5 (65); 2) The midpoint of the last transition in procaspase-3(C163S) unfolding is ~4.7 M versus ~5.4 M urea for the V266H mutant.

Unfolding data of procaspase-3(C163S,V266H) at pH 4.75 are shown in Figure 38. All probes suggest an unfolding mechanism described by a three-state process (Figure 38A-C), similar with the process at pH 5.0 (Figure 37). There is a cooperative decrease of the relative signal between 0 and 3.5 M urea corresponding to the first transition of the native protein, N, to an intermediate, I. The presence of the intermediate is expressed more clearly by a small shoulder in the signal at ~3.5 M urea, in the case of the experiments using fluorescence at 280 nm (Figure 38A). The midpoint of the first transition is ~2.4 M urea. The second transition shows a cooperative decrease of the signal between 4 and 9 M urea, representing the unfolding of the intermediate, I, to unfolded state, U. The midpoint of the last transition is ~4.8 M urea. Global fits of the data collected by fluorescence (Figure

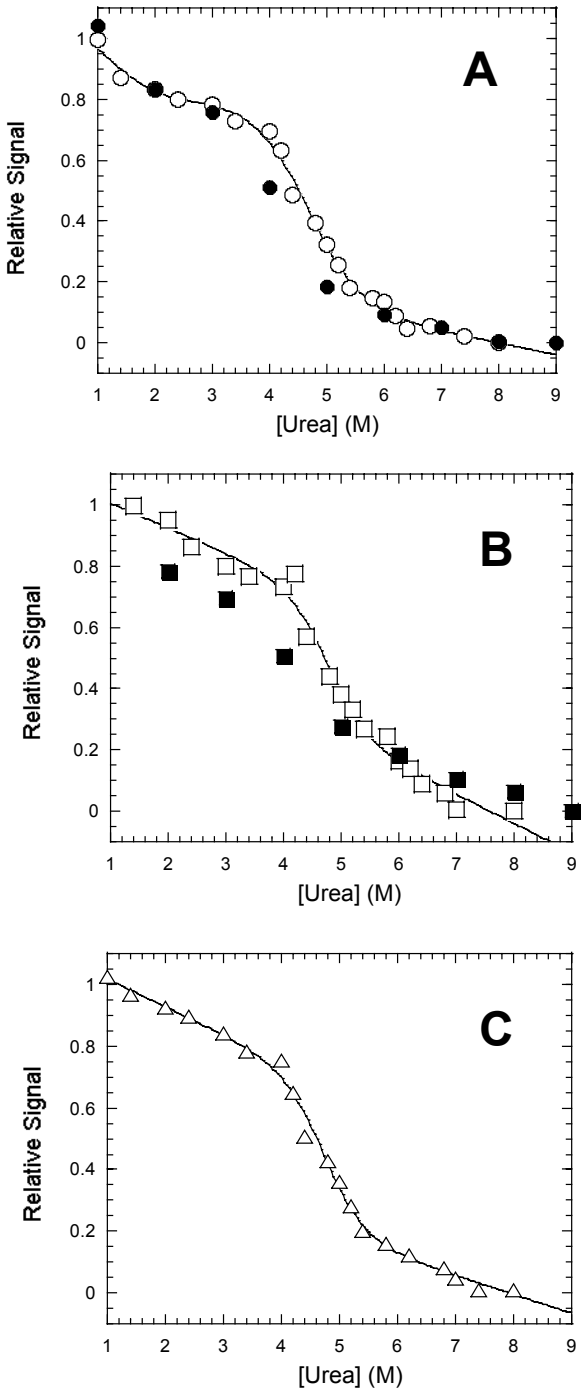

Figure 38. Equilibrium unfolding of procaspase-3(C163S,V266H) at pH 4.75. *Panel A*. Relative fluorescence signal with excitation at 280 nm (○). *Panel B*. Relative fluorescence signal with excitation at 295 nm (□). *Panel C*. Circular dichroism signal monitored at 228 nm (△). Closed symbols (●,■) represent refolding data at 1 μM concentration. For all panels, the data represents average of three data sets collected at protein concentrations of 1.0, 2.0, and 4.0 μM. The solid lines represent fits to the data described under Materials and Methods

38A and 38B) and circular dichroism (Figures 38C) generated the following thermodynamic parameters: ΔG_1=2.4 kcal/mol and m_1=-1.2 kcal/mol/M, for the first transition, and, respectively, ΔG_2=6.3±0.85 kcal/mol and m_2=-1.33±0.16 kcal/mol/M, for the second transition. The unfolding is reversibly and this is shown by the solid circles in the Figures 38A and 38C.

For pH 4.75, the unfolding of the procaspase-3(C163S) follows a four-state mechanism, similar to the mechanism at pH 5.0 (65). The last transition of the monomeric intermediate species to the unfolded state has a midpoint of ~4.4 M urea, and it is characterized by a ΔG of unfolding of ~5.0±0.2 kcal/mol and a *m* value of ~-1.1±0.05 kcal/mol/M (65).

Unfolding data of procaspase-3(C163S,V266H) at pH 4.25 are shown in Figure 39. For all three spectroscopic probes, the data are similar with the ones obtained for pH 4.75 (Figure 38). The unfolding is characterized by a three-state mechanism, with the native species, N, unfolding to an intermediate, I, between 0-3.5 M urea (ΔG_1=1.7 kcal/mol and m_1=-1.2 kcal/mol/M), that unfolds to the unfolded state, U, between 3.4 and 6 M urea (ΔG_2=4.4±0.58 kcal/mol and m_2=-1.07±0.05 kcal/mol/M). The midpoint for the first transition is ~2 M urea and ~4.4 M urea for the second transition (Figures 39A-C). In the case of procaspase-3(C163S), the unfolding at pH 4.25 is also characterized by a three-state process. The first transition (between 0 to 1.5 M urea), representing the formation of the monomeric intermediate, I, from the native dimer, N_2, has ΔG_1=1.3±0.3 kcal/mol and m_1=-1.46±0.2 kcal/mol/M. The second transition (unfolding of the intermediate, I, to the

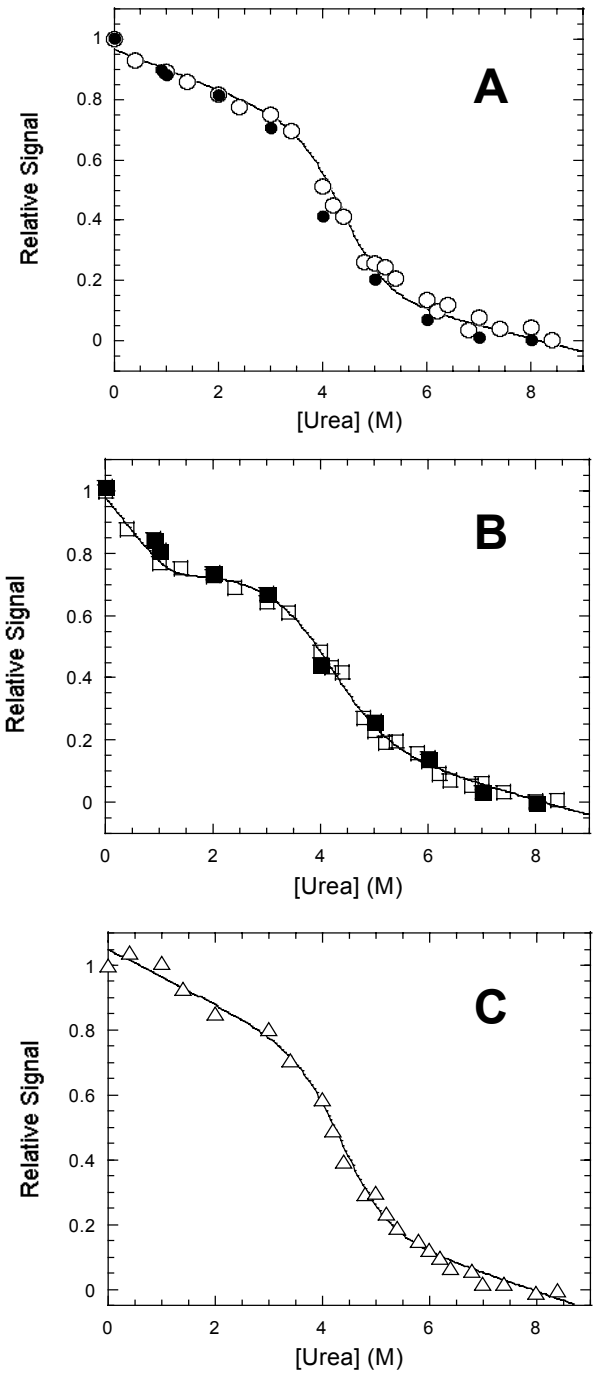

Figure 39. Equilibrium unfolding of procaspase-3(C163S,V266H) at pH 4.25. *Panel A*. Relative fluorescence signal with excitation at 280 nm (○). *Panel B*. Relative fluorescence signal with excitation at 295 nm (□). *Panel C*. Circular dichroism signal monitored at 228 nm (△). Closed symbols (●,■) represent refolding data at 1 μM concentration. For all panels, the data represents average of three data sets collected at protein concentrations 1.0, 2.0, and 4.0 μM. The solid lines represent fits to the data described under Materials and Methods.

unfolded state, U), occurs between 2.5 and 6 M urea, has ΔG_2=3.7±0.3 kcal/mol and m_2=-0.88±0.05 kcal/mol/M, and a midpoint of transition of ~3.9 M urea.

Unfolding data of procaspase-3(C163S,V266H) at pH 4.0 are shown in Figure 40. Although the unfolding curves at this pH are similar with the unfolding curves at pH 4.25 and 4.75 (Figures 38 and 39), the presence of an intermediate species is less obvious (Figure 40). We fit the data using a two-state equation as described in Methods, which does not affect significantly the thermodynamic parameters describing the main transition in case that an intermediate is present. Unfolding at pH 4.0 is described by a cooperative decrease between 0 and 3.4 M urea, which represents the pre-transition of the native species, N. Between 3.4 and 5 M urea, N unfolds to the unfolded state, U. The midpoint of the transition is ~4 M urea, characterized by the free energy of unfolding of ΔG=4.7±0.4 kcal/mol and the *m* value *m*=-1.14±0.09 kcal/mol/M. The unfolding is reversible as shown by the solid symbols in the Figures 40A and 40B. At pH 4.0, procaspase-3(C163S) also unfolds via a two-state model (65). In this case, the transition has the midpoint at ~3.2 M urea, and the parameters are ΔG=3.8±0.2 kcal/mol and *m*=-1.1±0.07 kcal/mol/M.

Overall, procaspase-3(C163S,V266H) is a much more stable protein than procaspase-3(C163S) over the pH range from 4.0 to 8.0. The free energy characterizing the unfolding of the monomeric species is within ~0.9 to 3.7 kcal/mol higher in the case of the V266 mutant at pH 4.0-5.0. This is reflected by the higher amounts of denaturant required to unfold this mutant, as midpoints of the transitions are shifted with ~0.5 to 0.7 M to higher urea concentrations (Figures 37-40). For the unfolding at higher pH values (pH 5.5 to 8.0), the thermodynamic

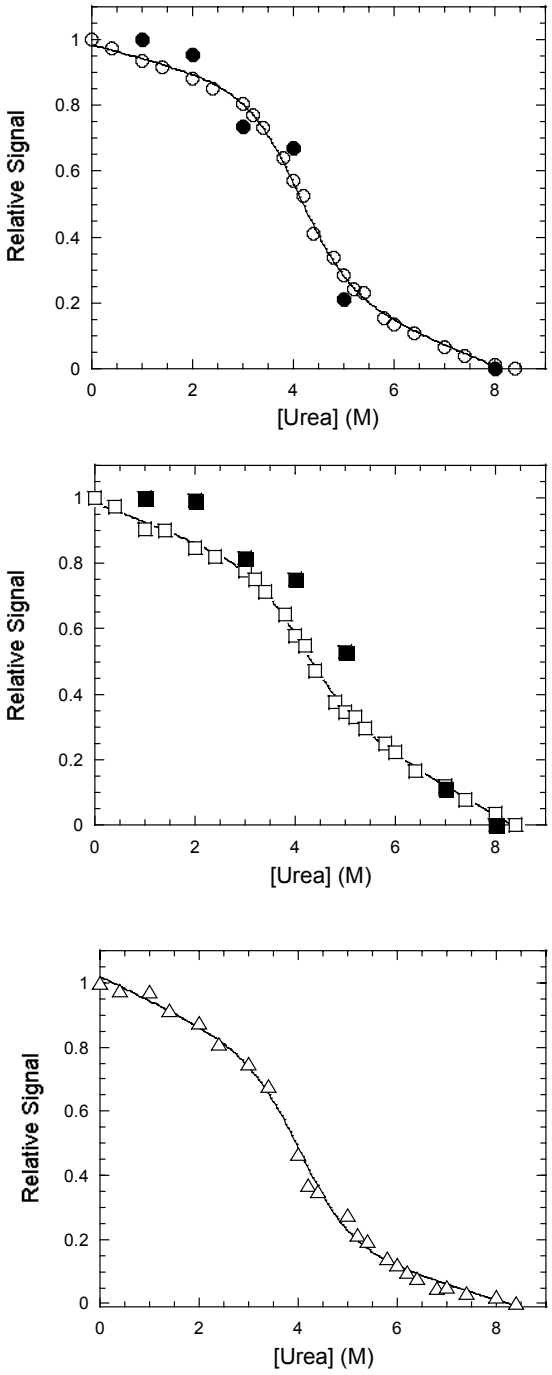

Figure 40. Equilibrium unfolding of procaspase-3(C163S,V266H) at pH 4.0. *Panel A*. Relative fluorescence signal with excitation at 280 nm (○). *Panel B*. Relative fluorescence signal with excitation at 295 nm (□). *Panel C*. Circular dichroism signal monitored at 228 nm (△). Closed symbols (●,■) represent refolding data at 1 μM concentration. For all panels, the data represents average of three data sets collected at protein concentrations of 0.5, 1.0 and 2.0 μM (Panels A and B) and 1.0, 2.0, and 4.0 μM (Panel C). The solid lines represent fits to the data described under Materials and Methods.

parameters of unfolding are not yet characterized. However, the pattern of the equilibrium unfolding curves (Figures 32-36) as well as the kinetics of unfolding (Figure30) makes it clear that V266H mutant is highly resistant to chemical denaturation. The midpoints for the unfolding transitions at pH 6.5-8.0 (Figures 32-24) are with ~1.5 to 2 M urea higher than the midpoints for unfolding curves of procaspase-3(C163S) (65). In addition, the time required for the unfolding at pH's>6.5 is at least double in the case of procaspase-3(C163S,V266H) in comparison with procaspase-3(C163S,V266H) (Table VII).

We noticed that during the unfolding of the V266H mutant at pH 7.2 and pH 8.0 the dissociation of the dimer occurred at urea concentrations as low as ~0.4-1 M (Figures 32-33). For procaspase-3(C163S), the dissociation occurred at >2.5 M urea (65). In addition, the size exclusion chromatography experiments show that procaspase-3(C163S,V266H) is a monomer at pH 4.75, while procaspase-3(C163S) is still a dimer at pH 4.25 (data not shown). Therefore, V266H dimer is less stable than the procaspase-3 dimer. We suggest that the high stability of procaspase-3(C163S,V266H) mutant shown by the unfolding studies is due to the formation of a monomeric intermediate of unfolding, which is much more stable than any of the procaspase-3(C163S) species formed during the unfolding.

It is interesting to notice that the midpoints of the transitions for unfolding at pH's 6.5, 7.2 and 8.0 are similar (Figures 32-34) and differ significantly of the values for unfolding at pH 5.0, 5.5 and 6.0, which are also similar (Figures 35-37). In addition, unfolding transitions at pH 4.0, 4.25 and 4.75 are comparable and form a distinct group of the unfolding transitions at higher pH values (Figure 38-40). We

have plotted the unfolding data monitored by fluorescence at 280 nm for all pH range studied, at one protein concentration (1 μM), and the results are shown in Figure 41. Indeed, the patterns of procaspase-3(C163S,V266H) unfolding between pH 4.0 and 8.0 can be divided into three groups: pH 4.0-4.75 group (shown in black), pH 5.0-6.0 group (shown in blue), and pH 6.5-8.0 group (shown in red) (Figure 41). For each group, the transitions cluster in the same region, giving similar midpoint values, which vary by at least 1 M urea concentration (Figure 41). Procaspase-3(C163S) does not display this feature (65). The described pattern of unfolding indicates that the V266H mutant undergoes two conformational changes following the decrease in the pH, so that the native species at pH 6.5-8.0 is not the same with the native species at pH 5.0-6.0, or pH 4.0-4.75. The first conformational change occurs between pH 6.5 to pH 6.0, and the second occurs between pH 5.0 to pH 4.75. We can indeed associate these two events to the change in the average emission wavelength (<λ>) measured over pH range 3.0 to 9.0, as described in Figure 20D. For the V266H mutant (white circles, Figure 20D), <λ> is constant between pH 9.0 and pH 6.6, followed by a slight blue shift (small inflexion) between pH 6.4 and 5.8. The second transition, which is more pronounced, occurs between pH 5.0 and pH 4.0, and is related with the dimer dissociation at low pH (data not shown).

It is interesting that for this mutant <λ> dependence on the pH is the same as in the case of procaspase-3(C163S) (92). Although not demonstrated yet, it is possible that the latter undergoes as well a conformational change between pH 6.5 and 6.0, which is not illustrated by the unfolding studies (65).

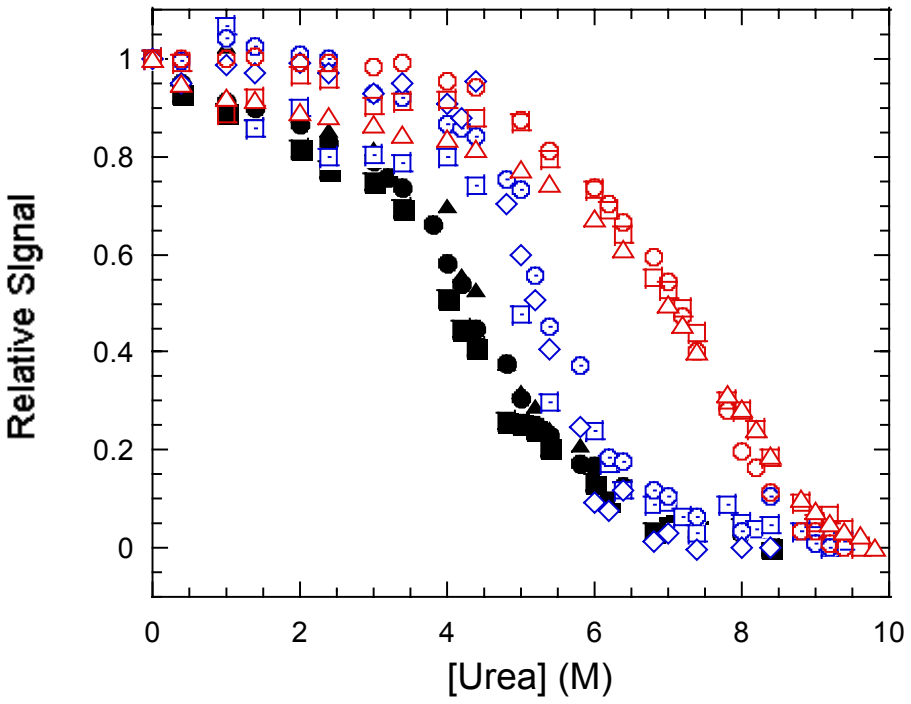

Figure 41. Unfolding of procaspase-3(C163S,V266H) at different pH's. The fluorescence signal at 280 nm was used to monitor the unfolding of 1 μM protein. The pH values were: pH 4.0 (●), pH 4.25 (■), pH 4.75 (▲) pH 5.0 (⊡), pH 5.5 (⊙), pH 6.0(◇), pH 6.5 (○), pH 7.2 (□), and pH 8.0 (△). Black symbols describe transitions with the midpoint at ~4.0 M urea. Blue symbols describe transitions with the midpoint at ~5 M urea. Red symbols describe transitions with the midpoint at ~7 M urea.

Unfolding of procaspase-3(C163S,V266H) resembles unfolding of procaspase-3(C163S) only at pH 5.5 (Figure 36) (65).

Equilibrium unfolding studies of procaspase-3(C163S,V266E)

We also performed equilibrium unfolding studies of procaspase-3(C163S,V266E), which was purified from the soluble fraction of bacteria (see Methods) as a dimeric species (see Figure 15A). The results are shown in Figure 42. In this case, we monitored the fluorescence signal at 340 nm after excitation at 280 nm, using one protein concentration (1μM). We first remarked that the protein unfolding at pH 7.2 is accompanied by a decrease in the fluorescence signal (blue-shift) (Figure 42), in contrast with the V266H mutant and procaspase-3(C163H) that showed exposure of the aromatic residues (Figures 32-40) (65). In Figures 32-40, the decrease in the relative signal is actually an increase in the fluorescence emission relative to the native protein (red-shift). Second, the V266E mutant unfolds via a two-state equilibrium process, from the native protein, N, to the unfolded state, U. The fluorescence signal is characterized by a slight increase between 0 and 3 M urea (pre-transition), followed by a significant quenching of the fluorescence between 3 and 6 M urea, and a post-transition between 6 M and 8 M urea (Figure 42). The thermodynamic parameters calculated by the fit are: the *m* value, m=-1.1$\pm$0.1, and the free energy of transition, ΔG= 4.9$\pm$0.4 kcal/mol, which is very small in comparison with the total free energy of unfolding for procaspase-3(C163S) at pH 7.2, ΔG_{tot}=26.1$\pm$2.1 kcal/mol (66). This indicates that V266E mutant is much

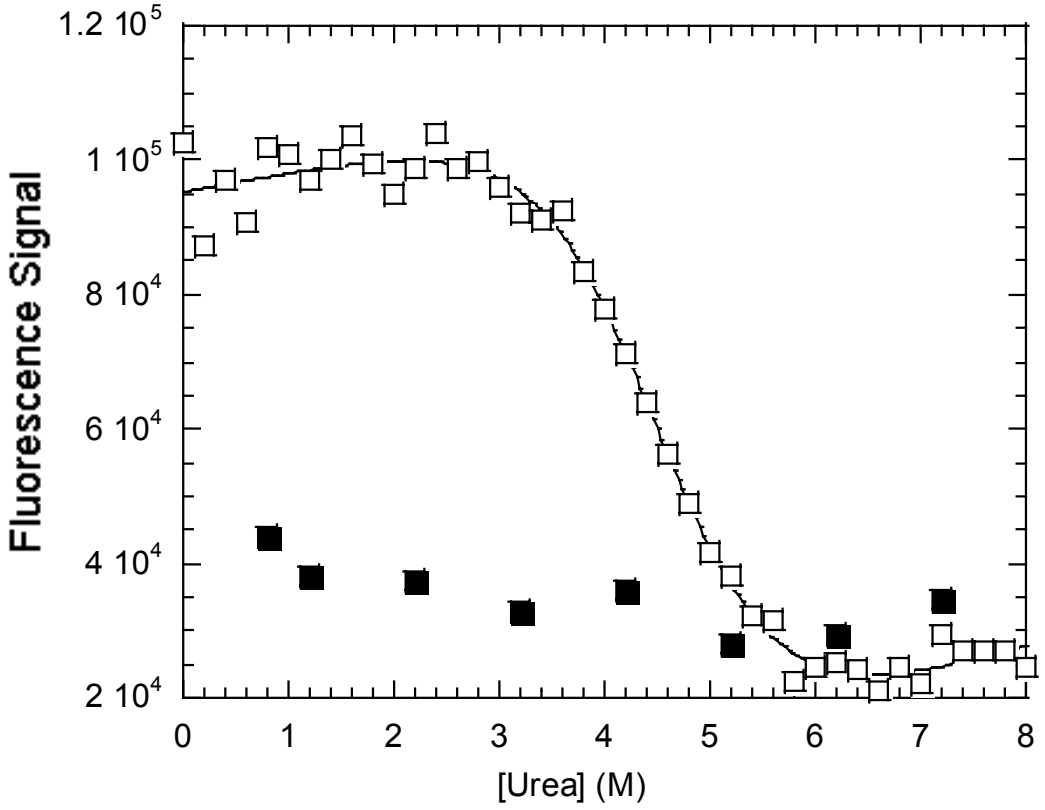

Figure 42. Unfolding of the procaspase-3(V266E) in urea at pH 7.2. Fluorescence signal at 340 nm was monitored following the excitation at 280 nm. The fluorescence signal is more quenched at higher urea concentrations. The open symbols represent unfolding data, while the solid symbols represent refolding data.

less stable than procaspsase-3(C163S). The midpoint of the unfolding transition is ~ 4.0 M urea versus 5.4 M for procaspsase-3(C163S). Interestingly, the thermodynamic parameters for this mutant are close to the thermodynamic parameters that characterize the unfolding of procaspase-3(C163S) monomer at pH 7.2 (last transition of unfolding), namely m=-1.21±0.1, and ΔG= 6.1±0.9 kcal/mol (66).

However, the unfolding of this protein is not reversible, as shown by the solid symbols in the Figure 42. The same results were obtained in the case of fluorescence excitation 295 nm (data not shown). The fluorescence of the refolded protein remains blue-shifted at a value similar to the value of the unfolded protein. We have tried to change the conditions of refolding from 8 M urea by varying the buffer (Tris or Phosphate) (Table I)), or by adding NaCl (0.15 to 0.5 M concentrations), and/or the detergent Tween II (data not shown). Under any of the conditions studied, the protein did not recover its native state following the refolding. As the mutant prepared from the insoluble fraction of *E. coli* is a monomer at pH 7.2 (Figure 15G), we concluded that procaspase-3(C163S,V266E) may be a kinetic trap that cannot undergo dimerization after it is unfolded in urea.

Due to this reason, we did not performed further equilibrium unfolding studies with this protein. Future studies using the protein isolated from the *E.coli* inclusion bodies are required to study in detail the thermodynamics of V266E mutant unfolding. This study will be helpful, as it will characterize the unfolding of a monomeric procaspase-3 mutant.

Conformational changes of procaspase-3(C163S,V266H) versus pH and activation of procaspase-3(D_3A,V266H)

Several conformational changes occur due to the change in pH in procaspase-3 containing the V266H mutation.

We first examined how the change in pH affects the residual activity of procaspase-3(D_3A,V266H) in the case of protein exposure at pH<7.2. Procaspase-3(D_3A,V266H) at pH 7.5 was dialyzed in buffers of different pH values at a final protein concentration of ~20 μM. After 16 h of dialysis, the protein was re-dialyzed in the initial solution of pH 7.5. All the solutions contained 1 mM DTT to ensure the maintaining of the catalytic cysteine in the reduced form. As a control, the same protein has been dialyzed for the same amount of time in a buffer at pH 7.5. Most of the samples at pH 3.0 and 4.0 precipitated following the second dialysis step and only a small percent of the protein could be recovered (see Methods). The protein samples were centrifuged and the exact concentration was determined.

We have shown that procaspase-3(D_3A,V266H) has very little residual activity at neutral pH, so that in comparison with caspase-3 the activity represents only 0.1% (Figure 16C). Appreciable enzymatic activity can be detected only at high protein concentration, i.e. at >500 nM, accounting for 100-500 times more than normal. We measured the initial velocity of the protein samples treated as above at 1 μM final protein concentration and at 100 μM substrate concentration.

Figure 43 shows the increase in the initial velocity of the samples dialyzed at the specified pH, and then re-dialyzed at pH 7.5 in comparison with the control

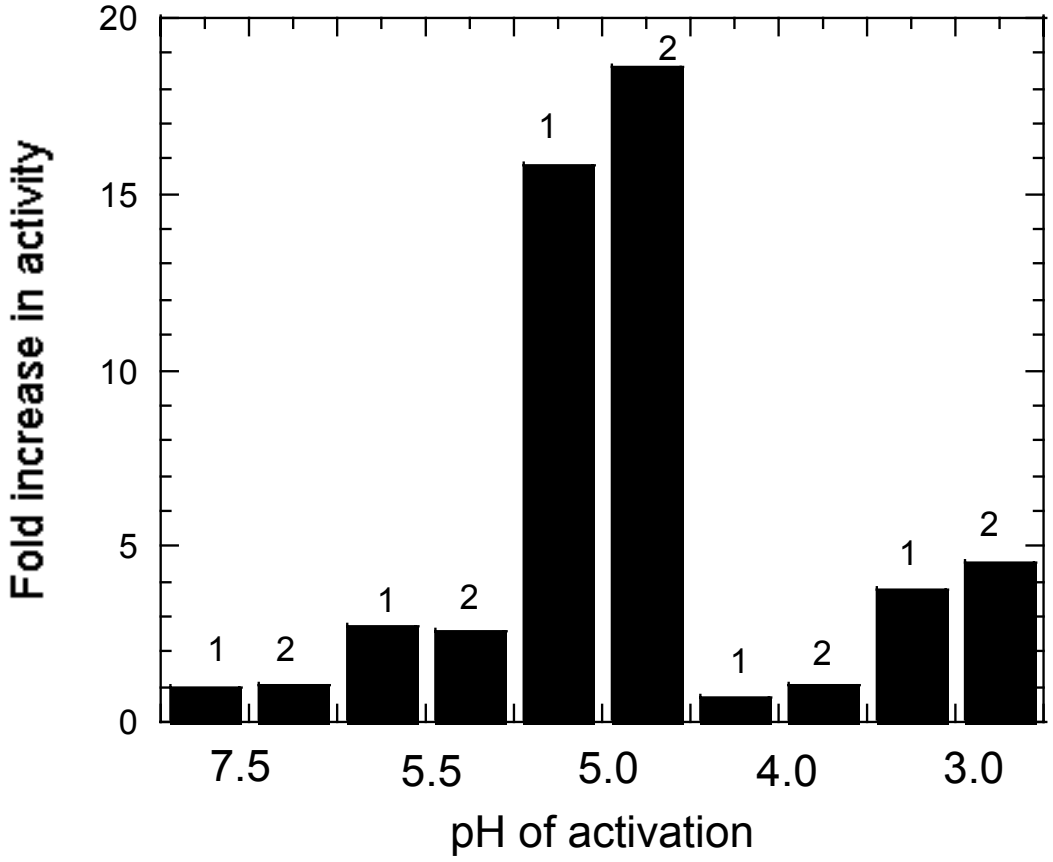

Figure 43. Activation of procaspase-3(D_3A,V266H) after dialysis at pH 3.0-5.5. All samples were dialyzed at the indicated pH and then re-dialyzed at pH 7.5. The initial velocity was measured in assay buffer at pH 7.5 (Table I). The activity is presented as fold increase in initial velocity relative to the velocity of the control sample, which was at kept pH 7.5. Two independent experiments were performed for each sample, symbolized with “1” and “2”.

sample. Interestingly, all samples dialyzed at low pH (except pH 4.0) showed an increase in the activity versus the control kept at pH 7.5. The highest change of the initial velocity is shown by the sample dialyzed at pH 5.0, which displays ~16-19 fold increase in the activity (Figure 43). Each experiment was performed twice. Work in our lab has shown that procaspase-3(D_3A) exposed in the same manner to low pH solutions preserves its catalytic activity after re-dialysis at pH 7.5 (data not shown).

Therefore, the V266H mutant undergoes a conformational change between pH 5.0-5.5 that allows the activation of the mutant.

Trypsin digestion and V8 protease assays were used to characterize these pH dependent modifications. First, we digested with trypsin procaspase-3(C163S,V266H) samples subjected to the pH change from 7.5 to 5.0 and then to 7.5. This assay is useful to indicate whether loop L3 containing the R207 maintains its overexposed position after the sample is kept at lower pH. The results are shown in Figure 44. Figure 44A is the same as Figure 19A. As shown, the kinetics of cleavage at R207 for procaspase-3(C163S,V266H) exposed at pH 5.0 (Figure 44B) is identical with the kinetics of cleavage for the control (Figure 44A). This suggests that overexposure of loop L3 may not be associated with the loss of V266H mutant activity, and if loop L3 exposure changes at low pH, then this change is reversible.

In order to determine how the exposure of the catalytic loops is affected by low pH, we did the limited proteolysis assays at pH 6.0 and 5.5 (trypsin) and pH 4.0, 5.0, 5.5 and 6.0 (V8 protease). Trypsin digestions of the procaspase-3(C163S,V266H) at pH 6.0 and 5.5 are shown in Figure 45. In comparison with the trypsin digestion at pH 7.5 (Figure 43A), more cleavages occur at pH 6.0 (Figure

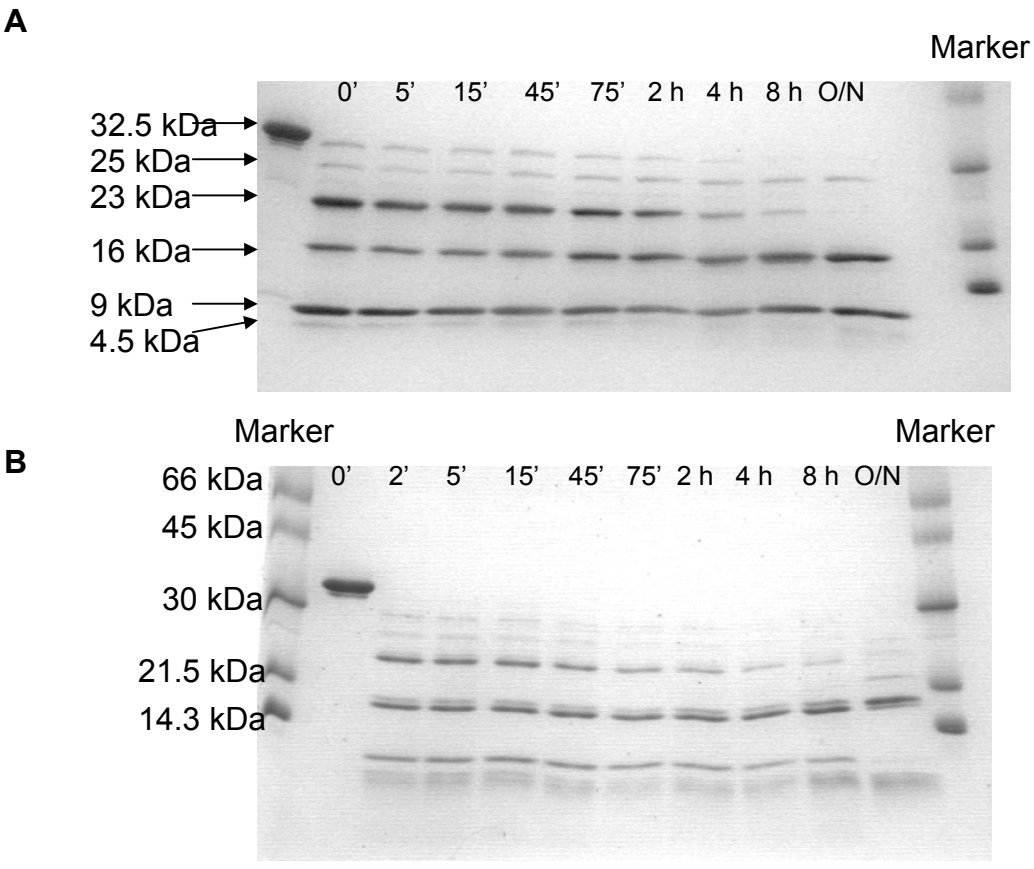

Figure 44. Trypsin digestion of the procaspase-3(C163S) at pH 7.5. *Panel A*. Digestion at pH 7.5 (see Figure 19A). *Panel B*. The protein was first dialyzed at pH 5.0 and then re-dialyzed at pH 7.5. The cleavage pattern and the kinetics of cleavage are the same.

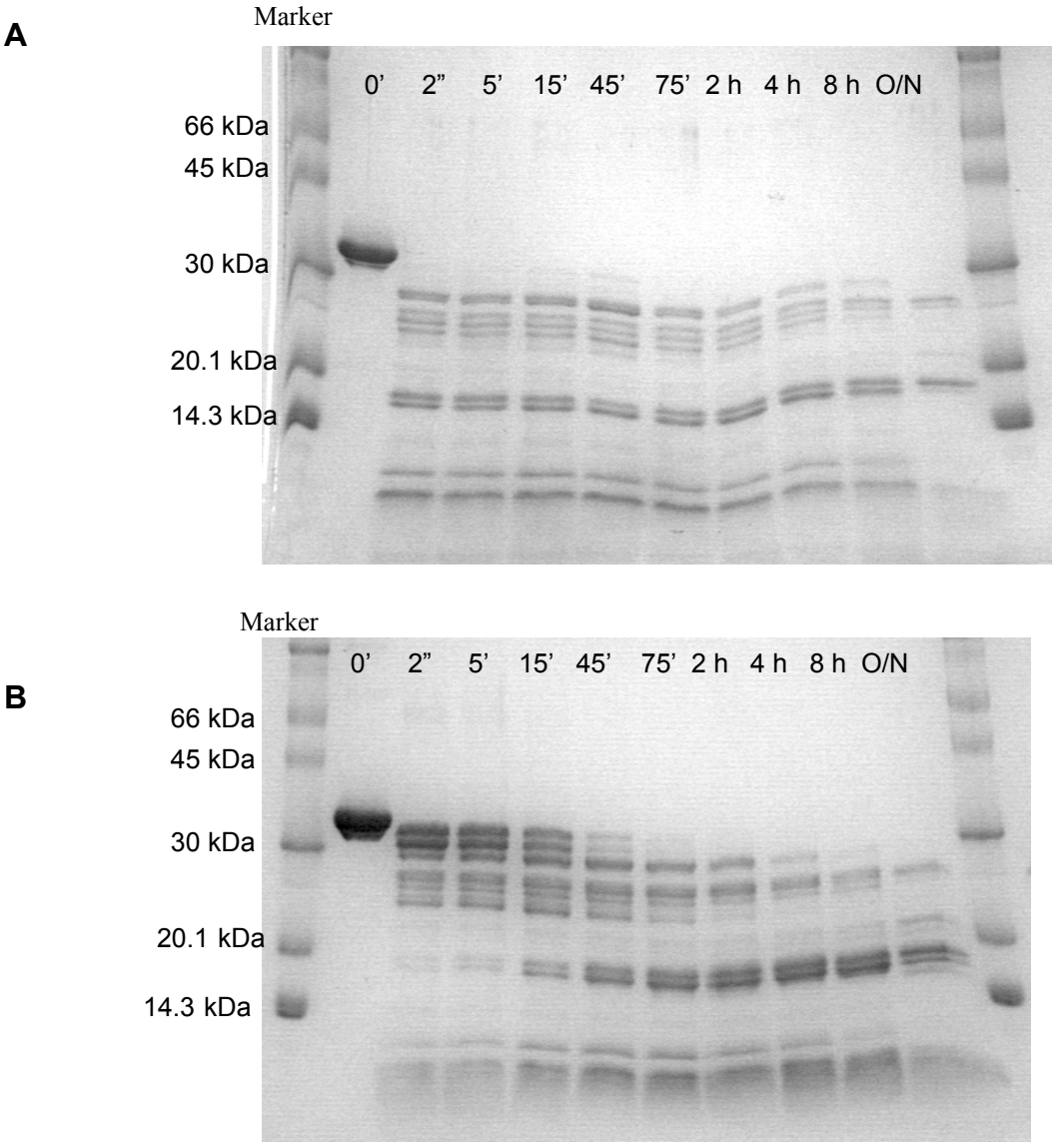

Figure 45. *Panel A*. Trypsin digestion of procaspase-3(C163S,V266H) at pH 5.5.

Panel B. Trypsin digestion of procaspase-3(C163S,V266H) at pH 6.0.

45A) and 5.5 (Figure 45B), suggested by the cluster of bands of ~20-25 kDa. These cleavages are not yet characterized. The remarkable feature of the proteolysis at pH 6 and pH 5.5 is that in both cases the cleavage at R207 (loop L3) occurs with a slower kinetics than at pH 7.5, similarly with the cleavage in procaspase-3(C163) at pH 7.5 (92). This means that the drop in pH may have recovered the orientation of loop L3 to the same orientation as in the wild-type procaspase-3. Due to the fact that trypsin has less activity at pH 5.0, we could not perform trypsin digestion assays below pH 5.5, which could have been indicative of more structural changes that allow activation of the V266H mutant at low pH. Control studies using procaspase-3(C163) have not been performed.

V8 protease displays little change in the activity over the pH range 4.0 to 9.0 (92). We used V8 protease limited proteolysis of procaspase-3(C163S,V266H) at pH 4.0, 5.0, 5.5 and 6.0 and the results are shown in Figure 46. V8 digestion at pH 6.0 shows cleavages at the residues D9, E25 (pro-domain), and D248/E253 (Loop L4) (bands at 26-30 kDa and 4 kDa)) (Figure 46A). However, there is very little cleavage at the residues E98, E106, E173, and D190 (no bands at ~8-16 kDa), as it is the case for the digestion at pH 7.5 (see Figure 19E). Interestingly, at pH 5.5, cleavage at the residues E98, E106, E173, and D190 is more obvious (Figure 46B). Furthermore, cleavage at pH 5.0 (Figure 46C) shows the same bands as the cleavage at pH 7.5 (see Figure 19E), except that the high molecular species contain only one band instead of three bands. This suggests that there is no cleavage in the pro-domain probably due to the high mobility and disorder of the N-terminus in solution at this pH. At last, V8 proteolysis of procaspase-3(C163S,V266H) at pH 4.0

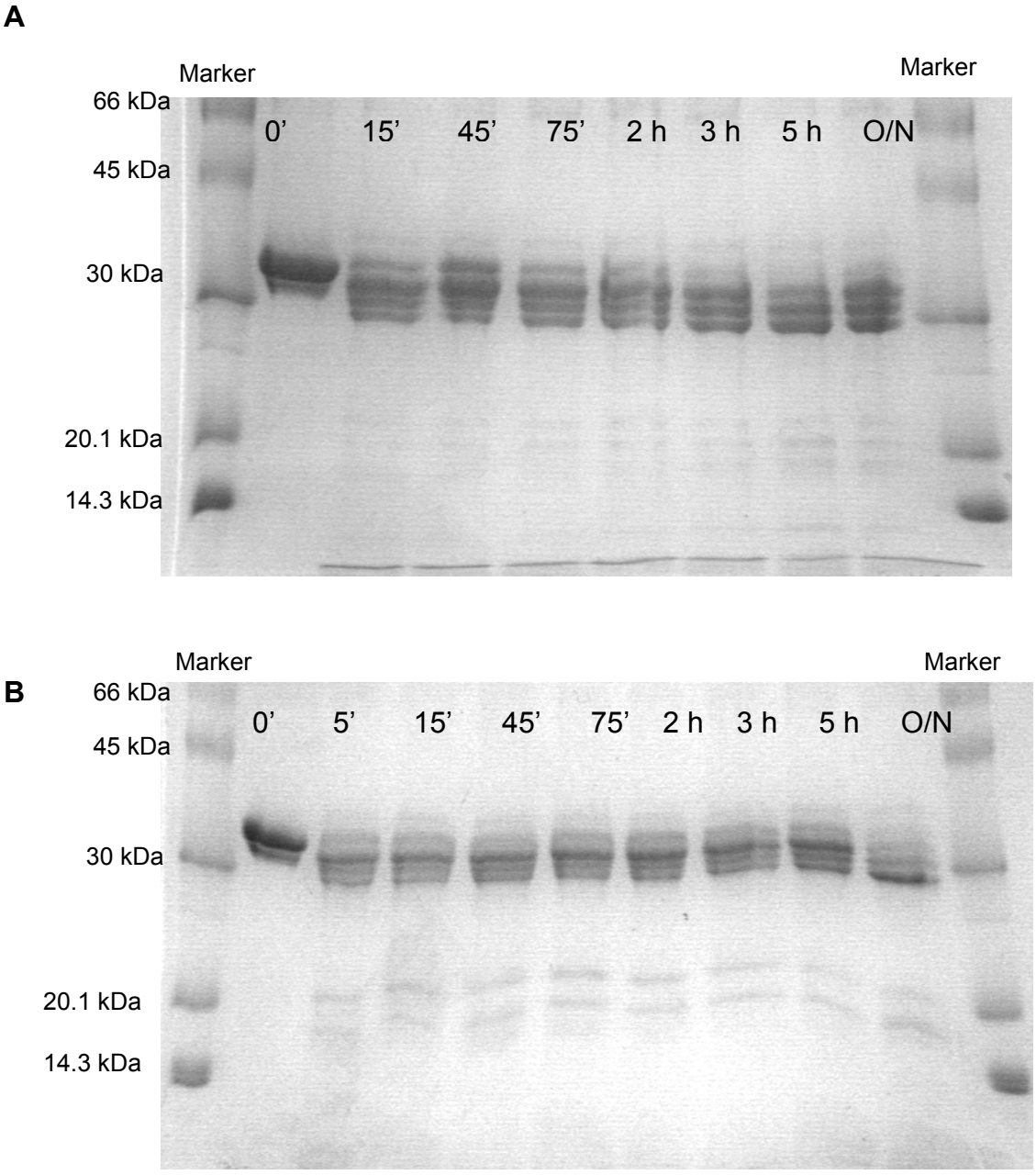

Figure 46. V8 protease digestion of procaspase-3(C163S,V266H) at pH 6.0 (*Panel A*) and pH 5.5 (*Panel B*).

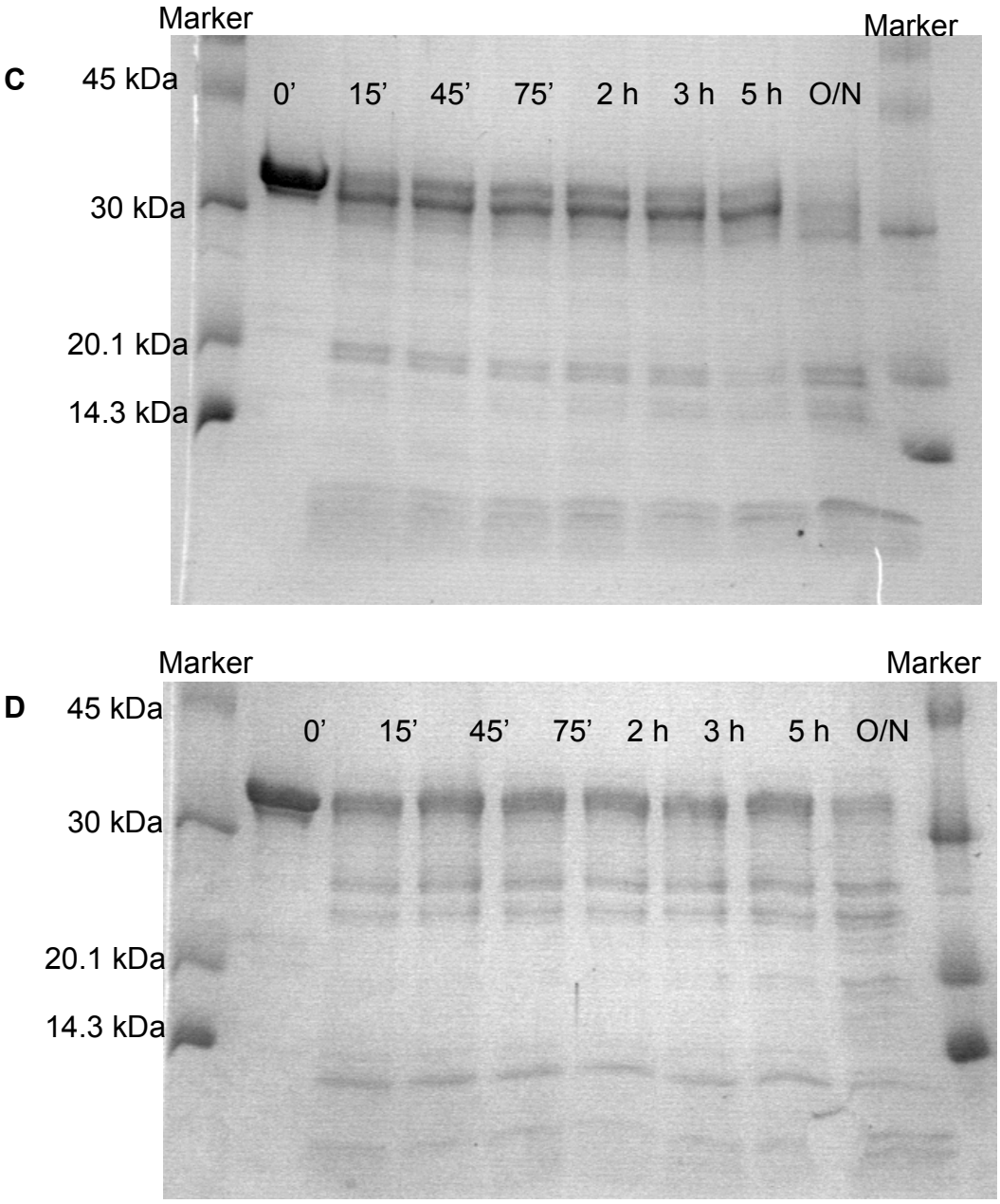

Figure 46. V8 protease digestion of procaspase-3(C163S,V266H) at pH 5.0 (*Panel C*) and pH 4.0 (*Panel D*).

displays a completely different pattern in comparison with the other pHs (Figure 46D). In this case, the cleavage generates at least two bands of ~23-25 kDa, one band of ~ 9kDa and two bands of less than 6 kDa (Figure 46D). These bands are not attributed yet to the protein fragments and the cleavage sites are not characterized.

The conformational changes predicted by the equilibrium unfolding results may be therefore reflected by the limited proteolysis with trypsin and V8 protease. Between pH 7.2 and 6, there is a conformational change that affects the intersubunit linker and makes it less accessible to V8 proteolysis. This is shown by the lack of cleavage at residues E173 and D190 (loop L2) by the V8 protease, as there are no fragments at ~ 8-16 kDa (Figure 46A). The transition from pH 7.2 to 6.0 also affects the regions containing E98 and E106 (Figure 46A). As the pH decreases at 5.5, residues from loop L2 and E98/E106 become more exposed, while loop L4 somehow becomes unavailable for proteolysis (the band at ~4 kDa is not visible in the gel) (Figure 46B). We observed increase in the activity by exposing procaspase-3(D_3A,V266H) at pH 5.5 by ~3 times (Figure 43). It is possible that this modification in the exposure of the loops L2 and L4 may affect the activation of V266H mutant. At pH 5.0, loop L4 becomes again accessible to V8 proteolysis, while the pro-domain is not cleaved (Figure 46C). The most remarkable change in the structure is shown by pH 5.0 to pH 4.0 transition (Figure 46D), which coincides with the dissociation of the procaspase-3(C163S,V266H) dimer (data not shown). More experiments need to be done in order to characterize the cleavage pattern at pH 4.0.

In conclusion, a significant structural change must happen between pH 7.5 and pH 5.0 that is able to allow the proper folding of the catalytic site. It would be

interesting to find those modifications occurring at low pH that are not reversible when the protein is brought at neutral pH. This can be tested by V8 proteolysis assays at the protein exposed at low pH and then re-dialyzed at pH 7.5. In addition, it is necessary to determine the k_{cat} or K_m values of the activated V266H mutant and compare these values with the wild-type catalytic parameters.

Most importantly, an inactive mutant of procaspase-3 that can be activated by the decrease in the pH can raise considerable interest in the field of cancer therapeutics by making use of targeting cellular death in a controllable manner.

DISCUSSION

Investigating the oligomeric properties of the enzymes in relation with protein stability and function is essential for elucidating the cause of various diseases. Many cellular processes are dependent on protein association or interaction. In pathological situations, investigators can control the regulation of these processes by designing tools that stimulate or inhibit protein oligomerization. For example, specific interface inhibitors against HIV-protease-1 (95) have already been developed in order to inhibit the catalytic activity of this protease in AIDS infected cells. In many other cases, investigators design site-directed mutants in order to enhance the thermal stability of the proteins **(96)**.

Dimerization of the initiator procaspases is a pre-requisite for enzymatic activation (17). For full activation, the effector procaspases require the cleavage of the intersubunit linker (33). Recently, our studies and other works have shown that effector procaspases are stable dimers (65).

1. Oligomerization properties of procaspase-3 and role of the pro-domain

We have shown that human procaspase-3 is a dimer in solution, and we estimate the upper limit for the equilibrium dissociation constant to be ~50 nM. Removal of the pro-peptide has little effect on the equilibrium dissociation constant of the dimer or on the spectroscopic properties of the dimer, indicating that the dimeric structure is likely to be unaltered in the pro-less mutant. Two other effector procaspases, procaspase-6 and -7, are also dimers *in vitro* as shown by analytical

ultracentrifugation studies and crystallography (27, 30, 90). Expression of procaspase-3 in yeast or bacterial cells promotes autocleavage. This means that there is sufficient intrinsic activity at high concentrations to initiate maturation. However, the inter-subunit cleavage site, IETD, is a poor substrate for caspase-3 itself (21), which explains why at the low intracellular concentration of ~100 nM (23), procaspase-3 remains inactive.

Results from fluorescence anisotropy (Figure 12), circular dichroism (Figure 11), and FTIR studies (not shown) also suggest that the pro-peptide interacts weakly with the dimer. In addition, the data suggest that the pro-peptide adopts a β-structure or an extended conformation when in contact with the protein, either covalently attached (in *cis*), as for the procaspase-3, or when added in *trans*, as for the pro-less variant. Surprisingly, while the pro-peptide does not inhibit the activity of the mature caspase-3 heterotetramer, we have shown that the pro-peptide is a poor substrate for the enzyme (68).

Also, Cohen and coworkers (97, 98) demonstrated that procaspase-3 from THP.1 cell lysates eluted as a dimer from a gel filtration column. This occurred in both control (non-apoptotic) and apoptotic cells (97). Together the data strongly suggest that procaspase-3 is a dimer *in vivo*. We should note that our results and those of Cohen and coworkers are in contrast to those described by Kumar and coworkers (89), in which they examined oligomerization by yeast two-hybrid assays. While results from their studies indicated that fewer than 10% of the colonies were positive for dimerization of procaspase-3(C163G), Kim and coworkers (99) have

shown recently that the yeast two-hybrid system may under-represent homodimeric interactions, such as the well-known Gcn4p coiled-coil homodimer.

These results are important because they suggest that dimerization is an early event in procaspase-3 maturation, similar to that described for procaspase-1 and activator procaspases (31).

Although not involved in dimerization, the pro-domain seems to be important for the proper formation of the active site of the procaspase-3 (Figure 13A). More work is required to establish why the absence of the pro-peptide does not allow the correct folding of the catalytic site.

2. Interface mutations in the (pro)caspase-3

We have shown that a point mutation of valine 266, the residue at the center of procaspase-3 dimer interface, to hydrophilic residues (glutamate, histidine, or arginine) does not affect the oligomerization state. The interface of (pro)caspase-3 is mainly hydrophobic, although few additional electrostatic interactions stabilize the association (26). Single mutations in the charged interface of initiator procaspase-1, -8 and -9 dramatically affect the dimerization and activation. For example, interface substitution of the T467 from procaspase-8 and F405 from procaspase-9 with aspartate prevents the protein association and consequently the activation (see Figure 7) (20). The charged reversal mutation, R391E, within the procaspase-1 interface prevents the oligomerization, whereas E390R mutation has no effect (31). Interestingly, mutation of the H322 residue, buried next to caspase-1 interface, with alanine, lysine or glycine eliminates caspase-1 activity (24).

This suggests that the initiator (pro)caspases are more vulnerable to interface point mutations than the effectors, where other surrounding interactions can compensate for the substitution, preventing dissociation.

Interestingly, the V266E or V266R mutations result in a 25-fold increase in the activity of procaspase-3, equivalent for activation of the caspase-3 (Tables III and VI). The mechanisms of activation seem to be different. In the case of the V266E mutant, the increase in activity is due to a change in the environment of the catalytic C163, resulting in a decrease in the pK_a of this group. Limited proteolysis assays, activity studies and quenching experiments show that the V266E mutants have features of both caspase and procaspase. In the case of the V266R mutant, the environment of the both catalytic C163 and H121 is affected. In both types of mutants, the effect is likely the result of stabilizing contacts in the loop bundle, including loop L4, which are mediated by movements in the intersubunit linker. The exposure of loop L3 is reduced in both mutants; however only in the V266E mutant do loops L1, L2 and L4 change their location. This is observed by limited proteolysis studies with trypsin and V8 protease (Figures 19B and 19F). These changes affect the electrostatic environment of the tryptophans (W296 and W214, in L3), as shown by potassium iodide quenching experiments (Figure 20A).

We propose that pseudo-activation “without cleavage” of the procaspase-3 containing V266E and V266R mutations is mediated by “concealing” the charged residues into buried salt bridges at the interface. The consequence of these interactions propagates to the catalytic loops in a manner similar to the mechanism of activation of the initiator procaspases following dimerization (20, 29). It is

interesting that processed caspase-9 occurs as a inactive monomer in the absence of the substrate (29) and the dimeric form allows formation of only one active center due to steric clashes at the interface. We do not have any evidence for the number of active catalytic sites in the V266E/R mutants. We estimate that the final effect of these mutations is only partially favorable for the catalytic activity, as the cleavage of the intersubunit linker does not restore full caspase activity.

There are only a few examples in literature of interface substitutions that positively affect the catalytic centers situated far away of the interface. One example belongs to the Cu,Zn superoxide dismutase from *Photobacterium leiognathi*. Mutations in the dimer interface promote dynamic perturbations to the active site region, inducing substrate active site accessibility. The overall effect is a decrease in the K_m and an increase in the k_{cat} (55, 100).

In contrast with V266E and V266R mutations, the V266H interface mutation leads to inactivation of both procaspase-3 and caspase-3. The oligomeric properties are not affected. We propose that H266 sterically clashes with Y197 in the vicinity and does not allow the proper insertion of the catalytic loops (Figure 22C). Small residues like alanine and cysteine substituting for Y197 can partially rescue the activity of procaspase(D_3A,V266H), and the activity of caspase(V266H) (Tables IV and V). Y197A and Y197C mutations are somewhat perturbing to the (pro)caspase-3 activity, suggesting the significance of Y197 in stabilizing the active site environment (Tables IV and V).

The main structural change in the V266H mutants is the overexposure of the catalytic loop L3, which is responsible for substrate binding due to R207 (in the S3

binding site). This change may be sufficient for inducing the inactivity of the V266H (pro)caspase-3. In the crystal structure of procaspase-7 solved at pH 5.5, loop L3 is also unraveled and solvent exposed, which motivated the authors to attribute the inactivity of procapase-7 in the physiological conditions to this reason (27, 30). Our laboratory has evidence that at pH 7.2-7.5 procaspase-3 has a well-formed catalytic pocket and loop L3 is not unraveled (92). Additional evidence is necessary to show that procaspase-3 undergoes structural changes below pH 7.

Many interface mutations that harm the activity and stability of the dimeric enzymes, with non-interface active sites, have been reported in literature. A few examples are: Y96C mutation in hypoxanthine-guanine-xanthine phosphoribosyltransferase (HGXPRT) (101), double mutant (E, R) in Triosephosphate isomerase (102), W52S in Yeast (Saccharomyces cerevisiae) pyrophosphatase (103). Usually, the effect of the interface mutations translates into space toward the active site, which is structurally affected.

Overall, (pro)caspase-3 containing hydrophilic mutations in the dimer interface maintains its quaternary structure at the expense of alterations of the catalytic activity and loop conformation.

3. Unfolding of procaspase-3(C163S,V266H) in urea and pH-dependent conformational changes

We have shown that procaspase-3(C163S,V266H) mutant is a much more stable protein in comparison with procaspase-3(C163S). First, this mutant requires a considerable amount of time to complete the unfolding in 9.4M urea at pH >6 (Table VII). For example, at pH 8, the half-time of unfolding is more than 23 h (Table VII). In

addition, the refolding of the protein at high pH values also require a long time (~72 h) and does not seem to follow the unfolding pathways (Figure 31 and Figures 32-34). The equilibrium unfolding studies show that the transition of unfolding in urea is with 1-2.5 M urea concentration higher in the case of procaspase-3 V266H mutant than in the case of procaspase-3(C163S) (Figures 32-40).

Procaspase-3(C163S,V266H) unfolding in urea involves at least four stages at pH 5.5, 7.2, and 8.0 (Figures 36, 32, 33), and three stages at pH 4.25-6.5 (Figures 34-40). It is interesting that unfolding at pH 6.5-8.0 (midpoint of transition ~7 M urea) forms a distinct group of the unfolding at pH 5.0-6.0 (midpoint of transition ~7 M urea), and of the unfolding group at pH 4.0-4.75 (midpoint of transition ~4 M urea) (Figure 41). This suggests that the mutant undergoes at least two conformation changes, one between pH 6.5 and pH 6.0, and another one between pH 5.0 and pH 4.75. If the latter is associated with the pH-dependent dissociation of the dimer (data not shown), the first may be due to re-location of the loops L3 and L2, as shown by the trypsin and V8 protease assays at pH 6.0 (Figures 45B and 46A). Exposure of the protein at pH lower than 6.0 also coincides with increase in the activity of the procaspase-3(D_3A,V266H) mutant after the protein is re-dialyzed at pH 7.5 (Figure 43). We know that the change in the exposure of loop L3 at pH 5.0 is reversible when the protein is re-dialyzed at pH 7.5 (Figure 44), which suggests that re-location of loop L3 may not be the cause for the low activity of the V266H mutant. At pH 5.5, loop L4 is less accessible to digestion by to V8 protease (Figure 46B), but both loops L2 and L4 recover the cleavage by V8 protease at pH 5.0 (Figure 46C). The highest increase in pH-dependent activation of V266H mutant occurs after protein exposure

at pH 5.0 (Figure 43). It is possible that one of the changes associated with the pH-dependent exposures of the loops L2 and L4 is not reversible after protein is dialyzed at pH 7.5, and this change is beneficial to the protein catalytic activity. Judging from this point of view, procaspase-3 containing V266H mutation is a misfold of the wild-type protein that needs to experience low pH for activation.

The reason for the high stability of V266H mutant during chemical denaturation is not known. We believe that the dimer of procaspase-3(C163S,V266H) is less stable than the dimer of procaspase-3(C163S), based on the experiments monitoring the dimer dissociation versus pH (data not shown) and on the equilibrium unfolding studies at pH 7.2 and pH 8.0 (Figures 32-33). However, we suggest that procaspase-3(C163S,V266H) forms a monomeric intermediate of unfolding that is considerable more stable than the intermediate species formed by procaspase-3(C163S) (65). We have performed trypsin and chymotrypsin digestions in 4 M urea, as well as circular dichroism studies in solutions containing 4 M urea for the two mutants (data not shown). In both types of the experiments, the secondary and tertiary structures, as well as loop accessibility to proteolysis for the V266H mutant were almost unchanged versus the structures in the native conditions (not shown). By contrast, procaspase-3(C163S) showed little secondary structure and almost no tertiary organization in this kind of experiments, coupled with high accessibility of the sequence for the cleavage by proteases (data not shown).

Future studies will elucidate the mechanism of unfolding of procaspase-3(C163S,V266H) at pH >6.5.

Overall, mutating the dimer interface of procaspase-3 may have various effects on the activity and stability of the protein, reflected by structural changes that take place at more than 10-20 Å away of the dimer interface. Understanding these changes will help to decipher the mechanism of procaspase-3 activation in various conditions.

4. Physiological significance

About a hundred thousand cells are produced every second by mitosis in the human body and a similar number die by apoptosis (104). The malfunction of cell death machinery is therefore summed to “too little or too much apoptosis”, which in the long term prepares the foundation for some pathological situations (105). Due to amplified apoptosis occur some neurodegenerative disorders (Alzheimer, Parkinson, and Huntington ’s disease), hematological disorders (Fanconi anemia, Hodgkin’s disease), autoimmune disorders (multiple sclerosis, fulminate hepatitis), ischemic injury, toxin-induced disease, and bacterial and viral infections (105). Insufficient cell death results in cancer, premalignant disease, autoimmune disorders (systemic lupus erythematosus), metabolic disease (osteoporosis) and some viral infections. However, the involvement of apoptosis in disease is not always straightforward. For example, cancer is not only the result of net gain of cells due to ineffective cell death, but also the consequence of apoptosis of the patrolling immune cells due to cancerous cells themselves (105). Also, the primary cause of T cell depletion in AIDS is not apoptosis but rather the inability of CD4-T cells to be replaced during lymphopoiesis (105). Consequently, the fine line between life and death must be

maintained by a complex network of regulators from both the intracellular and the extracellular environments.

Cancers arise due to gene mutations that lead to the dysregulation of normal apoptotic death. Cells that overexpress normal *ras* or *myc* protooncogenes induce tumors with high rates of both apoptosis and mitosis (106). Mutations in the p53 protein, also known as “the guardian of the genome,” are the most common chromosomal aberrations in human cancers, although p53 is dispensable for normal development (107). Mutations in other pro-survival genes, like Bcl-2 family, have been observed in several types of cancers (105). In addition, a decreased expression of Bax and Bak, pro-apoptotic members of Bcl-2 family, has also been reported in some tumors (108). Bcl-2 proteins play an enormous role in the apoptosis by controlling the release of cytochrome c from the intramembranar space of mitochondria and hence regulate the initiation of caspase activation via the intrinsic pathway. *Bcl-2*$^{-/-}$ newborn mice are viable but die at few months of renal failure (104).

Other important regulation points of apoptosis beside Bcl-2 are the Fas receptor (APO-1 or CD95) and the IAP inhibitors. Fas is a key regulator of apoptosis within the immune system. As a result of mutations in the Fas and Fas ligand gene, the mice develop profound autoimmune disease (109). IAPs (inhibitors of apoptosis) regulate the activity of caspases, and there is no report for procaspase interaction with IAPs. For example, XIAP specifically binds and inactivates caspase-3,-7, and -9 via two different mechanisms. XIAP mRNA levels are relatively high in many types of cancer cell lines (110). Deletions of IAP genes in mammals have not been

described. However, NAIP, one of the IAP genes, is mutated in the case of inherited neuronal disease spinal muscular atrophy (111).

The role of several other cellular components in cell death has been also established by gene knock-outs. *Caspase-1*$^{-/-}$ mice develop normally but are deficient in producing IL-β (112), while *Caspase-8*$^{-/-}$ mouse embryos die at day 11 with abnormal function of the heart (113). Mutations of *caspase-3* and *caspase-9* genes are also lethal and mainly affect the brain (114, 115).

As the evidence for apoptosis participation in human disease is overwhelming, the question that remains to be asked is: can apoptosis be safely targeted for therapy? Indiscriminate inhibition of apoptosis could lead to the survival of genetically damaged cells, whereas inappropriate promotion of apoptosis might lead to undesirable tissue degeneration (105). Several therapies can be utilized in conjunction with other treatments: a) injectable molecules targeted at the upstream modulators of apoptosis; b) small molecules designed to regulate expression or activation of Bcl-2 proteins, caspases or p53; and c) gene therapy, that is overexpression of either *Bcl-2* or *p53* genes. (Pro)caspase-3 interface mutants may be used to trigger apoptosis in cancerous cells by using the first approach.

Mutants of caspases with altered properties can be first tested in studies using induced cell death in cellular cultures. For example, V266E and V266R procaspase-3 mutants undergo *in vitro* activation without the need of cleavage. If this feature is preserved in cellular cultures, then these mutants can be useful in some systems that lack the initiator caspases. Such systems are similar to the organism of *C. elegans* that contains only one type of caspase with intermediate

properties between initiators and effectors (116). It would be interesting to know why it is advantageous for the evolved eumetazoans to develop two types of caspases for completing the programmed cell death.

In addition, it is important to test whether these procaspase mutants can undergo inactivation following the interaction with their natural inhibitors, IAPs. If this is not the case, then active procaspase mutants can be used in systems that contain unusual amounts of caspase inhibitors and prevent substrate cleavage by caspases during apoptosis.

On the other hand, procaspase-3 containing the V266H mutation may be a valuable tool in therapeutics, considering the controllable manner of activation of this mutant by using the exposure at low pH. This property can be useful *in vivo* if, after the synthesis, the protein is initially triggered to the cellular compartments with low pH (for example the lysosomes) and then is released in the cytoplasmic environment of neutral pH where it will undergo activation. This mechanism of activation is in contrast with the cathepsin proteases, which are active at pH 5, but are inhibited at neutral pH (117). The amount of technical details required to achieve such goal is massive and is above the discussion presented here.

Another therapeutic application of the interface mutants is the design of specific caspase inhibitors. Usually, protease inhibitors are designed based on the conformation of the active site pocket, which in many cases are similar. It becomes more and more common to synthesize inhibitors that prevent protein oligomerization and hence the function, like in the case of HIV-1 protease (96). V266H and Y197A (pro)caspase mutants enabled us to decipher the possible amino acid interaction

network that connects the active site and the dimer interface. Specific caspase-3 inhibitors can be developed either to freeze these interactions or to prevent protein association, with consequences on the catalytic activity. Such an approach eliminates the inhibitor cross-interaction with other caspases or proteases that have similar catalytic pockets. Not less appealing is the design of small molecules that are able to specifically activate the effector procaspases by a mechanism that avoids the intersubunit cleavage. Unquestionably, reaching this objective requires intense characterization of the manner by which the catalytic loops of (pro)caspase communicate with the rest of the structure and involves detailed mutagenesis studies coupled with crystallography experiments and advanced organic chemical synthesis.

Overall, studying the interface of (pro)caspase-3 is important for bringing more understanding in the mechanism of protein folding and enzyme activation as well as in the design of therapeutic tools used in the fight against lethal diseases.

.

CONCLUSIONS

The overall conclusions of these studies are:

1. Procaspase-3(C163S) is a stable dimer in solution at 25 ^{o}C and pH 7.2, with K_d of dissociation < 50 nM.
2. The pro-domain of procaspase-3 interacts with the zymogen in micromolar range and does not contribute to the dimer formation. The pro-peptide presence *in cis* is required for correct active site formation.
3. Substituting the valine266 from the hydrophobic interface of (pro)caspase-3 with histidine, glutamate and arginine does not affect the oligomeric properties of the resulting mutants.
4. Interface mutations severely alter the activity and the conformational change of the catalytic loops, located at more than 20 Å away.
5. V266E or V266R interface substitutions promote pseudo-activation of the procaspase-3 dispensing the need of inter-subunit linker cleavage, similarly with the initiator procaspases.
6. V266H interface mutation eliminates the activity of both caspase-3 and procaspase-3 by promoting the re-location of the catalytic loop L3. the activity is recovered following protein exposure at pH 5.
7. The effect of V266H mutation on the (pro)caspase-3 activity is mediated by tyrosine197. Y197A and Y197C substitutions partially rescue the activity of, respectively, procaspase-3 and caspase-3 containing the V266H mutation.
8. V266H interface mutation substantially increases the stability of procaspase-3(C163S) by stabilizing the monomer during chemical denaturation.

FUTURE STUDIES

Several aspects that remained unanswered require future investigation:

I. **Mechanism of pseudo-activation of procaspase-3 containing V266E and V266R mutations**

It is obvious that the two mutations influence the activity loop conformation by a different mechanism. We propose that the activation occurs via buried salt bridges at the interface. This model can be studied by introducing a double mutation “ER” in the hydrophobic interface. In addition, designing double mutants, (V266E,R164E) and (V266R,E124R) in the context of uncleavable procaspase-3 will confirm whether R164, respectively E124, are the potential electrostatic partners for the interface E266 and R266 residues.

II. **Investigating the structural reasons for the high stability of procaspase-3(C163S,V266H).**

Procaspase-3(C163S,V266H) will be analyzed by differential calorimetric studies. In addition, unfolding studies using the mutant procaspase-3(C163S,V266H,Y197A) will be performed in order to see whether the Y197A mutation will revert the effect of V266H mutation upon the stability of procaspase-3. Unfolding studies using procaspase-3(C163S,V266H) that has been pre-dialyzed at pH 5.0 will indicate whether the conformational change occurring at low pH will have an influence upon the stability of the procaspase-3(C163S,V266H) mutant during unfolding studies. If the stability is weaker, it means that the mutant synthesized by *E. coli* is an intermediate of the procaspase-3 unfolding which did not complete the folding.

REFERENCES

1. Yuan, J., S. Shaham, S. Ledoux, H. M. Ellis, and H. R. Horvitz. 1993. The C. elegans cell death gene ced-3 encodes a protein similar to mammalian interleukin-1β-converting enzyme. *Cell 75:641*.
2. Green, D. R. 1998. Apoptotic pathways: the roads to ruin. *Cell 94:695*.
3. Golstein, P., Aubry L., and L. J.P. 2003. Cell-death alternative model organisms: why and which? *Nat Rev Mol Cell Biol 4:798*.
4. Strasser, A., O'Connor, L,, Dixit, V.M. 2000. Apoptosis signaling. *Annu Rev Biochem 69:217*.
5. Hanahan, D., Weinberg, R.A. 2000. The hallmarks of cancer. *Cell 100:57*.
6. Kerr, J. F. 1972. Apoptosis: a basic biological phenomenon with wide ranging implications in tissue kinetics. *Br J Cancer 26:239*.
7. Budihardjo, I., H. Oliver, M. Lutter, X. Luo, and X. Wang. 1999. Biochemical pathways of caspase activation during apoptosis. *Annu Rev Cell Dev Biol 15:269*.
8. Kaufmann, S., H,, Hengartner, M,O. 2001. Programmed cell death: alive and well in the new millennium. *Trends Cell Biol 11:526*.
9. Earnshaw, W. C., L. M. Martins, and S. H. Kaufmann. 1999. Mammalian caspases: structure, activation, substrates, and functions during apoptosis. *Annu Rev Biochem 68:383*.

10. Acehan, D., Jiang, X., Morgan, D.G., Heuser, J.E., Wang, X., Akey, C.W. 2002. Three-dimensional structure of the apoptosome: implications for assembly, procaspase-9 binding, and activation. *Mol Cell 9:423*.

11. Shi, Y. 2002. Mechanisms of caspase activation and inhibition during apoptosis. *Mol Cell 9:459*.

12. Alnemri, E. S., D. J. Livingston, D. W. Nicholson, G. Salvesen, N. A. Thornberry, W. W. Wong, and J. Yuan. 1996. Human ICE/CED-3 protease nomenclature. *Cell 87:171*.

13. Andrade, F., Casciola-Rosen, L.A., Rosen, A. 2004. Granzyme B-induced cell death. *Acta Haematol 111:28*.

14. Grutter, M. G. 2000. Caspases: key players in programmed cell death. *Curr Opin Struct Biol 10:645*.

15. Schwerk, C., Schulze-Osthoff, K. 2003. Non-apoptotic functions of caspases in cellular proliferation and differentiation. *Biochem Pharmacol 66:1453*.

16. Philchenkov, A. A. 2003. Caspases as regulators of apoptosis and other cell functions. *Biochemistry (Mosc) 68:365*.

17. Boatright, K. M., and G. S. Salvesen. 2003. Mechanisms of caspase activation. *Curr Opin Cell Biol 15:725*.

18. Denault, J. B., Salvesen, G.S. 2002. Caspases: keys in the ignition of cell death. *Chem Rev 102:4489*.

19. Donepudi, M., Mac Sweeney, A., Briand, C., Grutter, M.G. 2003. Insights into the regulatory mechanism for caspase-8 activation. *Mol Cell 11:543*.

20. Boatright, K. M., Renatus, M., Scott, F.L., Sperandio, S., Shin, H., Pedersen, I.M., Ricci, J.E., Edris, W.A., Sutherlin, D.P., Green, D.R., Salvesen, G.S. 2003. A unified model for apical caspase activation. *Mol Cell 11:529*.

21. Thornberry, N. A., T. A. Rano, E. P. Peterson, D. M. Rasper, T. Timkey, M. Carcia-Calvo, V. M. Hotzager, P. A. Nordstrom, S. Roy, J. P. Vaillancourt, K. T. Chapman, and D. W. Nicholson. 1997. A combinatorial approach defines specificities of members of the caspase family and granzyme B. *J Biol Chem 272:17907*.

22. Tawa, P., Hell, K., Giroux, A., Grimm, E., Han, Y., Nicholson, D.W., Xanthoudakis, S. 2004. Catalytic activity of caspase-3 is required for its degradation: stabilization of the active complex by synthetic inhibitors. *Cell Death Differ.11:439*

23. Stennicke, H. R., J. M. Jurgensmeier, H. Shin, Q. Deveraux, B. B. Wolf, X. Yang, Q. Zhou, M. Ellerby, L. M. Ellerby, D. Bredesen, D. R. Green, J. C. Reed, C. J. Froelich, and G. S. Salvesen. 1998. Pro-caspase-3 is a major physiologic target of caspase-8. *J Biol Chem 273:27084*.

24. Wilson, K. P., J.-A. F. Black, J. A. Thomson, E. E. Kim, J. P. Griffith, M. A. Navia, M. A. Murcko, S. P. Chambers, R. A. Aldape, S. A. Raybuck, and D. J. Livingston. 1994. Structure and mechanism of interleukin-1β converting enzyme. *Nature 370:270*.

25. Schweizer, A., Briand, C., Grutter, M.G. 2003. Crystal structure of caspase-2, apical initiator of the intrinsic apoptotic pathway. *J Biol Chem 278:42441*.

26. Mittl, P. R. E., S. DiMarco, J. F. Krebs, X. Bai, D. S. Karanewsky, J. P. Priestle, K. J. Tomaselli, and M. G. Grutter. 1997. Structure of recombinant human CPP32 in complex with the tetrapeptide acetyl-asp-val-ala-asp fluoromethyl ketone. *J Biol Chem 272:6539*.

27. Chai, J., E. Shiozaki, S. M. Srinivasula, Q. Wu, P. Dataa, E. S. Alnemri, and Y. Shi. 2001. Structural basis of caspase-7 inhibition by XIAP. *Cell 104:769*.

28. Blanchard, H., L. Kodandapani, P. R. E. Mittl, S. Di Marco, J. F. Krebs, J. C. Wu, K. J. Tomaselli, and M. G. Grutter. 1999. The three-dimensional structure of caspase-8: an initiator enzyme in apoptosis. *Structure 7:1125*.

29. Renatus, M., Stennicke, H.R., Scott, F.L., Liddington, R.C., Salvesen, G.S. 2001. Dimer formation drives the activation of the cell death protease caspase 9. *Proc Natl Acad Sci U S A. 98:14250*.

30. Riedl, S. J., Fuentes-Prior, P., Renatus, M., Kairies, N., Krapp, S., Huber, R., Salvesen, G.S., Bode, W. 2001. Structural basis for the activation of human procaspase-7. *Proc Natl Acad Sci U S A 98:14790*.

31. Gu, Y., J. Wu, C. Faucheu, J.-L. Lalanne, A. Diu, D. J. Livingston, and M. S.-S. Su. 1995. Interleukin-1β converting enzyme requires oligomerization for activity of processed forms in vivo. *EMBO J 14:1923*.

32. Ramage, P., D. Cheneval, M. Chvei, P. Graff, R. Hemmig, R. Heng, H. P. Kocher, A. Mackenzie, K. Memmert, L. Revesz, and W. Wishart. 1995. Expression, refolding, and autocatalytic proteolytic processing of the interleukin-1β-converting enzyme precursor. *J Biol Chem 270:9378*.

33. Han, Z., E. A. Hendrickson, T. A. Bremner, and J. H. Wyche. 1997. A sequential two-step mechanism for the production of the mature p17:p12 form of caspase-3 *in vitro*. *J Biol Chem 272:13432*.

34. MacCorkle, R. A., K. W. Freeman, and D. M. Spencer. 1998. Synthetic activation of caspases: Artificial death switches. *Proc Natl Acad Sci U S A 95:3655*.

35. Sulpizi, M., Rothlisberger, U., Carloni, P. 2003. Molecular dynamics studies of caspase-3. *Biophys J 84:2207*.

36. Piana, S., Sulpizi, M., Rothlisberger, U. 2003. Structure-based thermodynamic analysis of caspases reveals key residues for dimerization and activity. *Biochemistry 42:8720*.

37. Thornberry, N. A., H. G. Bull, J. R. Calaycay, K. T. Chapman, A. D. Howard, M. J. Kostura, D. K. Miller, S. M. Molineaux, J. R. Weidner, J. Aunins, K. O. Elliston, J. M. Ayala, F. J. Casano, J. Chin, G. J.-F. Ding, L. A. Egger, E. P. Gaffney, G. Limjuco, O. C. Palyha, S. M. Raju, A. M. Rolando, J. P. Salley, T.-T. Yamin, T. D. Lee, J. E. Shively, M. MacCross, R. A. Mumford, J. A. Schmidt, and M. J. Tocci. 1992. A novel heterodimeric cysteine protease is required for interleukin-1β processing in monocytes. *Nature 356:768*.

38. Katoh, I., Tomimori, Y., Ikawa, Y., Kurata, S.I. 2004. Dimerization and processing of procaspase-9 by redox stress in mitochondria. *J Biol Chem*.

39. Pain, H. R. 2000. *Mechanism of protein folding, Oxford University Press:279*.

40. Zutsh, i. R., Brickner, M., Chmielewski, J. 1998. Inhibiting the assembly of protein-protein interfaces. *Curr Opin Chem Biol 2:62*.

41. Sigler, P. B., Z. Xu, H. S. Rye, S. G. Burston, W. A. Fenton, and A. L. Horwich. 1998. Structure and function in GroEL-mediated protein folding. *Annu Rev Biochem 67:581*.

42. Groll, M., Ditzel, L., Lowe, J., Stock, D., Bochtler, M., Bartunik, H.D, Huber, R. 1997. Structure of 20S proteasome from yeast at 2.4 A resolution. *Nature 386:463*.

43. Ackers, G. K. 1998. Deciphering the molecular code of hemoglobin allostery. *Adv Protein Chem 51:185*.

44. Lipscomb, W. N. 1994. Aspartate transcarbamylase from Escherichia coli: activity and regulation. *Adv Enzymol Relat Areas Mol Biol 68:67*.

45. Schulz, G. E. a. S., R.H. 1979. Principles of protein structure. *Principles of protein structure Springer Verlag, New York:314*.

46. Eriani, G., Cavarelli, J., Martin, F., Dirheimer, G., Moras, D., Gangloff, J. 1993. Role of dimerization in yeast aspartyl-tRNA synthetase and importance of the class II invariant proline. *Proc Natl Acad Sci U S A 90:10816*.

47. Ishima, R., Torchia, D.A., Lynch, S.M., Gronenborn, A.M., Louis, J.M. 2003. Solution structure of the mature HIV-1 protease monomer: insight into the tertiary fold and stability of a precursor. *J Biol Chem 278:43311*.

48. Achari, A., Marshall, S.E., Muirhead, H., Palmieri, R.H., Noltmann, E.A. 1981. Glucose-6-phosphate isomerase. *Philos Trans R Soc Lond B Biol Sci 293:145*.

49. Goldstein, B. M., Colby, T.D. 1999. IMP dehydrogenase : structural aspects of inhibitor binding. *Curr Med Chem 6:519*.

50. Chang, G. G., Tong, L. 2003. Structure and function of malic enzymes, a new class of oxidative decarboxylases. *Biochemistry 42:12721*.

51. Lindner, H. A., Lunin, V.V., Alary, A., Hecker, R., Cygler, M., Menard, R. 2003. Essential roles of zinc ligation and enzyme dimerization for catalysis in the aminoacylase-1/M20 family. *J Biol Chem 278:44496*.

52. Hearn, A. S., Fan, L., Lepock, J.R., Luba, J.P., Greenleaf, W.B., Cabelli, D.E., Tainer, J.A., Nick, H.S., Silverman, D.N. 2004. Amino Acid substitution at the dimeric interface of human manganese superoxide dismutase. *J Biol Chem 279:5861*.

53. Zhang, B., Gao, Y., Moon, S.Y., Zhang, Y., Zheng, Y. 2001. Oligomerization of Rac1 gtpase mediated by the carboxyl-terminal polybasic domain. *J Biol Chem 276:8958*.

54. Falconi, M., Stroppolo, M.E., Cioni, P., Strambini, G., Sergi, A., Ferrario, M., Desideri, A. 2001. Dynamics-function correlation in Cu, Zn superoxide dismutase: a spectroscopic and molecular dynamics simulation study. *Biophys J. 80:2556*.

55. Aparicio, R., Ferreira, S.T., Polikarpov, I. 2003. Closed conformation of the active site loop of rabbit muscle triosephosphate isomerase in the absence of substrate: evidence of conformational heterogeneity. *J Mol Biol 334:1023*.

56. Anderson, P. M. 1986. Carbamoyl-phosphate synthetase: an example of effects on enzyme properties of shifting an equilibrium between active monomer and active oligomer. *Biochemistry 25:5576*.

57. Micheau, O., Thome, M., Schneider, P., Holler, N., Tschopp, J., Nicholson, D.W., Briand, C., Grutter, M.G. 2002. The long form of FLIP is an activator of caspase-8 at the Fas death-inducing signaling complex. *J Biol Chem 277:45162*.

58. Chang, D. W., Xing, Z., Pan, Y., Algeciras-Schimnich, A., Barnhart, B.C., Yaish-Ohad, S., Peter, M.E., Yang, X. 2002. c-FLIP(L) is a dual function regulator for caspase-8 activation and CD95-mediated apoptosis. *EMBO J 21:3704*.

59. van Wijk, R., Huizinga, E.G., Prins, I., Kors, A., Rijksen, G., Bierings, M., van Solinge, W.W. 2004. Distinct phenotypic expression of two de novo missense mutations affecting the dimer interface of glucose-6-phosphate dehydrogenase. *Blood Cells Mol Dis 32:112*.

60. Gable, K., Han, G., Monaghan, E., Bacikova, D., Natarajan, M., Williams, R., Dunn, T.M. 2002. Mutations in the yeast LCB1 and LCB2 genes, including those corresponding to the hereditary sensory neuropathy type I mutations, dominantly inactivate serine palmitoyltransferase. *J Biol Chem 277:10194*.

61. Saarela, J., Laine, M., Oinonen, C., Schantz, C., Jalanko, A., Rouvinen, J., Peltonen, L. 2001. Molecular pathogenesis of a disease: structural consequences of aspartylglucosaminuria mutations. *Hum Mol Genet 10:983*.

62. Healy, D. G., Abou-Sleiman, P.M., Valente, E.M., Gilks, W.P., Bhatia, K., Quinn, N., Lees, A.J., Wood, N.W. 2004. DJ-1 mutations in Parkinson's disease. *J Neurol Neurosurg Psychiatry 75:144*.

63. Neet, K. E., Timm, D.E. 1994. Conformational stability of dimeric proteins: quantitative studies by equilibrium denaturation. *Protein Sci 3:2167*.

64. Bose, K. 2004. Folding, stability and active site conformation of procaspase-3. *PhD Dissertation, North Carolina State University*.

65. Bose, K., Clark, A.C. 2001. Dimeric procaspase-3 unfolds via a four-state equilibrium process. *Biochemistry 40:14236*.

66. Wiederanders, B. 2000. The function of propeptide domains of cysteine proteinases. *Adv Exp Med Biol. 477:261*.

67. Pop, C., Chen, Y.R., Smith, B., Bose, K., Bobay, B., Tripathy, A., Franzen, S., Clark A.C. 2001. Removal of the pro-domain does not affect the conformation of the procaspase-3 dimer. *Biochemistry 40:14224*.

68. Klein-Seetharaman, J., Oikawa, M., Grimshaw, S.B., Wirmer, J., Duchardt, E., Ueda, T., Imoto, T., Smith, L.J., Dobson, C.M., Schwalbe, H. 2002. Long-range interactions within a nonnative protein. *Science 295:1719*.

69. Pace, C. N., B. A. Shirley, and J. A. Thomson. 1989. Measuring the conformational stability of a protein. In *Protein Structure and Function, A Practical Approach*. T. Creighton, ed. IRL Press, New York, p. 311.

70. Fernandes-Alnemri, T., Litwack, G, Alnemri, ES. 1995. Mch2, a new member of the apoptotic Ced-3/Ice cysteine protease gene family. *Cancer Res. 55:2737*.

71. Clark, A. C., Ramanathan, R., Frieden, C. 1998. Purification of GroEL with low fluorescence background. *Methods Enzymol 290*.

72. Edelhoch, H. 1967. Spectroscopic determination of tryptophan and tyrosine in proteins. *Biochemistry 6:1948*.

73. Stennicke, H. R., and G. S. Salvesen. 1997. Biochemical characteristics of caspases-3, -6, -7, and -8. *J Biol Chem 272:25719*.

74. Haugland, R. P. 1995. Coupling of monoclonal antibodies with fluorophores. *Methods Mol Biol 45:205*.

75. Connolly, K. M., Ilangovan U, J. M. Wojciak, M. Iwahara, and R. T. Clubb. 2000. Major groove recognition by three-stranded beta-sheets: affinity determinants and conserved structural features. *J Mol Biol 300:841*.

76. Stennicke, H. R., and G. S. Salvesen. 1999. Caspases: preparation and characterization. *Methods 17:313*.

77. Davies, G. E., Stark, G.R. 1970. Use of dimethyl suberimidate, a cross-linking reagent, in studying the subunit structure of oligomeric proteins. *Proc Natl Acad Sci U S A. 66:651*.

78. Royer, C. A., C. J. Mann, and C. R. Matthews. 1993. Resolution of the fluorescence equilibrium unfolding profile of *trp* aporepressor using single tryptophan mutants. *Protein Sci 2:1844*.

79. Clark, A. C., Sinclair, J.F., Baldwin, T.O. 1993. Folding of bacterial luciferase involves a non-native heterodimeric intermediate in equilibrium with the native enzyme and the unfolded subunits. *J Biol Chem 268:10773*.

80. Hedegs, J., S. Sarrafzadeh, J. D. Lear, and D. K. McRorie. 1984. *Modern Anal Ultracentrif*. Birkhäuser, Boston MA.

81. Johnson, M. L., I. J. Correa, D. A. Yphantis, and H. R. Halvorson. 1981. Analysis of data from the analytical ultracentrifuge by nonlinear least-squares techniques. *Biophys. J. 36:575*.

82. Tang, S. S., Chang, G.G. 1996. Kinetic characterization of the endogenous glutathione transferase activity of octopus lens S-crystallin. *J Biochem (Tokyo) 119:1182*.

83. Eftink, M. R., Ghiron, C.A.. 1981. Fluorescence quenching studies with proteins. *Anal Biochem 114:199*.

84. Santoro, M. M., and D. W. Bolen. 1988. Unfolding free energy changes determined by the linear extrapolation method. 1. Unfolding of phenylmethanesulfonyl α-chymotrypsin using different denaturants. *Biochemistry 27:8063*.

85. Thomson, J. A., B. A. Shirley, G. R. Grimsley, and C. N. Pace. 1989. Conformational stability and mechanism of folding of ribonuclease T1. *J Biol Chem 264:11614*.

86. Meergans, T., A.-K. Hildebrandt, D. Horak, C. Haenisch, and A. Wendel. 2000. The short prodomain influences caspase-3 activation in HeLa cells. *Biochem J 349:135*.

87. Van Criekinge, W., R. Beyaert, M. Van de Craen, P. Vandenabeele, P. Schotte, D. De Valck, and W. Fiers. 1996. Functional characterization of the prodomain of interleukin-1β-converting enzyme. *J Biol Chem 271:27245*.

88. Colussi, P. A., N. L. Harvey, L. M. Shearwin-Whyatt, and S. Kumar. 1998. Conversion of procaspase-3 to an autoactivating caspase by fusion to the caspase-2 prodomain. *J Biol Chem 1998:26566*.

89. Kang, B. H., Ko, E., Kwon, O.K., Choi, K.Y. 2002. The structure of procaspase 6 is similar to that of active mature caspase 6. *Biochem J. 364:629*.

90. Lewis, S. D., F. A. Johnson, and J. A. Shafer. 1981. Effect of cysteine-25 on the ionization of histidine-159 in papain as determined by proton nuclear magnetic resonance spectroscopy. Evidence for a His-159-Cys-25 ion pair and its possible role in catalysis. *Biochemistry 20:48*.

91. Bose, K., & Pop, C. Feeney, B, Clark, A.C. 2003. Procaspase-3 has a lower catalytic efficiency but an intact substrate binding pocket compared to mature caspase-3. *Biochemistry 42:12298*.

92. Walker, N. P. C., R. V. Talanian, K. D. Brady, L. C. Dang, N. J. Bump, C. R. Ferenz, S. Franklin, T. Ghayur, M. C. Hackett, L. D. Hammill, L. Herzog, M. Hugunin, W. Houy, J. A. Mankovich, L. McGuiness, E. Orlewicz, M. Paskind, C. A. Pratt, P. Reis, A. Summani, M. Terranova, J. P. Welch, L. Xiong, A. Moller, D. E. Tracey, R. Kamen, and W. W. Wong. 1994. Crystal structure of the cysteine protease interleukin-1β-converting enzyme: a $(p20/p10)_2$ homodimer. *Cell 78:343*.

93. Kaneko, K., Peretz, D., Pan, K.M., Blochberger, T.C., Wille, H., Gabizon, R., Griffith, O.H., Cohen, F.E., Baldwin, M.A., Prusiner, S.B. 1995. Prion protein

(PrP) synthetic peptides induce cellular PrP to acquire properties of the scrapie isoform. *Proc Natl Acad Sci U S A 92:11160*.

94. Boggetto, N., Reboud-Ravaux, M. 2002. Dimerization inhibitors of HIV-1 protease. *Biol Chem 383:1321*.

95. Vinayagam, A., Pugalenthi, G., Rajesh, R., Sowdhamini, R. 2004. DSDBASE: a consortium of native and modelled disulphide bonds in proteins. *Nucleic Acids Res 32*.

96. Cain, K., D. G. Brown, C. Langlais, and G. M. Cohen. 1999. Caspase activation involves the formation of the aposome, a large (~700 kDa) caspase-activating complex. *J Biol Chem 274:22686*.

97. Bratton, S. B., G. Walker, S. M. Srinivasula, X.-M. Sun, M. Butterworth, E. S. Alnemri, and G. M. Cohen. 2001. Recruitment, activation and retention of caspases-9 and -3 by Apaf-1 apoptosome and associated XIAP complexes. *EMBO J 20:998*.

98. Newman, J. R., E. Wolf, and P. S. Kim. 2000. A computationally directed screen identifying interacting coiled coils from Saccharomyces cerevisiae. *Proc Natl Acad Sci U S A. 97:13203*.

99. Stroppolo, M. E., Pesce, A., D'Orazio, M., O'Neill, P., Bordo, D., Rosano, C., Milani, M., Battistoni, A., Bolognesi, M., Desideri, A. 2001. Single mutations at the subunit interface modulate copper reactivity in Photobacterium leiognathi Cu,Zn superoxide dismutase. *Mol Biol 308:555*.

100. Subbayya, I. N., Balaram, H. 2002. A point mutation at the subunit interface of hypoxanthine-guanine-xanthine phosphoribosyltransferase impairs activity: role of oligomerization in catalysis. *FEBS Lett 521:72*.

101. Schliebs, W., Thanki, N., Jaenicke, R., Wierenga, R.K. 1997. A double mutation at the tip of the dimer interface loop of triosephosphate isomerase generates active monomers with reduced stability. *Biochemistry 36:9655*.

102. Salminen, A., Parfenyev, A.N., Salli, K., Efimova, I.S., Magretova, N.N., Goldman, A., Baykov, A.A., Lahti, R.. 2002. Modulation of dimer stability in yeast pyrophosphatase by mutations at the subunit interface and ligand binding to the active site. *J Biol Chem 277:15465*.

103. Cygler, M., and J. S. Mort. 1997. Proregion structure of members of the papain superfamily. Mode of inhibition of enzymatic activity. *Biochimie 79:645*.